GEORG-AUGUST-UNIVERSITÄT
GÖTTINGEN

Characterization of a novel regulator of the unfolded protein response in Ustilago maydis and mammals

Dissertation

for the award of the degree

“Doctor rerum naturalium”

of the Georg-August-Universität Göttingen

within the doctoral program *Microbiology and Biochemistry*

of the Georg-August University School of Science (GAUSS)

submitted by

Domenica Martorana

from Ludwigshafen am Rhein

Göttingen 2019

Thesis Committee

apl.-Prof. Dr. Kai Heimel

Department of Molecular Microbiology and Genetics, Georg-August-Universität Göttingen

Prof. Dr. Gerhard Braus

Department of Molecular Microbiology and Genetics, Georg-August-Universität Göttingen

Prof. Dr. Stefanie Pöggeler

Department of Genetics of Eukaryotic Microorganisms, Georg-August-Universität Göttingen

Members of the Examination Board

Referee:

apl.-Prof. Dr. Kai Heimel

Department of Molecular Microbiology and Genetics, Georg-August-Universität Göttingen

2nd Referee:

Prof. Dr. Gerhard Braus

Department of Molecular Microbiology and Genetics, Georg-August-Universität Göttingen

Further members of the Examination Board

Prof. Dr. Stefanie Pöggeler

Department of Genetics of Eukaryotic Microorganisms, Georg-August-Universität Göttingen

PD Dr. Marcel Wiermer

Department of Plant Cell Biology, Georg-August-Universität Göttingen

Prof. Dr. Rolf Daniel

Department of Genomic and Applied Microbiology, Georg-August-Universität Göttingen

PD Dr. Michael Hoppert

Department of General Microbiology, Georg-August-Universität Göttingen

Date of oral examination: 5th of June 2019

Declaration of Independence

I hereby declare that the dissertation entitled “Characterization of a novel regulator of the unfolded protein response in *Ustilago maydis* and mammals” was written independently and without any other aids and sources than stated. This work has not been previously submitted, either in the same or in a similar form to any other university or tertiary institution.

_____ _____

Place, Date Signature

This work was accomplished in the group and under the supervision of apl.-Prof. Dr. Kai Heimel at the Department of Molecular Microbiology and Genetics, Institute of Microbiology and Genetics, Georg-August-Universität Göttingen and in the group of Prof. Dr. Harald Stenmark, Department of Molecular Cell Biology, Institute for Cancer Research, Oslo University Hospital under the supervision of Dr. Kay Oliver Schink from 2015 to 2019.

If you do what you've always done,
you'll get what you've always got.
- Mark Twain -

Summary

The endoplasmic reticulum (ER) is an eukaryotic organelle which is the entry point into the secretory pathway and responsible for protein synthesis and processing. The amount of proteins to be folded in the ER lumen is highly variable and depends on different factors, such as the physiology and the environment of a cell. Accumulation of unfolded proteins in the ER activates the unfolded protein response (UPR) which functions to counter ER stress. Once activated, the UPR restores ER homeostasis or, if ER stress remains unresolved, induces apoptosis. In higher eukaryotes, the UPR is a dynamic signaling network regulated by three main transducers, ATF6, PERK and IRE1α.
Activated IRE1α unconventionally splices the constitutively expressed *XBP1* mRNA encoding the bZIP transcription factor XBP1^{s} which, in turn, transcriptionally regulates the expression of UPR target genes. Under unstressed conditions, as well as during the recovery phase of ER stress, the unspliced *XBP1* mRNA is translated into XBP1^{u}, a highly unstable protein containing a bZIP domain. XBP1^{u} has previously been demonstrated to function as a negative regulator of XBP1^{s}. However, an increasing number of recent studies indicate that XBP1^{u} plays a more important role in UPR regulation than assumed so far. A comprehensive understanding of the regulatory role of XBP1^{u} in the ER stress response as well as the molecular details are still missing.

In the course of this work XBP1^{u} was shown to restore cell survival and promote cell proliferation under unstressed and partly under ER stress conditions. Moreover, ER stress resistance was increased in the presence of XBP1^{u} without affecting the expression of common UPR target genes and fully independent of a functional DNA-binding domain or transcriptional activity. Additionally, the deletion of *XBP1* resulted in morphological aberrations of the ER that were suppressed by *XBP1^{u}*.
Similar to the situation in higher eukaryotes, fungi activate the UPR to resolve ER stress but only rely on the conserved IRE1 signaling pathway. In the fungus *U. maydis*, the bZIP transcription factor Cib1^{s} represents the main UPR regulator. The Cib1^{u} protein, which is derived from the unspliced *cib1* mRNA, is homologous to XBP1^{u} and functions in the ER stress response independent of Cib1^{s}. Analogous to XBP1^{u}, Cib1^{u} mediates increased ER stress resistance and this does not require a functional DNA-binding domain. Consistently, genome-wide analysis revealed that expression of common UPR target genes is not affected. Finally, it was demonstrated that Cib1^{u} and XBP1^{u} are functionally interchangeable.

Collectively, these data strongly suggest a novel, previously undescribed, role of XBP1^{u} in the UPR, which is likely to be evolutionary conserved.

Zusammenfassung

Die Aufrechterhaltung der zellulären Homöostase ist von zentraler Bedeutung für die Anpassungsfähigkeit von Zellen an neue Umgebungen oder Umweltreize.

Das endoplasmatische Retikulum (ER) bildet als eines der größten Kompartimente ein Kontinuum mit der Doppelmembranhülle des Zellkerns. Am Zellkern erfolgt die Synthese, Faltung und Glykosylierung von sekretierten oder Membranproteinen. Ein Ungleichgewicht zwischen Proteinimport in das ER und Proteinexport aus dem ER wird als ER Stress bezeichnet und führt zur Aktivierung eines konservierten eukaryotischen Signalweges, der "**U**nfolded **P**rotein **R**esponse" (UPR). Dies ermöglicht eine erhöhte Faltungskompetenz, einen vergrößerten Reaktionsraum und den Abbau von potenziell toxischen, falsch gefalteten Proteinaggregaten und hilft die ER-Homöostase wiederherzustellen.
In höheren Eukaryoten wird die UPR durch drei Transmembranproteine reguliert: PERK, ATF6 sowie IRE1α, welches den einzigen evolutionär konservierten Signalweg steuert. Unter ER Stress Bedingungen wird IRE1α durch ungefaltete Proteine aktiviert. Dies führt dazu, dass die für den UPR-spezifischen Regulator kodierende *XBP1* mRNA im Zytoplasma prozessiert wird. Durch diesen als unkonventionelles Spleißen bezeichneten Prozess wird die Translation des bZIP Transkriptionsfaktors $XBP1^{s}$ ermöglicht. Unter ungestressten Bedingungen bleibt die *XBP1* mRNA ungespleißt und wird in das Protein $XBP1^{u}$ translatiert. Vor einiger Zeit wurde gezeigt, dass $XBP1^{u}$ als negativer Regulator von $XBP1^{s}$ fungiert. Neuere Studien weisen allerdings auf eine umfassendere Rolle von $XBP1^{u}$ bei der ER Stress Antwort hin. Umfangreiche mechanistische Untersuchungen dazu fehlen jedoch.

Die Ergebnisse dieser Arbeit legen nahe, dass $XBP1^{u}$ sowohl unter ER Stress als auch unter ungestressten Bedingungen das Überleben der Zellen und deren Proliferation begünstigt ohne dabei die Expression von UPR Zielgenen zu beeinflussen. Darüber hinaus konnte beobachtet werden, dass $XBP1^{u}$ dafür weder eine funktionale bZIP Domäne noch transkriptionelle Aktivität benötigt. Auch morphologische Änderungen am ER, die durch eine Deletion von *XBP1* hervorgerufen wurden, konnten durch $XBP1^{u}$ komplementiert werden. Ähnlich wie in höheren Eukaryoten, wird die UPR in dem Basidiomycet *U. maydis* durch den IRE1 Signalweg reguliert. Dabei stellt der bZIP Transkriptionsfaktor $Cib1^{s}$ den Hauptregulator und $Cib1^{u}$ das Homolog von $XBP1^{u}$ dar. Interessanterweise, konnte auch für $Cib1^{u}$ eine Beteiligung an der UPR Regulation und eine Funktionalität in höheren Eukaryoten gezeigt werden.

Zusammenfassend deuten diese Daten auf eine bisher nicht erforschte, evolutionär konservierte Funktion von $XBP1^{u}$ in der UPR hin.

Abbreviations

aa	amino acids
ATF6	activating transcription factor 6
bp	base pair(s)
C-terminal	carboxy-terminal
cDC1S	type 1 conventional dendritic cells
CDK	cyclin-dependent kinase
cDNA	complementary DNA
Cib1	Clp1 interacting bZIP 1
Cntrl	control
CoIP	co-immunoprecipitation
CRISPR	clustered regularly interspaced short palindromic repeats
DNA	deoxyribonucleic acid
DNase	deoxyribonuclease
EC	endothelial cell
e.g.	exempli gratia
et al.	et alii
EM	electron microscopy
ER	endoplasmic reticulum
ERAD	ER-associated degradation pathway
ERSE	ER stress response elements
Exp	experiment
Fig.	figure
FSC	forward scatter
GFP	green fluorescent protein
HEK	human embryonic kidney
h	hour(s)
IRE1	inositol-requiring enzyme 1
kDa	kilodalton
KO	knock-out
m	multiple integration
MEF	mouse embryonic fibroblast
min	minute(s)
mRNA	messenger RNA
N-terminal	amino-terminal
NES	nuclear export signal
NLS	nuclear localization sequence
ORF	open reading frame
PC12	pheochromocytoma cells
PCR	polymerase chain reaction
PERK	PKR-like ER kinase
pers.	personal
qRT-PCR	quantitative real-time PCR
RIDD	IRE1-dependent decay of mRNA
RNA	ribonucleic acid
RNase	ribonuclease
RNC	ribosome-nascent chain
ROI	region of interest
RPE	retinal pigmented epithelium
RPKM	reads per kilobase million
rpm	rounds per million
RT	room temperature
s	second(s)
s	single integration
SEM	standard error of the mean
SPP	signal peptide peptidase
Tab.	table
TM	tunicamycin
TP	translational pausing
uORF	upstream open reading frame
UPR	unfolded protein response
UPRE	UPR elements
UTR	untranslated region
V	volt
WT	wild type
XBP1	X-box binding protein 1
Δ	deletion

Table of Contents

List of Figures

List of Tables

1. Introduction

1.1. ER stress provokes the Unfolded Protein Response (UPR)

Eukaryotic cells contain a number of different organelles that represent optimized compartments for specific cellular processes. One such organelle is the endoplasmic reticulum (ER). The ER with its complex membrane network orchestrates numerous cellular processes such as lipid metabolism, drug detoxification and calcium storage (Alberts et al., 2002; Cribb et al., 2005; Treiman, 2002). More importantly, it is the site of synthesis, folding and post-translational modifications of secretory and membrane-anchored proteins (Hegde and Lingappa, 1999; Ma and Hendershot, 2002). Approximately, this accounts for 30 % of the cellular proteome. Thus, in order to maintain cellular homeostasis, the ER has to constantly adapt to the influx of proteins to be processed (Schröder, 2008). The protein load of the ER is dependent on environmental factors and the physiological status of a cell. Challenges like nutrient deprivation, perturbation of the intracellular Ca^{2+} storage or oxygen deficiency can disrupt ER homeostasis and lead to the so-called ER stress – an imbalance between the protein folding demand and the ER folding capacity (Kozutsumi et al., 1988; Lee, 2001; Ma and Hendershot, 2002). In order to prevent accumulation of unfolded proteins in the ER and to sustain ER homeostasis, the Unfolded Protein Response (UPR) signaling pathway is activated (Cox and Walter, 1996; Mori et al., 1996). The UPR copes with misfolded proteins in the ER lumen by repressing global translation while increasing the production of chaperones and folding catalysts. In addition, it increases the capacity of the ER to fold and secrete proteins by promoting ER expansion (Cox and Walter, 1996; Hurtley et al., 1989; Kaufman, 1999; Murray et al., 2004; Schuck et al., 2009). Misfolded proteins are potentially toxic to the cell and are eliminated via an increased activity of the ER-associated degradation pathway (ERAD). Thus, unfolded proteins are transported back to the cytosol and degraded by the 26S proteasome (Friedlander et al., 2000; Smith et al., 2011; Travers et al., 2000). If ER stress cannot be alleviated in a certain time frame or exceeds a certain threshold, the UPR switches from pro-survival to pro-apoptotic signaling events (Ron and Walter, 2007; Rutkowski et al., 2006; Shore et al., 2011). In general, the UPR is a highly conserved mechanism across eukarya that

developed along with the ER. Even organisms lacking complex transcriptional regulation are able to react to ER stress e.g. via translational changes or alterations in mRNA stability. Overall, the presence as well as the meticulous regulation of the UPR are inevitable since malfunction may result in dire consequences (Hollien, 2013).

1.2. Three interconnected signaling pathways regulate the UPR in mammals

Mammals are composed of hundreds of different specialized cell types (Arendt, 2008; Lodish et al., 2000). The folding capacity of the ER varies among these cell types since every cell type has individual requirements in order to function properly. They encounter different levels of stress depending on the cellular function and environment. Macrophages for example are regularly exposed to various harmful substances whereas secretory cells such as pancreatic β-cells, that are susceptible to chronic stress, produce and secrete up to one million insulin molecules in a single minute (Hollien, 2013; Rutkowski and Kaufman, 2007). Hence, UPR activation not only results from protein folding perturbations, infections and diseases but also from cellular differentiation processes (Kaufman, 2002; Marciniak and Ron, 2006). Despite the different UPR requirements of the cells, the signaling pathways that maintain ER homeostasis are conserved. The stress response in mammals is mainly defined by three ER-localized transducers: Inositol-requiring enzyme 1 (IRE1), activating transcription factor 6 (ATF6) and PKR-like ER kinase (PERK). The three UPR branches elicit different outputs in the cell while operating in-parallel as a complex interconnected signaling network. These outputs can function on a transcriptional, on a translational and on a protein level, affecting intracellular signaling and development as well as differentiation and morphology of whole organs such as liver and secretory glands (Fig. 1). Depending on the cell type, specific combinations of IRE1, ATF6 and PERK are required to modulate the stress response according to their current need (Hetz and Papa, 2018; Lee et al., 2005; Todd et al., 2008).

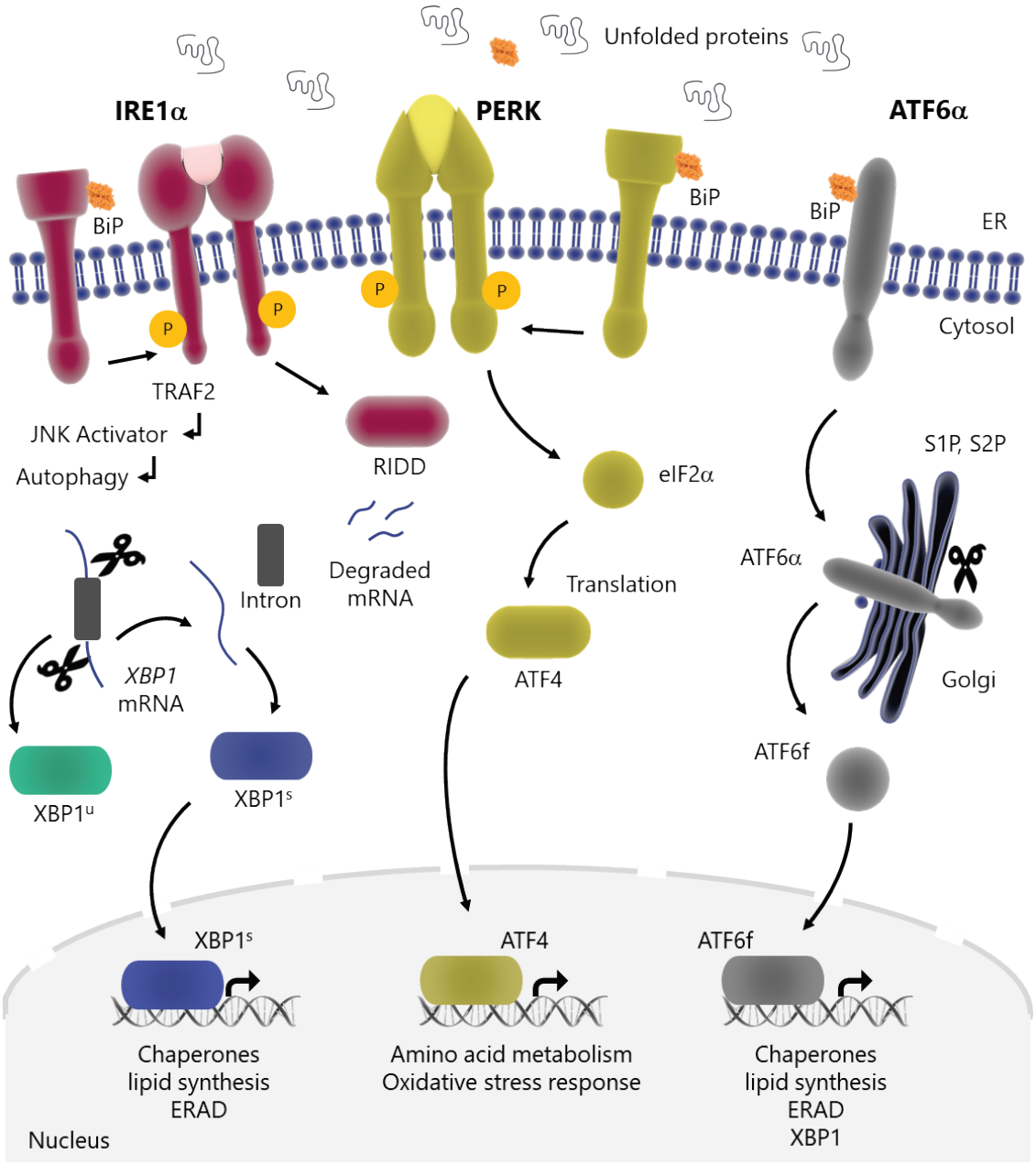

Figure 1: Signaling through the UPR

Accumulation of misfolded proteins in the ER leads to the activation of the transducers IRE1α, PERK and ATF6. The three UPR branches are highly interconnected and allow for the preservation of ER homeostasis. While IRE1α and ATF6 induce the expression of chaperones as well as proteins involved in lipid synthesis and ERAD, PERK attenuates global translation via eIF2α and makes an impact on amino acid metabolism, oxidative stress response and apoptosis. Figure modified after Ribeiro and Lubamba, 2017.

1.2.1. **PERK**

PERK is a transmembrane kinase that is present in higher eukaryotes including insects, worms and mammals (Fig. 1, middle). The ER luminal part shows high

similarity to IRE1 and is important for the activation of the pathway (Janssens et al., 2014; Schröder and Kaufman, 2005). Under unstressed conditions, BiP, a molecular HSP70 chaperone, is bound to PERK inhibiting its activation. Upon stress induction, BiP preferentially binds to misfolded proteins in the ER lumen. The depletion of PERK-bound BiP leads to the activation of the cytoplasmic kinase domain, autophosphorylation and oligomerization of PERK. In addition, un-or misfolded proteins can also directly bind to and activate PERK (Carrara et al., 2015; Gething, 1999; Wang et al., 2018, 2016). Once activated, PERK phosphorylates several substrates such as the ubiquitous eukaryotic initiation factor 2 (eIF2α) and the bZIP Cap 'n' Collar transcription factor Nrf2, which procures an antioxidant response (Cullinan et al., 2003; Venugopal and Jaiswal, 1998). Phosphorylation of eIF2α globally inhibits mRNA translation in order to facilitate recovery from ER stress and to prevent additional stress induction. By contrast, phosphorylation of eIF2α leads to an increased abundance of ATF4 by overcoming the 5' upstream open reading frame (uORF)-dependent inhibition of ATF4 ORF translation under stressed conditions (Harding et al., 2000; Hinnebusch, 1997; Scheuner et al., 2001). ATF4 is a bZIP transcription factor that coordinates the transcriptional program of amino acid metabolism and resistance to oxidative stress. ATF4 regulates genes such as growth arrest DNA damage gene 34 (GADD34) and C/EBP-homologous protein (CHOP). GADD34 is a negative feedback regulator that dephosphorylates eIF2α, whereas CHOP induces apoptosis under chronic stress conditions (Harding et al., 2009, 2000; Ma et al., 2002; Marciniak et al., 2004; Tsaytler et al., 2011).

Overall, the PERK branch is strongly protective under modest levels of ER stress but can also induce signaling to cell death. Cells lacking PERK are sensitive to ER stress even though the other two branches, IRE1 and ATF6, are fully functional (Harding et al., 2000). This implies that all three signaling pathways are interconnected and codependent.

1.2.2. **ATF6**

ATF6 is a type II transmembrane protein present in mammals, plants and *C. elegans* (Liu et al., 2007; Nagashima et al., 2011; Shen et al., 2001) (Fig. 1, right). Two homologous proteins, ATF6α and ATF6β coexist in mammals. Both

proteins show similar properties and deletion leads to embryonic lethality. However, ATF6β seems to occupy a minor role in UPR regulation (Adachi et al., 2008; Haze et al., 1999; Lee et al., 2003; Thuerauf et al., 2007). The ER luminal domain of both proteins contains a Golgi-localization sequence that is masked by BiP under unstressed conditions (Shen et al., 2002). Depletion of ATF6-associated BiP during ER stress leads to a translocation of ATF6 to the Golgi via COPII vesicles where it is sequentially cleaved by site 1 and site 2 proteases (S1P and S2P) (Chen et al., 2002). This proteolytic processing is reminiscent of the well characterized SREBP transcription factor activation (Ye et al., 2000). Afterwards, the amino-terminal cytosolic domain, ATF6f, which contains a bZIP domain, is released and upregulates the expression of several UPR target genes such as BiP, components of the ERAD pathway (e.g. EDEM1) as well as components involved in lipid synthesis. To this end, ATF6f specifically recognizes ER stress response elements (ERSEs) (Roy and Lee, 1999; Yan Wang et al., 2000; Yoshida et al., 1998, 2000) (Tab. 1).

Table 1: Overview of cis-regulatory elements in mammals and *S. cerevisiae*

The promoters of *bona fide* UPR target genes contain cis-regulatory elements which substantially differ between *S. cerevisiae* and higher eukaryotes.

Organism	Motif	Sequence
Mammals	UPRE	TGACGTGG/A
	ERSE I	CCAAT-N9-CCACG
	ERSE II	ATTGG-N-CCACG
S. cerevisiae	UPRE I	GGACAGCGTGTCG
	UPRE II	CTACGTGTCT

Interestingly, ATF6f also regulates the expression of the HSP40 family protein, protein kinase inhibitor p58 ($p58^{IPK}$). $p58^{IPK}$ has been shown to be an important component of a negative feedback loop inhibiting PERK activity (van Huizen et al., 2003). Another essential target gene of ATF6f is *X-box binding protein 1* (XBP1), the transcription factor controlling the IRE1 pathway. XBP1 is not only a target of ATF6f but also an interaction partner. Heterodimer formation leads to a

modulated stress response (Shoulders et al., 2013; Yamamoto et al., 2007). Once more, this highlights further branching of the three UPR signaling pathways.

1.2.3. **IRE1**

The IRE1 branch of UPR signaling is most conserved and best studied (Fig. 1, left). So far, it is the only UPR pathway that has been demonstrated to regulate ER stress response in fungi (Wang et al., 1998; Welihinda and Kaufman, 1996). In mammals, the IRE1 pathway regulates, among others, the expression of ERAD components, lipid biosynthetic enzymes as well as chaperones (Acosta-Alvear et al., 2007; Lee et al., 2003). Two isoforms, IRE1α and IRE1β could be discovered so far. Deletion of the ubiquitously expressed IRE1α provokes embryonic lethality in mice while deletion of IRE1β, which is only expressed in epithelial cells lining the gut and lungs, provokes susceptibility towards dextran sodium sulfate induced colitis (Bertolotti et al., 2001; Tirasophon et al., 1998; Wang et al., 1998). IRE1α is a bifunctional type I transmembrane protein. The ER luminal part contains a dimerization domain and senses ER stress, whereas the cytoplasmic fraction consists of a serine-threonine kinase and a unique endoribonuclease (RNase) domain (Liu et al., 2002; Shamu and Walter, 1996; Welihinda and Kaufman, 1996). Under unstressed conditions BiP keeps IRE1α in a monomeric, inactive form. Upon stress induction, BiP dissociates resulting in IRE1α self-association, trans-autophosphorylation via the kinase domain and conformational changes. This cascade leads to the activation of the endogenous RNase domain (Bertolotti et al., 2000; Calfon et al., 2002; Shen et al., 2001; Yoshida et al., 2001). How exactly activation occurs is still a matter of ongoing research. What is presumed so far, is that the phosphate transfer plays a subsidiary role in that process. Analogous to PERK, misfolded proteins can also directly bind to IRE1α and initiate the stress response pathway in a BiP independent manner (Gardner and Walter, 2011). Once the RNase domain is functional, the IRE1α mRNA substrate *XBP1* is unconventionally spliced in the cytoplasm. For that, two distinct stem loop structures in the pre-mRNA are prerequisite. Overall, splicing makes for a removal of the 26 bp intron and for a shift of the *XBP1* ORF. The mature *XBP1* mRNA is translated into the active bZIP transcription factor XBP1^{s}, whereas expression of the pre-mRNA results in the synthesis of the bZIP domain

containing protein XBP1^{u} (more in chapter 1.2.4) (Cox and Walter, 1996; Yoshida et al., 2001). Deletion of *XBP1* results in embryonic lethality, cardiomyopathy and liver hypoplasia (Masaki et al., 1999; Reimold et al., 2000).

Furthermore, IRE1α also shows a more promiscuous endonuclease activity by a direct endonucleolytic cleavage of multiple ER-localized mRNAs thereby lowering protein influx and ER protein load. This mechanism is called IRE1-dependent decay of mRNA (RIDD) and was initially described in *Drosophila melanogaster*. What exactly makes a subset of mRNAs to RIDD targets is not entirely resolved so far. Most likely multiple factors like the sequence and secondary structure of the mRNA as well as the oligomeric state of IRE1α play an important role (Hollien and Weissman, 2006; Maurel et al., 2014; Moore and Hollien, 2015; Tam et al., 2014).
Besides functioning as endonuclease, IRE1α also regulates autophagy levels under ER stress conditions by directly interacting with tumour-necrosis factor-receptor-associated factor 2 (TRAF2). This promotes activation of JUN N-terminal kinase (JNK) and consequently initiates autophagy (Castillo et al., 2011). All in all, the three UPR branches are not only internally linked but also linked to other cellular effectors (Castillo et al., 2011).

1.2.4. **XBP1^{s} & XBP1^{u}**

Under unstressed conditions IRE1α is inactive. Therefore, the *XBP1* pre-mRNA is directly translated into the highly unstable protein XBP1^{u} which is degraded by the 26S proteasome (Navon et al., 2010). Upon stress induction, IRE1α gets activated. This leads to unconventional cytoplasmic splicing of the *XBP1* pre-mRNA which is afterwards translated into XBP1^{s} (Yoshida et al., 2001). The latter is a bZIP transcription factor and a major regulator of the IRE1α signaling pathway. It regulates a plethora of target genes that vary between tissues and stress stimuli. Thereto, XBP1^{s} binds to the cis-regulatory UPR elements (UPRE), ERSE I & II where only binding to ERSE I additionally requires the nuclear transcription factor Y (NF-Y) (Tab. 1). This induces the expression of ERAD components (e.g. EDEM1), ER-localized chaperones such as ERDJ4 (DNAJ4 protein), p58^{IPK}, RAMP4 (ribosomal associated membrane protein 4), PDI-P5 (protein disulfate isomerase P5) and components involved in lipid biosynthesis

and ER biogenesis (Lee et al., 2008, 2003; Sriburi et al., 2004; Yamamoto et al., 2004). Further modulation of the transcriptional response is achieved by the heterodimerization of XBP1^{s} with several transcription factors (Hetz, 2012; Lee et al., 2003). Beyond that XBP1^{s} has been implied to be involved in endothelial cell (EC) proliferation, autophagy response as well as apoptosis (Margariti et al., 2013; Zeng et al., 2013, 2009).

From a structural point of view XBP1^{s} and XBP1^{u} show close resemblance. The N-termini are identical containing a NLS and a bZIP domain whereas the C-termini are specific for both proteins (Fig. 2b). Nevertheless, both proteins hold distinct functions. So far, for XBP1^{u}, neither transcriptional activity has been observed, as it lacks a transactivation domain, nor has it been observed to act as a transcriptional repressor in a homodimeric state (Calfon et al., 2002). However, the last five years of research revealed XBP1^{u} to be involved in fundamental biological processes (Fig. 2a). XBP1^{u} suppresses autophagy through interaction with and following degradation of forkhead box protein O1 (FoxO1) (Zhao et al., 2013). Moreover, the formation of a protein complex with HDAC3 (Histone deacetylase 3), mTOR (serine/protein kinase mTOR) and ACT1 (Rac-α serine/threonine protein kinase) promotes survival of EC under oxidative stress conditions (Martin et al., 2014). Additionally, a XBP1^{u} function in regulating the suppressor p53/p21 axis, which controls cell cycle progression through interaction and stabilization of MDM2 (mouse double minute homolog 2), was identified. XBP1^{u} suppression induces cell cycle arrest in G0-G1, thus repressing cell proliferation (Huang et al., 2017). Furthermore, XBP1^{u} negatively influences the ER stress response (e.g. after prolonged ER stress) by forming a heterodimer with XBP1^{s} and most probably with ATF6f (Newman and Keating, 2003), sequestering the transcription factors from the nucleus and targeting the complexes for proteasomal degradation (Yoshida et al., 2009, 2006). XBP1^{u} contains, besides an NLS and a bZIP domain, a nuclear export signal (NES), a signal for proteasome-mediated degradation, a hydrophobic membrane interacting stretch (HR2) and a translational pausing region (TP) at the C-terminus (Fig. 2b). The function of the last two domains is controversial. One model proposes that XBP1^{u} regulates the efficiency of its own transcript splicing by recruiting the ribosome-nascent chain complex (RNC) during translation to the ER membrane while the RNC complex is stalled at the translational pausing

region. This would place the *XBP1* pre-mRNA in close proximity to IRE1α for efficient splicing and represent an elegant way of coupling co-translational protein targeting to mRNA maturation. In that case, XBP1^{u} acts as a membrane associated protein (Kanda et al., 2016; Yanagitani et al., 2009, 2011). In contrast, the second model suggests that XBP1^{u} is a type II transmembrane protein (via the hydrophobic stretch) and the substrate of a signal peptide peptidase (SPP). This SPP forms a complex with an ERAD protein Derlin1 and the E3 ubiquitin ligase TRC8 which leads to cleavage and degradation of XBP1^{u} (C. Chen et al., 2014).

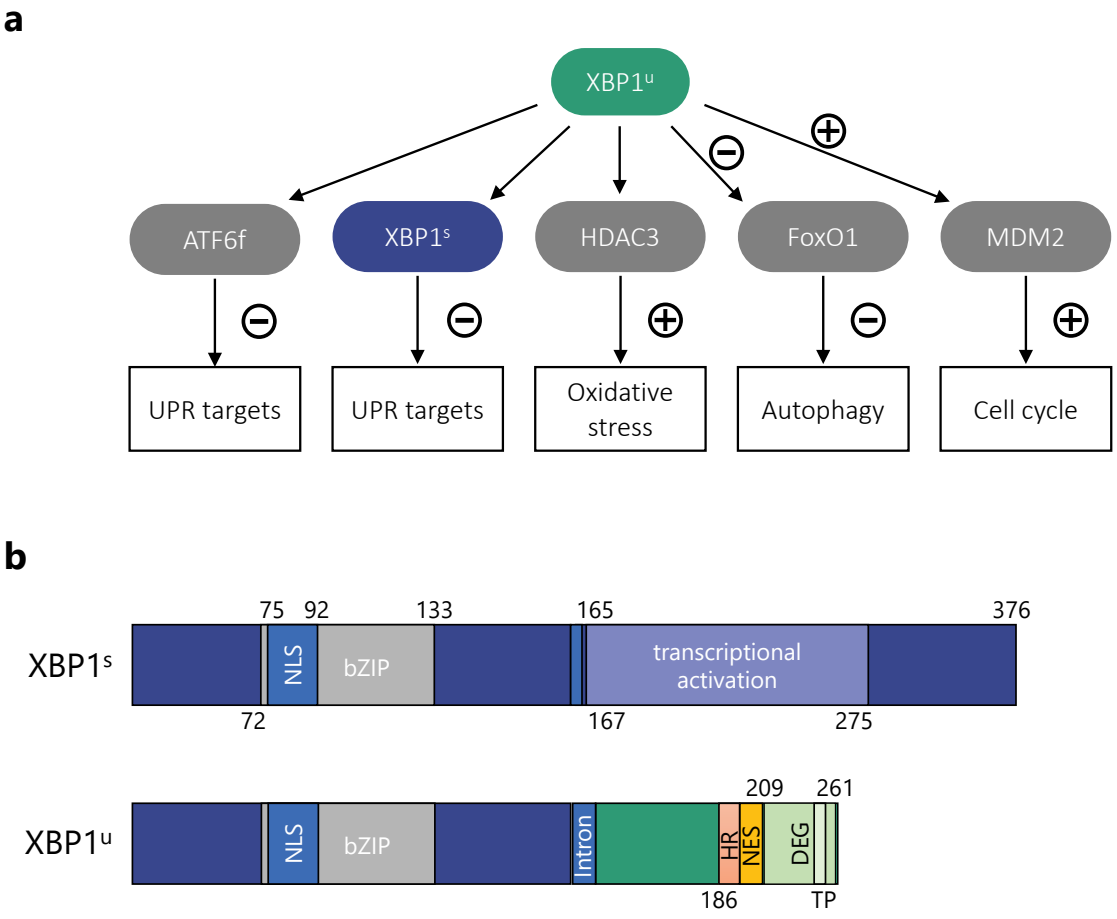

Figure 2: XBP1^{u} assumes auxiliary roles besides regulating the UPR

(a) Upon stress induction the bZIP transcription factors ATF6f and XBP1^{s} induce the expression of a plethora of UPR target genes. In order to modulate the stress response, XBP1^{u} negatively influences the UPR target gene expression by physically interacting with XBP1^{s} and ATF6f. In addition, XBP1^{u} has an impact on autophagy and the cell cycle through the interaction with FoxO1 and MDM2, respectively. (b) Scheme of XBP1^{u} with its domains.

Overall, the role of XBP1^{u} remains poorly characterized. The increasing number of recent studies strongly indicate that XBP1^{u} assumes a more important function in the UPR regulation and beyond that in the regulation of further cellular processes than has been expected so far.

1.3. The UPR is an important signaling pathway for fungal development and adaptation to the environment

The fungal kingdom with its more than 1.5 million estimated species, shows a high degree of diversification. In the process of their adaptation to e.g. different ecological niches they developed different lifestyles. Comparable to other organisms, fungi are able to quickly and adequately react to changes in their environment (Hawksworth, 2001). Saprophytic fungi, for example, depend on the secretion of large quantities of extracellular enzymes in order to make nutrients from dead organic material available. Plant pathogenic fungi, on the other hand, are dependent on secreted effector molecules that counteract host defense mechanisms. In doing so UPR plays a decisive role. Moreover, fungi necessitate the UPR for stress resistance, infection-associated development, virulence as well as for vegetative growth (Cheon et al., 2011; Heimel, 2015; Joubert et al., 2011; Richie et al., 2009). Contrary to higher eukaryotes, only little is known about the role of UPR during fungal development. In mammals three distinct pathways addressing the UPR have been discovered and characterized. However, in fungi IRE1 is the only sensor of ER stress, jointly regulating UPR with other proteins (Cox et al., 1993; Hollien, 2013; Mori et al., 1993). The multitude of stress responses function similarly in fungi and higher eukaryotes through conserved interactions of the UPR with other intracellular signaling pathways (Guo and Polymenis, 2006; Heimel et al., 2013; Jung et al., 2016).

1.3.1. UPR in *Saccharomyces cerevisiae*

The IRE1 branch is the most conserved UPR signaling pathway and present from fungi to higher eukaryotes. Ire1p was initially found in a screen to play an essential role in inositol auxotrophy (Nikawa and Yamashita, 1992). Later it could

be shown that Ire1p is crucial for the regulation of UPR as it is the sole sensor of ER stress (Cox et al., 1993; Hollien, 2013; Mori et al., 1993). Neither the ATF6 nor the PERK branch could be identified to date, even though the latter is closely related to the Gcn4 (homologue of ATF4) system which regulates the amino acid control network and influences the UPR (Harding et al., 2003; Herzog et al., 2013; Patil et al., 2004). Since the IRE1 pathway closely resembles the one described for mammals in chapter 1.2.3., at this point only the differences will be highlighted. Briefly, the presence of misfolded proteins in the ER lumen initiates Ire1p oligomerization, trans-autophosphorylation as well as activation of the endonuclease (RNase) domain. This, in turn, promotes removal of the intron of the *HAC1* pre-mRNA which is the homologue of *XBP1* (Cox and Walter, 1996; Mori et al., 1996; Sidrauski et al., 1996). The unconventional splicing in the cytoplasm consists of two site-specific cleavages and linkage of the exons mediated by the tRNA ligase Rlg1p/Trl1p (Sidrauski et al., 1996). Neither the spliceosome nor the intranuclear splicing machinery are required by which the process more closely resembles tRNA rather than mRNA splicing (Gonzalez et al., 1999). The spliced *HAC1* mRNA is then translated into the bZIP transcription factor Hac1^{s}p which translocates to the nucleus and binds as a homodimer to cis-acting UPR elements (UPRE I & II) in the promoter regions of UPR target genes (Fordyce et al., 2012; Kohno et al., 1993; Mori et al., 1992) (Tab. 1). Among these, genes coding for ER-resident chaperones that increase the protein folding capacity (e.g. *BIP*, *PDI1*, *FKB2*), genes involved in the secretory and ERAD pathway, and genes regulating fatty acid and cell wall synthesis, can be found (Heimel, 2015; Mori et al., 1998; Travers et al., 2000). All in all, the expression of Hac1^{s}p is regulated on a post-transcriptional level like XBP1^{s} although remarkable differences arise concerning the expression of *HAC1* pre-mRNA. In budding yeast, the translation of *HAC1* pre-mRNA is blocked due to the formation of a stem-loop structure formed between the 5'UTR and the intron which impedes translation initiation (Di Santo et al., 2016; Ruegsegger et al., 2001). This stem-loop structure increases the splicing efficiency by targeting the pre-mRNA to Ire1p for splicing which is in good accordance with the observation of ER-associated *HAC1* pre-mRNA (Aragón et al., 2009; Diehn et al., 2000). Hence, removal of the intron is necessary and sufficient for the regulation of Hac1p expression (Chapman and Walter, 1997). Interestingly, an additional regulatory level

preventing accumulation of Hac1^{u} has been detected by Di Santo and colleagues in 2016. Besides preventing inappropriate translation, in case of the inhibitory secondary structure being bypassed, Hac1^{u}p contains a degradation domain (instead of the transactivation domain present in Hac1^{s}p) leading to accelerated protein degradation. With this fail-safe mechanism it is accomplished that the *HAC1* pre-mRNA is completely repressed (Chapman and Walter, 1997; Di Santo et al., 2016; Kawahara et al., 1997).

Although the IRE1 pathway is conserved among fungi, marked differences exist on several levels one of which is the size of the intron that in general ranges from non-existent in certain *Candida* related species, over 20-23 bp in ascomycetes, 56-65 bp in basidiomycetes right up to 252 bp in *S. cerevisiae*. Concomitantly, the strategy for silencing the expression of unspliced *HAC1* mRNA differs (Cox and Walter, 1996; Heimel, 2015; Heimel et al., 2013; Mori et al., 1996; Saloheimo et al., 2003). The same holds true for the importance of RIDD among fungal species. The fission yeast, *Schizosaccaromyces pombe*, for example lacks a Hac1p homologue and copes with ER stress primarily via RIDD, which, in turn, plays a minor role in *S. cerevisiae* (Kimmig et al., 2012; Tam et al., 2014). However, the role of RIDD in filamentous fungi remains unexplored. Future research will show to what extent an interaction with the main IRE1 branch exists and how this will affect adaptation of the stress response to the respective fungal needs.

1.3.2. **UPR in *Cryptococcus neoformans***

Cryptococcus neoformans is ubiquitous in different environmental niches and a human pathogenic fungus that belongs to the basidiomycetes. It causes severe pulmonary infections and fatal meningoencephalitis mostly in immune-compromised populations. During the process of host infection, *C. neoformans* encounters several other stress sources besides ER stress such as oxidative and thermal stress as well as high levels of CO_2. In order to cope with that the UPR is required. UPR in *C. neoformans* is regulated by Ire1 which is conserved and shares all functional domains with Ire1p from *S. cerevisiae* and higher eukaryotes. *IRE1* deletion leads to increased thermo-sensitivity, ER stress-sensitivity and sensitivity towards cell wall damaging agents. Additionally, knock-

out (KO) mutants are avirulent since the antiphagocytic capsule which enables the fungus to escape from the host immune system is defective. This demonstrates that UPR is not only important for the ER stress response but also indispensable for virulence. For a long time, the counterpart of *HAC1*/*XBP1* remained undiscovered. In 2011, Cheon and co-workers identified an orthologue *HXL1* (Hac1 and XBP1-like gene 1) that encodes a bZIP transcription factor. Although *HXL1* shows no sequence homology to *HAC1/XBP1* outside of the moderately conserved bZIP domain, they share the unconventional splicing under ER stress conditions. Upon ER stress Ire1p facilitates the removal of the 56 bp intron which gives rise to the potent transcription factor Hxl1. Interestingly, the post-transcriptional regulation is not only mediated by the intron but also by Puf4 (member of the pumilio-FBF family of mRNA binding proteins) affecting splicing efficiency and decay of the *HXL1* mRNA (Glazier et al., 2015).
Overall, *C. neoformans* is a perfect example for the UPR being more than just a regulator of stress response. The UPR is crucial for antiphagocytic capsule formation, thermo-tolerance, azole drug resistance, maintenance of cell wall integrity as well as for sexual mating and unisexual differentiation, hence, for virulence. This opens up new possibilities for the research of novel antifungal therapeutic targets (Cheon et al., 2014, 2011; Jung et al., 2016).

1.3.3. **UPR in *Ustilago maydis***

Ustilago maydis is a facultative biotrophic basidiomycetous fungus that exclusively infects *Zea mays* and its progenitor Teosinte (*Zea mays subsp. parviglumis*) (Doebley, 1992). In 2013, Heimel and co-workers identified the regulators of the UPR Ire1 (homolog of Ire1p in baker's yeast and IRE1α in mammals) and Cib1 (Clp1 interacting bZIP 1; homolog of Hac1/XBP1) in the smut fungus (Heimel et al., 2013). *cib1* has been previously demonstrated to code for a bZIP transcription factor and the splice sites at the intron/exon borders correspond to the consensus splice sites of *HAC1* (Heimel et al., 2010, 2013). Besides the IRE1 signaling pathway no other ER stress regulating pathway could be identified. Under unstressed conditions deletion of either *ire1* or *cib1* has no influence on vegetative growth, whereas under ER stress inducing conditions growth is heavily impaired. Upon accumulation of unfolded proteins Ire1 gets

activated and unconventionally splices the *cib1* pre-mRNA (*cib1*^{u}). The mature *cib1* mRNA (*cib1*^{s}) is then translated into Cib1^{s} which induces the expression of UPR target genes encoding proteins such as chaperones or protein disulfide isomerase. So far there are no indications for the 65 bp intron attenuating translation of *cib1*^{u} mRNA. On the contrary, Cib1^{u} seems to have a rather important function in the regulation of the UPR by counteracting UPR hyperactivation similar to XBP1^{u} (Heimel et al., 2013). As a result, this makes *U. maydis* the first fungus in which the protein resulting from the pre-mRNA exerts a regulatory function in the stress response pathway (Fig. 3).

The UPR, apart from being a coordinator of cellular homeostasis, is also indispensable for pathogenic development. The life cycle of *U. maydis* can be split into a saprophytic and a biotrophic phase. The biotrophic stage is initiated on the surface of a plant leaf by the fusion of two haploid, budding yeast-like sporidia, that differ in their mating types (Bölker et al., 1992; Schulz et al., 1990). Afterwards a dikaryotic infectious filament, arrested in the G2 cell cycle phase, is formed. This morphogenetic transition to the filamentous pathogenic form is mediated by the heterodimeric homeodomain transcription factor bEast/bWest (bE/bW) which also controls, in cooperation with other proteins, the maintenance of the cell cycle arrest and plant penetration (Bölker et al., 1995; Brachmann et al., 2001; Gillissen et al., 1992; Heimel et al., 2010; Kämper et al., 1995; Snetselaar, 1993; Snetselaar and Mims, 1992; Wahl et al., 2010). All these processes are independent of a functional UPR. Activation of the UPR is specifically induced after successful plant penetration, which is enabled through the activity of secreted lytic enzymes (Heimel et al., 2013; Schirawski et al., 2005). At this point, an active UPR is essential to allow for increased production and secretion of effectors (476 secreted proteins encoded). Those effectors are necessary for *U. maydis* to successfully evade the plant immune system (Lanver et al., 2018; Lo Presti et al., 2016, 2015; Schuster et al., 2018). Cib1^{s} has been shown, for example, to regulate the expression of two effectors, Pit2 and Tin1-1 (Hampel et al., 2016). However, a premature UPR activation negatively affects fungal virulence by the suppression of bE/bW expression (Heimel et al., 2013). After plant penetration the G2 cell cycle arrest needs to be resolved. Therefore, the protein clampless 1 (Clp1) represses the bE/bW signaling pathway resulting in massive proliferation of the dikaryotic hyphae which leads to the formation of

tumor-like galls following hyphal fragmentation and spore formation (Banuett and Herskowitz, 1996; Heimel et al., 2010). Interestingly, Heimel and co-workers were able to demonstrate physical interaction between Clp1 and Cib1 by which Cib1 stabilizes Clp1 (Heimel et al., 2013). Overall, the UPR in the phytopathogen is not only a regulator for the stress response, but it is also an important determinant for the pathogenic lifestyle.

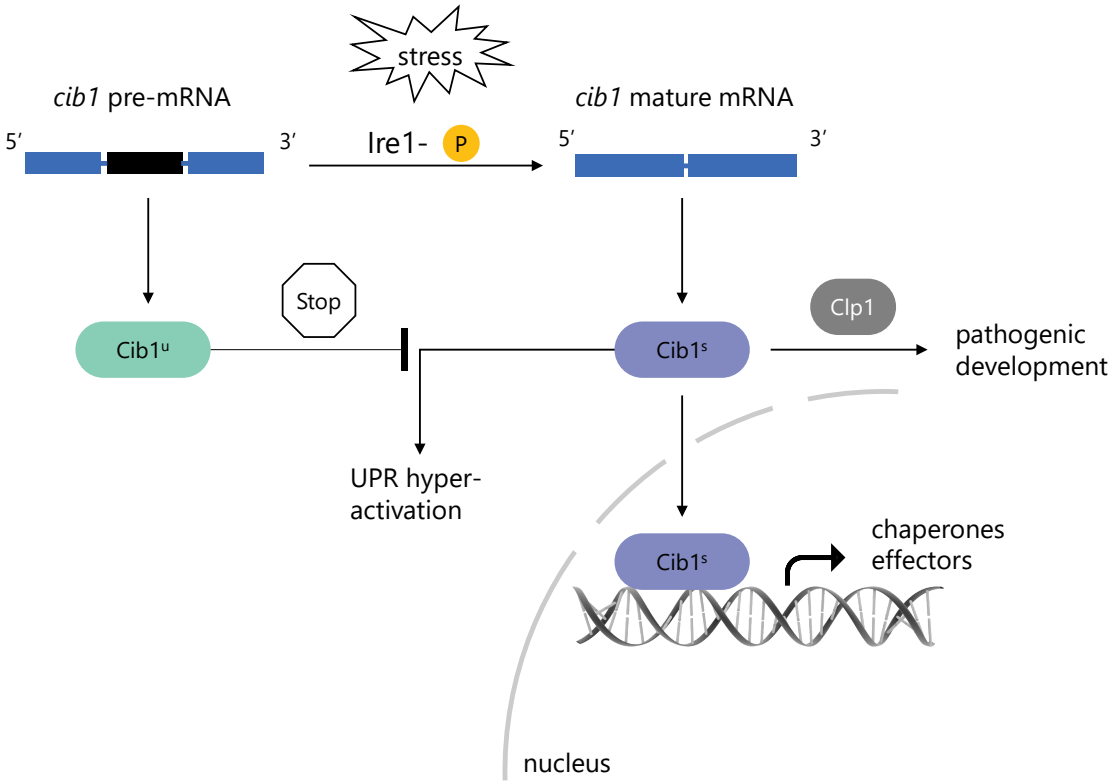

Figure 3: The IRE1 branch is the sole signaling pathway regulating UPR in *Ustilago maydis*

Upon induction of ER stress IRE1 gets activated and leads to an unconventional cytoplasmic splicing event of the *cib1* pre-mRNA. The mature *cib1* mRNA is then translated into the bZIP transcription factor Cib1^{s}, which induces the expression of UPR targets such as chaperones or effectors important for pathogenic development. Cib1^{s} further affects pathogenic development through the interplay with Clp1. Under unstressed conditions the *cib1* pre-mRNA remains unspliced giving rise to Cib1^{u}, which prevents UPR hyperactivation by counteracting Cib1^{s}.

1.4. RPE1 cells and *U. maydis* are ideal model systems to study UPR

UPR in higher eukaryotes is regulated via three highly interconnected pathways. This makes the mechanistic analysis difficult, as modifications to a component of one pathway might influence the other two branches. Moreover, UPR varies considerably depending on the cell type. As a result, certain cell types are more suitable to certain research questions. For example, in immortalized retinal pigmented epithelial cells (RPE1) UPR can be induced by the accumulation of unfolded proteins and all three UPR branches are present. RPE1 cells roughly double every 24 hours and are comparably large in size which makes them ideal for cell biological analyses. They can be easily grown in culture and are capable of extended proliferation. More importantly, the adherent human RPE1 cell line is near-diploid containing 46 chromosomes and can easily be genetically modified (Rambhatla et al., 2002). Thus, RPE1 cells are an attractive model system for studying the UPR on a more mechanistic level.

When analyzing the regulatory machinery of the IRE1 UPR branch, fungi represent a good alternative to higher eukaryotes. The filamentous fungus *U. maydis* is particularly well suited for that. The whole UPR is driven by the IRE1 pathway and is highly conserved with the mammalian IRE1 branch which is unique within the fungal kingdom (Heimel, 2015; Heimel et al., 2013). *U. maydis* combines the advantages of a unicellular organism whilst sharing important cellular processes with mammals (Steinberg and Perez-Martin, 2008). Furthermore, the whole genome sequence of the fungus, which can easily be genetically modified, is available (Brachmann et al., 2004; Kämper et al., 2006). All in all, the combination of RPE1 cells and *U. maydis* allows for an in-depth analysis of the IRE1 pathway. Knowledge obtained from the fungus can directly be transferred to RPE1 cells in which it can be analyzed jointly with the other ER stress response pathways.

1.5. The UPR is relevant for a wide range of applications

The UPR with its signaling pathways is an important mechanism, that copes with ER stress and adapts the cell to changing environments and metabolic conditions. Albeit conserved, there are substantial differences in the signaling network of the UPR depending on the organism or cell type. The down side of adopting to such a crucial pathway is that dysfunction may have severe consequences. Additionally, either rogue cells or pathogens may exploit UPR to ensure their survival. On the other hand, this also allows researchers to develop a better understanding and take advantage of it for biotechnological purposes.

1.5.1. **Medical relevance**

The importance of the UPR is reflected by the fact that dysregulation is often associated with diseases. Among these diseases are metabolic diseases, neurodegenerative disorders, inflammation, and cancer, which seem disparate at first, but all share one commonality: a misregulated UPR factor (Ma and Hendershot, 2004; Wang and Kaufman, 2014, 2012). Considering the complex regulatory network a misregulation of one factor can easily occur. XBP1, for example, has been demonstrated to promote tumorigenicity and progression in triple negative breast cancer, a highly aggressive malignancy with limited options for treatment (X. Chen et al., 2014). On the other hand, in some cases UPR has been shown to increase chemosensitivity of tumors thus protecting the host (Ma and Hendershot, 2004). Although there has been considerable progress, there is still a lack in identifying all intra- and inter-connecting links of the three pathways, which will ultimately lead to better treatment opportunities for the aforementioned diseases.

1.5.2. **Biotechnological relevance**

Over the last 50 years, filamentous fungi have been established as a platform for biotechnological products, such as primary and secondary metabolites and proteins. One of the key factors in optimizing the secretion is the UPR and its regulation of ER folding capacity. However, these optimization efforts are still mostly tailored to specific proteins and therefore not universally usable for a wider

range of proteins. Hence, increasing the understanding of wanted and unwanted UPR effects is high on the agenda of researchers (Heimel, 2015). One application of UPR control in white biotechnology is the production of itaconic acid (IA). Due to its chemical characteristics, IA is used as a compound for the production of polymers, coatings, chemical compounds and biofuels (Hermann and Patel, 2007). The energy department of the United States of America rated IA as one of the twelve most important bio-based chemical building blocks with an annual production volume of 80,000 tons (Lee et al., 2011; Okabe et al., 2009). Relatively low production rates as well as a rather high market price, justify an increased research interest.

1.6. Aim of the thesis

The stress response in *U. maydis* is regulated exclusively by the IRE1 pathway. Herein, the translation of *cib1* pre-mRNA leads to the protein Cib1^{u} which seems to assume quite a vital role in the regulation of ER stress. In addition to preventing UPR hyperactivation, preliminary experiments point to a partial regulation of the stress response by Cib1^{u}, independent of Cib1^{s}. However, so far the molecular details and mechanism how Cib1^{u} affects the ER stress response have not been investigated, yet. Apparently, the pathway is highly conserved with the one in mammals. While it is known that XBP1 is fully functional in *U. maydis*, a comprehensive understanding of the regulatory role of XBP1^{u} in higher eukaryotes is still missing as well. The number of recent studies reporting new functions of XBP1^{u} suggests that besides its function as a counterpart of XBP1^{s}, it is also involved in several cellular processes such as autophagy and cell cycle progression. Against this background, the aim of this thesis is to shed light on further roles of XBP1^{u} in the stress regulation of RPE1 cells and to what extent this has an impact on the other pathways. Furthermore, a potential conservation with *U. maydis* should be analyzed. The analysis of the UPR in this dual system of fungus and higher eukaryotes allows for the parallel characterization of Cib1^{u} and XBP1^{u}. Hence, this thesis combines the best of two worlds, the simplicity of *U. maydis* and the universality of the more complex system in mammals.

2. Results

2.1. Generation of homozygous *XBP1* knock-out and rescue cell lines

The UPR in metazoa is regulated via three interconnected signaling pathways. This makes it challenging to define each pathway's contribution to the regulation of the ER stress response. Only the IRE1 branch is conserved between fungi and mammals which might reflect its superordinate role (Hollien, 2013). Besides IRE1, XBP1^{s} and XBP1^{u} exert important regulatory functions. Both proteins are encoded by a single gene and their expression is regulated on a post-transcriptional level (Yoshida et al., 2006). This further complicates the analysis of the individual contributions of XBP1^{s} and XBP1^{u} to the UPR and their regulatory function within the UPR.

2.1.1. *XBP1* was successfully deleted in RPE1 cells

In order to analyze the role of XBP1 related to the UPR and the extent to which this has an impact on RPE1 cells (WT) under different conditions, an *XBP1* KO cell line was generated via CRISPR/Cas9 mediated genome editing. Therefore, two guide RNAs (gRNA1 and gRNA3), within which the nuclease Cas9 induces double-strand breaks that are repaired through non-homologous end joining, were designed according to Bauer et al., 2015 and Ran et al., 2013. The *XBP1* gene is located on chromosome 22 and contains five exons. gRNA1 recognizes a region directly upstream of the *XBP1* start codon, whereas gRNA3 is complementary to a region within exon 5 (Fig. 4a). In this way, an almost complete deletion of the *XBP1* ORF was achieved. Since several additional downstream start codons are present in the *XBP1* ORF, a deletion of the entire ORF is of particular importance to prevent pervasive transcription and translation of shortened XBP1 related mutant proteins. Clones harboring a successful deletion of *XBP1* were identified via PCR (Fig. 4b) and further validated on transcript and protein level via qRT-PCR and Western blot analysis, respectively. This resulted in the identification of two independent RPE1 cell lines in which neither an XBP1 protein (Fig. 4c) nor an *XBP1* transcript (Fig. 5) was detectable.

The first KO cell line contains a full deletion of the *XBP1* ORF on one allele and an inversion on the second corresponding allele (KO_1), while the deletion of *XBP1* was confirmed to be homozygous in the other cell line (KO_2) (Fig. 4b). These two *XBP1* KO cell lines laid the foundations for all further analyses.

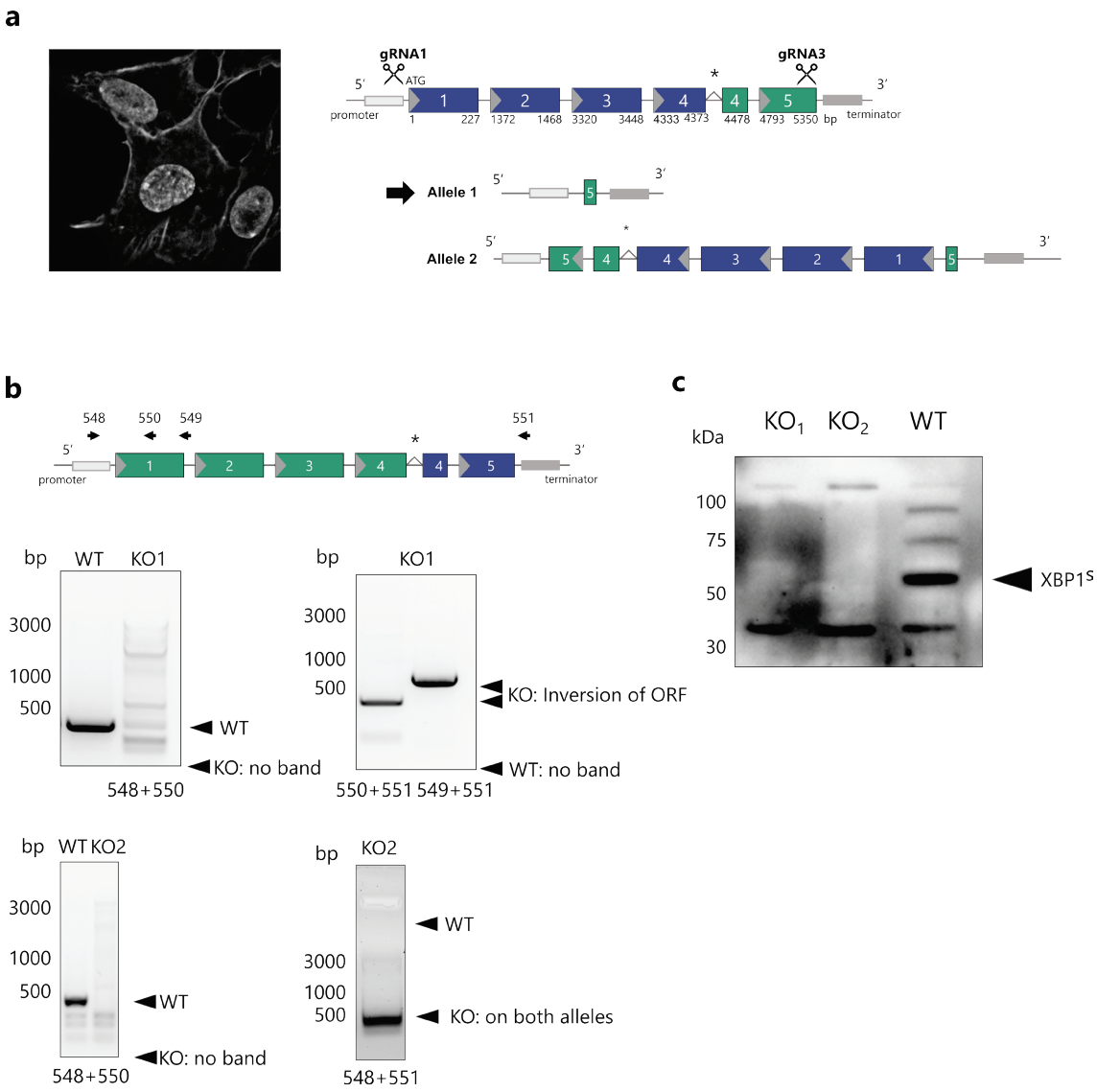

Figure 4: CRISPR/Cas9-generated *XBP1* KO cell lines were characterized on a DNA and a protein level

Characterization of CRISPR-generated *XBP1*$^{-/-}$ cell lines. (a) Schematic display of the intron-exon structure of *XBP1* and localization of gRNAs as well as genomic organization of the *XBP1* KO_1/KO_2 cell lines used. (b) PCR analysis from KO_1 and KO_2 cell lines using different primer combinations. (c) Western blot showing complete absence of XBP1 in KO_1 and KO_2.

2.1.2. *XBP1^{s}/XBP1^{u}* were reintroduced separately into the *XBP1$^{-/-}$* cell line

XBP1^{s} and *XBP1^{u}* are similar on a protein level where merely the C-terminus differs (Fig. 2b). Yet, on a functional level, it is quite the opposite. While the regulatory function of XBP1^{s} has been comprehensively investigated, the knowledge on XBP1^{u} is comparably scarce. In order to address this gap of knowledge, either *XBP1^{s}* or *XBP1^{u}* were reintroduced into the genome of the RPE1 KO$_1$ cell line via a lentiviral system (Fig. 5a). The lentiviral system used for the generation of the cell lines leads to random integration of *XBP1^{s}/XBP1^{u}* into the genome with different integration frequencies. Furthermore, the expression of *XBP1^{s}/XBP1^{u}* is driven by the constitutive *PGK* promoter. In contrast, the endogenous *XBP1* promoter is subject to an XBP1^{s}-mediated autoregulation to amplify XBP1 gene expression (Acosta-Alvear et al., 2007).

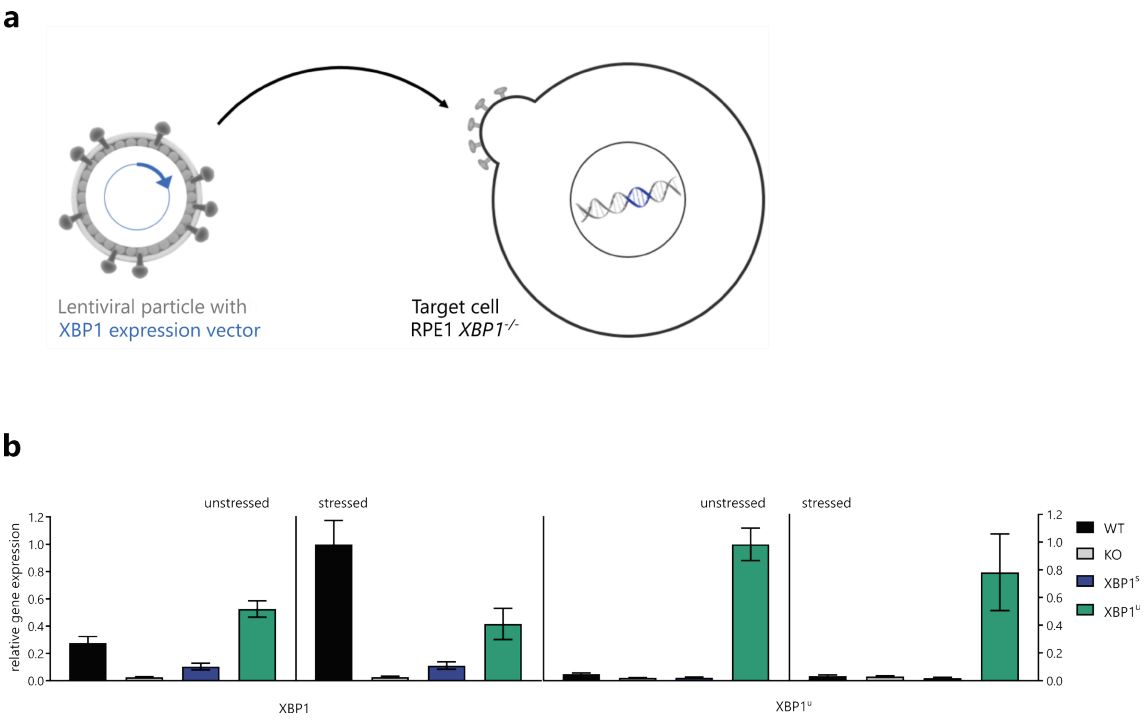

Figure 5: *XBP1* and *XBP1^{u}* are expressed in the respective rescue cell lines

Characterization of XBP1^{s}/XBP1^{u} rescue cell lines via qRT-PCR. (a) *XBP1^{s}* and *XBP1^{u}* were randomly integrated into the genome of the RPE1 *XBP1$^{-/-}$* cell line by using a lentiviral system. (b) Expression of *XBP1* and *XBP1^{u}* was analyzed in WT, KO and the generated rescue cell lines under unstressed and stressed (1 µg/mL TM for 4.5 h) conditions. *GAPDH* was used for normalization. Expression values are derived from one representative experiment with two technical replicates each. Error bars represent standard error of the mean (SEM).

As a consequence, expression levels between the cell lines are not necessarily comparable nor do they necessarily match the endogenous levels. In the following, the RPE1 *XBP1*$^{-/-}$ cell line expressing XBP1^{u} will be referred to as "XBP1^{u}" or "XBP1^{u} rescue cell line". Analogous naming will be used for the RPE1 *XBP1*$^{-/-}$ cell line expressing XBP1^{s}. Expression of XBP1^{u} was enabled by the introduction of an unspliceable version of XBP1^{u} in which the amino acid sequence was retained, but the splice sites as well as the secondary structure required for recognition and cleavage by IREα, were disrupted (Hampel, 2016; Peschek et al., 2015; Yoshida et al., 2001). Successful integration of *XBP1*^{s}*/XBP1*^{u} in the rescue cell lines was confirmed by qRT-PCR using specific oligonucleotides for either *XBP1,* which recognizes both *XBP1* isoforms, or *XBP1*^{u}*,* which recognizes only the unspliceable isoform (Fig. 5). Gene expression was analyzed under unstressed and stressed conditions. ER stress was induced by tunicamycin (TM), which inhibits N-linked glycosylation preventing protein folding and transit through the ER (Oslowski and Urano, 2011). Under both conditions, neither *XBP1* nor *XBP1*^{u} were expressed in KO_1 further confirming the validity of the cell line. The levels of *XBP1/XBP1*^{u} gene expression in the corresponding rescue cell lines were comparable in both treated and untreated cells. All in all, the generated rescue cell lines enable the independent dissection of the regulatory involvement of XBP1^{s} and XBP1^{u} in the IRE1 branch.

2.2. Physiological characterization of the *XBP1*$^{-/-}$ and XBP1^{s}/XBP1^{u} rescue cell lines

The UPR enables cells to adapt to highly diverse environments and conditions with specific requirements like starvation and differentiation processes (Schröder, 2008). All cells encounter different levels of ER stress, though they are minimal sometimes (Selye, 1975). Nevertheless, these low stress levels will be referred to as "unstressed" in the following.

2.2.1. **ER stress resistance and clonogenic survival are reduced in RPE1 *XBP1*$^{-/-}$ cells**

In mouse embryonic fibroblast (MEF) cells XBP1^{s} plays an essential role in the regulation of cellular survival and proliferation (Romero-Ramirez et al., 2004). To address whether XBP1^{u} is also involved, clonogenic survival was investigated in RPE1 WT, KO and XBP1^{s}/XBP1^{u} rescue cell lines under unstressed and stressed conditions. Therefore, the cells were plated in culture dishes as single-cell suspensions at low densities. Untreated cells were directly incubated until they had formed sufficiently large colonies (8-10 days), whereas stressed cells were treated with 0.5 µg/mL TM for 4.5 h before incubation (Fig. 6a). Under unstressed conditions an average 65 % of the WT and only 20 % of *XBP1* KO cells were able to grow into a colony (Fig. 6c, d), revealing a significantly reduced clonogenic survival in *XBP1* KO cells. Moreover, their size and density were markedly reduced compared to WT (Fig. 6b). This suggests that, already under unstressed conditions, XBP1 plays an important role with respect to cell proliferation. Surprisingly, in both XBP1^{s} and XBP1^{u} rescue cell lines the ability to form colonies was restored (Fig. 6c). XBP1^{u} was even able to fully compensate the defect. These data imply that not only XBP1^{s} but also XBP1^{u}, independent from each other, are involved in the regulation of cell proliferation under unstressed conditions, pointing to a so far unknown regulatory function of XBP1^{u}.

Under stressed conditions less than 50 % of WT and 10 % of KO cells formed colonies (Fig. 6c). This defect was fully rescued by XBP1^{s} and to some degree by XBP1^{u}, which demonstrates that not only the expression of XBP1^{s}, but also the expression of XBP1^{u} increases ER stress resistance.

a

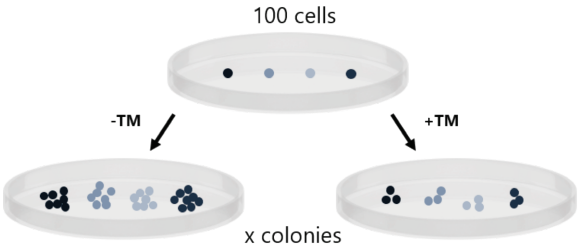

b

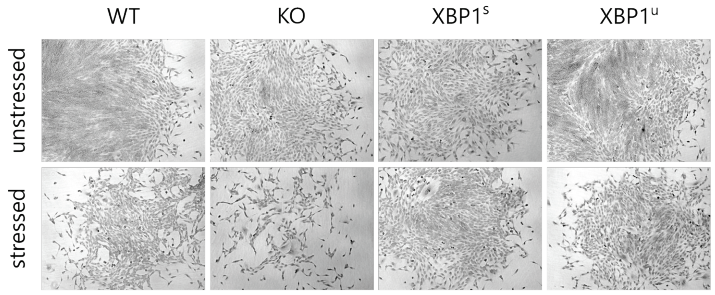

c

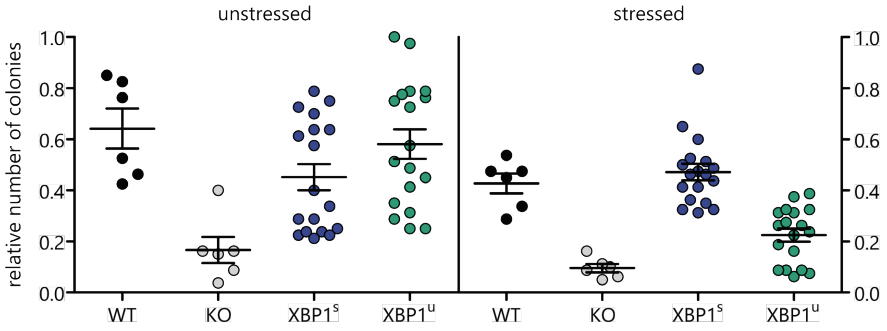

d

unstressed

Dunn's multiple comparisons test	Adjusted P Value	Summary
WT vs. KO	0.003	**
WT vs. XBP1^{s}	0.36	ns
WT vs. XBP1^{u}	>0.99	ns
KO vs. XBP1^{s}	0.09	ns
KO vs. XBP1^{u}	0.002	**

stressed

Dunn's multiple comparisons test	Adjusted P Value	Summary
WT vs. KO	0.004	**
WT vs. XBP1^{s}	>0.99	ns
WT vs. XBP1^{u}	0.03	*
KO vs. XBP1^{s}	<0.001	***
KO vs. XBP1^{u}	>0.99	ns

* p<0.05, ** p<0.01, *** p<0.001

Figure 6: XBP1^{s} and XBP1^{u} partially restore clonogenic survival and ER stress resistance in *XBP1$^{-/-}$* cells

Analysis of clonogenic survival and ER stress resistance via clonogenic assays. (a) Scheme of a clonogenic assay. (b) Size and density of WT, KO and XBP1^{s}/XBP1^{u} colonies formed after 9 days of incubation. Cells in bottom row were treated with 0.5 µg/mL TM for 4.5 h. (c) Number of colonies formed in WT and derivatives relative to maximum number of colonies. Each data point represents the mean of three technical replicates of one experiment. Error bars represent SEM. (d) P-values and significance levels are based on Dunn's multiple comparisons test.

2.2.2. **RPE1 *XBP1*$^{-/-}$ cells do not display cell cycle defects**

Progression through the cell cycle requires the coordinated action of various regulatory proteins such as cyclins and cyclin-dependent kinases (CDK). Since XBP1 is also involved in controlling the cell cycle in pancreatic β-cells and human osteosarcoma (Xu et al., 2014; Yang et al., 2015), which might be the reason for reduced clonogenic survival, the DNA profile as well as the number of cells undergoing mitosis were examined by flow cytometry. To do so, 70-80 % confluent WT, KO and XBP1^{s}/XBP1^{u} rescue cells were fixed either directly or after 4.5 h treatment with 1 µg/mL TM and stained with Hoechst 33342 (DNA marker) and H_3P (marker of mitotic cells). In all analyzed cell lines the number of cells undergoing mitosis remained relatively constant (Fig. 7e). Moreover, no pronounced cell cycle defects were observed. Merely, the fraction of cells in S-phase was increased in the tested cell lines under stressed conditions (Fig. 7a). Nonetheless, as opposed to WT, the percentage of KO cells in subG1-phase increased from 1.5 % under unstressed conditions to 4 % under stressed conditions (Fig. 7d). The subG1-fraction usually contains cells with fractional DNA as in apoptotic cells. However, also hypodiploid and necrotic cells peak into the subG1-fraction (Riccardi and Nicoletti, 2006). The percentage of XBP1^{s}/XBP1^{u} cells in the subG1-phase was on par with WT cells (Fig. 7b, d) suggesting that the expression of both XBP1^{s} and XBP1^{u} might protect cells from DNA fragmentation under stressed conditions.

Figure 7: Deletion of *XBP1* does not provoke cell cycle defects

Cell cycle analysis of unstressed and stressed (1 µg/mL TM for 4.5 h) WT, KO and XBP1^{s}/XBP1^{u} cells by flow cytometry. (a), (b), (c) Hoechst area histograms of DNA content show subG1- (P1), G1-, S- and G2/M-phases of the cell cycle (top). Discrimination of mitotic cells by means of H_3P area versus Hoechst area (bottom). 10000 single cells were analyzed. (d) Percentage of cells in subG1-phase. (e) Percentage of mitotic cells.

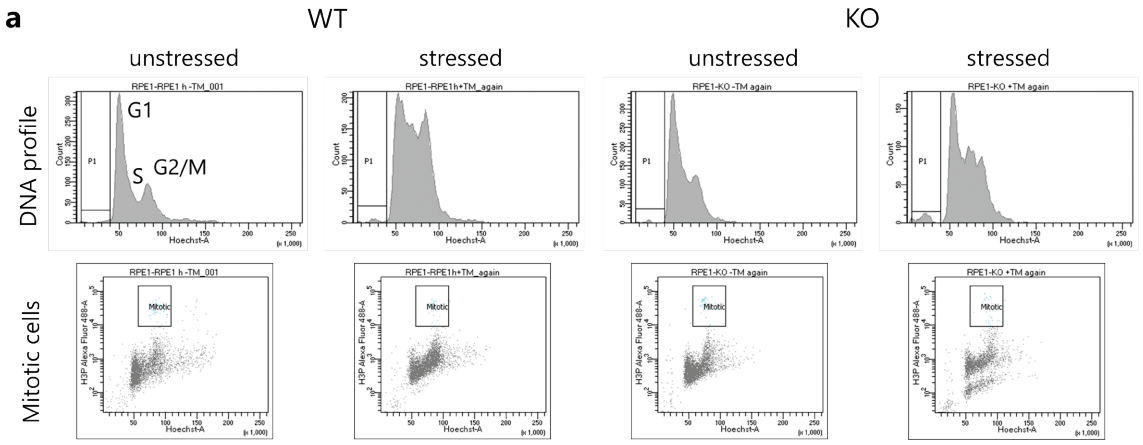

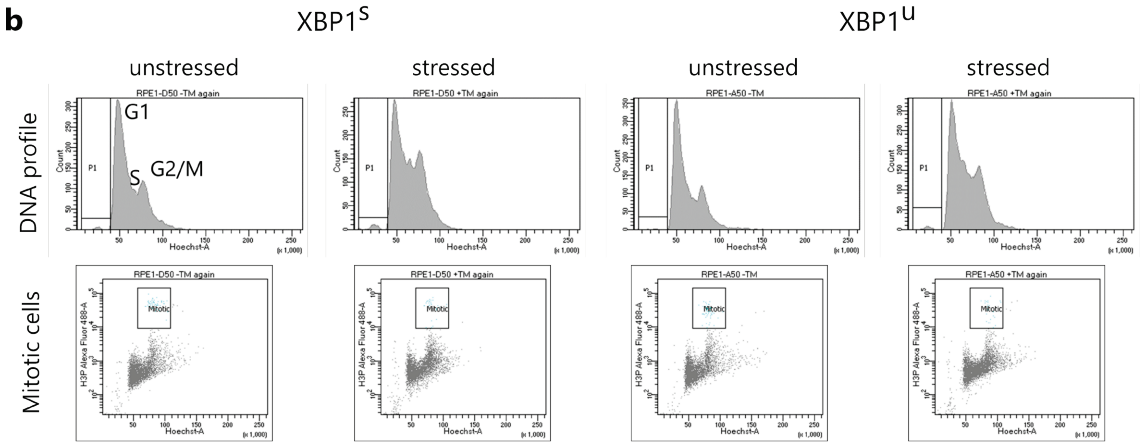

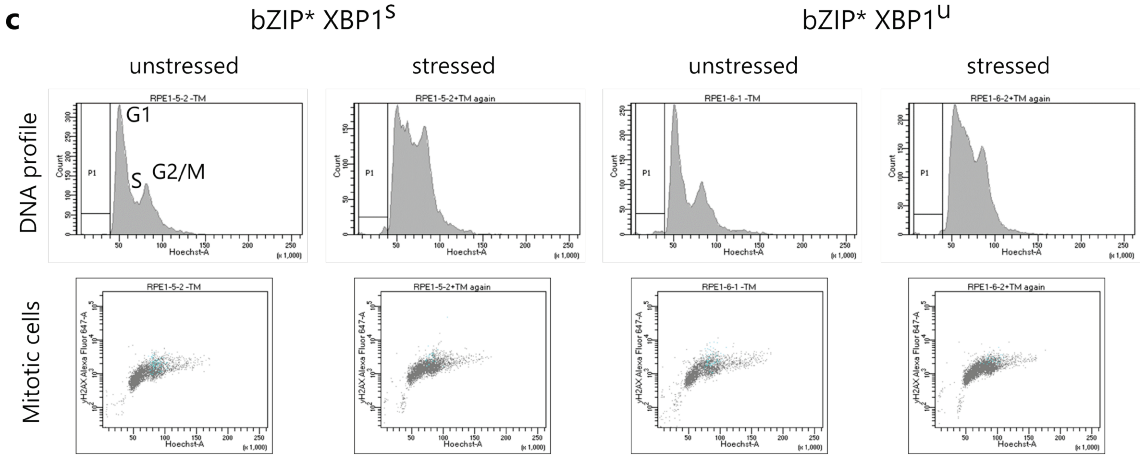

d

P1 [%]	unstressed	stressed
WT	2.1	1.6
KO	1.5	4.0
XBP1^{S}	1.5	2.1
XBP1^{U}	1.0	1.4
bZIP* XBP1^{S}	0.8	1.5
bZIP* XBP1^{U}	2.2	0.9

e

Mitotic cells [%]	unstressed	stressed
WT	1.6	0.7
KO	1.4	1.1
XBP1^{S}	1.6	0.9
XBP1^{U}	1.6	0.7
bZIP* XBP1^{S}	1.8	0.7
bZIP* XBP1^{U}	2.2	0.5

2.3. Characterization of the *XBP1*$^{-/-}$ and XBP1^{s}/XBP1^{u} rescue cell lines on a transcriptional level

XBP1^{s} is a potent transcriptional activator that induces the expression of a subset of UPR target genes in order to cope with ER stress (Lee et al., 2003; Shoulders et al., 2013). It contains an amino-terminal bZIP domain which enables binding to specific promoter regions (UPREs) of genes to control their expression. Furthermore, the bZIP domain allows for heterodimerization with other transcription factors within the bZIP transcription factor family, which results in changes in the DNA-binding specificity, thus, increasing the number of recognized DNA sequences. Genome-wide analysis revealed a subset of genes such as *CHOP* and *BiP,* that were induced upon ER stress induction. Another subset of genes, on the other hand, was uncovered to be dependent on XBP1^{s}. This includes, among others, *ERDJ4*, *RAMP4* and *EDEM1* (Lee et al., 2003). Although XBP1^{u} and XBP1^{s} contain an identical bZIP domain, a role as transcriptional transactivator has not been described for XBP1^{u}, yet. To investigate a possible involvement of XBP1^{u} in the transcriptional regulation of the ER stress response, the expression levels of the above mentioned UPR target genes and *GADD34* were determined under unstressed as well as under ER stress (1 µg/mL TM for 4.5 h) conditions in WT, KO and XBP1^{s}/XBP1^{u} rescue cells via qRT-PCR. As expected, the expression of the UPR targets *BiP*, *CHOP* and *GADD34* was not induced under unstressed conditions. Under ER stress conditions, the expression of all three genes was markedly increased. However, the expression levels of *BiP*, *CHOP* and *GADD34* did not differ significantly among the tested cell lines suggesting that the induction of gene expression does not require XBP1 (Fig. 8a). In contrast, the expression of *EDEM1*, *RAMP4* and *ERDJ4* was not only induced in response to ER stress but also in response to XBP1^{s}. Interestingly, KO and XBP1^{u} rescue cells showed similar *EDEM1*, *RAMP4* and *ERDJ4* expression levels (Fig. 8b).

Based on these observations, it is most likely that XBP1^{u} does not regulate UPR target gene expression.

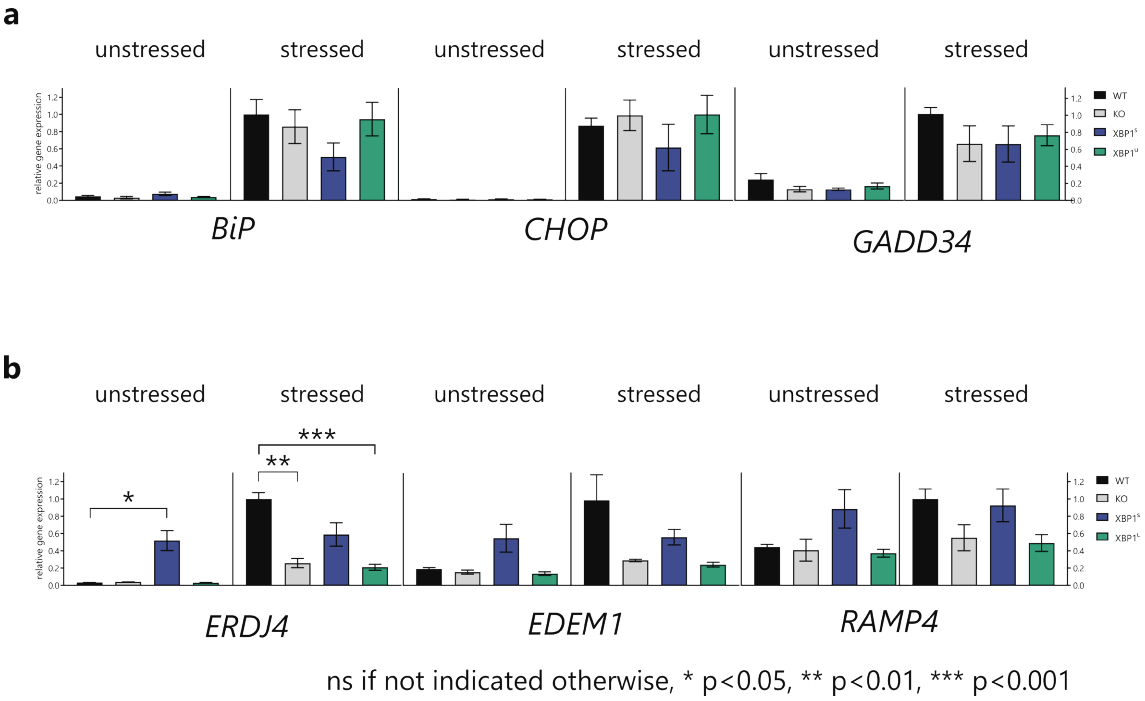

Figure 8: XBP1^{s} but not XBP1^{u} regulates the expression of a subset of UPR target genes

Analysis of UPR target gene expression in WT, KO and XBP1^{s}/XBP1^{u} rescue cell lines under unstressed and stressed (1 µg/mL TM for 4.5 h) conditions by qRT-PCR. (a) Expression of *BiP*, *CHOP* and *GADD34* was measured in (a) and *ERDJ4*, *EDEM1* and *RAMP4* in (b). *β-Actin* was used for normalization. The expression values represent the mean of biological replicates (WT: n=3, KO: n=2, XBP1^{s}/XBP1^{u}: n=4) with two technical duplicates each. Error bars represent SEM. Significance levels are based on Bonferroni's multiple comparisons test.

2.4. The DNA-binding domain is dispensable for the functionality of XBP1^{u} but required for XBP1^{s} function

The bZIP transcription factor XBP1^{s} is a major regulator of the ER stress response. In this respect, the basic DNA-recognition domain's mediation of sequence specific DNA-binding is crucial. However, for the regulation of glucose homeostasis via FoxO1 in mouse, the DNA-binding domain is dispensable (Zhou et al., 2011). As described in section 2.2.1, XBP1^{s} and XBP1^{u} conciliate clonogenic survival and ER stress resistance in *XBP1*$^{-/-}$ cells. However, the contributions of individual protein domains to mediate these functions are currently unknown. To further investigate a potential involvement of the DNA-binding domain in the XBP1^{u} functionality, stable RPE1 *XBP1*$^{-/-}$ cell lines

expressing either XBP1^{s} or XBP1^{u} (unspliceable variant), in which the DNA-binding domain was replaced with an artificial NLS according to Zhou et al., 2011, were generated. In the following, RPE1 *XBP1*$^{-/-}$ cell lines expressing XBP1^{s} or XBP1^{u} with a mutated DNA-binding domain will be referred to as “bZIP* XBP1^{s}” and “bZIP* XBP1^{u}”, respectively. To this end, the impact of the mutation on clonogenic survival and ER stress resistance was analyzed under unstressed and stressed conditions in the bZIP* XBP1^{s}/XBP1^{u} cell lines. WT, KO and XBP1^{s}/XBP1^{u} rescue cells served as additional controls. Consistent with previous results, the size and density of the colonies formed under unstressed conditions were reduced in the KO cell line in comparison to the WT control. Remarkably, not only the expression of XBP1^{s}/XBP1^{u} but also of bZIP* XBP1^{s}/XBP1^{u} was sufficient to restore the colony phenotype (Fig. 9a, top). By contrast, colonies formed by all tested cell lines treated with TM (0.6 µg/mL for 4.5 h) were reduced in size and density (Fig. 9a, bottom). Interestingly, the DNA-binding domain in XBP1^{s}/XBP1^{u} did not affect the colony formation ability under unstressed conditions. Under stressed conditions only the expression of XBP1^{s} but not bZIP* XBP1^{s} in *XBP1*$^{-/-}$ cells restored ER stress resistance. On the other hand, the XBP1^{u} and bZIP* XBP1^{u} cell lines produced similar numbers of colonies (Fig. 9b,c). These data imply, that the bZIP domain of XBP1^{u} does not play a decisive role in the regulation of cell proliferation and that the regulatory role of XBP1^{u} is most likely independent of the ability to bind DNA.

a

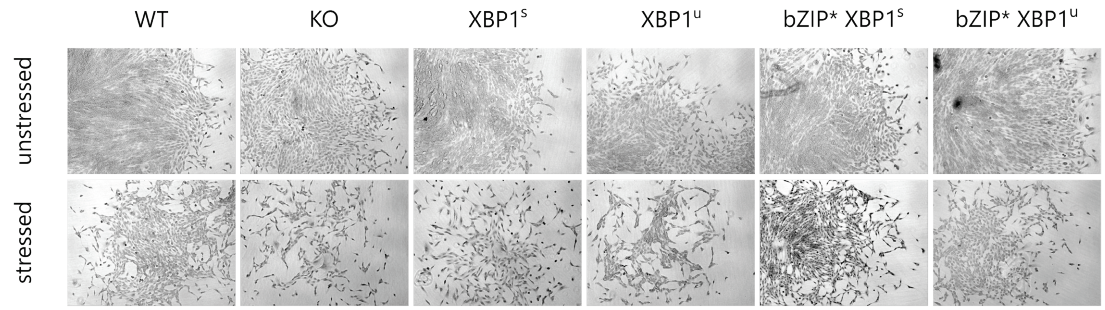

b

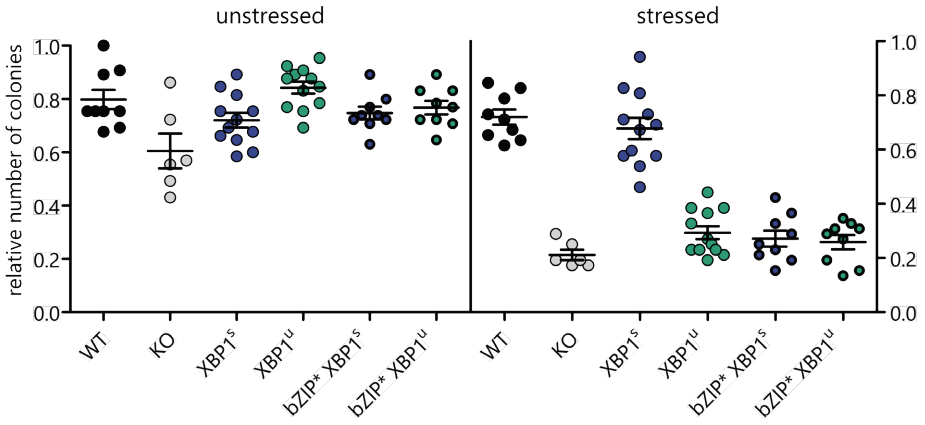

c

unstressed

Dunn's multiple comparisons test	Adjusted P Value	Summary
WT vs. KO	0.006	**
WT vs. XBP1^{s}	>0.99	ns
WT vs. XBP1^{u}	>0.99	ns
WT vs. bZIP* XBP1^{s}	>0.99	ns
WT vs. bZIP* XBP1^{u}	>0.99	ns
KO vs. XBP1^{s}	0.31	ns
KO vs. XBP1^{u}	<0.001	***
KO vs. bZIP* XBP1^{s}	0.11	ns
KO vs. bZIP* XBP1^{u}	0.04	*

stressed

Dunn's multiple comparisons test	Adjusted P Value	Summary
WT vs. KO	<0.001	***
WT vs. XBP1^{s}	>0.99	ns
WT vs. XBP1^{u}	<0.001	***
WT vs. bZIP* XBP1^{s}	<0.001	***
WT vs. bZIP* XBP1^{u}	<0.001	***
KO vs. XBP1^{s}	<0.001	***
KO vs. XBP1^{u}	>0.99	ns
KO vs. bZIP* XBP1^{s}	>0.99	ns
KO vs. bZIP* XBP1^{u}	>0.99	ns

* p<0.05, ** p<0.01, *** p<0.001

Figure 9: Mutation of the DNA-binding domain only hampers XBP1^{s}-mediated clonogenic survival

Analysis of clonogenic survival and ER stress resistance in XBP1 rescue cell lines with a mutated DNA-binding domain. (a) Size and density of WT, KO, XBP1^{s}/XBP1^{u} and bZIP* XBP1^{s}/bZIP* XBP1^{u} colonies formed after 10 days of incubation. Cells in bottom row were treated with 0.6 µg/mL TM for 4.5 h. (b) Number of colonies formed in WT and derivatives relative to maximum number of colonies. Each data point represents the mean of three technical replicates of one experiment. Error bars represent SEM. (c) P-values and significance levels are based on Dunn's multiple comparisons test.

2.5. XBP1^{u} is unlikely to be transcriptionally active

Although XBP1^{u} contains a DNA-binding domain, neither a transcriptional transactivation domain nor target genes were identified to date. In the presence of basal ER stress levels, XBP1^{u} induces clonogenic survival independent of XBP1^{s}. However, it is yet to be determined on which level this regulation occurs. Assuming that this happens on a transcriptional level, XBP1^{u} should be able to activate the transcription of certain targets.

To investigate this possibility, luciferase reporter assays were performed. To this end, the consensus UPRE motif, which is specifically recognized by XBP1, was fused to the firefly luciferase reporter (Yan Wang et al., 2000). WT, KO, XBP1^{s}/XBP1^{u} as well as bZIP* XBP1^{s}/bZIP* XBP1^{u} cells were transiently transfected with the reporter construct and the luciferase activity measured 24 h post-transfection. For normalization purposes the reporter construct additionally contained the renilla luciferase under the control of an SV40 minimal promoter (Fig. 10a). Only basal luciferase activity was measured in KO_1 and KO_2, indicating that the UPRE motif used is a specific binding site for XBP1. In XBP1^{s} rescue cells the luminescence was significantly increased, confirming transcriptional activity of XBP1^{s}. As expected, mutation of the DNA-binding domain completely abolished reporter activity. By contrast, only basal firefly luciferase activity was detected in *XBP1*$^{-/-}$ cells expressing XBP1^{u} or bZIP* XBP1^{u} (Fig. 10b). In order to test if the lack of reporter activity results from the absence of a transactivation domain in XBP1^{u}, a VP16-derived minimal transactivation domain was fused to *XBP1*^{u} (unspliceable) expressed under the control of the constitutive *CMV* promoter and transiently co-transfected with the luciferase reporter construct in *XBP1*$^{-/-}$ cells (Fig. 10c). Luciferase activity in cells expressing XBP1^{u}-VP16 was significantly increased compared to cells expressing XBP1^{u} and to WT cells, which provides direct evidence that XBP1^{u} is acting on a post-transcriptional level (Fig. 10d).

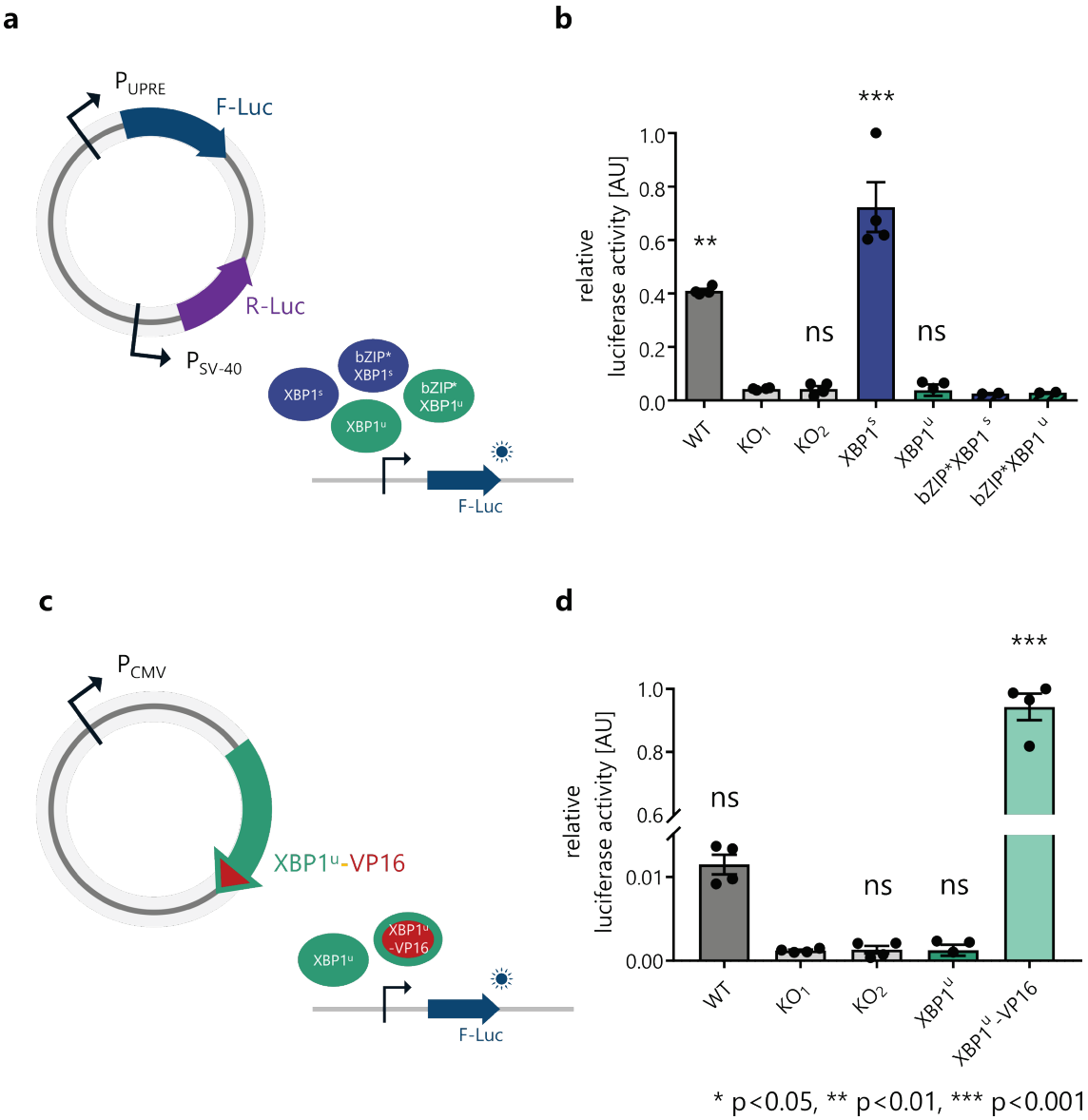

Figure 10: XBP1^{u} does not activate the expression of the luciferase reporter

Analysis of the transcriptional activity of XBP1^{u} and XBP1^{s} via dual luciferase reporter assays. (a) Schematic display of the pUPRE-firefly-luciferase reporter construct. (b) WT, KO, XBP1^{s}/XBP1^{u} and bZIP* XBP1^{s}/bZIP* XBP1^{u} cells were transfected with the UPRE-luciferase reporter. Luciferase activity was measured 24 h post-transfection. The renilla luciferase was used for normalization. Each data point represents the mean of two technical replicates of one experiment. Significance levels are based on Bonferroni's multiple comparisons test. (c) Schematic display of the XBP1^{u}-VP16 fusion plasmid. (d) WT, KO and XBP1^{u} cells were treated as described in (b). In addition, KO cells were transfected with an expression plasmid containing an XBP1^{u}-VP16 fusion. Luciferase activity was measured 24 h post-transfection. The renilla luciferase was used for normalization. Each data point represents the mean of two technical replicates of one experiment. Significance levels are based on Bonferroni's multiple comparisons test.

2.6. Analysis of XBP1^{u} interactors under unstressed and stressed conditions

Besides the already known functions of XBP1^{u}, the protein is probably also involved in the regulation of cell proliferation as well as in the mediation of ER stress resistance. In addition, XBP1^{u} potentially takes part in protecting cells from DNA fragmentation under unstressed conditions. The way these regulations occur is most likely on a post-transcriptional level.

To further investigate the molecular function of XBP1^{u} and to identify potential interactors (in the following called interactors for simplicity), affinity purification of GFP-tagged XBP1^{u} (unspliceable, expressed in KO cells) followed by mass spectrometry was performed. Therefore, protein lysates of 70-80 % confluent unstressed or stressed (1 µg/mL TM for 4.5 h) cells were used. To eliminate unspecific interactors, *XBP1*$^{-/-}$ cells expressing either GFP-XBP1^{s} or cytosolic eGFP (Cntrl) were analyzed in the same way. For the identification of XBP1^{u} interactors, the protein intensities were calculated as the sum of all related peptide intensities. The latter, in turn, were calculated as the sum of the extracted ion currents from all identified peptide ions. The intensities of two independent experiments (Exp 1 and Exp 2) were jointly analyzed.

Figure 11: Interactors of XBP1^{s} and XBP1^{u} under unstressed conditions

Analysis of XBP1^{s}/XBP1^{u} interactors in unstressed *XBP1*$^{-/-}$ *GFP-XBP1^{s}/XBP1^{u}* cells by mass spectrometry. (a) Venn diagram of XBP1^{u}-specific (green), XBP1^{s}-specific (blue) and common interacting proteins. The diagram only includes proteins for which the difference between intensity of Cntrl and XBP1^{s}/XBP1^{u} is at least 1 on a log2 scale (equivalent to 2 fold change). Data represent intersection of two independent experiments. (b) Bar chart of protein intensities of XBP1^{u} interactors over calculated intensities in the GFP-XBP1^{s} trap. Negative values (blue gradient) depict higher intensities in the GFP-XBP1^{s} purification, whereas positive values (red gradient) depict higher intensities in the XBP1^{u} trap. Blue and green dots represent XBP1^{s} and XBP1^{u} interactors, respectively. (c) Analysis of protein-protein interaction networks among XBP1^{u} interactors via STRING. (d) Analysis of protein-protein interaction networks among XBP1^{s} interactors via STRING.

a

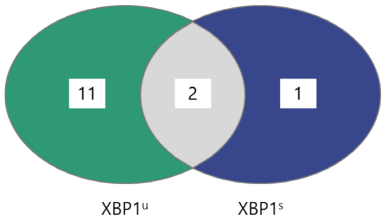
11
2
1
XBP1u
XBP1s

b

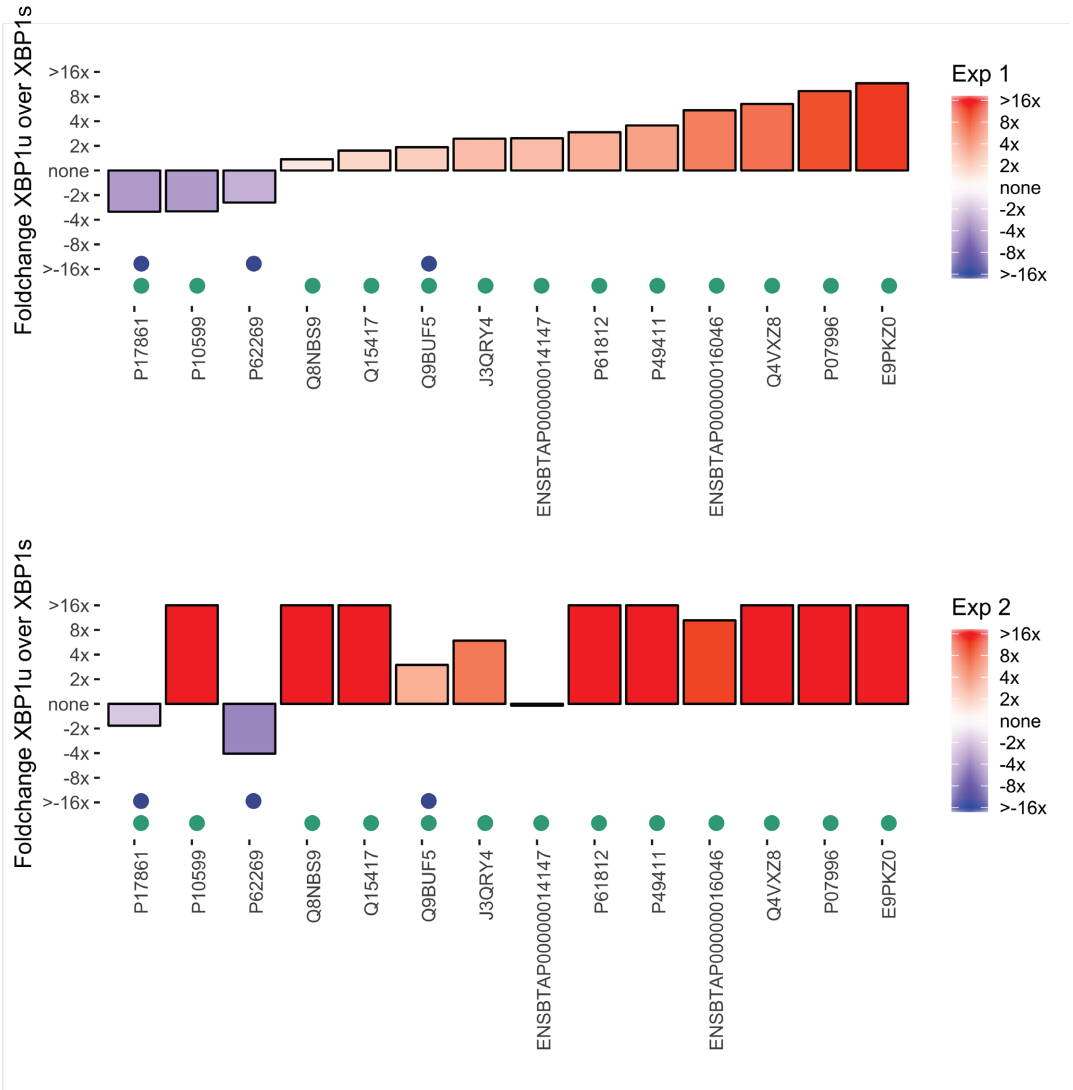
Foldchange XBP1u over XBP1s
>16x
8x
4x
2x
none
-2x
-4x
-8x
>-16x
P17861
P10599
P62269
Q8NBS9
Q15417
Q9BUF5
J3QRY4
ENSBTAP00000014147
P61812
P49411
ENSBTAP00000016046
Q4VXZ8
P07996
E9PKZ0
Exp 1
Exp 2

c

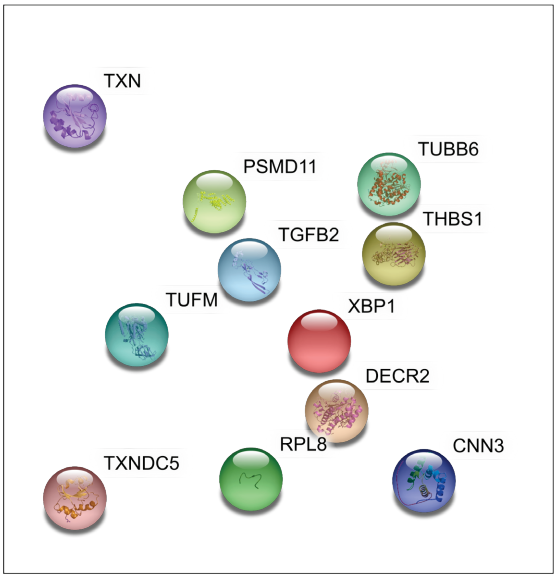

Protein IDs	Gene name	Protein name
J3QRY4	PSMD11	Proteasome 26S subunit
P17861	XBP1	X-box binding protein 1
P61812	TGFB2	Transforming growth factor
Q4VXZ8	DECR2	2,4-dienoyl CoA reductase 2 (peroxisomal)
ENSBTAP00000014147	unknown	unknown
Q15417	CNN3	Calponin 3
Q8NBS9	TXNDC5	Thioredoxin domain containing protein 5
ENSBTAP00000016046	unknown	unknown
E9PKZ0	RPL8	Ribosomal protein L8
P49411	TUFM	Tu translation elongation factor
P07996	THBS1	Thrombospondin 1
Q9BUF5	TUBB6	Tubulin, beta 6 class V
P10599	TXN	Thioredoxin

d

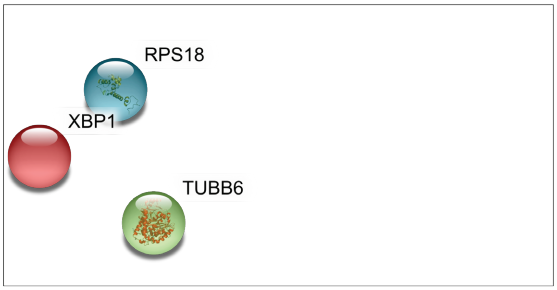

Protein IDs	Gene name	Protein name
P17861	XBP1	X-box binding protein 1
P62269	RPS18	Ribosomal protein S18
Q9BUF5	TUBB6	Tubulin, beta 6 class

Under unstressed conditions, only one protein was identified that was specifically co-purified with GFP-XBP1^{s} (Fig. 11a): Ribosomal protein S18 (RPS18). RPS18 is involved in the translational initiation and its calculated protein intensity was 4 fold increased over the intensity calculated in the GFP-XBP1^{u} trap (Fig. 11b). Additionally, eleven proteins that were specifically pulled-down with GFP-XBP1^{u} were identified (Fig. 11a). In the following, the three most promising proteins will be described in more detail. Firstly, thrombospondin 1 (THBS1, P07996), which protects pancreatic β- cells from lipotoxicity via the PERK pathway and interacts with ATF6 (Cunha et al., 2016; Lynch et al., 2012), was identified as a potential XBP1^{u}-specific interactor. The calculated protein intensities were more than 8 times higher than in the GFP-XBP1^{s} trap (Fig. 11b). In addition, THBS1 was only identified under unstressed conditions (Fig. 12). Secondly, calponin 3 (CNN3, Q15417), critical, e.g., for coordinated contractility of actin stress fibers (Ciuba et al., 2018), showed intensities at least twice as high as in the GFP-XBP1^{s} trap, albeit with divergence between Exp 1 and Exp 2, and the protein was also found as an XBP1^{u} interactor under stressed conditions (Fig. 12). Thirdly, 26S proteasome regulatory subunit 11 (PSMD11, J3QRY4), which is involved in regulating increased proteasome activity in embryonic stem cells (Vilchez et al., 2012). In general, the proteasome function is, among other things, tightly linked to ER stress as one of the consequences of inhibiting its activity is increased ER stress (Lee et al., 2013). Intensity levels of PSMD11 were 2-5 times higher than in the GFP-XBP1^{s} trap and the protein was co-purified with GFP-XBP1^{s} under stressed conditions, too (Fig. 11b, Fig. 12).
Overall, protein-protein interaction network analyses (STRING) for all eleven XBP1^{u} interacting candidates did not point to a specific cellular role (Fig. 11c, d).

Under stressed conditions, 24 potential XBP1^{s} interactors, mostly involved in biological processes such as negative regulation of cell death and apoptosis, RNA- and RNA Poly(A)-binding as well as protein processing in the ER, were identified (Fig. 12a, b, d). On the other hand, only two potential XBP1^{u}-specific interactors, PDLIM5 (Q96HC4) and CNN3, were detected. However, the intensity level differences between the GFP-XBP1^{u} and GFP-XBP1^{s} traps for these two candidates in Exp 1 could not be confirmed in Exp 2 (Fig. 12b).

Like under unstressed conditions, the STRING analysis did not reveal a specific cellular role for the interacting candidates (Fig. 12c).

All in all, three potential interactors of XBP1^{u} were identified. However, the results obtained from mass spectrometry did not provide sufficient information for further network analyses. The potential interactors could not be mapped unambiguously to biological processes, making it hard to tell on which level regulation takes place and which other proteins might be involved in the process. For that reason, the two experiments were re-analyzed individually in order to explore the full spectrum of potential interactors and to minimize technical challenges.

Figure 12: Interactors of XBP1^{s} and XBP1^{u} under stressed conditions

Analysis of XBP1^{s}/XBP1^{u} interactors in TM treated (1 µg/mL for 4.5 h) *XBP1$^{-/-}$ GFP-XBP1^{s}/XBP1^{u}* cells by mass spectrometry. (a) Venn diagram of XBP1^{u}-specific (green), XBP1^{s}-specific (blue) and common interacting proteins. The diagram only includes proteins for which the difference between intensity of Cntrl and XBP1^{s}/XBP1^{u} is at least 1 on a log2 scale (equivalent to 2 fold change). Data represent intersection of two independent experiments. (b) Bar chart of protein intensities of XBP1^{u} interactors over calculated intensities in the GFP-XBP1^{s} trap. Negative values (blue gradient) depict higher intensities in the GFP-XBP1^{s} purification, whereas positive values (red gradient) depict higher intensities in the XBP1^{u} trap. Blue and green dots represent XBP1^{s} and XBP1^{u} interactors, respectively. (c) Analysis of protein-protein interaction networks among XBP1^{u} interactors via STRING. (d) Analysis of protein-protein interaction networks among XBP1^{s} interactors via STRING.

a

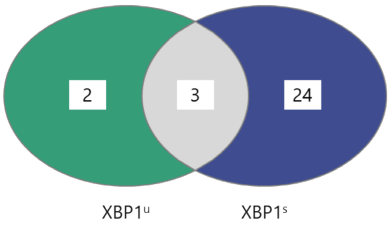
2
3
24
XBP1u
XBP1s

b

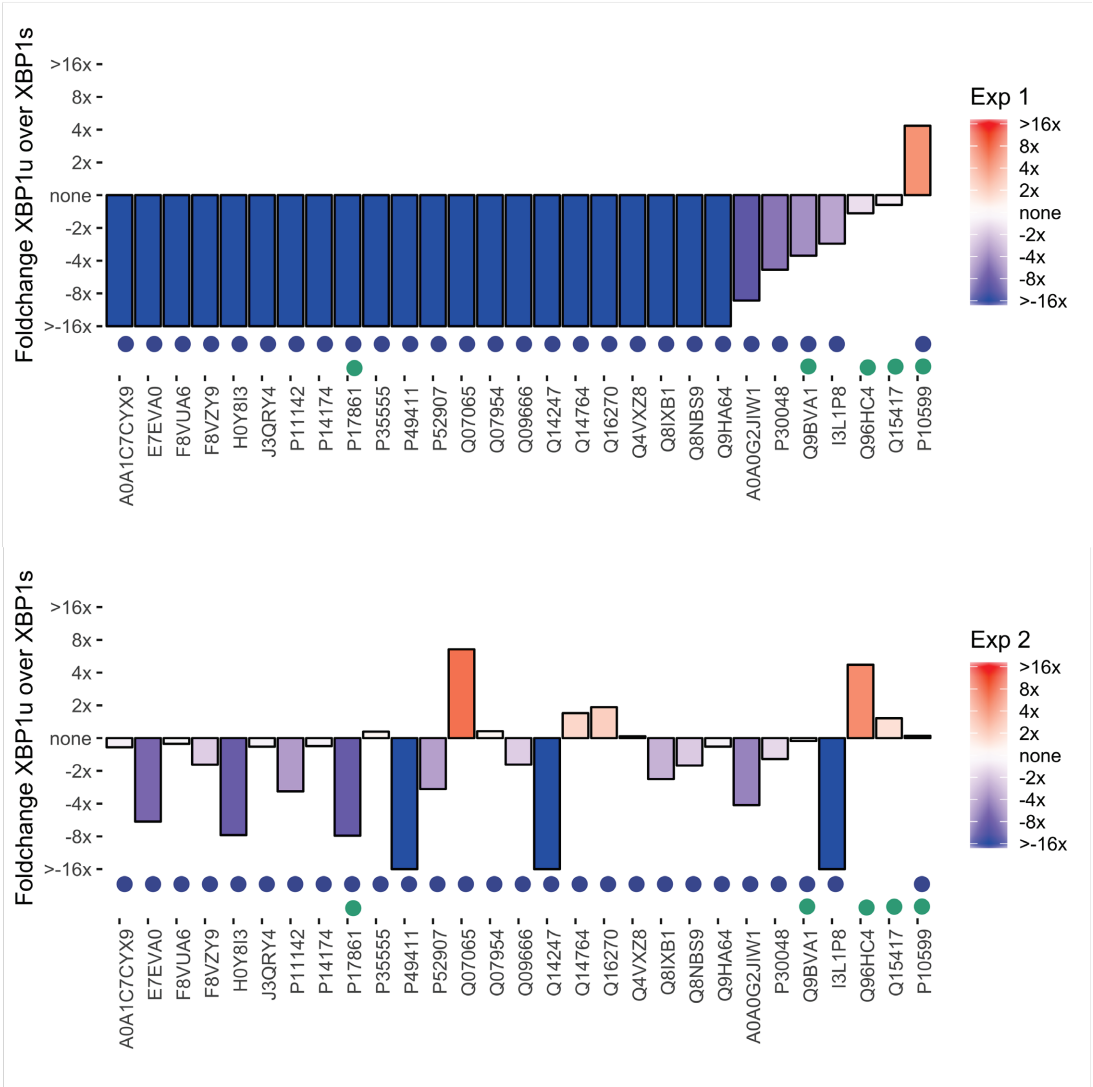
Foldchange XBP1u over XBP1s
>16x
8x
4x
2x
none
-2x
-4x
-8x
>-16x
Exp 1
A0A1C7CYX9
E7EVA0
F8VUA6
F8VZY9
H0Y8I3
J3QRY4
P11142
P14174
P17861
P35555
P49411
P52907
Q07065
Q07954
Q09666
Q14247
Q14764
Q16270
Q4VXZ8
Q8IXB1
Q8NBS9
Q9HA64
A0A0G2JIW1
P30048
Q9BVA1
I3L1P8
Q96HC4
Q15417
P10599
Exp 2

c

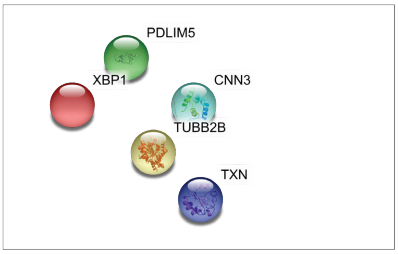

Protein IDs	Gene name	Protein name
P17861	XBP1	X-box binding protein 1
Q9BVA1	TUBB2B	Tubulin, beta 2B class lib
Q96HC4	PDLIM5	PDZ and LIM domain 5
Q15417	CNN3	Calponin 3
P10599	TXN	Thioredoxin

d

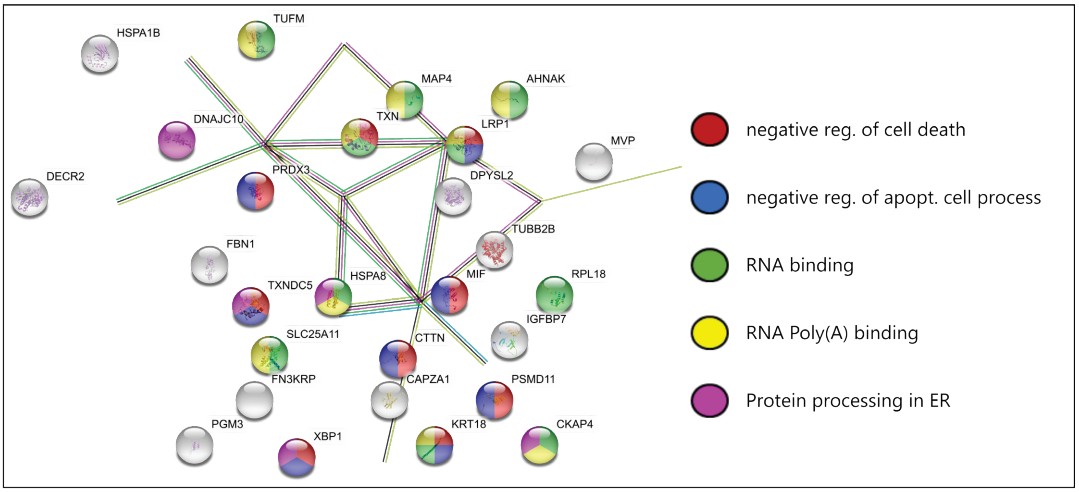

Protein IDs	Gene name	Protein name
J3QRY4	PSMD11	Proteasome 26S subunit
P17861	XBP1	X-box binding protein 1
Q9BVA1	TUBB2B	Tubulin, beta 2B class lib
Q9BVA1	PGM3	Phosphoglucomutase 3
P35555	PRDX3	Peroxiredoxin 3
P30048	unknown	unknown
Q14247	CTTN	Cortactin
A0A0G2JIW1	HSPA1B	Heat shock 70kDa protein 1B
Q4VXZ8	DECR2	2,4-dienoyl CoA reductase 2 (peroxisomal)
E7EVA0	MAP4	Microtuble-associated protein 4
Q07954	LRP1	Low density lipoprotein receptor-related protein 1
Q8NBS9	TXNDC5	Thioredoxin domain containing protein 5
I3L1P8	SLC25A11	Solute carrier family 25
Q07065	CKAP4	cytoskeleton-associated protein 4
F8VUA6	RPL18	Ribosomal protein L18
F8VZY9	KRT18	Keratin18
Q9HA64	FN3KRP	Fructosamine 3 kinase related protein
Q09666	AHNAK	AHNAK nucleoprotein
P49411	TUFM	Tu translation elongation factor
A0A1C7CYX9	DPYSL2	Dihydropyrimidinase-like 2
P52907	CAPZA1	Capping protein (actin filament) muscle Z-line alpha 1
Q14764	MVP	Major vault protein
P14174	MIF	Macrophage migration inhibitory factor(glycosylation-inhibiting factor)
Q8IXB1	DNAJC10	DnaJ (Hsp40) homolog
Q16270	IGFBP7	Insuline-like growth factor binding protein 7
P11142	HSPA8	Heat shock 70kDa protein 8
P10599	TXN	Thioredoxin

At this point, only the analysis of XBP1^{u} interactors under stressed conditions will be described. For a complete analysis, refer to Appendix B. 9 potential XBP1^{u}-specific interactors could be identified in Exp 1 and 52 in Exp 2 (Fig. 13a, b). Looking at the corresponding network analyses, it is obvious that there is a large discrepancy between Exp 1 and Exp 2 (Fig. 13b, c). Proteins identified in Exp 1 were mapped to biological processes such as catabolic processes, response to lipids, external stimuli and glucose starvation as well as regulation of peptidase activity (Fig. 13c). Proteins identified in Exp 2 were mainly associated with mitotic cell cycle checkpoint control as well as catabolic and protein metabolic processes (Fig. 13d). Identified proteins potentially interacting with XBP1^{u} under ER stress conditions barely overlap between the two replicates, which makes it challenging to distinguish between valid and false positive interactors. Further repetitions are necessary to validate these preliminary results and to clarify the molecular function of XBP1^{u}.

Figure 13: Detailed analysis of XBP1^{u} interactors upon induction of ER stress

Analysis of XBP1^{u} interactors in TM treated (1 µg/mL for 4.5 h) *XBP1$^{-/-}$ GFP-XBP1^{s}/XBP1^{u}* cells by mass spectrometry. (a, b) Venn diagrams of XBP1^{u}-specific (green), XBP1^{s}-specific (blue) and common interacting proteins. The diagrams only include proteins for which the difference between intensity of Cntrl and XBP1^{s}/XBP1^{u} is at least 1 on a log2 scale (equivalent to 2 fold change). Each diagram represents data of one experiment (a: Exp 1, b: Exp 2). (c) Analysis of protein-protein interaction networks among XBP1^{u} interactors via STRING (Exp 1). (d) Analysis of protein-protein interaction networks among XBP1^{u} interactors via STRING (Exp 2).

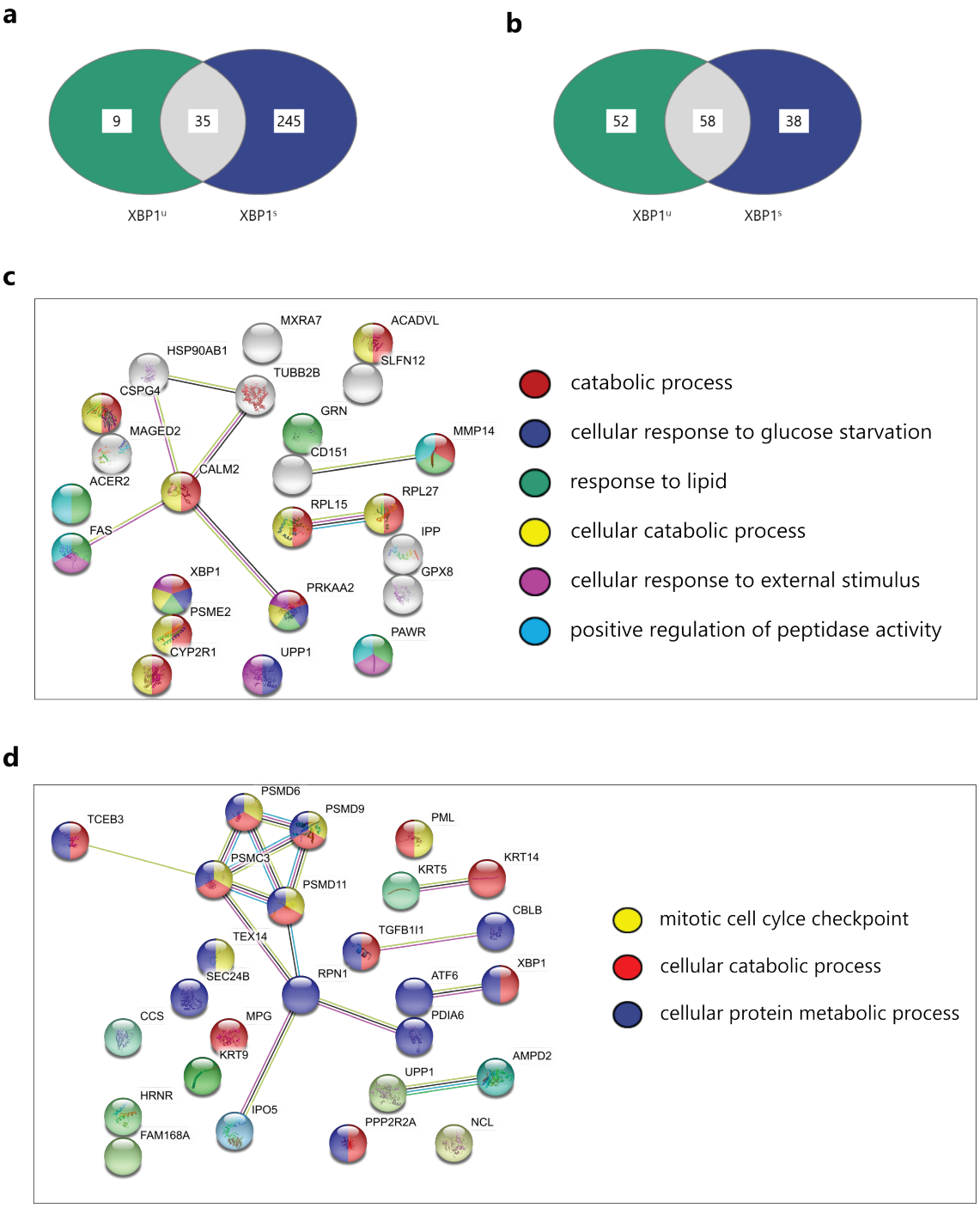

2.7. Analysis of the cellular impact of XBP1^{s}/XBP1^{u}

An effective interplay between XBP1^{u} and XBP1^{s} is crucial for dealing with the accumulation of unfolded proteins in the ER and for maintaining ER homeostasis. XBP1^{s} is produced and specifically translocated into the nucleus upon stress induction. When ER stress has subsided, XBP1^{s} is no longer synthesized giving

rise to the production of XBP1^{u}, which is localized to both the nucleus and the cytoplasm (Fig. 14). In this way, XBP1^{u} is able to act as a negative feedback regulator specific to XBP1^{s} (Yoshida et al., 2006).

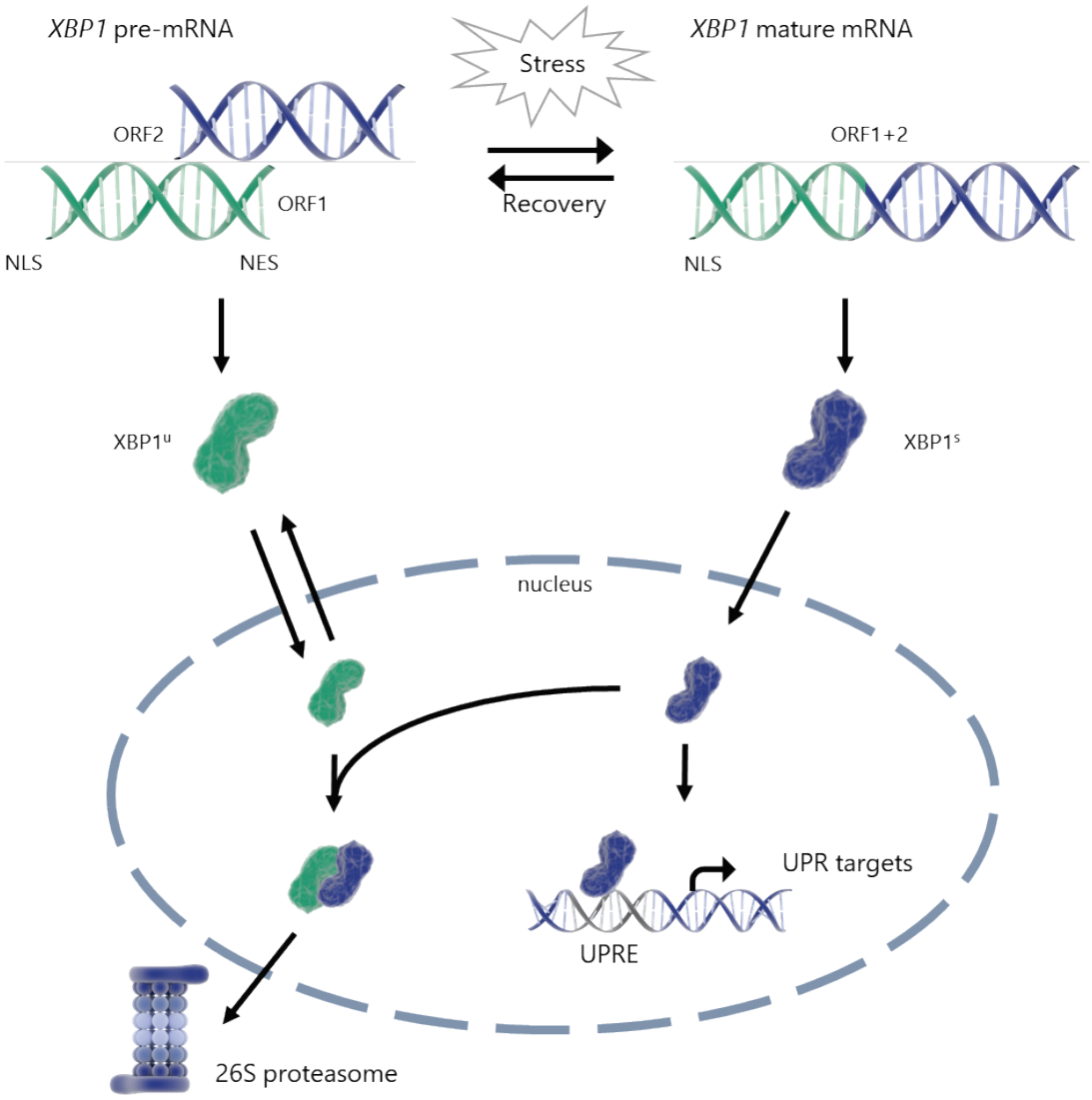

Figure 14: XBP1^{u} as a negative regulator of the ER stress response

Upon ER stress induction the bZIP transcription factor XBP1^{s} is produced and translocated into the nucleus where it regulates gene expression of UPR targets. After prolonged ER stress XBP1^{s} is no longer produced, instead XBP1^{u}, which contains an NES besides an NLS, is formed. These two domains enable shuttling from the cytoplasm to the nucleus and back. In the nucleus XBP1^{u} supposedly forms a heterodimer with XBP1^{s} which is exported out of the nucleus where it is degraded by the proteasome. Figure modified according to Yoshida et al., 2006.

2.7.1. **GFP-XBP1^s and GFP-XBP1^u reside in the ER and the nucleus**

The subcellular localization of proteins often provides important information on their cellular functions. However, this connection cannot be leveraged for XBP1^s and XBP1^u as their localizations have only been poorly characterized so far. XBP1^s localized predominantly to the nucleus, whereas XBP1^u was found in the nucleus and the cytoplasm (Yoshida et al., 2006). In order to clarify the regulatory function of XBP1^u, the subcellular localization of XBP1^s and XBP1^u was further characterized in *XBP1*$^{-/-}$ cells under both unstressed and ER stress inducing conditions. Therefore, stable RPE1 *XBP1*$^{-/-}$ cell lines expressing either *GFP-XBP1^s* or *GFP-XBP1^u* (unspliceable) were generated using a lentiviral system. Afterwards, cells were seeded on coverslips and remained either untreated (unstressed) or were treated with 1 µg/mL TM for 12 h (stressed) before fixation and immunostaining. The subcellular localization was analyzed by confocal microscopy. Vesicle-associated membrane protein-associated protein A (VapA) served as a reticular ER marker, whereas Hoechst was used for nuclear staining. Both, GFP-XBP1^s and GFP-XBP1^u were localized to the ER and to the nucleus. From a qualitative perspective, the localization of both fusion proteins did not change upon stress induction. However, in comparison to GFP-XBP1^u, GFP-XBP1^s showed a stronger nuclear localization (Fig. 15a).

Figure 15: GFP-XBP1^s and GFP-XBP1^u show nuclear and ER localization

Qualitative and quantitative analysis of GFP-XBP1^s and GFP-XBP1^u localization in RPE1 *XBP1*$^{-/-}$ cells. a) Representative confocal single plane images of immunostained *XBP1*$^{-/-}$ cells expressing either GFP-XBP1^s or GFP-XBP1^u under unstressed and stressed (1 µg/mL TM for 12 h) conditions. VapA marks the reticular ER and Hoechst the nuclei. Scale bars represent 15 µm. b) Scatter plots of GFP-XBP1^s/GFP-XBP1^u intensities under unstressed and stressed (1 µg/mL TM for 12 h) conditions. Maximum GFP-XBP1^s/GFP-XBP1^u intensity across all plots was used to scale the data between 0 and 1. Each data point represents the GFP-XBP1^s/GFP-XBP1^u intensity in one nucleus. Significance levels were computed using the non-parametric two-tailed Mann-Whitney-U test.

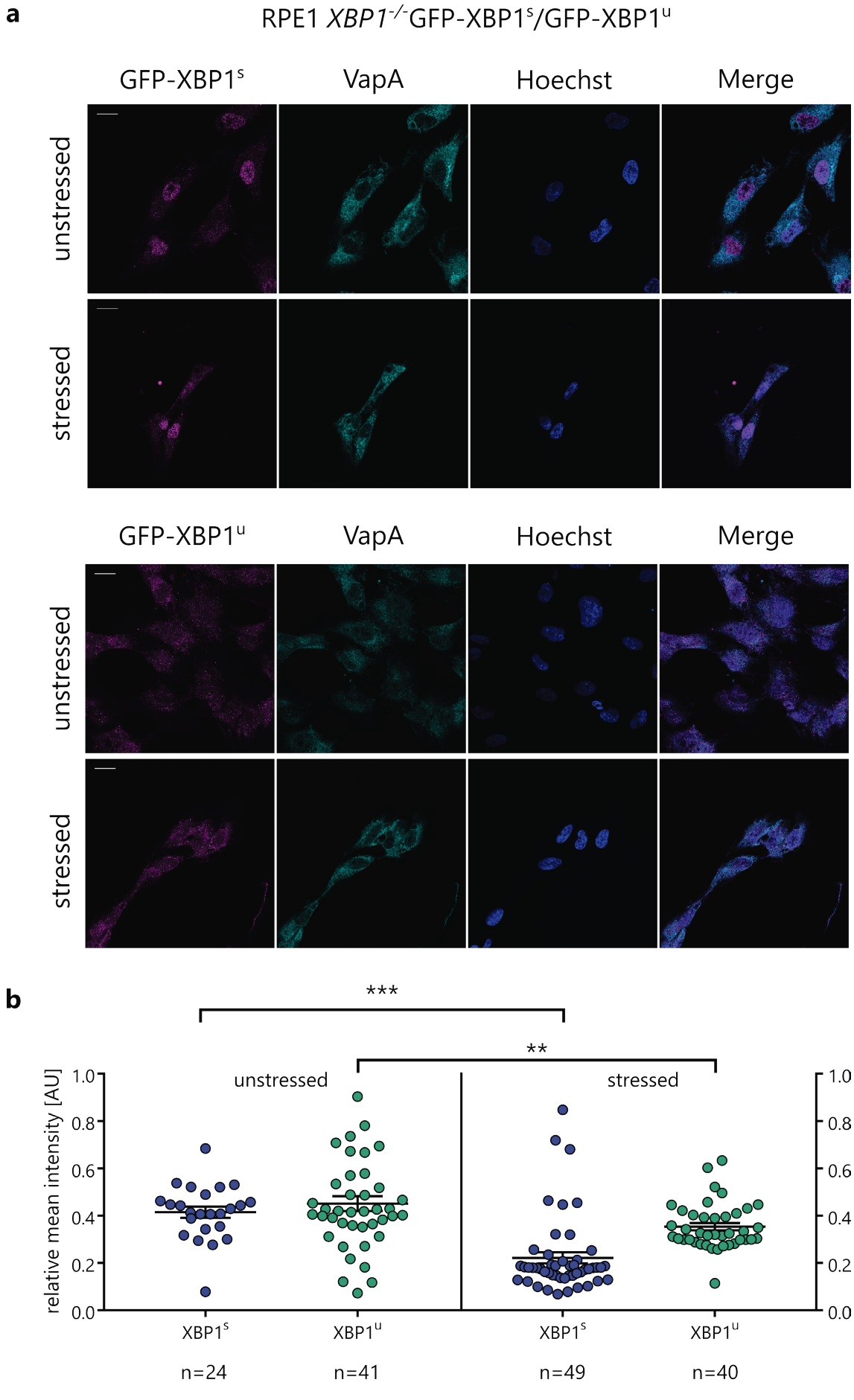
a
RPE1 XBP1-/- GFP-XBP1s/GFP-XBP1u
GFP-XBP1s
VapA
Hoechst
Merge
unstressed
stressed
GFP-XBP1u
VapA
Hoechst
Merge
unstressed
stressed
b
***
**
unstressed
stressed
relative mean intensity [AU]
1.0
0.8
0.6
0.4
0.2
0.0
XBP1s
XBP1u
XBP1s
XBP1u
n=24
n=41
n=49
n=40

Next, the nuclear GFP-XBP1^{s}/GFP-XBP1^{u} intensity was quantified in a two-step procedure: Firstly, nuclei were segmented in order to define the region of interest (ROI) in each cell. Secondly, the intensity of GFP-XBP1^{s}/GFP-XBP1^{u} was measured within this ROI. Intensity levels for both GFP-XBP1^{s} and GFP-XBP1^{u} decreased significantly upon ER stress induction. While mean intensities under unstressed conditions only differed marginally, the difference was more pronounced under stressed conditions (Fig. 15b). Although the GFP-XBP1^{s} fluorescence appeared stronger in the nucleus, quantitatively the intensity levels were not higher compared to GFP-XBP1^{u} (Fig. 15).

2.7.2. **Fast fluorescence recovery of GFP-XBP1^{u} and mCherry-XBP1^{s} within the nucleus after photobleaching**

In order to simultaneously monitor the subcellular localization of XBP1^{u} and XBP1^{s}, a multi-gene expression system, which enabled the co-expression of GFP-XBP1^{u} (unspliceable) and mCherry-XBP1^{s} from one polycistronic mRNA, was leveraged in living cells. Therefore, a construct with a T2A peptide (2A peptide from thosea asigna virus) fused in-between mCherry-XBP1^{s} and GFP-XBP1^{u}, was generated. The 2A peptide mediates cleavage of the polypeptide during protein translation resulting in two proteins (Szymczak and Vignali, 2005). The fusion proteins mCherry-XBP1^{s} and GFP-XBP1^{u} were expressed under the control of the constitutive *CMV* promoter. Localization of both proteins was investigated in RPE1 cells under unstressed conditions by live fluorescence microscopy. While mCherry-XBP1^{s} was localized predominantly to the nucleus, GFP-XBP1^{u} could be found in the whole cell with a preference to the nucleus (Fig. 16a). Afterwards, the dynamics of mCherry-XBP1^{s} and GFP-XBP1^{u} within a cell were analyzed via Fluorescence Recovery after Photobleaching (FRAP). This method allows for investigating the molecular mobility in living cells. To this end, either a small area inside the nucleus or the entire nucleus were photobleached, and changes in fluorescence intensity of mCherry-XBP1^{s} and GFP-XBP1^{u} were measured across the cell and over time. After photobleaching a small area, the nuclear mean intensities of GFP and mCherry were reduced by at least 70 %. Fast recovery was observed within the bleaching area.

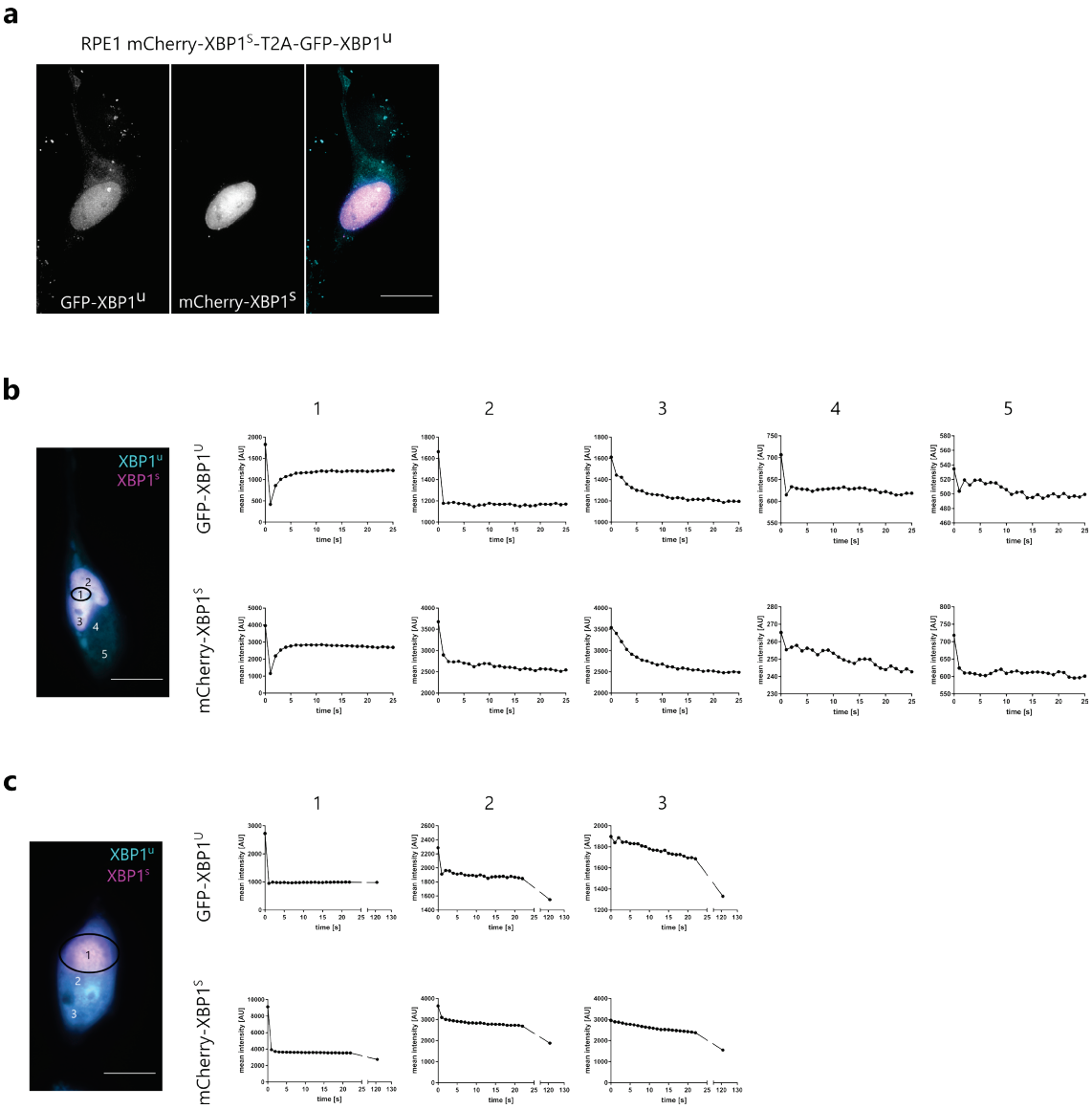

Figure 16: GFP-XBP1^{u} and mCherry-XBP1^{s} seem to be mobile within the nucleus

Analysis of intracellular dynamics of GFP-XBP1^{u} and mCherry-XBP1^{s} by live cell fluorescence microscopy. (a) Subcellular localization of GFP-XBP1^{u} and mCherry-XBP1^{s}. RPE1 cells were transfected with a single plasmid encoding both fusion proteins separated by a T2A peptide. Cells were imaged 24 h post-transfection. Maximum projection of one representative cell is shown. Scale bar represents 15 µm. (b) FRAP analysis of RPE1 mCherry-XBP1^{s}-T2A-GFP-XBP1^{u} cells. Region of photobleaching (at 1 s) within the nucleus is highlighted. Areas 1-5 were used to measure GFP and mCherry intensities. Fluorescence recovery was monitored for 25 s. One representative measurement is depicted. Scale bar corresponds to 15 µm. (c) FRAP analysis of RPE1 mCherry-XBP1^{s}-T2A-GFP-XBP1^{u} cells. The entire nucleus was photobleached at time point 1 s. GFP and mCherry intensities were measured within the areas 1-3. Fluorescence recovery was monitored for 121 s. One representative measurement is depicted. Scale bar corresponds to 15 µm.

However, full fluorescence recovery back to levels before bleaching was not achieved. Fluorescence in adjacent areas inside the nucleus was also reduced by up to 30 %. In these areas, recovery of fluorescence could not be observed. In the cytoplasm, too, the GFP and mCherry fluorescence decreased by 5-15 % without recovery (Fig. 16b). These data indicate that GFP-XBP1^{u} and mCherry-XBP1^{s} are similarly dynamic inside the nucleus. After photobleaching the entire nucleus, the mean intensity of GFP-XBP1^{u} and mCherry-XBP1^{s} in the nucleus dropped by an average of 60 % and did not recover. A non-recovering reduced fluorescence intensity was also measured in the cytoplasm (Fig. 16c).

2.7.3. **Deletion of *XBP1* provokes alterations in ER morphology**

Cells constantly modulate their compartments in order to alleviate stress and maintain homeostasis. To further investigate the regulatory role of XBP1 on organelle morphology, WT and *XBP1*$^{-/-}$ cells were scrutinized in terms of actin, Golgi, nucleus and ER by fluorescence microscopy. WT and KO cells were seeded on coverslips and remained either untreated (unstressed) or were treated with 1 µg/mL TM for 12 h before fixation and immunostaining. F-actin and the nuclei were stained by Phalloidin and Hoechst, respectively. VapA was used as a reticular ER marker and GM130 was used to visualize the cis-Golgi. In WT and KO cells, TM treatment did not affect the morphology of actin filaments and nuclei. However, differences were observed concerning the Golgi and ER morphology (Fig. 17, top). The Golgi increased in size and appeared more fragmented compared to unstressed WT cells. In line with that, the ER also showed a more fragmented phenotype. Interestingly, in KO cells the ER appeared fragmented already under unstressed conditions and induction of ER stress further increased ER fragmentation (Fig. 17, bottom). Considering that, XBP1 seems to be important for maintenance of the ER and Golgi morphology under unstressed and ER stress conditions.

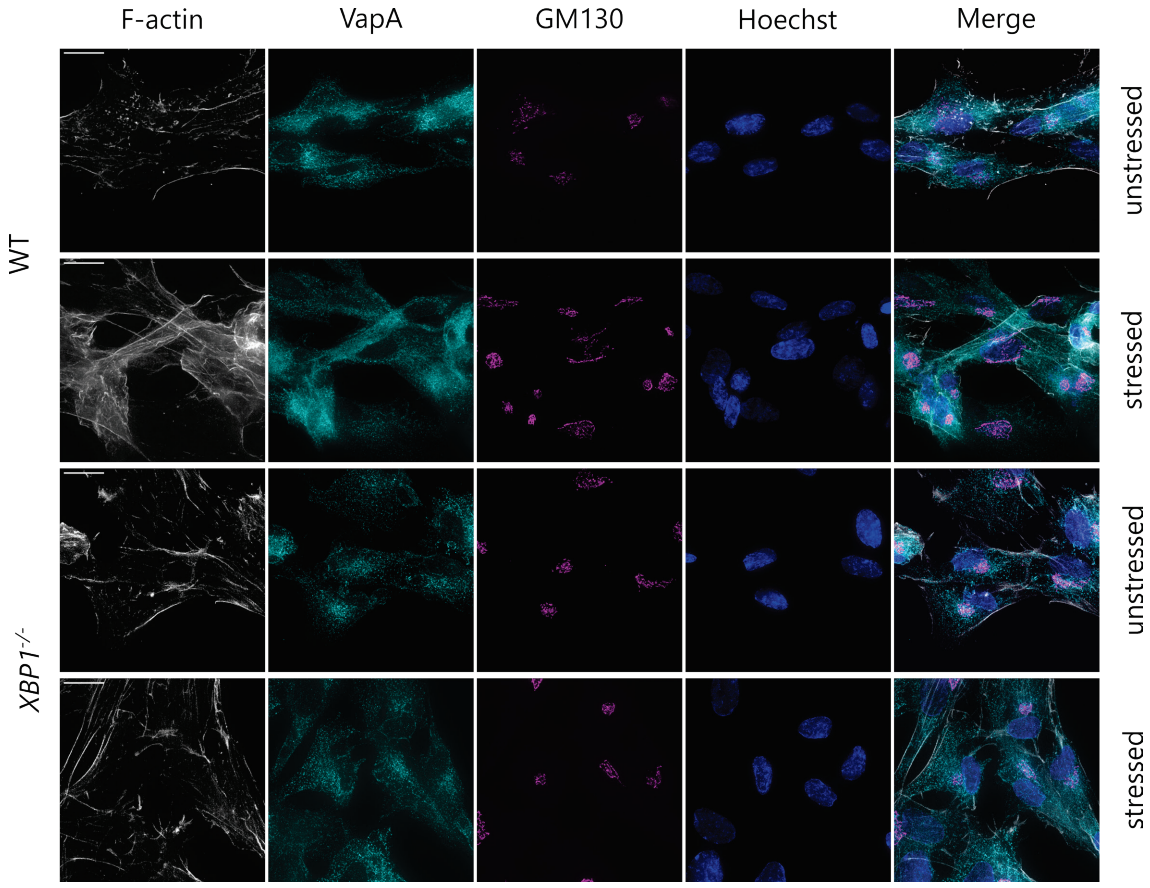

Figure 17: The ER and Golgi morphology is altered in RPE1 *XBP1*$^{-/-}$ cells

Morphology analysis of actin, ER, Golgi and nuclei in RPE1 WT and *XBP1* KO cells by immunofluorescence microscopy. Cells were seeded on coverslips. TM (1 µg/mL) was added for 12 h in order to induce ER stress. Afterwards cells were fixed and stained. Phalloidin and Hoechst were used to stain actin and nuclei, respectively. VapA was used as a marker for the reticular ER and GM130 as a marker of the cis-Golgi. Shown are maximum projections of representative images. Scale bars correspond to 15 µm.

2.7.4. XBP1^{u} is sufficient to restore ER stress induced aberrations in ER morphology

Interestingly, even in untreated *XBP1* KO cells the ER morphology deviates from the one in WT cells, which indicates that the ER is already restructured at basal ER stress levels. It remains to be answered if the expression of XBP1^{u} is sufficient to complement this phenotype. To address this question, a detailed analysis of the ER morphology in WT, KO_1 and KO_2 cells was performed. For this purpose, unstressed as well as stressed cells (1 µg/mL TM) were fixed and the ER immunostained for fluorescence microscopy analysis. Under unstressed

conditions, the ER in KO_1 and KO_2 showed increased fragmentation in comparison to the WT control. In addition, a reduced ER density was observed (Fig. 18a, top). This phenotype became even more pronounced in KO cells treated with TM for 12 h, whereas the WT ER did not show increased fragmentation under these conditions (Fig. 18a, bottom). Subsequently, the integrated ER densities for WT, KO_1 and KO_2 were calculated. As a basis for this, a brightness threshold of 1000 was applied to single plane images and an ROI selected in which the integrated density (IntDen) was measured. The ER density was monitored in the course of ER stress treatment (0 h, 3 h, 6 h, 12 h). Under unstressed conditions the mean IntDen in KO_1 was only slightly reduced in comparison to WT. KO_2, on the other hand, showed significant differences to WT. Starting from 6 h of stress induction, both KO cell lines showed significant differences to WT, which had an approximately twofold increased ER density (Fig. 18b). These observations strongly indicate that the deletion of *XBP1* affects ER morphology in particular under prolonged ER stress exposure.

Lastly, it was tested whether expression of either $XBP1^s$ or $XBP1^u$ is sufficient to restore ER morphology. To do so, the ER of WT, KO and $XBP1^s$/$XBP1^u$ rescue cell lines was analyzed via fluorescence microscopy differentiating between extended (as in WT) and fragmented ER (as shown in KO in Fig. 18a). Under unstressed conditions, an extended ER was observed in approximately 70 % of the WT, 80 % of the KO_1 and 40 % of the KO_2 cells. Surprisingly, only 30 % of the KO cells expressing $XBP1^s$ showed an extended ER, whereas this was the case for 70 % of $XBP1^u$ rescue cells.

Figure 18: Deletion of *XBP1* leads to an increase of fragmented ER and a decrease of ER density

Qualitative and quantitative analysis of the ER morphology in WT, KO and $XBP1^s$/$XBP1^u$ rescue cells. (a) Micrographs of WT and KO under unstressed and stressed (1 µg/mL TM for 12 h) conditions. VapA was used as a marker of the reticular ER. Scale bars represent 15 µm. (b) Scatter plots of the IntDen of the ER in WT, KO_1 and KO_2 after 0 h, 3 h, 6 h and 12 h TM treatment. Brightness threshold was set to 1000 for density measurements. Significance levels are based on Dunn's multiple comparisons test. (c) Rating of extended and fragmented ER in WT, KO and $XBP1^s$/$XBP1^u$ rescue cell lines.

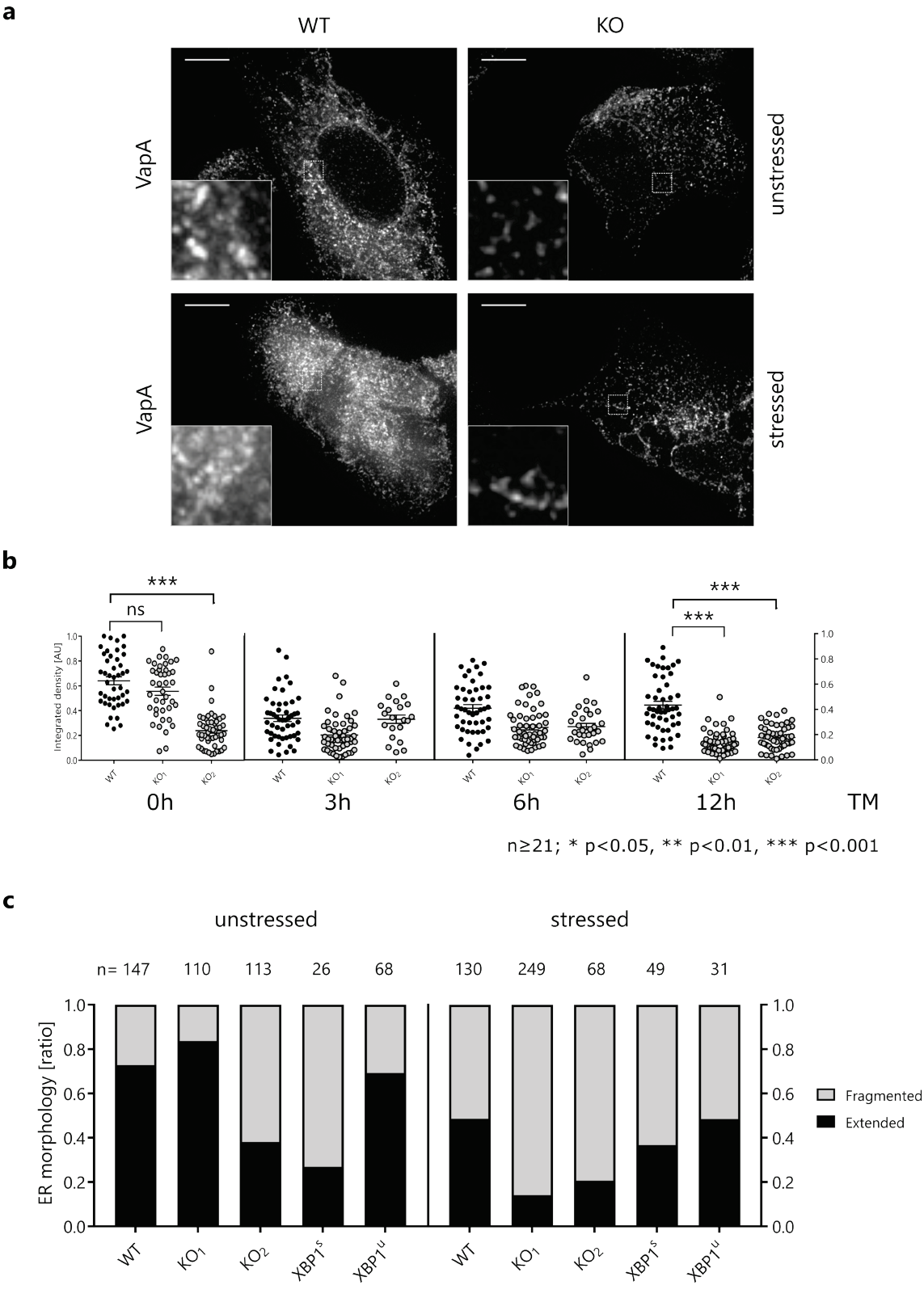
a
WT
KO
VapA
unstressed
VapA
stressed
b
***
ns
***
***
Integrated density [AU]
WT
KO1
KO2
0h
3h
6h
12h
TM
n≥21; * p<0.05, ** p<0.01, *** p<0.001
c
unstressed
stressed
n= 147
110
113
26
68
130
249
68
49
31
ER morphology [ratio]
Fragmented
Extended
WT
KO1
KO2
XBP1s
XBP1u

Due to the fact that KO_1 and KO_2 show very different ER morphologies, it is difficult to draw conclusions with respect to $XBP1^u$ functionality. Still, expression of $XBP1^s$ under unstressed conditions did not have a positive impact on the ER. Under stressed conditions (12 h TM treatment), an increased number of cells showed a fragmented ER morphology compared to WT. This was suppressed by the expression $XBP1^s$ and fully rescued by $XBP1^u$ (Fig. 18c). Thus, $XBP1^u$ appears to have important functions to maintain ER morphology under these conditions.

Taken together, it was shown that clonogenic survival and ER stress resistance were reduced in KO cells. Moreover, the number of presumably apoptotic cells was increased. On a cellular level, alterations compared to WT were noticed, such as a fragmented and less dense ER. Importantly, all these phenotypes can be at least partially rescued by $XBP1^u$. Yet, how $XBP1^u$ functions on a mechanistic level remains unresolved. Since DNA-binding and transcriptional activity were dispensable in this process, the data strongly suggest a previously undescribed mode of action for $XBP1^u$.

It is important to note that the ER stress response in higher eukaryotes is not only regulated by the IRE1-XBP1 pathway but also by the PERK and ATF6 signaling pathways. Hence, the function of the $XBP1^u$ regulator might include an interplay with the latter two UPR branches. To distinguish between these possibilities and to test for a putatively conserved function, the role of the $XBP1^u$ homolog $Cib1^u$ was characterized in *U. maydis.* In this fungus the UPR is exclusively regulated by the IRE1 pathway, which facilitates the functional analysis independent of the crosstalk between additional UPR branches.

2.8. Characterization of *U. maydis* Cib1 on a physiological level

The UPR in the filamentous fungus *U. maydis* is exclusively regulated by the IRE1 signaling pathway. Induction of ER stress gives rise to the bZIP transcription factor $Cib1^s$ regulating the expression of UPR target genes. Under unstressed conditions, the *cib1* pre-mRNA remains unspliced. Despite the presence of the

65 nt intron, the pre-mRNA is translated into Cib1^{u}, which is rather unique among fungi (Hampel, 2016; Heimel et al., 2013).

2.8.1. **Cib1^{u} restores ER stress resistance in a dose-dependent manner**

Up until now, Cib1^{u} was demonstrated to counteract UPR hyperactivation. Furthermore, preliminary data indicate that Cib1^{u} has a Cib1^{s}-independent impact on the ER stress response (Hampel, 2016; Heimel et al., 2013). However, the molecular details remain to be discovered. For that reason, first it was determined under which conditions Cib1^{u} exerts its regulatory function. Therefore, cell growth of a *U. maydis* WT strain (SG200), a *cib1* deletion strain (Δ*cib1*) and two Δ*cib1* strains containing either a single copy (s) or multiple copies (m) of *cib1^{us}* expressed under the control of the constitutive *etef* promoter were analyzed on YNB plates (Fig. 19b, -TM). The *cib1^{us}* gene introduced is a mutated version in which the secondary structure is altered and unconventional splicing prevented. The resulting Cib1^{u} protein is identical to the protein expressed from the wild type gene (Hampel, 2016). As a control, a Δ*cib1* strain was used, which harbors the wild type gene *cib1* (Fig. 19a, -TM). As expected, neither the Δ*cib1* strain, nor its derivatives showed reduced growth under unstressed conditions, confirming that Cib1 per se is dispensable for cell growth under these conditions (Fig. 19a, b, -TM). Next, cell growth of those strains was tested on solid media supplemented with 0.6 µg/mL TM. The *cib1* deletion mutant showed reduced ER stress resistance compared to WT. This hypersensitivity to ER stress was fully suppressed by the expression of *cib1* and partly complemented by Cib1^{u}. Interestingly, the degree of complementation seemed to be dependent on the quantity of Cib1^{u}. The Δ*cib1 cib1^{us}* (m) strain showed an increased ER stress resistance in comparison to Δ*cib1 cib1^{us}* (s) (Fig. 19a, b, +TM). These results demonstrate that Cib1^{u} is able to partially suppress ER stress susceptibility of Δ*cib1* strains. However, it remains unexplained how Cib1^{u} mediates this function. Initially, an involvement of the bZIP domain, which is identical in Cib1^{s} and Cib1^{u}, was analyzed. Assuming ER stress resistance was mediated on a transcriptional level, the mutated bZIP domain should prevent regulation and suppression of ER stress susceptibility. The basic domain responsible for binding to DNA was mutated by replacing all arginines with alanines. Afterwards, the mutated

constructs *bZIP* cib1*^{s} (intron removed) and *bZIP* cib1*^{us} (unspliceable) were introduced into SG200 Δ*cib1* and cell growth as well as ER stress resistance were tested.

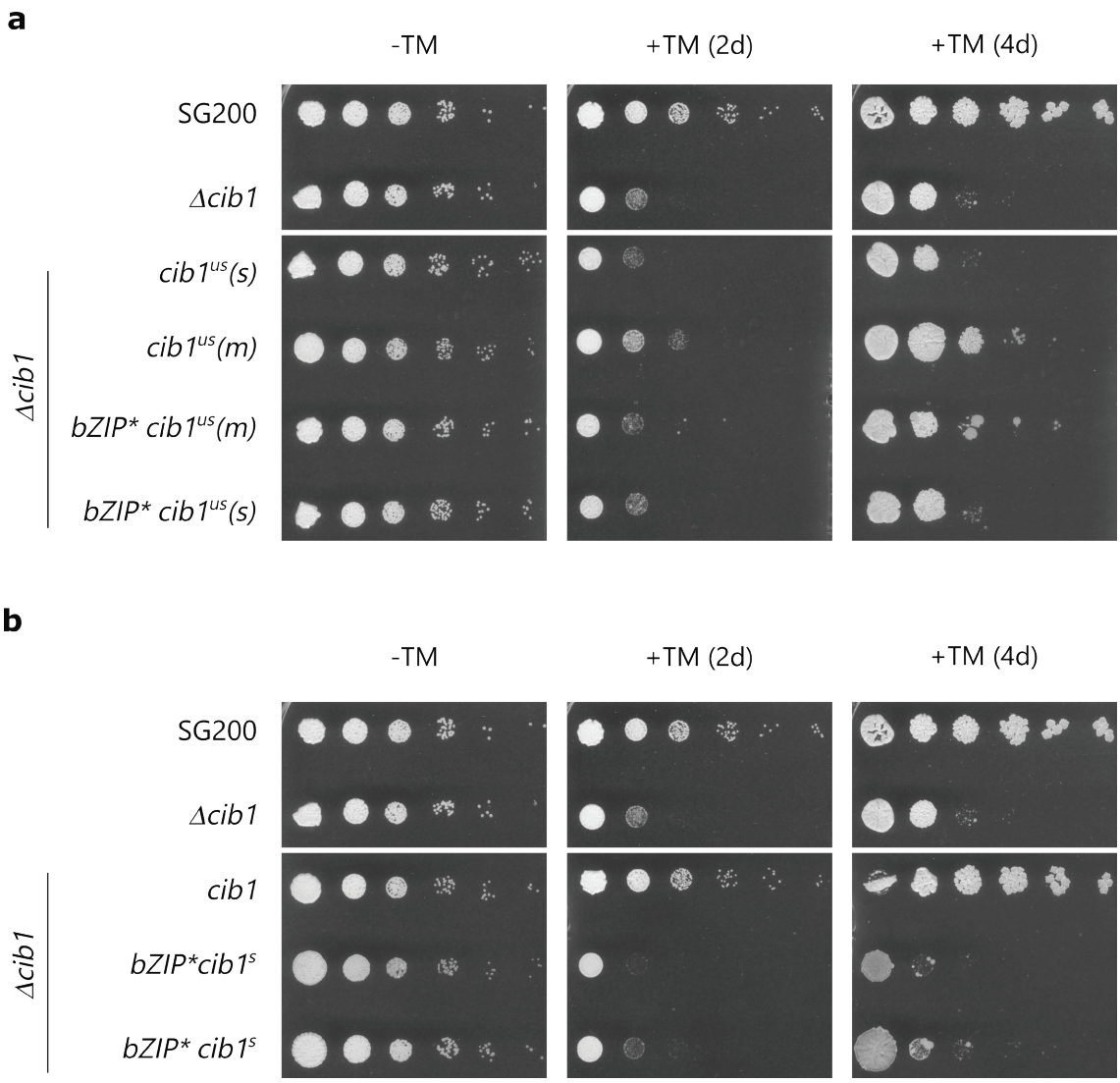

Figure 19: bZIP domain of Cib1^{u} is dispensable for mediating ER stress resistance

Analysis of cell growth and ER stress resistance in WT and derivatives. (a) Serial 10-fold dilutions of WT, Δ*cib1* and Δ*cib1 cib1*^{us} strains were spotted on YNB plates supplemented with glucose as carbon source. ER stress was induced by 0.6 µg/mL TM. Plates were incubated at 28°C. (b) Serial 10-fold dilutions of WT, Δ*cib1* and Δ*cib1 cib1*^{s} strains were spotted on YNB plates supplemented with glucose as carbon source. ER stress was induced by 0.6 µg/mL TM. Plates were incubated at 28°C.

The mutated bZIP domain in Cib1^{s} and in Cib1^{u} did not affect cell growth under unstressed conditions. However, the bZIP domain was essential for the functionality of Cib1^{s} but not of Cib1^{u} under ER stress conditions (Fig. 19). These observations suggest that Cib1^{s} mediates resistance to ER stress on a transcriptional level, whereas Cib1^{u} rather acts on a post-transcriptional level.

2.8.2. **Deletion of *cib1* has no influence on the cell cycle during vegetative growth**

Under optimal environmental conditions *U. maydis* has a doubling time of approximately 120 minutes. A very short G1-phase is distinctive for its cell cycle and S-phase begins shortly after cytokinesis.

Similar to other organisms, *U maydis* adjusts its cell cycle when adapting to different environmental conditions. Under starvation conditions, for example, the generation time is prolonged as a result of longer G1- and G2-phases (Pérez-Martín et al., 2006). In an effort to analyze the impact of the UPR on the cell cycle, exponentially grown WT and Δ*cib1* cells under unstressed and stressed conditions were analyzed via flow cytometry. To minimize experimental variations and to be able to analyze unstressed and stressed (1.5 µg/mL for 4 h) WT cells as well as unstressed and stressed (1.5 µg/mL for 4 h) Δ*cib1* cells as one sample each, cells were labeled with different concentrations of Pacific Blue. This barcoding procedure which enhances the comparability of the cell cycle profiles, was applied before combining and staining the DNA with Sytox Green. No significant differences were observed between the cell cycle profiles of WT and Δ*cib1* cells under unstressed conditions. Upon induction of ER stress, cells peaking into the G1-phase disappeared, while the number of cells with a more than 2C DNA content increased equally in WT and Δ*cib1* strains (Fig. 20). All in all, these results suggest that induction of ER stress, most probably independent from Cib1, provokes changes in the cell cycle.

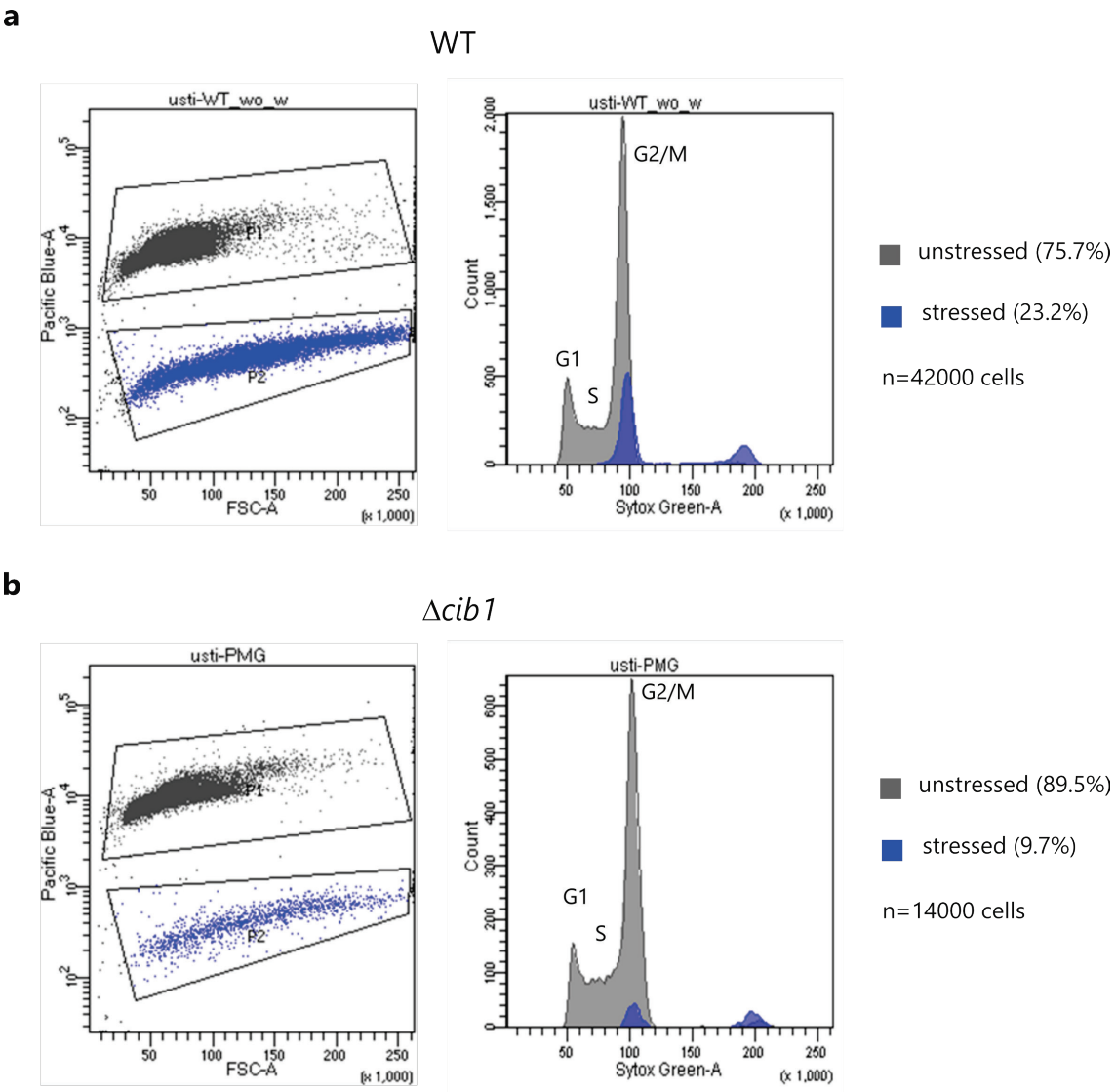

Figure 20: ER stress induction provokes changes in cell cycle

Analysis of the cell cycle in SG200 and SG200 Δ*cib1* under unstressed and stressed (1.5 µg/mL for 4 h) conditions via flow cytometry. (a) Scatter plot of FSC area versus Pacific Blue area of WT unstressed (grey, 75.7 %) and WT stressed (blue, 23.2 %) cells (left). Sytox Green area histograms of DNA content show G1-, S- and G2/M-phases of the cell cycle (right). 42000 cells were analyzed. (b) Scatter plot of FSC area versus Pacific Blue area of Δ*cib1* unstressed (grey, 89.5 %) and Δ*cib1* stressed (blue, 9.7 %) cells (left). Sytox Green area histograms of DNA content show G1-, S- and G2/M-phases of the cell cycle (right). 14000 cells were analyzed.

2.8.3. **Reduced virulence of the SG200 *cib1* deletion strain cannot be rescued by Cib1^{u}**

The UPR regulates biotrophic development in *U. maydis*. The exact timing of

UPR activation is decisive for virulence, which is reduced in case of premature activation. Also, the deletion of *cib1* results in the loss of virulence and subsequently in weak plant disease symptoms (Heimel et al., 2013). At this point, in order to investigate if expression of Cib1^{u} is sufficient to restore virulence and to determine to which extent the bZIP domain is required for that, maize plant infection assays were performed.

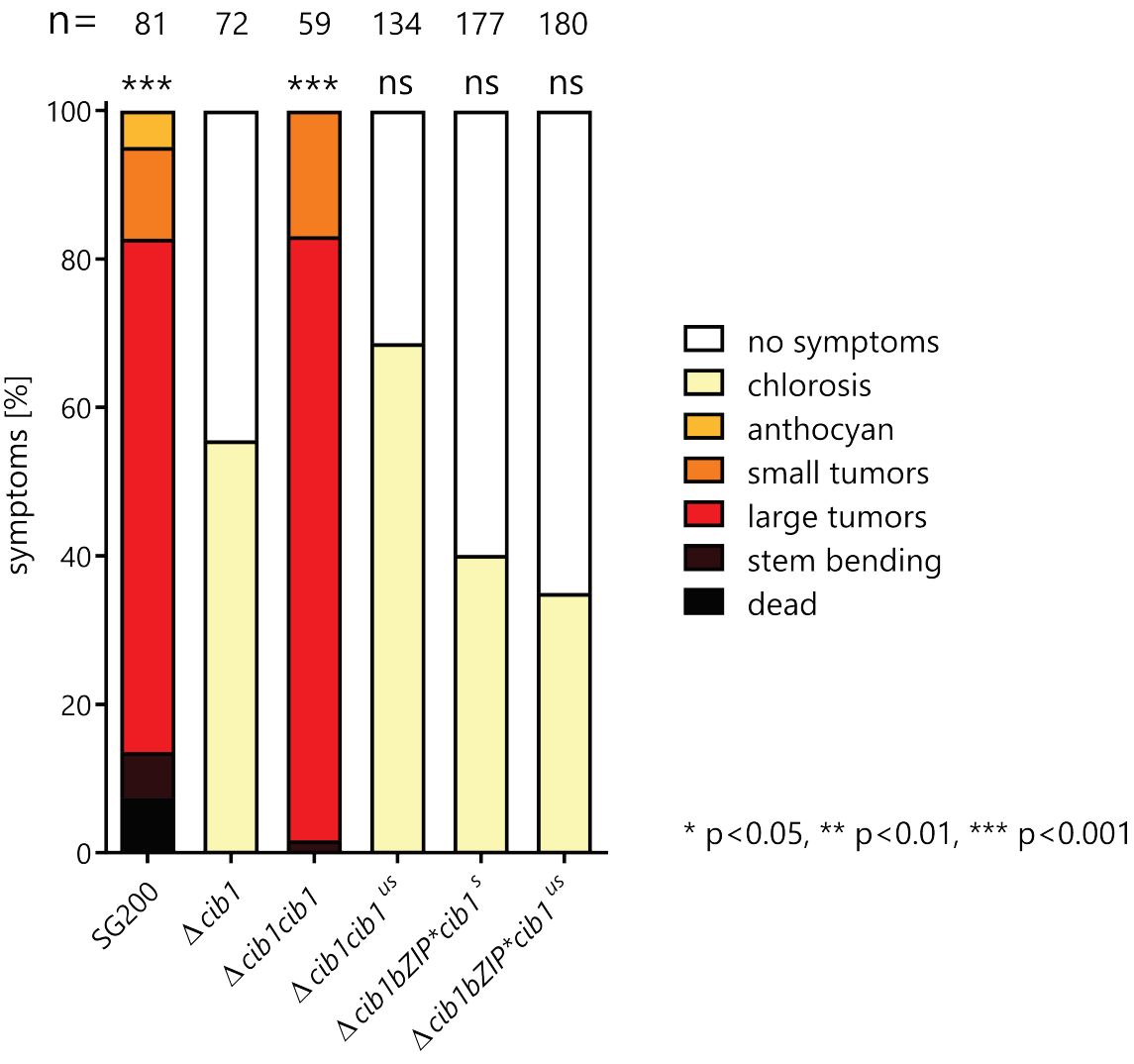

Figure 21: Cib1^{u} is not able to restore virulence in *cib1* deletion strains

Maize plant infection assays of SG200 and derivatives. *U. maydis* strains were inoculated into 8 days old maize seedlings. Disease symptoms were rated 8 days after inoculation. Assays were performed with three biological replicates each. n corresponds to the number of infected plants. Statistical significance levels are based on Dunn's multiple comparisons test.

To this end, the haploid pathogenic strain SG200, which infects plants without prior mating, and its derivatives were used (Kämper et al., 2006). As expected, virulence of SG200 Δ*cib1* was significantly reduced in comparison to SG200. SG200 Δ*cib1 cib1* but not SG200 Δ*cib1 cib1*^{us} displayed complementation of the virulence defect indicating that Cib1^{u} is not sufficient for this purpose. SG200 Δ*cib1 bZIP* cib1*^{us} displayed slightly weaker infection symptoms compared to SG200 Δ*cib1 cib1*^{us}. However, the mutated bZIP domain in Cib1^{s} had a strong influence on the fungal virulence, confirming that the transcriptional activity of Cib1^{s} is crucial for virulence (Fig. 21).

2.9. Characterization of *U. maydis* Cib1 on a transcriptional level

Under ER stress conditions, the UPR is activated and regulates the expression of UPR target genes. This contributes to the maintenance of ER homeostasis. In *U. maydis* the bZIP transcription factor Cib1^{s} mediates the transcriptional response to ER stress (Heimel et al., 2013).

2.9.1. Cib1^{u} is not involved in the transcriptional regulation of common UPR target genes

The bZIP domain in Cib1^{s} and Cib1^{u} is identical. However, transcriptional activity has only been described for Cib1^{s} (Hampel, 2016). Initially, in order to investigate if Cib1^{u} is also involved in regulating the ER stress response on a transcriptional level, the expression of common UPR target genes was analyzed in SG200 Δ*cib1 cib1*^{us} under unstressed and stressed (3 µg/mL TM for 4 h) conditions via qRT-PCR. Subsequently, it was tested to what extent bZIP domain mutations, which prevent binding to DNA, would affect expression of UPR targets. For that, expression levels of UPR target genes were analyzed in SG200 Δ*cib1* bZIP* *cib1*^{us} via qRT-PCR. The expression of the following five genes that code for ER chaperones, a protein disulfide isomerase and a signal peptide peptidase, was examined: *bip1*, *cne1*, *lhs1*, *mpd1* and *spp1* (Heimel et al., 2013). As already described in Hampel, 2016, expression of the UPR targets

was exclusively dependent on Cib1^{s} under both unstressed and stressed conditions. Expression of Cib1^{u} in Δ*cib1* did not influence their transcript levels. Mutations in the bZIP domain of Cib1^{u} did not elicit any difference (SG200 Δ*cib1* bZIP* *cib1^{us}*). Merely, the mutated bZIP domain in Cib1^{s} (SG200 Δ*cib1* bZIP* *cib1^{s}*) impeded the induction of target gene expression (Fig. 22).

Collectively, these results strongly indicate that Cib1^{u} does not play a role in the transcriptional regulation of the ER stress response.

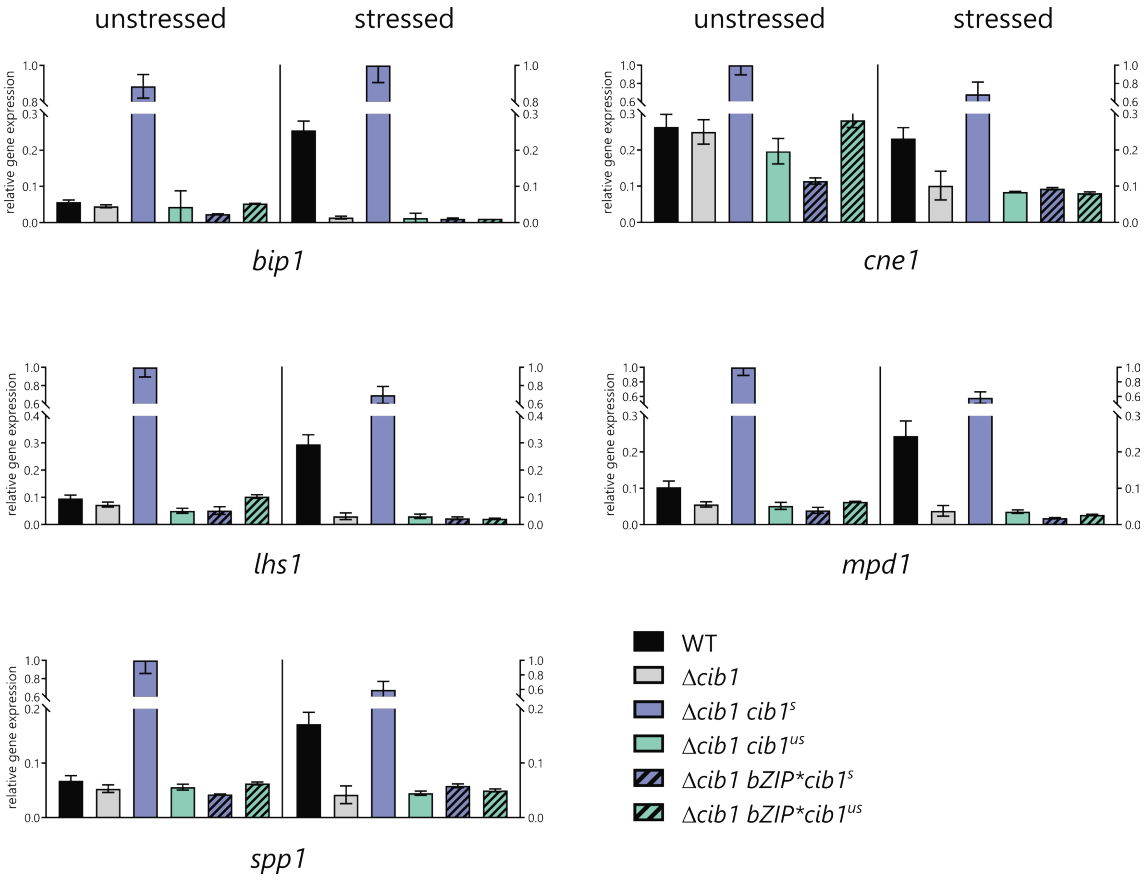

Figure 22: Cib1^{u} does not induce expression of common UPR target genes

Characterization of UPR target gene expression in SG200 and derivatives via qRT-PCR. Expression was analyzed in unstressed cells and cells in which ER stress was induced with 3 µg/mL TM for 4 h (stressed). *eIF2b* was used for normalization of the relative gene expression. Expression values are from one representative experiment with two technical replicates each. Error bars represent SEM.

2.9.2. **Transcriptome-wide analysis of Cib1^{u}-regulated genes**

So far, no Cib1^{u}-dependent regulation of common UPR target genes has been identified (Hampel, 2016). This supports the observation that ER stress resistance can be mediated by Cib1^{u} with a mutated bZIP domain. However, it cannot be completely ruled out that Cib1^{u} affects the expression of other genes in response to ER stress. In order to distinguish among these possibilities, RNAseq analysis was performed. To this end, the transcriptomes of SG200, SG200 Δ*cib1* and SG200 Δ*cib1 cib1^{us}* were analyzed under unstressed and stressed (5 µg/mL TM for 4 h) conditions. For the analysis, log2 fold changes of reads per kilobase million (RPKM) expression values were computed via MultiDESeq2. RPKM values are calculated by dividing the number of reads mapped to a gene by the product of the total number of mapped reads from a given library and the gene length in bp. Based on these, comparisons between SG200, SG200 Δ*cib1* und SG200 Δ*cib1 cib1^{us}* under unstressed and stressed conditions were made. Only genes with at least twofold up- or down-regulation in those comparisons were included. First of all, gene expression upon stress induction was explored. In SG200, 645 genes were differentially regulated between unstressed and stressed growth conditions (Fig. 23a). In a Functional Catalogue (FunCat) analysis, the identified genes were mapped to a variety of cellular processes ranging from ER to Golgi transport to enzyme inhibition (Fig. 23c). These data clearly suggest that upon stress induction not only the expression of the well-studied UPR target genes changes, but also the expression of numerous others is up-or downregulated. 320 of the 645 genes found are WT-specific, 40 were shared with SG200 Δ*cib1* and 17 with SG200 Δ*cib1 cib1^{us}*. However, among the latter, four genes were upregulated in SG200 and downregulated in SG200 Δ*cib1 cib1^{us}* and vice versa (Fig. 23b). These include *um06467*, *um00013*, *um11083* and *um05352*. *um06467* encodes an Ustilagic acid glycosyl transferase, *um11083* a protein related to p24, *um05352* a disulfide isomerase related protein and *um00013* a yet uncharacterized protein.

Surprisingly, comparing Δ*cib1* and SG200 Δ*cib1 cib1^{us}* there were 787 genes similarly expressed, none of them in opposite direction (Appendix C). This observation is emphasized by looking at the FunCat results, where multiple

overlaps like ribosome biogenesis, translation and secondary metabolism were ranked highest in both Δ*cib1* and SG200 Δ*cib1 cib1*^{us} (Fig. 23c). Hence, upon stress induction, SG200 Δ*cib1 cib1*^{us} more closely resembles SG200 Δ*cib1* than SG200 with respect to gene expression.

Figure 23: After ER stress induction expression of several other genes besides known UPR targets is changed

Analysis of transcriptome-wide changes in gene expression upon ER stress induction. (a) Venn diagram of differentially expressed genes in WT (black), SG200 Δ*cib1* (grey), SG200 Δ*cib1 cib1*^{us} (turquoise). The diagram only includes genes for which the expression is increased or decreased by at least 1 on a log2 scale. (b) Bar chart of RPKM log2 fold changes. (c) Functional categories (FunCat) analysis of differentially expressed genes.

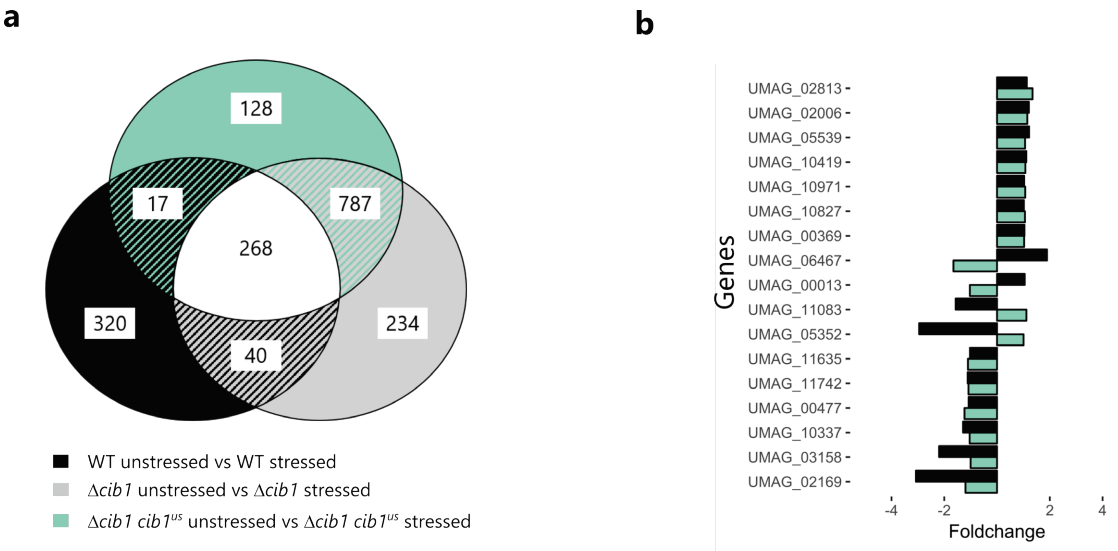

c

WT unstressed vs WT stressed

FunCat description	Adjusted p-value	# genes / category	# genes / input	# genes / input [%]
ER to Golgi transport	1,15E-07	25 / 72	25 / 645	3,88%
polysaccharide binding	3,82E-04	9 / 17	9 / 645	1,40%
non-vesicular ER transport	3,82E-04	7 / 10	7 / 645	1,09%
polysaccharide metabolism	4,58E-04	23 / 98	23 / 645	3,57%
C-compound and carbohydrate transport	1,06E-03	23 / 104	23 / 645	3,57%
transport facilities	1,92E-03	36 / 211	36 / 645	5,58%
non-vesicular cellular import	1,97E-03	17 / 68	17 / 645	2,64%
secondary metabolism	5,42E-03	40 / 259	40 / 645	6,20%
cellular export and secretion	6,15E-03	20 / 97	20 / 645	3,10%
vesicle formation	9,76E-03	9 / 27	9 / 645	1,40%
C-compound and carbohydrate metabolism	1,07E-02	60 / 459	60 / 645	9,30%
protein transport	1,12E-02	34 / 220	34 / 645	5,27%
sugar binding	1,12E-02	6 / 13	6 / 645	0,93%
drug/toxin transport	1,51E-02	14 / 62	14 / 645	2,17%
intracellular transport vesicles	2,06E-02	9 / 31	9 / 645	1,40%
perception of nutrients and nutritional adaptation	2,57E-02	11 / 45	11 / 645	1,71%
unfolded protein response (e.g. ER quality control)	3,28E-02	14 / 68	14 / 645	2,17%
protein folding and stabilization	3,70E-02	20 / 117	20 / 645	3,10%
heavy metal ion transport (Cu+, Fe3+, etc.)	3,70E-02	10 / 41	10 / 645	1,55%
viral proteins	4,23E-02	3 / 4	3 / 645	0,47%
lysosomal protein degradation	4,23E-02	3 / 4	3 / 645	0,47%
vesicular transport (Golgi network, etc.)	4,45E-02	26 / 172	26 / 645	4,03%
enzyme inhibitor	4,74E-02	6 / 18	6 / 645	0,93%

Δ*cib1* unstressed vs Δ*cib1* stressed

FunCat description	Adjusted p-value	# genes / category	# genes / input	# genes / input [%]
ribosomal proteins	2,23E-17	82 / 156	82 / 1329	6,17%
ribosome biogenesis	1,86E-16	84 / 172	84 / 1329	6,32%
translation	8,34E-07	68 / 166	68 / 1329	5,12%
secondary metabolism	1,42E-04	87 / 259	87 / 1329	6,55%
non-vesicular cellular import	6,19E-06	31 / 68	31 / 1329	2,33%
C-compound and carbohydrate metabolism	6,19E-06	124 / 459	124 / 1329	9,33%
cellular import	8,44E-06	44 / 116	44 / 1329	3,31%
polysaccharide metabolism	2,83E-05	38 / 98	38 / 1329	2,86%
C-compound and carbohydrate transport	4,88E-05	39 / 104	39 / 1329	2,93%
metabolism of amines	4,13E-04	11 / 16	11 / 1329	0,83%
drug/toxin transport	8,63E-04	25 / 62	25 / 1329	1,88%
metabolism of energy reserves (e.g. glycogen, trehalose)	1,76E-03	21 / 50	21 / 1329	1,58%
transport facilities	3,56E-03	59 / 211	59 / 1329	4,44%
biosynthesis of arginine	4,47E-03	9 / 14	9 / 1329	0,68%
extracellular / secretion proteins	5,12E-03	5 / 5	5 / 1329	0,38%
metabolism of urea (urea cycle)	6,60E-03	8 / 12	8 / 1329	0,60%
amine / polyamine transport	7,34E-03	12 / 24	12 / 1329	0,90%
degradation of glutamate	7,34E-03	9 / 15	9 / 1329	0,68%
detoxification	7,91E-03	31 / 96	31 / 1329	2,33%
homeostasis of cations	1,41E-02	13 / 29	13 / 1329	0,98%
sugar, glucoside, polyol and carboxylate catabolism	1,91E-02	34 / 114	34 / 1329	2,56%
vitamine/cofactor transport	1,91E-02	13 / 30	13 / 1329	0,98%
allantoin and allantoate transport	1,91E-02	9 / 17	9 / 1329	0,68%
vacuolar protein degradation	1,91E-02	8 / 14	8 / 1329	0,60%
detoxification by export	2,03E-02	18 / 49	18 / 1329	1,35%
biosynthesis of isoleucine	3,17E-02	7 / 12	7 / 1329	0,53%
metabolism of urea cycle, creatine and polyamines	4,36E-02	5 / 7	5 / 1329	0,38%
biosynthesis of glycine	4,43E-02	9 / 19	9 / 1329	0,68%
heavy metal ion transport (Cu+, Fe3+, etc.)	4,67E-02	15 / 41	15 / 1329	1,13%
biosynthesis of valine	4,95E-02	6 / 10	6 / 1329	0,45%

Δ*cib1 cib1*^{us} unstressed vs Δ*cib1 cib1*^{us} stressed

FunCat description	Adjusted p-value	# genes / category	# genes / input	# genes / input [%]
ribosomal proteins	1,64E-19	83 / 156	83 / 1200	6,92%
ribosome biogenesis	1,10E-14	81 / 172	81 / 1200	6,75%
translation	3,36E-07	67 / 166	67 / 1200	5,58%
secondary metabolism	4,47E-06	88 / 259	88 / 1200	7,33%
C-compound and carbohydrate metabolism	1,88E-06	122 / 459	122 / 1200	10,17%
metabolism of amines	3,64E-05	12 / 16	12 / 1200	1,00%
C-compound and carbohydrate transport	1,76E-04	37 / 104	37 / 1200	3,08%
polysaccharide metabolism	2,60E-04	35 / 98	35 / 1200	2,92%
non-vesicular cellular import	9,94E-04	26 / 68	26 / 1200	2,17%
drug/toxin transport	1,47E-03	24 / 62	24 / 1200	2,00%
biosynthesis of glycine	2,33E-03	11 / 19	11 / 1200	0,92%
assimilation of ammonia, metabolism of the glutamate group	2,33E-03	11 / 19	11 / 1200	0,92%
extracellular / secretion proteins	4,60E-03	5 / 5	5 / 1200	0,42%
vitamine/cofactor transport	4,60E-03	14 / 30	14 / 1200	1,17%
degradation of glutamate	6,23E-03	9 / 15	9 / 1200	0,75%
cellular import	7,24E-03	35 / 116	35 / 1200	2,92%
metabolism of energy reserves (e.g. glycogen, trehalose)	7,57E-03	19 / 50	19 / 1200	1,58%
transport facilities	1,61E-02	54 / 211	54 / 1200	4,50%
polysaccharide binding	1,61E-02	9 / 17	9 / 1200	0,75%
biosynthesis of arginine	1,61E-02	8 / 14	8 / 1200	0,67%
vacuolar protein degradation	1,61E-02	8 / 14	8 / 1200	0,67%
amine / polyamine transport	1,85E-02	11 / 24	11 / 1200	0,92%
degradation of glutamine	2,38E-02	6 / 9	6 / 1200	0,50%
biosynthesis of isoleucine	2,52E-02	7 / 12	7 / 1200	0,58%
metabolism of urea (urea cycle)	2,52E-02	7 / 12	7 / 1200	0,58%
detoxification by export	3,35E-02	17 / 49	17 / 1200	1,42%
metabolism of urea cycle, creatine and polyamines	3,53E-02	5 / 7	5 / 1200	0,42%
cellular export and secretion	3,53E-02	28 / 97	28 / 1200	2,33%
ABC transporters	3,92E-02	16 / 46	16 / 1200	1,33%
biosynthesis of valine	3,92E-02	6 / 10	6 / 1200	0,50%
biosynthesis of glutamate	4,19E-02	11 / 27	11 / 1200	0,92%
chemoperception and response	4,67E-02	14 / 39	14 / 1200	1,17%
degradation of methionine	4,78E-02	4 / 5	4 / 1200	0,33%
allantoin and allantoate transport	4,99E-02	8 / 17	8 / 1200	0,67%

Next, the three strains were compared with each other under unstressed conditions. In short, five genes were differentially expressed plus *cib1,* which is absent in KO, and the *sdh1* gene, in the locus of which *cib1*^{us} was introduced. Thus, under unstressed conditions, there were hardly any transcriptome-wide differences (Fig. 24).

a

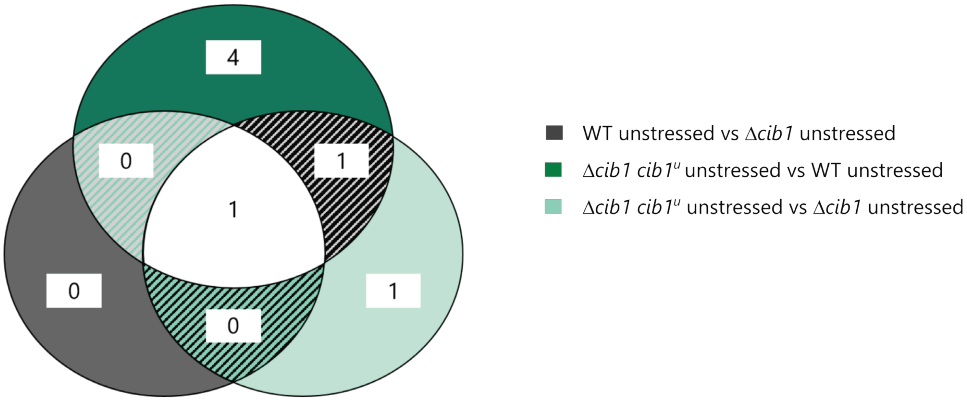

b

stable_id	WT unstressed vs Δ*cib1 cib1* ^{u} unstressed (log2FC)	Gene description
um11782	-3,230920627	Cib1
um00844	-2,445696401	succinate dehydrogenase [ubiquinone] iron-sulfur protein, mitochondrial precursor
um02139	-1,19762419	effector family protein Eff1-9
um11249	-1,129674163	related to cyclopropane-fatty-acyl-phospholipid synthase
um03411	-1,013913164	probable endo-1,4-beta-xylanase
um03138	1,083221495	hypothetical protein

stable_id	WT unstressed vs Δ*cib1* unstressed (log2FC)	Gene description
um11782	3,896185075	Cib1

stable_id	Δ*cib1 cib1*^{u} unstressed vs Δ *cib1* unstressed (log2FC)	Gene description
um11782	7,135180882	Cib1
um00844	2,472210911	succinate dehydrogenase [ubiquinone] iron-sulfur protein, mitochondrial precursor
um00842	1,118023714	probable aflatoxin efflux pump AFLT

Figure 24: Deletion of *cib1* has marginal influence on the transcriptome under unstressed conditions

Analysis of differentially expressed genes comparing SG200, SG200 Δ*cib1* and SG200 Δ*cib1 cib1*^{us} with each other under unstressed conditions. (a) Venn diagram of differentially expressed genes. The diagram only includes genes for which the expression is increased or decreased by at least 1 on a log2 scale. (b) Lists of differentially expressed genes including RPKM log2 fold changes.

Finally, the same comparisons were made under stressed conditions. 12 genes were differentially expressed in both SG200 and SG200 Δ*cib1 cib1*^{us} compared to SG200 Δ*cib1* (Fig. 25a).

Figure 25: Transcriptome of SG200 Δ*cib1 cib1*^{us} more closely resembles the one of SG200 Δ*cib1* compared to SG200

Analysis of differentially expressed genes comparing SG200, SG200 Δ*cib1* and SG200 Δ*cib1 cib1*^{us} with each other under stressed conditions. (a) Venn diagram of differentially expressed genes. The diagram only includes genes for which the expression is increased or decreased by at least 1 on a log2 scale. (b, c, d) Bar charts of RPKM log2 fold changes from selected intersections. (e, f, g, h). Functional categories (FunCat) analysis of differentially expressed genes.

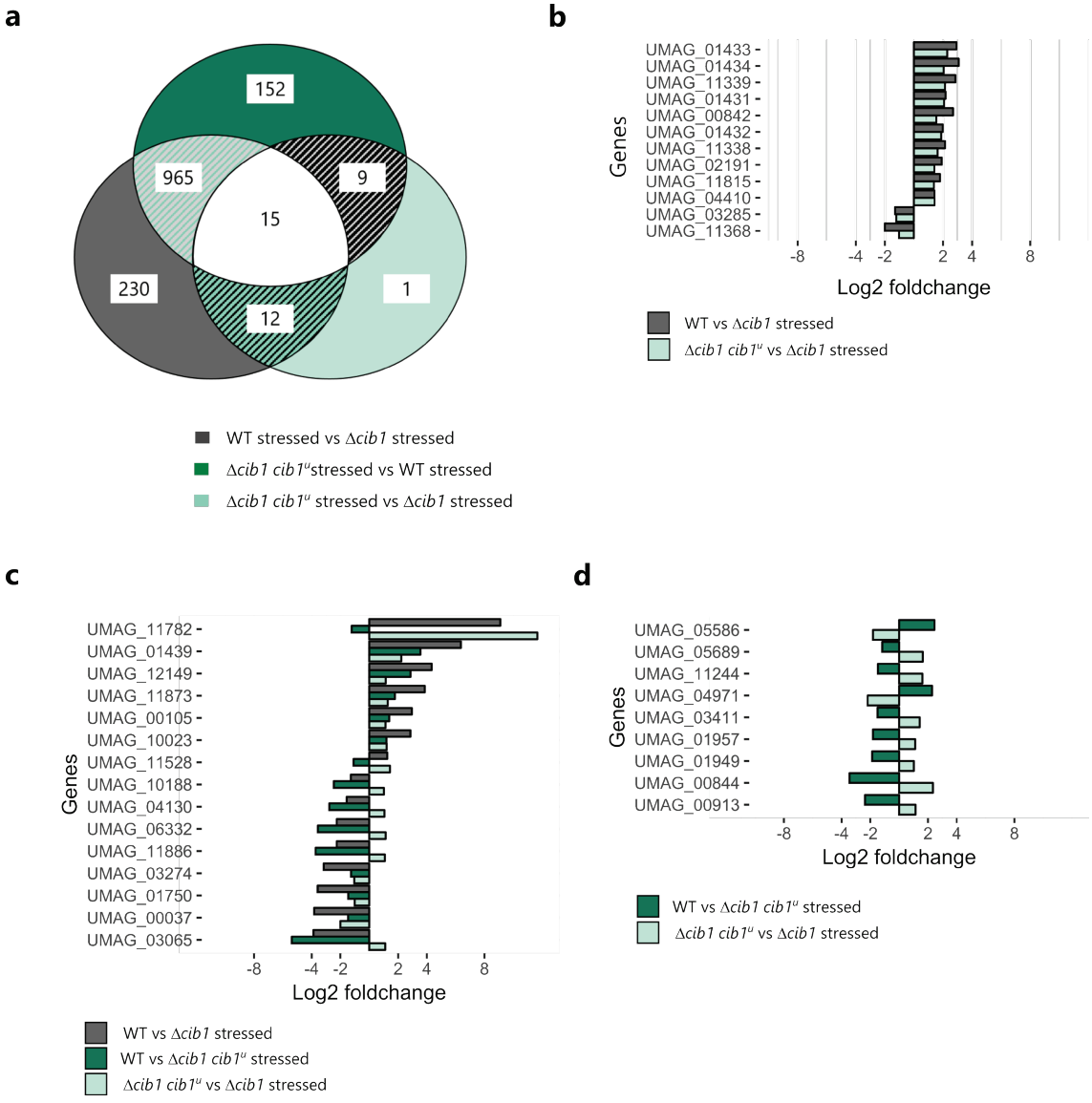

e

Intersection WT stressed vs Δ*cib1* stressed & WT stressed vs Δ*cib1 cib1*^{u} stressed

FunCat description	Adjusted p-value	# genes / category	# genes / input	# genes / input [%]
C-compound and carbohydrate metabolism	5,58E-07	113 / 459	113 / 965	11,71%
C-compound and carbohydrate transport	9,07E-06	41 / 104	41 / 965	4,25%
secondary metabolism	1,78E-03	68 / 259	68 / 965	7,05%
cellular export and secretion	3,09E-03	35 / 97	35 / 965	3,63%
polysaccharide metabolism	1,34E-06	34 / 98	34 / 965	3,52%
transport facilities	1,37E-05	54 / 211	54 / 965	5,60%
non-vesicular cellular import	9,31E-05	24 / 68	24 / 965	2,49%
ER to Golgi transport	2,60E-04	24 / 72	24 / 965	2,49%
detoxification by export	8,01E-04	18 / 49	18 / 965	1,87%
non-vesicular ER transport	2,02E-03	7 / 10	7 / 965	0,73%
drug/toxin transport	2,02E-03	20 / 62	20 / 965	2,07%
cellular import	3,29E-03	30 / 116	30 / 965	3,11%
chemoperception and response	2,25E-02	13 / 39	13 / 965	1,35%
vitamine/cofactor transport	2,25E-02	11 / 30	11 / 965	1,14%
detoxification	2,25E-02	24 / 96	24 / 965	2,49%
extracellular / secretion proteins	3,23E-02	4 / 5	4 / 965	0,41%
degradation of glutamate	3,24E-02	7 / 15	7 / 965	0,73%
virulence, disease factors	3,24E-02	7 / 15	7 / 965	0,73%
resistance proteins	3,24E-02	11 / 32	11 / 965	1,14%
amine / polyamine transport	4,17E-02	9 / 24	9 / 965	0,93%
sugar, glucoside, polyol and carboxylate catabolism	4,22E-02	26 / 114	26 / 965	2,69%
fermentation	4,34E-02	7 / 16	7 / 965	0,73%

f

Intersection WT stressed vs Δ*cib1* stressed & Δ*cib1 cib1*^{u} stressed vs Δ*cib1* stressed

FunCat description	Adjusted p-value	# genes / category	# genes / input	# genes / input [%]
drug/toxin transport	5,89E-04	4 / 62	4 / 12	33,33%
secondary metabolism	6,91E-03	5 / 259	5 / 12	41,67%
siderophore-iron transport	1,48E-02	2 / 20	2 / 12	16,67%

g

Intersection WT stressed vs Δ*cib1* stressed & WT stressed vs Δ*cib1 cib1*^{u} stressed & Δ*cib1 cib1*^{u} stressed vs Δ*cib1* stressed

FunCat description	Adjusted p-value	# genes / category	# genes / input	# genes / input [%]
siderophore-iron transport	5,54E-05	3 / 20	3 / 15	20,00%
heavy metal ion transport (Cu+, Fe3+, etc.)	2,56E-04	3 / 41	3 / 15	20,00%
homeostasis of metal ions (Na, K, Ca etc.)	3,69E-03	3 / 114	3 / 15	20,00%
extracellular lignin degradation	4,15E-02	1 / 5	1 / 15	6,67%
inorganic chemical agent resistance (e.g. heavy metals)	4,15E-02	1 / 7	1 / 15	6,67%
cellular import	4,15E-02	2 / 116	2 / 15	13,33%
anaerobic respiration	4,15E-02	1 / 9	1 / 15	6,67%
metabolism of melanins	4,15E-02	1 / 9	1 / 15	6,67%
amino acid metabolism	4,56E-02	2 / 138	2 / 15	13,33%

h

Intersection Δ*cib1 cib1*^{u} stressed vs Δ*cib1* stressed & WT stressed vs Δ *cib1 cib1*^{u} stressed

FunCat description	Adjusted p-value	# genes / category	# genes / input	# genes / input [%]
electron transport and membrane-associated energy conservation	1,09E-02	3 / 79	3 / 9	33,33%
tricarboxylic-acid pathway (citrate cycle, Krebs cycle, TCA cycle)	4,57E-02	2 / 45	2 / 9	22,22%

All 12 genes were similarly up- or downregulated and are involved in iron/toxin transport, secondary metabolism as well as in siderophore-iron transport (Fig. 25b, f).

Additionally 965 genes, whose expression in SG200 Δ*cib1* and SG200 Δ*cib1 cib1*^{us} differed from SG200, were identified (Fig. 25a). These genes can be mapped to a wide spectrum of biological processes such as carbohydrate metabolism and transport, secondary metabolism and cellular export and secretion (Fig. 25e). Comparing the gene expression in SG200 Δ*cib1 cib1*^{us} and SG200 Δ*cib1* only 37 genes were differentially expressed, whereas 1141

differentially expressed genes were identified comparing SG200 and SG200 Δ*cib1 cib1*^{us} (Fig. 25a). Hence, the transcriptome of SG200 Δ*cib1 cib1*^{us} highly resembles the one of SG200 Δ*cib1* indicating that Cib1^{u} most likely does not assume a major transcriptional function related to ER stress response. 15 genes, which were differentially expressed in SG200, SG200 Δ*cib1 cib1*^{us} and SG200 Δ*cib1*, were discovered and mapped to a variety of cellular processes ranging from siderophore-iron transport to secondary metabolism (Fig. 25a, g). Among these, the RPKM log2 fold changes of *um10188*, *um04130*, *um06332*, *um11886* and *um03065* were higher in SG200 Δ*cib1 cib1*^{us} than in SG200 and SG200 Δ*cib1* indicating that Cib1^{u} may potentially assume an inducing role in those cases. The RPKM log2 fold changes of *um01439*, *um12149*, *um11873*, *um00105* and *um10023* in SG200 Δ*cib1 cib1*^{us} were higher than in SG200 Δ*cib1* but lower than in SG200, suggesting that in these cases Cib1^{u} is involved in the regulation of their gene expression but not to the same extent as in SG200 (Fig. 25c). Remarkably, all of the characterized genes encode proteins of the siderophore metabolism (Appendix C). In case of *um00037, um03274 and um01750* the RPKM log2 fold changes were higher in SG200 Δ*cib1* compared to SG200 Δ*cib1 cib1*^{us} and SG200, indicating that Cib1^{u} partially reduces their expression. Nine Cib1^{u}-specific regulated genes were discovered, two of them (*um04971*, *um05586*) repressed and seven of them induced (Fig. 25d). These genes code for proteins that, among others, relate to electron transport and membrane-associated energy conservation processes as well as the tricarboxylic acid pathway (Fig. 25h).

All in all, transcriptome-wide analysis revealed only a couple of Cib1^{u}-dependently regulated genes. An obvious connection to the transcriptional regulation of the ER stress response could not be observed.

2.10. Characterization of *U. maydis* Cib1 on a protein level

As opposed to other fungi in which UPR has been investigated, translation of the *cib1* pre-mRNA is not prevented in *U. maydis*. Hence, in the absence of ER stress

the protein Cib1^{u} is produced. Upon activation of IRE1, the *cib1* pre-mRNA is spliced, giving rise to the intron-free *cib1^{s}* mRNA which, in turn, is translated into the bZIP transcription factor Cib1^{s} (Heimel et al., 2013).

2.10.1. **Cib1^{u} is only produced under unstressed conditions**

In higher eukaryotes, the presence of XBP1^{s} mostly precludes the production of XBP1^{u}. In case of prolonged ER stress, both proteins coexist. To determine the ratio of Cib1^{u} in comparison to Cib1^{s} under unstressed and stressed (1 µg/mL TM or 3 mM DTT for 4 h) conditions in *U. maydis,* the quantities of Cib1^{u} and Cib1^{s} in SG200 expressing *3xHA-cib1* controlled by the constitutive *etef* promoter were measured. Surprisingly, under unstressed conditions exclusively 3xHA-Cib1^{u} whereas under stressed conditions only 3xHA-Cib1^{s} was detected. This indicates that induction of ER stress efficiently promotes splicing of the *cib1* pre-mRNA (Fig. 26).

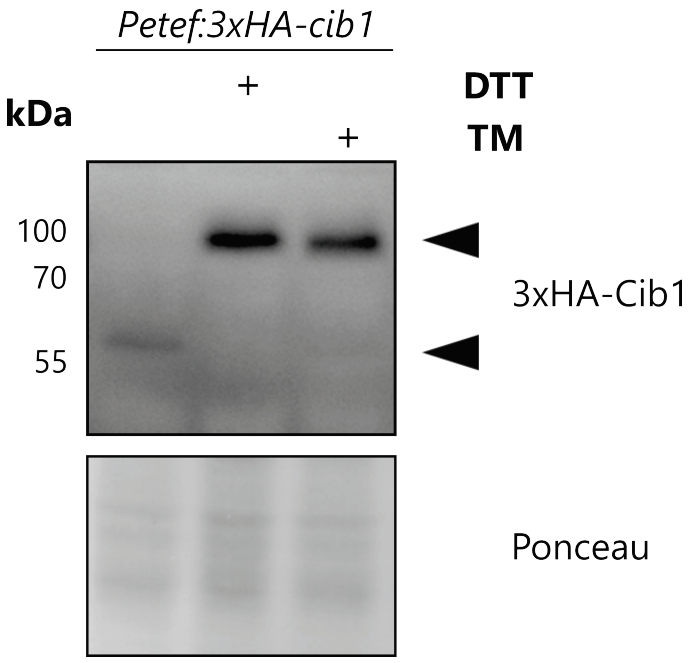

Figure 26: Cib1^{u} is exclusively synthesized under unstressed conditions

Analysis of Cib1^{s} and Cib1^{u} ratio under unstressed and stressed conditions. 3xHA-Cib1^{s} and 3xHA-Cib1^{u} were expressed in SG200 under unstressed and stressed conditions. ER stress was induced by treatment with either TM (1 µg/mL) or DTT (3 mM) for 4 h. Proteins were detected on a Western Blot. Ponceau staining served as a loading control.

2.10.2. **Cib1^{u} is considerably less stable than Cib1^{s}**

From *S. cerevisiae* and higher eukaryotes it is known that Hac1^{u}/XBP1^{u} are highly unstable. The C-terminal tail of Hac1^{u} in *S. cerevisiae,* for example, serves as a degron which results in a calculated Hac1^{u} half-life of 50 seconds (Di Santo et al., 2016; Yoshida et al., 2006). Such a destabilizing element has not been described for Cib1^{u}, yet. For this reason, first, the stability of Cib1^{u} in comparison to Cib1^{s} was analyzed in SG200 Δ*cib1* strains that contain either *cib1^{us}-3xHA* or *cib1^{s}-3xHA* controlled by the arabinose inducible *crg* promoter. This enables the production of comparable levels of Cib1^{u}-3xHA and Cib1^{s}-3xHA. Stability of both proteins was measured under unstressed and stressed (1 µg/mL TM for 4 h) conditions. The cells were therefore treated with cycloheximide (CHX) for 15 minutes, 30 minutes, 60 minutes and 90 minutes. CHX is an antibiotic that interferes with translational elongation and is applied as an inhibitor of protein biosynthesis. Under both growth conditions, Cib1^{s}-3xHA was relatively stable. A noticeable decrease of relative protein quantity was observed after about an hour. The protein degradation was accelerated by induction of ER stress.

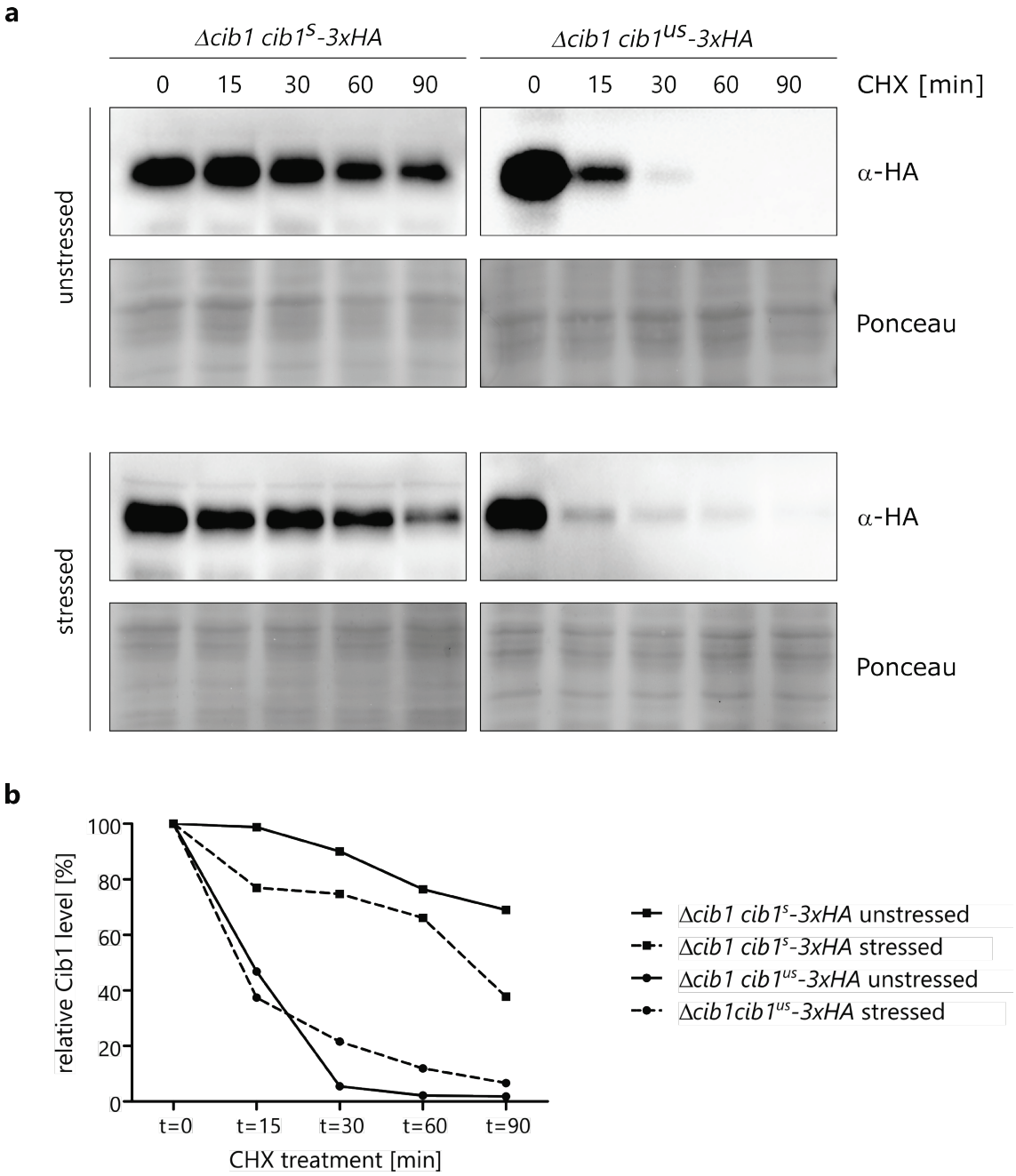

Figure 27: Cib1^{u} stability is marginally affected by ER stress

Western Blot analysis of Cib1^{s}-3xHA and Cib1^{u}-3xHA stability. (a) Unstressed or stressed (1 µg/mL TM for 4 h) SG200 Δ*cib1* cells expressing either Cib1^{s}-3xHA or Cib1^{us}-3xHA were treated with CHX up to 90 minutes. Proteins were taken before the addition of CHX as well as at every indicated time point. (b) Quantification of relative protein amount in the course of CHX treatment. Ponceau staining served as a loading control for normalization. Half-life was estimated by linear interpolation.

While, the half-life of Cib1^{s} was above 90 minutes under unstressed conditions, it was an estimated 77 minutes under stressed conditions. Cib1^{u}-3xHA was much more unstable. The half-life under unstressed conditions was an estimated

14 minutes and ER stress had only a minor impact on stability (half-life of 12 minutes) (Fig. 27)

2.10.3. **Cib1^{s} and Cib1^{u} interact via their bZIP domain**

Preliminary data indicate that the formation of Cib1^{u} and Cib1^{s} heterodimers is not only mediated by the bZIP domain but also via their C-termini (Hampel, 2016). In order to test this initial observation, co-immunoprecipitation (CoIP) analyses were performed. To this end, several *U. maydis* strains expressing either full-length Cib1^{s} (aa 1-574) or full-length Cib1^{u} (aa 1-434), or the N-terminus of Cib1 (aa 1-273), or the C-terminus of Cib1^{s} (aa 274-574) or the C-terminus of Cib1^{u} (aa 274-434) were generated (Fig. 28). The interaction of two proteins, one of which was tagged with 3xHA and the other one tagged with GFP, was tested *in vivo* (Fig. 28a). The GFP-fusion protein was always used as bait and pulled-down by GFP-Trap. As controls, strains expressing eGFP and the corresponding interaction partners to be tested were used. Interactions between Cib1^{s}-GFP and Cib1^{s}-3xHA as well as between Cib1^{u}-GFP and Cib1^{u}-3xHA were observed, strongly indicating that they are able to form homodimers (Fig. 28b). Unspecific interaction with the GFP tag alone was not observed (Fig. 28g). Furthermore, heterodimer formation between Cib1^{u} and Cib1^{s} was discovered (Fig. 28c). In addition, an interaction between Cib1^{u} and Cib1^{s} with the N-terminus of Cib1 containing the bZIP domain was identified (Fig. 28d). Unspecific interaction with the GFP tag could be excluded (Fig. 28g). By contrast, an interaction between the C-terminus of Cib1^{s} with Cib1^{s}-GFP or Cib1^{u}-GFP was not observed (Fig. 28e). Interestingly, a weak interaction was discovered between the C-terminus of Cib1^{u} and Cib1^{s}-GFP but not with Cib1^{u}-GFP (Fig. 28f). Collectively, these data imply that homo- and heterodimer formation is mainly mediated by the bZIP domain. Nevertheless, the C-terminus of Cib1^{u} might potentially be involved in this interaction as well.

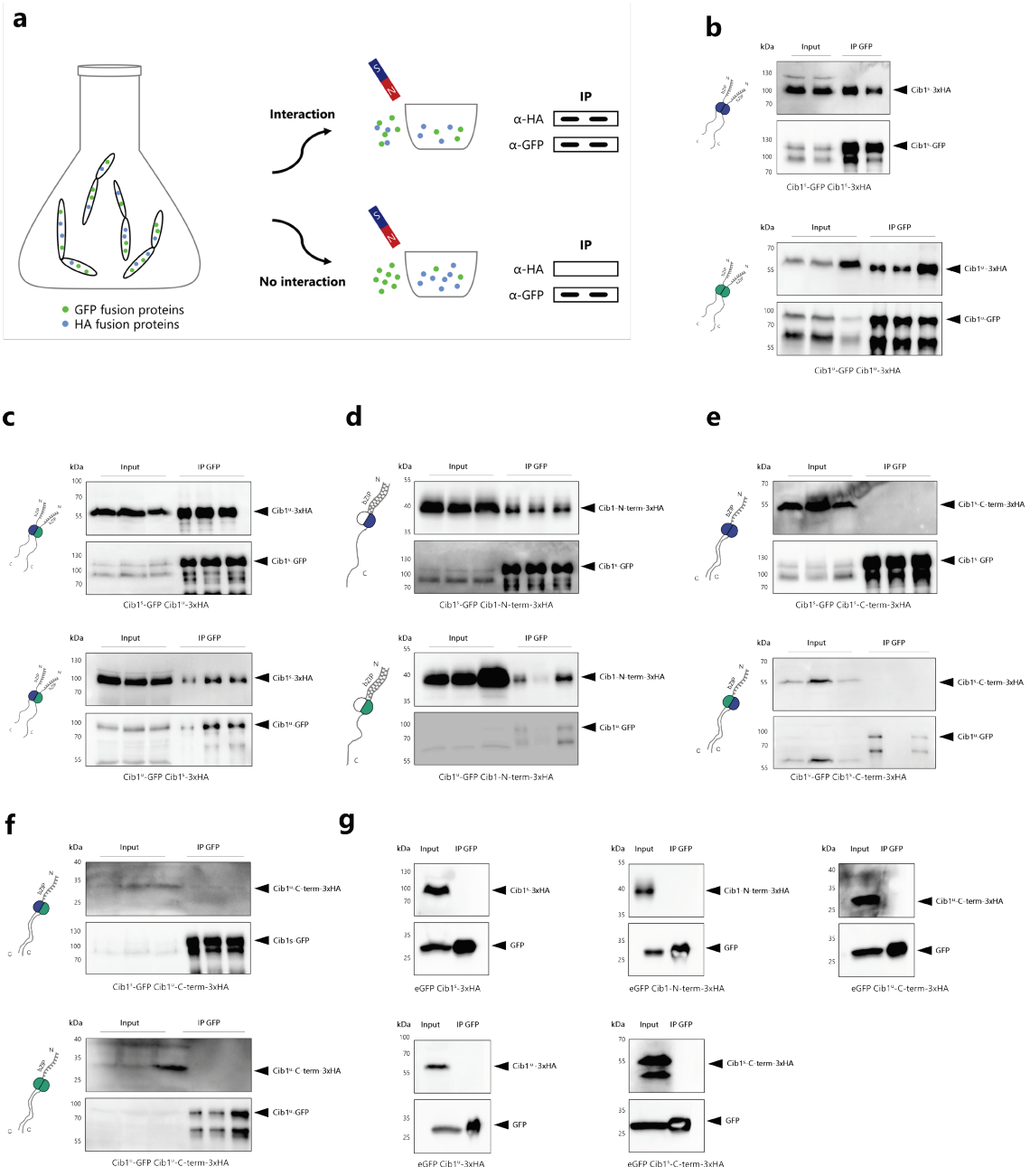

Figure 28: N-termini of Cib1^{s} and Cib1^{u} are crucial for homo- and heterodimer formation

Analysis of Cib1^{s} and Cib1^{u} interaction via CoIP. (a) Scheme of the CoIP procedure and the subsequent Western Blot analysis. (b) Western blot of CoIPs of Cib1^{s}-GFP and Cib1^{s}-3xHA (top) as well as Cib1^{u}-GFP and Cib1^{u}-3xHA (bottom), (c) Cib1^{s}-GFP and Cib1^{u}-3xHA as well as Cib1^{u}-GFP and Cib1^{s}-3xHA, (d) Cib1^{s}-GFP and Cib1-N-term-3xHA as well as Cib1^{u}-GFP and Cib1-N-term-3xHA, (e) Cib1^{s}-GFP and Cib1^{s}-C-term-3xHA as well as Cib1^{u}-GFP and Cib1^{s}-C-term-3xHA, (f) Cib1s-GFP and Cib1^{u}-C-term-3xHA as well as Cib1^{u}-GFP and Cib1^{u}-C-term-3xHA. In all cases, 1/100 of the whole protein lysate was loaded in the input lanes. IP represents the proteins bound by the GFP-Trap® beads. Interaction was tested in three biological replicates (exception (b) top). (g) Western Blot of control CoIPs between eGFP and Cib1 derivatives. One representative replicate for each interaction combination is shown.

2.11. Characterization of *U. maydis* Cib1 on a cellular level

For mammalian XBP1^{s} and XBP1^{u} not only a nuclear localization but also an ER localization was observed under both unstressed and stressed conditions. Also, morphological changes of the ER were observed as a response to ER stress, which was also reported for *S. cerevisiae*. ER stress induces an expansion of the ER which, in turn, alleviates ER stress (Schuck et al., 2009).

2.11.1. **Cib1^{u}-GFP and Cib1-GFP are localized to the nucleus**

So far, in *U. maydis* it was shown that Cib1^{s}-3xGFP localizes to the nucleus upon ER stress induction (Heimel et al., 2013). The intracellular localization of Cib1^{u} remained unresearched. In order to find out under which condition Cib1^{u} is present in which part of a cell, the localization of Cib1^{u}-GFP in SG200 Δ*cib1* was analyzed by fluorescence microscopy. Additionally, the localization of Cib1-GFP, for which the GFP-fusion protein is only built after successful splicing of the intron, was analyzed. A nuclear localization of Cib1^{u}-GFP was observed under unstressed and stressed (1 µg/mL TM for 4 h) conditions indicating that induction of ER stress did not affect subcellular localization. By contrast, a distinct nuclear localization of Cib1-GFP in SG200 could only be observed in stressed cells. Under unstressed conditions, only a weak nuclear localization was visible suggesting that efficient splicing occurs in response to ER stress (Fig. 29).

Figure 29: Cib1^{u}-GFP is localized to the nucleus

Analysis of the subcellular localization of Cib1^{u}-GFP and Cib1-GFP. Localization of both GFP-fusion proteins was investigated by fluorescence microscopy of logarithmically growing unstressed and stressed (1 µg/mL TM for 4 h) cells. Scale bar represents 5 µm.

2.11.2. **Impact of ER stress on the ER morphology**

In *S. cerevisiae* it was demonstrated that ER stress leads to an enlargement of the ER through the formation of ER sheets (Schuck et al., 2009). To address if ER stress also affects the ER morphology in *U. maydis*, the ER in SG200 and SG200 Δ*cib1* was further investigated by electron microscopy (EM). On base of this analysis, there were no obvious morphological differences visible between the two strains (Fig. 30).

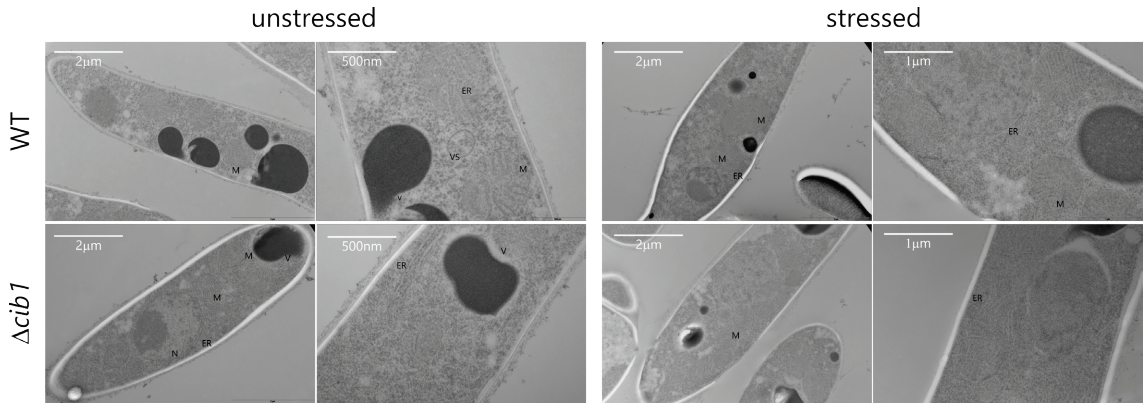

Figure 30: Deletion of *cib1* does not seem to affect ER morphology

Analysis of ER morphology in SG200 and SG200 Δ*cib1* under unstressed and stressed (1.5 µg/mL TM for 4 h) conditions by electron microscopy. Representative images are shown. N-nucleus, V-vacuole, M-mitochondria, ER-endoplasmic reticulum and VE-vesicle.

Collectively, it was shown that deletion of *cib1* in *U. maydis* resulted in reduced ER stress resistance, which was restored by Cib1^{u} without affecting the gene expression of common UPR target genes. Yet, how the regulation works on a mechanistic level remains unresolved. Nevertheless, several parallels to XBP1^{u} in higher eukaryotes could be identified, which suggest that the regulatory function of XBP1^{u} may be evolutionarily conserved in *U. maydis.*

2.12. Evolutionary conservation of the IRE1 signaling pathway between mammals and *U. maydis*

The metazoan UPR is regulated by three main sensors of ER stress, IRE1, PERK and ATF6. The UPR in fungi is mainly controlled by the IRE1 signaling pathway, which appears to be well conserved from fungi to higher eukaryotes. Despite the distinctive parallels in the UPR regulation, the IRE1 branch underwent some degree of specialization. Due to the fact that the IRE1 pathway is present in metazoans, fungi and plants, it is referred to as the most ancient pathway (Hollien, 2013).

2.12.1. **Only the bZIP domains in XBP1^{u} and Cib1^{u} are conserved**

Under unstressed conditions, the protein XBP1^{u} is produced in mammals and Cib1^{u} in the basidiomycete *U. maydis*. Both proteins contain a conserved bZIP domain and were demonstrated to counteract UPR hyperactivation (Heimel et al., 2013; Yoshida et al., 2006). Moreover, XBP1^{u} is able to mediate ER resistance in *U. maydis* in a dose-dependent manner. The more XBP1^{u} is produced, the more resistant cells become towards ER stress (Hampel, 2016). Hence, with respect to mediating ER stress resistance, Cib1^{u} and XBP1^{u} are apparently conserved. On closer inspection of the protein domains and amino acid sequences, it becomes evident that similarities are limited. The N-termini containing NLSs and bZIP domains are quite conserved with a similarity of 50.6 % (calculated using the Smith-Waterman algorithm), whereas the C-termini exhibit no significant similarities. While the C-terminus of XBP1^{u} containing a hydrophobic stretch, a NES and a degron is well characterized, the C-terminus of Cib1^{u} remains unexplored (Fig. 31a). Amino acid sequence alignment of XBP1 and Cib1 merely revealed homology in the area of the bZIP domains (Fig. 31b).

Figure 31: C-termini of Cib1 and XBP1 do not show conservation

Comparison of protein domains and sequence alignment of XBP1 and Cib1. (a) Scheme of protein domains in XBP1^{s} and XBP1^{u} as well as in Cib1^{s} and Cib1^{u}. Numbers represent the first and the last amino acid of the corresponding protein domain. (b) Protein sequence alignment of XBP1^{s} and Cib1^{s}. Alignment was performed by 'CLUSTAL format alignment by MAFFT (v7.416)'.

a

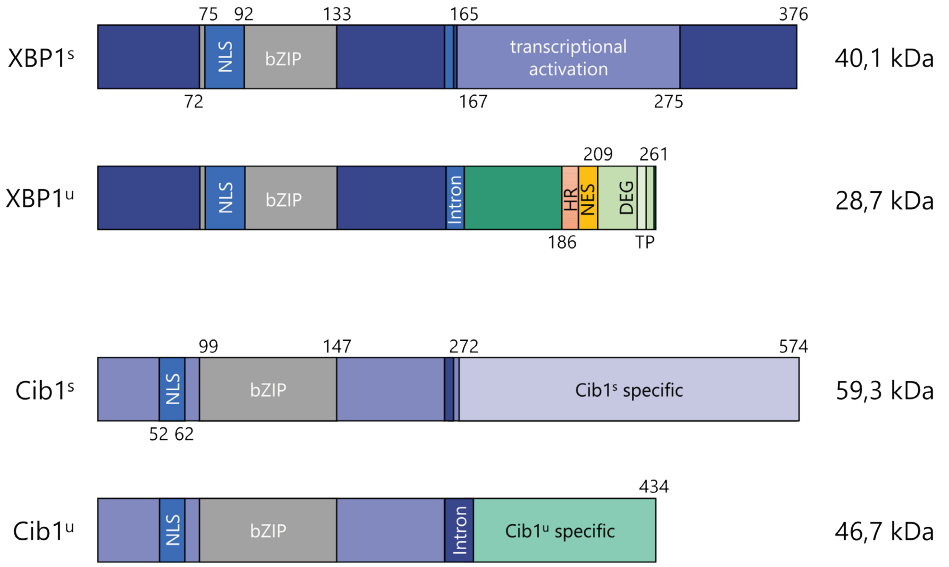

b

```
XBP1            MVV---------------------------------------VAAAPNPADGTPKVLLL
Cib1            MTSTTTSTPPMFAVAQASTPSSPSAFASSSRLSETPVKQETHHIALADACSNSSKKRKLI
                *.                                         :* *   ::.: *  *:

XBP1            SGQPASAAGAPAGQALPLMVPAQRGASPEAASGGLPQARKRQRLTHLSPEEKALRRKLKN
Cib1            DERDDHDEDVDDSSSSPSASP-----SKSSNTGGRRKASDEERKARLEA------RQARN
                . :     ..  ..: *   *     * .: :**  :* ..:* ::*..      *: :*

XBP1            RVAAQTARDRKKARMSELEQQVVDLEEENQKLLLENQLLREKTHGLVVENQELRQRLGMD
Cib1            RLSAQYSRERKKAYVETLEGSL-------NALKAENTLLRQQRE----QDQALQQTLDAK
                *::** :*:**** :. ** .:       : *  ** ***:: .    ::* *:* *. .

XBP1            ALVAEEEAEAKGNEVRPVAGSAESAAGAGPVVT-PPEHLPMDSGGIDSSDSESDILLGIL
Cib1            LKDAQLRVNTLETILRTLAPSLVPLLGPSSLLSLPSSSNPSVLATSPASSLAPQFDAGLS
                   *: ..::  . :*.:* *  .  *...::: *..  *   .   :*.  .::  *:

XBP1            DNLDPVMFFKCPSPEPASLEELPEVYPEGPSSLPASLSLSVGTSS---AKLEAINELIRF
Cib1            ANLASASVQDNSSASKEVPLSLAIAAPASTVSTPFSFGTLAQQSSNEGVRLPAADALTQF
                 ** .. . . .*..     .*. . * .. * * *:.  .  **   .:* * : * :*

XBP1            DHIYTKPLVLEIPSETESQANVVVKIEEAPLSPSENDHPEFIVSVKEEPVEDDLVPELGI
Cib1            ESVAGKQSALEKAGNNVDVNGSSIVNQGYPLA------SQISVSAPEQP-----------
                : :  *  .** ..:. .  .  :  :  **:      .:: **. *:*

XBP1            SNLLSSSHCPKPSSCLLDAYSDCGYGGS--LSPFSDMSSLLG------------------
Cib1            SSFAASAQVPLPQHVVEAKAAGVAREAEALLSNFIDLDAKLANGDAKTAAQDQGAPTSAT
                *.: :*:: * *.  :    :. .  ..  ** * *:.: *.

XBP1            ------------------------------------------------------------
Cib1            PSEPVSVGEGYAAAAGNALRSASAAAGDLASLSAASSADSGDGSSGSSDGSKTNNENGGS


XBP1            -------VNHS------------------------WE---DTFANELF-----------
Cib1            TIFNTISLSHADNKDQDLEKRFQLLTSPLLATERNVWELVTDTMLQDLYSGSDEVGAISG
                      :.*:                          **   **: ::*:

XBP1            ---PQL-------------------------------------------------------
Cib1            NADPALTPSEVDMSAGSSPFDLVDLDIEIEEPLQVNIGLETEDAVHGGLLGFGHEKPDAG
                   * *

XBP1            ----------ISV
Cib1            VPDWSGLMASIVA
                         * .
```

2.12.2. **Cib1^{u} and Cib1^{s} partially rescue clonogenic survival and ER stress resistance in RPE1 *XBP1*$^{-/-}$ cells**

XBP1 was demonstrated to be functional and mediate ER stress resistance in *U. maydis* (Hampel, 2016). However, it has not been tested, if Cib1 is able to take over the function of XBP1 in mammals. To investigate this possibility, stable RPE1 *XBP1*$^{-/-}$ cell lines expressing either Cib1^{s}-1xHA (Cib1^{s}) or Cib1^{u}-3xHA (Cib1^{u}) were generated (Fig. 32a). Afterwards, the clonogenic survival, ER stress resistance and the colony morphology of both cell lines were tested via clonogenic assays under unstressed and stressed (0.55 µg/mL TM for 4.5 h) conditions. RPE1 WT as well as *XBP1*$^{-/-}$ and XBP1^{s}/XBP1^{u} rescue cell lines served as references. Under unstressed conditions, colonies formed by *XBP1* KO cells were smaller in size and reduced in density. This colony phenotype was entirely complemented by the expression of Cib1^{s}-1xHA or Cib1^{u}-3xHA. Yet, under ER stress inducing conditions, neither Cib1^{s} nor Cib1^{u} were able to fully restore colony size and density to WT levels. Expression of Cib^{s}-1xHA in RPE1 *XBP1*$^{-/-}$, similar to XBP1^{s}, resulted in a partial rescue of the colony phenotype, whereas the production Cib1^{u}-3xHA had no effect on the colony appearance (Fig. 32b). These data suggest that, at least under unstressed conditions, Cib1^{s} and Cib1^{u} may be functional in mammals. Furthermore, expression of Cib1^{u}-3xHA and Cib1^{s}-1xHA positively influenced clonogenic survival.

Figure 32: Expression of *U. maydis* Cib1^{u} and Cib1^{s} in RPE1 *XBP1*$^{-/-}$ cells increase clonogenic survival and ER stress resistance

Analysis of Cib1^{u} and Cib1^{s} functionality in RPE1 *XBP1*$^{-/-}$ cells via clonogenic assays. (a) Verification of generated RPE1 *XBP1*$^{-/-}$ cell lines expressing either Cib1^{u}-3xHA or Cib1^{s}-1xHA under unstressed and stressed (1 µg/mL TM for 4.5 h) conditions on a protein level. One representative Western Blot is shown. (b) Size and density of colonies formed by WT and derivatives after 9 days of incubation. Cells in bottom row were treated with 0.55 µg/mL TM for 4.5 h. (c) Number of colonies formed in WT and derivatives relative to maximum number of colonies. Each data point represents the mean of three technical replicates of one experiment. Error bars represent SEM. (d) P-values and significance levels are based on Dunn's multiple comparisons test.

a

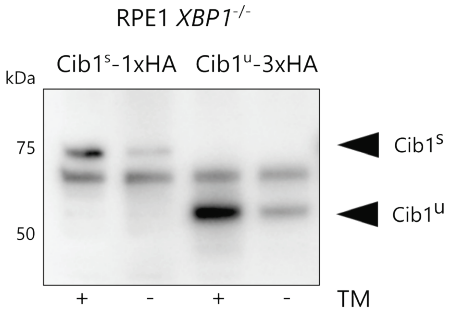

b

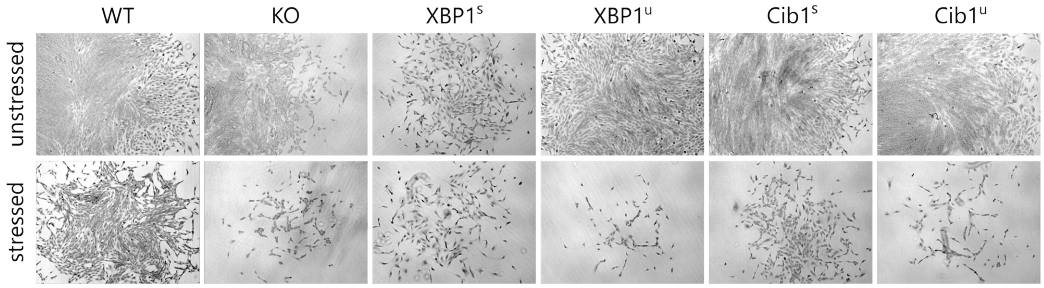

c

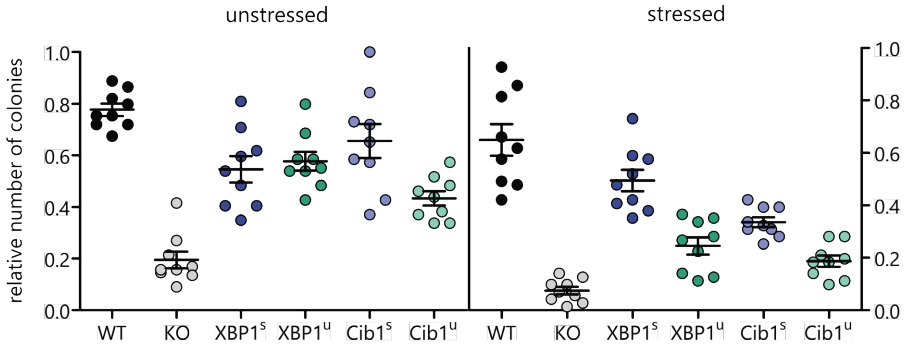

d

unstressed

Dunn's multiple comparisons test	Adjusted P Value	Summary
WT vs. KO	<0.001	***
WT vs. XBP1^{s}	0.21	ns
WT vs. XBP1^{u}	0.57	ns
WT vs. Cib1^{s}	>0.99	ns
WT vs. Cib1^{u}	0.003	**
KO vs. XBP1^{s}	0.04	*
KO vs. XBP1^{u}	0.01	*
KO vs. Cib1^{s}	<0.001	***
KO vs. Cib1^{u}	>0.99	ns

stressed

Dunn's multiple comparisons test	Adjusted P Value	Summary
WT vs. KO	<0.001	***
WT vs. XBP1^{s}	>0.99	ns
WT vs. XBP1^{u}	0.007	**
WT vs. Cib1^{s}	0.27	ns
WT vs. Cib1^{u}	<0.001	***
KO vs. XBP1^{s}	<0.001	***
KO vs. XBP1^{u}	0.46	ns
KO vs. Cib1^{s}	0.02	*
KO vs. Cib1^{u}	>0.99	ns

* p<0.05, ** p<0.01, *** p<0.001

Under unstressed conditions, 80 % of the RPE1 WT cells grew into a colony, whereas only an average of 20 % of the *XBP1*$^{-/-}$ cells formed colonies. Clonogenic survival was significantly increased in Cib1^{s} cells. Approximately 70 % of the cells

grew into a colony. Nevertheless, only approximately 40 % of the cells expressing Cib1^{u}-3xHA were able to form colonies. In case of the XBP1^{s}/XBP1^{u} rescue cell lines approximately 60 % of the cells formed colonies. These results suggest that under unstressed conditions Cib1^{u} and especially Cib1^{s} are involved in regulating cell proliferation. Under ER stress conditions, expression of Cib1^{s} and XBP1^{s} in *XBP1*$^{-/-}$ cells led to a significantly increased ER stress resistance (compared to KO) that even reached WT level (Fig. 32c, d). Collectively, both proteins Cib1^{u} and Cib1^{s} appear to be functional in mammals, at least to a certain extent.

2.12.3. **Cib1^{s} is sufficient to drive expression of the mammalian UPRE reporter**

In luciferase reporter assays, the bZIP domain of XBP1^{s} was shown to bind to the UPRE consensus motif thereby activating transcription of the luciferase reporter gene. In case of XBP1^{u} no transcriptional activity was measured.

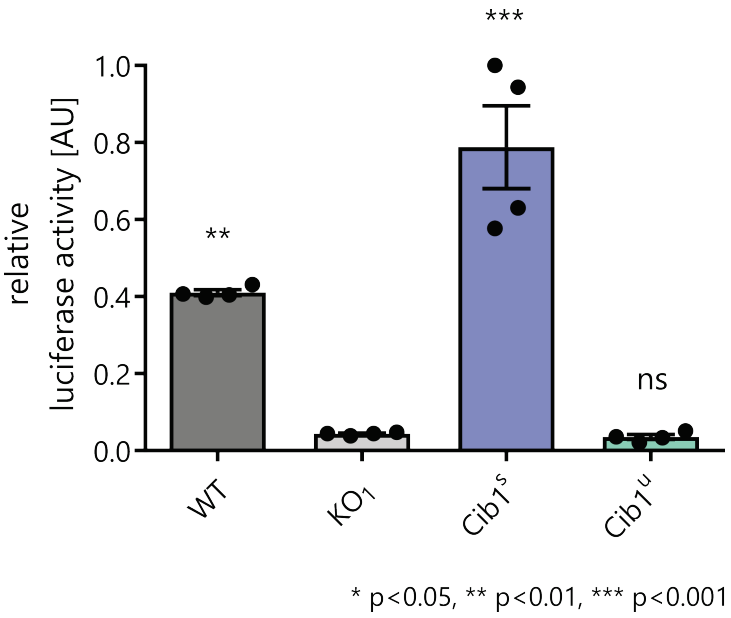

Figure 33: Cib1^{s} but not Cib1^{u} activates the expression of the luciferase reporter

Analysis of the transcriptional activity of Cib1^{u} and Cib1^{s} via a dual luciferase reporter assay. WT, KO and Cib1^{s}/Cib1^{u} cells were transfected with the UPRE-luciferase reporter. Luciferase activity was measured 24 h post-transfection. The renilla luciferase was used for normalization. Each data point represents the mean of two technical replicates of one experiment. Significance levels are based on Bonferroni's multiple comparisons test.

The proteins Cib1^{s} and Cib1^{u} are functional in mammals and mediate clonogenic survival and ER stress resistance. To establish whether a transcriptional activity is present, the luciferase reporter system with the UPRE consensus sequence described in section 2.5 was employed. RPE1 *XBP1*$^{-/-}$ cells expressing either Cib1^{s}-1xHA or Cib1^{u}-3xHA were transfected with the luciferase reporter construct and the luciferase activity measured 24 h post-transfection. Only in cells expressing Cib1^{s} luciferase activity was detected, whereas luciferase activity in Cib1^{u} cells was not increased and similar to the KO control (Fig. 33). This indicates that Cib1^{s}, but not Cib1^{u}, is transcriptionally active in mammals, providing further support for the evolutionary conservation of XBP1^{s}/XBP1^{u} functions.

In conclusion, these data show that XBP1^{s}/XBP1^{u} and Cib1^{s}/Cib1^{u} respectively functionally resemble each other. Not only do XBP1^{u}/XBP1^{s} mediate ER stress resistance in *U. maydis* but also Cib1^{u}/Cib1^{s} in mammals. Structurally, only the bZIP domains of the proteins are conserved. In addition, Cib1^{s} is likely to adopt the regulatory function of XBP1^{s} and Cib1^{u} the regulatory function of XBP1^{u}. Although this function remains to be explored on a mechanistic level, it seems to be evolutionary conserved between *U. maydis* and higher eukaryotes.

3. Discussion

The focus of many studies investigating the IRE1 signaling pathway of the UPR in mammals was on the analysis of the bZIP transcription factor XBP1^{s} and its regulatory role. Not much attention was paid to XBP1^{u} (Hetz, 2012; Karagöz et al., 2019; Walter and Ron, 2011). The main focus of this thesis was to shed light on the molecular details and mechanism how XBP1^{u} influences the ER stress response and to what extent its regulatory role is conserved in the fungus *U. maydis*. The analyses of this work revealed a novel, evolutionary conserved function of XBP1^{u}. XBP1^{u}, independent of XBP1^{s}, plays an essential role in the regulation of cellular survival and cell proliferation without the need of DNA-binding or transcriptional activity.

3.1. XBP1^{u} as a regulator of cell proliferation

3.1.1. Connection between XBP1^{u} and cell survival

In the work at hand it was shown that a deletion of *XBP1* leads to reduced cell survival, which can be restored by XBP1^{s} and XBP1^{u}. Also in other studies, XBP1 was demonstrated to play an essential role in regulating the ER stress response and during developmental processes. A global deletion of *XBP1* in mice results in embryonic lethality by embryonic day 14.5. At this developmental stage, XBP1 reaches maximum expression levels in WT mice. Liver-specific expression of XBP1 prolongs embryonic survival, yet, it leads to early postnatal lethality due to severe liver and pancreas damages (Lee et al., 2005; Reimold et al., 2000). XBP1 does not only have a crucial function in the development of highly secretory exocrine cells but also in plasma cell differentiation (Reimold et al., 2001). Also, survival of type 1 conventional dendritic cells (cDC1s) may depend on XBP1 expression. While loss of XBP1 in lung cDC1s leads to cell death, deletion in intestinal as well as splenic cDC1s does not affect cell survival (Tavernier et al., 2017). In *XBP1* depleted mouse embryonic fibroblast (MEF) cells, no reduction of cell survival was observed under unstressed conditions (Romero-Ramirez et al., 2004). However, as shown in the work at hand, deletion of *XBP1* in RPE1 cells caused a significant reduction in cell survival already under unstressed

conditions.

At some point, every cell experiences stress, be it during early embryogenesis and differentiation processes or be it *in vivo* through, e.g., infections or hypoxia. Stress levels vary between cell types and in order to compensate for the loss of *XBP1* some of them have developed elaborate strategies (Puscheck et al., 2015). Intestinal cDC1s, for example, prevent cell death by IRE1α-dependent activation of RIDD, which rescues deleterious effects of *XBP1* deletion (Tavernier et al., 2017).

It is hardly surprising that *XBP1* deletion affects some cell types in a different way than others. *In vitro* stresses should not be neglected either: Cells grown in cultures are subjected to oxidative stress among others (Halliwell, 2003; Sherr and DePinho, 2000) and the way how cell lines are immortalized may play an important role as well. For instance, during the immortalization of MEFs only those cells are enriched that acquired growth advantages (Xu, 2005) and potentially accumulated beneficial suppressor mutations.

To the best of our knowledge it has not been investigated on a molecular level whether cell survival and proliferation are mediated by XBP1^{s} and XBP1^{u} individually or in dependence of each other under unstressed conditions. Due to the fact that XBP1^{u} is a highly unstable and short-lived protein, a potential involvement regarding the regulation of cellular processes is often underestimated. Furthermore, the abundance of XBP1^{u} varies between cell types which further complicates analyses (Acosta-Alvear et al., 2007). Although a regulatory function for XBP1^{u} was proposed, most often it is connected to XBP1^{s} (Yoshida et al., 2006) or to other transcription factors/proteins upon induction of ER stress (Huang et al., 2017; Martin et al., 2014; Zhao et al., 2013). In order to close this research gap, it was analyzed in this thesis to what extent XBP1^{s} and XBP1^{u} independently restore the reduced cell survival in RPE1 *XBP1*$^{-/-}$ cell lines under unstressed conditions. Thereby, it was discovered that expression of either protein is beneficial for cell survival under unstressed conditions. Interestingly, the DNA-binding domain, and thus the transcriptional activity, was dispensable for this function. This strongly indicates that XBP1^{u} can mediate cell survival in the absence of XBP1^{s}. However, an indirect involvement via interaction with other proteins cannot be excluded at this point. One possibility would be the formation

of XBP1^{u} heterodimers with other bZIP transcription factors, resulting in changes in the transcriptional response, which could promote cell survival or reduce ER stress levels. Moreover, it should be noted that XBP1 is not the sole regulator of the UPR. XBP1^{u} could ensure, for example, that ATF6 and PERK dominate the restoring of ER homeostasis. Another possibility would be that XBP1^{u} forms complexes with other proteins via its C-terminus accounting for their increased or decreased stability. Such a relation has already been reported in human colon carcinoma cells HCT116, in which the C-terminus of XBP1^{u} forms a complex with MDM2 leading to an increased stability of the latter and consequently to accelerated cell cycle progression as well as cell proliferation (Huang et al., 2017). In addition, it has been demonstrated that XBP1^{u} is able to increase the splicing efficiency of its own transcript via HR2 and TP domains located at the C-terminus, both of which are absent in XBP1^{s} (Kanda et al., 2016; Yanagitani et al., 2011, 2009).

Nevertheless, the C-terminal regions of XBP1^{u} and XBP1^{s} are not conserved and both proteins mediate cell survival. Assuming that XBP1^{u} and XBP1^{s} increase cell survival in the same way, a C-terminus-dependent regulatory role seems rather unlikely. Additional analyses will be needed to further narrow down the mechanistic details of the XBP1^{u} function.

3.1.2. **Connection between XBP1^{u} and the cell cycle**

For a number of human cancers it was demonstrated that XBP1 facilitates cell cycle progression and cell proliferation. An increased ratio of XBP1^{s} versus XBP1^{u} predicts a poor prognosis for myeloma patients (Gambella et al., 2014; Vincenz et al., 2013). Already in 1999, Brewer and co-workers reported that UPR inhibits cyclin D1 synthesis preventing cell cycle progression. Pharmacological induction of UPR triggered loss of cyclin D1 leading to a cell cycle arrest in G1-phase (Brewer et al., 1999). The same holds true for pancreatic β-cells in which a link exists between the IRE1 signaling pathway and the cell cycle checkpoint control. Proliferation of β-cells was achieved by the upregulation of cyclin D1 by XBP1^{s}, which drives cells from the G1- into the S-phase of the cell cycle (Xu et al., 2014). In the osteosarcoma cell lines MG63 and U2OS, on the contrary, silencing of *XBP1* increased the cell proportion in G2/M-phase (Yang et al.,

2015).

Cell cycle analysis in this work did not reveal severe cell cycle defects in WT and RPE1 *XBP1*$^{-/-}$ cells. Expression of XBP1^{s} or XBP1^{u} did not induce any changes either. Thus, cell cycle defects are presumably not the reason for the reduced clonogenic survival and therefore the cell cycle is not the cellular process affected by XBP1^{u}. Nevertheless, it cannot be excluded that the duration of cells in the corresponding cell cycle phase is prolonged, which would lead to reduced cell proliferation, too. There are a number of ways to investigate that, two of which flow cytometry-based. Firstly, the cell cycle status can be determined by analyzing proliferation specific markers and cellular DNA content. Secondly, the incorporation of 5'-bromo-2'-deoxyuridine (BrdU), a thymidine analog, can be measured, which allows to determine the duration through the cell cycle (Pozarowski and Darzynkiewicz, 2004).

Activation of the UPR may not only provoke cell cycle arrest but might also inhibit DNA synthesis. Cabrera and co-workers showed that activation of PERK results in an inhibition of replication fork progression and replication origin firing, which would lead to a prolonged S-phase (Cabrera et al., 2017). Such a scenario would not be resolved by the cell cycle analyses performed in this work. Thus, it appears possible that due to the lack of *XBP1*, increased activity of PERK results in reduced cell proliferation. Nevertheless, an increased abundance of proteins acting downstream of PERK, such as ATF4 and CHOP, was not observed (data not shown). Moreover, *p58*^{IPK}, for example, a gene described as a XBP1^{s} target, serves as an inhibitor of the PERK protein (Todd et al., 2008). A regulation via XBP1^{u} has not been described, yet. However, transcript analyses, which were performed for this thesis, did not provide evidence for a p58^{IPK} regulation by XBP1^{u}. Consequently, further pathways with a potential impact on the cell cycle should be considered when analyzing the regulatory function of XBP1^{u}.

3.1.3. **Connection between XBP1^{u} and cell death**

The reduced clonogenic survival of RPE1 *XBP1*$^{-/-}$ cells observed in the analyses for this work may be explained by the reduced cell proliferation but also by the untimely induction of cell death. ER stress provokes an activation of the UPR. In case that ER stress cannot be adequately resolved and ER homeostasis

restored, the UPR promotes cell death. Little is known about how exactly the transition from a pro-survival pathway to apoptosis is regulated (Walter et al., 2015; Walter and Ron, 2011). Two factors that lead to the activation of apoptosis are CHOP and JNK. CHOP stems from the activation of the PERK pathways, whereas JNK is activated by IRE1α. Both proteins are hyperactive under ER stress conditions in mice containing a liver-specific *XBP1* deletion. *XBP1* deletion results in progressive liver injuries and the activation of apoptosis. It remains unresolved which isoform, XBP1^{s} or XBP1^{u}, assumes this regulatory role (Olivares and Henkel, 2015).

On the basis of the data presented in this thesis, the deletion of *XBP1* in RPE1 cells led to an increased cell fraction in subG1-phase, which was reduced by XBP1^{u} besides XBP1^{s}. The DNA-binding property of both XBP1 isoforms was dispensable in this case. The reduction of cells in subG1-phase is unlikely to be derived from CHOP activity since protein levels were comparable in all tested cell lines (data not shown). However, in previous analyses, Gupta and co-workers suggested an alternative way to improve cell survival, inhibit ER stress induced apoptosis and support cells to adapt to chronic ER stress in rat pheochromocytoma cells (PC12) independent of CHOP. The molecular chaperone Hsp72 takes over the protective role by preventing cytochrome c release and by physically interacting with IRE1α which results in increased IRE1α activity. This regulatory role is dependent on XBP1^{s}, which initially needs to upregulate the synthesis of Hsp72 (Gupta et al., 2010).

Alternatively, RIDD has been shown to promote a pro-apoptotic response independent of CHOP and JNK. In certain cDC1s, RIDD may determine cell fate in the absence of XBP1. Interestingly, the regulation of apoptosis seems to vary between the cell lines as well. In some cDC1s, RIDD promotes a pro-apoptotic response, while in others it can assume a protective role (Tavernier et al., 2017). A potential connection between RIDD and XBP1^{u} has not been analyzed, yet. In addition, it is also worthwhile to have a closer look at autophagic processes, which are an alternative form of programmed cell death. The mammalian FoxO transcription factor family is involved in the regulation of several cellular processes such as cell cycle arrest, DNA repair, apoptosis and autophagy. Depletion of FoxO protein in Drosophila, mouse muscle cells and several cancer cell lines results in attenuation of autophagy. In MEF cells an interaction between

XBP1^{s} and FoxO1 causes degradation of FoxO1 by a not fully understood mechanism (Zhou et al., 2011). Interestingly, it has been shown that FoxO1 stability is linked to the phosphorylation state of XBP1^{u} in HCT116 cells in response to glutamine starvation. Phosphorylation of XBP1^{u} enables complex formation with FoxO1, which is thereafter degraded by the 20S proteasome. Accumulation of LC3-II, which is one of the autophagic hallmarks, reflects the level of autophagy induction. In glutamine starved HCT116 cells increased levels of LC3-II were observed (Zhao et al., 2013). In contrast, analyses of LC3 levels in RPE1 WT and *XBP1*$^{-/-}$ cell lines did not reveal a quantitative increase. Furthermore, depletion of FoxO1 in RPE1 *XBP1*$^{-/-}$ cells induced cell death already under unstressed conditions within 72 h. Cell cycle analyses after 48 h of depletion revealed a drastic increase of cells in subG1-phase (data not shown). Transcript levels of LC3, ATG5 (involved in autophagic vesicle formation), BECN1 (plays a central role in autophagy) and CHOP were increased compared to control cells (data not shown).

In conclusion, CHOP-dependent apoptosis and autophagic processes are improbable to be influenced by XBP1^{u}, at least for the experimental setup on which this analysis is based. The mechanism of cell death reduction through XBP1^{u} remains poorly understood and requires further analyses. For that, reverse phase protein array (RPPA) analysis in which abundance of more than 400 proteins extracted from mammalian cells is quantitatively examined, might represent a promising approach. Besides others, proteins involved in both apoptosis and autophagy are covered in this protein array. In addition, it would be worthwhile to have a closer look into the cell fraction in subG1-phase. Annexin V and TUNEL staining could clarify, whether the cells are indeed apoptotic and, if so, in which apoptotic stage they are.

All in all, XBP1^{u} and XBP1^{s} are able to mediate cell proliferation independent of DNA-binding. Functional studies in the baker's yeast *S. cerevisiae* showed that mammalian XBP1 is not functionally complementary with Hac1p, whereas the plant homolog bZIP60 is. Moreover, inter-species interactions between bZIP60, Hac1p and XBP1 were observed. As a consequence, it is reasonable to conclude that there is an evolutionary divergence besides the functional conservation in the most ancient UPR branch, IRE1 (Zhang et al., 2016). Remarkably enough,

the *U. maydis* homologs of XBP1^{u} and XBP1^{s}, Cib1^{u} and Cib1^{s}, respectively, are able to increase clonogenic survival in RPE1 *XBP1*$^{-/-}$ cells, too. Although the proteins appear to be divergent on a structural and sequence level, their function seems to be conserved. Hence, not only XBP1 in *U. maydis* is fully functional (Hampel, 2016) but also Cib1 in mammals in regard to cell proliferation under low levels of ER stress or under unstressed conditions, respectively. Consequently, the IRE1 pathway in *U. maydis* may be more closely related to the mammalian than to the *S. cerevisiae* pathway. This could serve as an important read-out when searching for the regulatory role of XBP1^{u}, as it might be a conserved function that is also present in less complex organisms.

3.2. XBP1^{u} and Cib1^{u} as mediators of ER stress resistance

3.2.1. XBP1^{u} and Cib1^{u} reduce ER stress susceptibility

The UPR presumably evolved to enable cells to flexibly adapt to different environmental and metabolic demands ensuring maintenance of ER homeostasis. It can be activated by different means. Pharmacologically, ER stress can be induced by tunicamycin or thapsigargin, which inhibits N-glycosylation and disrupts the calcium homeostasis in the ER, respectively (Walter and Ron, 2011). Physiological ways of inducing ER stress are nutrient deprivation and hypoxia. It should be taken into account that not every type of stressor necessarily activates the same stress response. Rather the overall response is the result of a superimposition of several defined and specific responses. For instance, when analyzing the IRE1 signal pathway under oxidative stress, the PERK pathway may increasingly be activated, which, in turn, could cause effects that are mistakenly attributed to the IRE1 pathway.

In the experiments for this work, ER stress was induced by treating the cells with TM. This leads to the activation of all three UPR branches. In combination with pleiotropic effects, this makes the analysis of the regulatory role of XBP1^{u} even harder. In previous studies, it has been shown that the proteome and transcriptome of cells in which the IRE1 pathway was exclusively activated differ from those in which either specifically ATF6 or ATF6 together with IRE1 were

activated (Shoulders et al., 2013).

In this work, the deletion of *XBP1* in RPE1 cells had a significant effect on ER stress resistance. Already in WT cells a reduced cellular survival was observed. However, in RPE1 *XBP1*$^{-/-}$ cells only 10 % of the cells did form colonies. Hence, as expected and shown in several previous studies, XBP1 seems to play a role in the regulation of cell proliferation under ER stress conditions. The observed reduction of cell survival was efficiently restored by XBP1^{s}. XBP1^{u}, on the other hand, only led to a minor increase of cell survival under ER stress conditions. Interestingly, colonies formed by RPE1 *XBP1*$^{-/-}$ cells under ER stress conditions could not be morphologically distinguished from colonies formed by WT and XBP1^{s} cells. Based on these observations, it can be concluded that the expression of XBP1^{u} positively influences the cell even though ER stress susceptibility was only partly reduced. Cells surviving ER stress did not show prolonged cell proliferation and XBP1^{s} seems to be the main regulator for the mediation of ER stress resistance.

Also, in MEF cells deletion of *XBP1* leads to reduced cell survival under ER stress conditions induced by hypoxia. Moreover, inhibited tumor growth was observed under these growth conditions in the absence of XBP1. Whether the expression of XBP1^{u} is sufficient for the rescue of the described phenotypes remains obscure (Romero-Ramirez et al., 2004).

Expression of *U. maydis cib1*^{s} and *cib1*^{u} in RPE1 *XBP1*$^{-/-}$ cells increased cell survival of RPE1 *XBP1*$^{-/-}$ cells. However, under ER stress conditions, only Cib1^{s} but not Cib1^{u} provoked a significant improvement. Moreover, Cib1^{u} and Cib1^{s} did not restore cell survival to the same extent as XBP1^{u} and XBP1^{s}. Colony, morphology of *cib1*^{u} expressing cells could not be distinguished from *XBP1*$^{-/-}$ cells.

Recently, in *U. maydis* it was demonstrated that Cib1^{s} negatively affects cell growth and does not restore ER stress resistance in Δ*cib1* strains. Cib1^{u}, on the other hand, is able to mediate ER stress resistance in a dose-dependent manner. The more Cib1^{u} is expressed the higher the ER stress resistance. However, a complementation was only observed under lower ER stress levels. Expression of Cib1^{u} in Δ*cib1* strains was not sufficient to cope with higher ER stress levels (Hampel, 2016).

This admits the interpretation that Cib1^{u} regulates some kind of ‘first line of

defense', but only if ER stress levels do not exceed a certain threshold. Analogously, such a regulation would also be possible in RPE1 cells. Under unstressed conditions, XBP1^{u} is sufficient to mediate cell survival, whereas under ER stress conditions, only a limited rescue was observed. This hypothesis would be backed by the observation that a reduction of the TM concentration or a shorter duration of stress induction in preliminary assays increased cell survival in RPE1 *XBP1*$^{-/-}$ cells under stressed conditions (data not shown).

Moreover, the dose-dependent mediation of ER stress resistance holds true for XBP1^{u}. The more XBP1^{u} is produced in *XBP1*$^{-/-}$ cells the higher the percentage of surviving cells. On the other hand, this does not hold true for the expression of XBP1^{s}. Already during the generation of the stable XBP1^{s} rescue cell lines, the survival rate of the cells which were transduced with low virus titer was significantly higher than of those transduced with high virus titer (data not shown). A lower XBP1^{s} expression seems to be more beneficial to cells regarding their ER stress resistance. Thus, the toxic effect of highly abundant Cib1^{s} in *U. maydis* might be reminiscent of the XBP1^{s}-dependent effects in RPE1 cells.
All in all, the function of XBP1^{u} with respect to ER stress resistance seems to be conserved with Cib1^{u} in *U. maydis*. The fact that the expression of *XBP1*^{u} in Δ*cib1* cells leads to an increase in ER stress resistance in a dose-dependent manner (Hampel, 2016) provides further support for this hypothesis.

3.2.2. **XBP1^{u} and Cib1^{u} mediate ER stress resistance independent of DNA-binding**

Under unstressed conditions, *XBP1*^{u} expression in RPE1 *XBP1*$^{-/-}$ cells is sufficient to restore cell proliferation up to WT level. The DNA-binding domain of XBP1^{u} is therefore not required and similar results were obtained for XBP1^{s}. However, under ER stress conditions only XBP1^{s} with an intact DNA-binding domain fully rescued the growth defect of RPE1 *XBP1*$^{-/-}$ cells. Thus, only under ER stress conditions the DNA-binding domain of XBP1^{s} and consequently the function as a transcription factor is decisive for cell survival. In contrast, even though XBP1^{u} only partially increased cell survival, mutating the DNA-binding domain did not affect the function any further, which may reflect a subordinate role of the DNA-binding domain for the XBP1^{u} function.

These results are in good accordance with was has been demonstrated in *U. maydis*. Hampel and co-workers showed that an intact DNA-binding domain is crucial for the Cib1 function to mediate ER stress resistance (Hampel, 2016). Also for the virulence of *U. maydis* an intact DNA-binding domain is prerequisite, too. On the other hand, the function of Cib1^{u} did not seem to be dependent on the DNA-binding domain. Neither the ability to mediate ER stress resistance nor pathogenicity was affected in Δ*cib1 bZIP* cib1^{us}* in comparison to Δ*cib1 cib1^{us}* strains.
In mice, hepatic overexpression of *XBP1^{s}* reduces serum glucose concentrations. Interaction of XBP1^{s} with FoxO1 promotes proteasomal degradation of FoxO1, which leads to reduced blood glucose levels and increased glucose tolerance. For that, the DNA-binding domain of XBP1^{s} is dispensable. This function of XBP1^{s} is most likely independent of ER stress (Zhou et al., 2011).

In essence, the regulatory roles of XBP1^{u} and Cib1^{u} are likely to be highly conserved. Both proteins were interchangeable with almost no loss of functionality and in both cases the DNA-binding domain was probably negligible. Assuming that the function of XBP1^{u} and Cib1^{u} is evolutionary conserved, this would narrow down the possibilities on how these proteins act on a mechanistic level, since Cib1^{u} arises from *U. maydis* in which UPR is exclusively regulated by the IRE1 pathway. Yet, it cannot be excluded that additional, so far undiscovered ER stress regulating pathways are present in *U. maydis*. In *S. cerevisiae*, a PERK related pathway, which regulates the amino acid control network and affects UPR via Gcn4p, the homolog of the mammalian bZIP transcription factor ATF4, does exist (Herzog et al., 2013). Nevertheless, in *U. maydis* a Gcn4p/ATF4 homolog has not been detected so far (Kai Heimel, personal communication).
Likewise, the fission yeast *S. pombe* has developed an extraordinary way of coping with ER stress. Since a Hac1 homolog is completely missing, ER homeostasis is mainly maintained by RIDD. To date, there is no study on RIDD in *U. maydis*. The results of the transcriptome analysis render this option very unlikely, since RIDD would provoke changes in gene expression which were not observed. Nevertheless, given that RIDD occurs in *U. maydis*, not only a regulatory role of XBP1^{u} and Cib1^{u} via the IRE1 signaling pathway but also via RIDD should be considered.

3.3. XBP1^{u} and Cib1^{u} acting as transcription factors

3.3.1. Regulatory role of XBP1^{u} on a transcriptional level

Transcriptome analyses in HEK 293 and MEF cells revealed several XBP1^{s} targets (Lee et al., 2003; Shoulders et al., 2013). Expression of *ERDJ4*, *p58^{IPK}*, *RAMP4* and *EDEM1* has been shown to be induced by XBP1^{s} under ER stress conditions. The specific activation of the *ERDJ4* expression via XBP1^{s} was additionally demonstrated in a luciferase reporter assay using approximately 500 bp of the promoter region (Lee et al., 2003). Unfortunately, a potential regulation by XBP1^{u} has not been tested, maybe due to the fact that in previous studies XBP1^{u} has been shown to be highly unstable and scarce and there were no indications of a transactivation domain. Nevertheless, a transcriptional activity of XBP1^{u} cannot be excluded. Acosta-Alvear and co-workers speculated that XBP1^{u} might also be able to access chromatin and bind targets if the protein is highly abundant so that the probability of complete degradation is low. Overall, XBP1^{u} abundance varies between cell types. In plasma cells and β-cells, for example, XBP1^{u} can be detected without proteasomal inhibition and XBP1^{u} mRNA levels were significantly higher compared to skeletal muscle myotubes (Acosta-Alvear et al., 2007). Hence, cell types with high XBP1^{u} abundance might be promising to gain further insights into a potential transcriptional role of XBP1^{u}. Based on the results obtained in this thesis, XBP1^{u} is unlikely to have transcriptional activity. The expression of common UPR targets was not responsive to XBP1^{u} neither under unstressed nor under ER stress conditions. While XBP1^{s}, as expected, regulated the expression of several UPR target genes, no XBP1^{u} targets were discovered. However, it appears possible that XBP1^{u} regulates another subset of genes which has not been tested in this work. Transcriptome-wide analyses should be considered.

Furthermore, luciferase reporter assays using the consensus UPRE motif as a binding site for XBP1^{s} and XBP1^{u} did confirm these observations. Surprisingly, the specific transcriptional activation of *ERDJ4* by XBP1^{s} using the same promoter region as described in Lee et al., 2003 could not be reproduced (data not shown). At this point, it should be noted that the *XBP1$^{-/-}$* MEF cells used in the studies of Lee and co-workers were treated with 1 µg/mL TM for 16 h prior to

measuring the luciferase activity. In contrast, luciferase activity in this work was determined without pharmacological induction of ER stress. While this does not have a direct effect on the expression of XBP1^{s}/XBP1^{u}, the abundance of other regulatory proteins might be affected, which would have an indirect effect on the transcriptional activation of *ERDJ4*.

Notably, a transcriptional activity has been attributed to XBP1^{u} regarding the regulation of oxidative stress. Some XBP1 targets are involved in redox homeostasis and oxidative stress responses. In *XBP1* deficient MEF cells, oxidative stress decreased cell viability and increased loss of mitochondrial membrane potential as well as ROS generation. mRNA expression of *SOD1*, *TRX1* and *Catalase* was decreased in those cells. Unexpectedly, not XBP1^{s} but XBP1^{u} clearly increased *Catalase* expression. In luciferase reporter assays using a segment of the catalase promoter, XBP1^{u} enhanced luciferase activity although this promoter does not contain distinct XBP1 binding sites. Instead, three CCAAT boxes were present. Consequently, for the XBP1^{u}-dependent expression of the *Catalase* the CCAAT motifs in the promoter as well as the contribution of NF-Y are pivotal (Liu et al., 2009). Previously, it has been shown that XBP1^{u}, under stressed conditions, can bind to the ERSE motif and activate reporter activity in the presence of NF-Y, even though XBP1^{u} is lacking a transactivation domain (Yoshida et al., 2001).

By contrast, this could not be confirmed in RPE1 cells although the UPRE reporter used in the luciferase assays contained five CCAAT motifs and it can be expected that the ubiquitous protein NF-Y was also present. Hence, it cannot be excluded that other motifs, which were missing in the UPRE reporter, were necessary for the transcriptional regulation of the catalase reporter by XBP1^{u}. On the other hand, XBP1^{u} fused to an artificial transactivation domain was able to activate the UPRE reporter, indicating that the lack of such a domain is likely the reason for the missing transcriptional activity.

Consistently, the UPRE reporter was activated by Cib1^{s} but not Cib1^{u}, which is providing further evidence for a functional conservation of XBP1^{s}/XBP1^{u} and Cib1^{s}/Cib1^{u}.

Overall, it seems highly unlikely that XBP1 regulates cell proliferation on a transcriptional level. The results of the transcript analyses and of the luciferase

assays are in line with the observation that the DNA-binding domain is not required to promote cell survival of *XBP1*$^{-/-}$ cells.

3.3.2. **Regulatory role of Cib1^{u} on a transcriptional level**

Analogous to the regulatory function of XBP1^{u} as negative regulator of XBP1^{s} described in mammals, overexpressed Cib1^{u} reduces ER stress resistance in WT and additionally negatively affects gene expression of common UPR target genes in a dose-dependent manner. This reflects once more a conserved regulatory role of XBP1^{u} and Cib1^{u}. In contrast, when expressed in Δ*cib1* cells, ER stress resistance is restored without affecting the gene expression of common UPR targets (Hampel, 2016). As in the case of XBP1^{u}, core UPR targets seem not to be transcriptionally regulated by Cib1^{u}, which is in line with the fact that the DNA-binding domain, which is essential for transcriptional activity, is dispensable for increasing cell growth under ER stress conditions.

However, transcriptome-wide analysis of Cib1^{u}-regulated genes under ER stress conditions revealed 12 targets (*um01433*, *um01434*, *um01431*, *um01432*, *um11339*, *um11338*, *um11369*, *um00842*, *um11815*, *um02191*, *um03285* and *um04410*) which were co-regulated in WT and Δ*cib1 cib1*^{us} cells but not in Δ*cib1* cells. Those observations indicate that Cib1^{u} might have a regulatory function on a transcriptional level, most likely indirectly via other proteins. Interestingly, 7 of the 12 genes have a putative function in the iron uptake system in *U. maydis*. *um04410* probably encodes a siderophore iron transporter, whereas the other 6 genes (*um01433*, *um01434*, *um01431*, *um01432*, *um11339* and *um11338*) are co-regulated and located in one of the three iron uptake clusters described in *U. maydis* (Eichhorn et al., 2006).

Several secondary metabolites are produced in *U. maydis*, among which are two types of siderophores, ferrichrome and ferrichrome A. Both are regulated in an iron-responsive way by the transcription factor Urbs1 (Bölker et al., 2008; Eichhorn et al., 2006). Iron is an essential metal required for successful survival of cells and is therefore absorbed, stored and delivered when required by siderophores (Raines et al., 2015).

The above-mentioned 6 genes seem to be involved in the biosynthesis of ferrichrome A and in the siderophore transport. In addition, under ER stress

conditions, 15 genes were identified which were differentially regulated in SG200, SG200 Δ*cib1* and SG200 Δ*cib1 cib1*^{us}. Those genes were mapped to a variety of cellular processes such as siderophore-iron transport, heavy metal-iron transport and secondary metabolism. Interestingly, also in this case, all siderophore-related genes were induced in the presence of Cib1^{u}.

In hepatocyte-derived cell lines exposed to ER stress it was shown that the expression levels of iron-related genes were increased (Oliveira et al., 2011). Vecchi and co-workers came to the same conclusion using a different experimental approach. Hepcidin is a peptide hormone that regulates iron homeostasis in mammals. Under ER stress conditions, the transcription factor CREBH is upregulated and leads to an induction of hepcidin (Vecchi et al., 2009). In summary, these studies clearly show a connection between the ER stress response and iron homeostasis. In several additional studies it has also been observed that an ER stress response can be activated by changes in the cellular iron levels and iron metabolism. As an example, it was shown in pancreatic cancer cells that the depletion of cellular iron resulted in an induction of oxidative stress and activation of the PERK pathway (Lane et al., 2014; Sahni et al., 2014). Such a system would also be conceivable in *U. maydis*. Increased production of siderophores leads to a decrease in the available iron pools which, in turn, would lead to an increased ER stress response. Since the PERK pathway is missing in *U. maydis*, it remains to be investigated how such a regulation could take place. A recent study in *S. cerevisiae* showed that Ire1p forms clusters to ensure ideal UPR activation. This cluster formation is dependent on a certain membrane composition which is determined by intracellular iron levels. Depletion of iron upon ER stress induction affects UPR activation in yeast and mammals by preventing IRE1 clustering and consequently slowing down IRE1 signaling (Cohen et al., 2017). Such a scenario cannot be ruled out in *U. maydis*, either. Nevertheless, although the molecular mechanism should be further analyzed, it can be concluded that there is a clear connection between UPR and iron homeostasis. More importantly, it remains to be clarified how the regulatory function of Cib1^{u} on a transcriptional level fits to the data, which clearly show that a functional DNA-binding domain is not necessary in Cib1^{u} to mediate ER stress resistance. An indirect regulation via other transcription factors/regulators (e.g.,

Urbs1), which specifically interact with Cib1^{u} but not Cib1^{s}, appears possible. Since Cib1^{s} and Cib1^{u} only differ from one another at the C-terminus, this region would be preferred for interaction with other proteins to ensure a certain specificity. Co-immunoprecipitation studies in this work provide first hints that heterodimerization with Cib1^{s} occurs not only via the N-terminus but also via the C-terminus.

In conclusion, it remains to be determined how exactly iron metabolism and ER stress response are linked and whether the regulatory roles of XBP1^{u} and Cib1^{u} are conserved in this respect.

3.4. XBP1^{u} acting on a post-transcriptional level

Activation of XBP1^{s} leads to a remodeling of the cellular proteome. Proteins involved in ER import, assisting folding or unfolding processes, quality control and degradation as well as intracellular trafficking are increasingly produced (Shoulders et al., 2013). Furthermore, the focus of XBP1^{s} analysis is mostly on its function as transcription factor. Comprehensive studies addressing a potential regulation of the ER stress response through protein-protein interaction with XBP1^{s} do not exist except for the interaction with other transcription factors in order to modulate the transcriptional response. Contrary to that, and despite the fact that a comparable proteome analysis does not exist, the scope of characterizing the regulatory function of XBP1^{u} has recently been on the interaction with other regulators through which XBP1^{u} can regulate ER stress. Huang and co-workers have discovered a specific interaction of MDM2 and XBP1^{u}, which resulted in a faster cell proliferation clearly showing a connection between XBP1^{u} and the tumor suppressor MDM2/p53 axis (more information in section 3.1.1.) (Huang et al., 2017). Additionally, XBP1^{u} has been demonstrated to directly interact with FoxO1 via the C-terminus under glutamine starvation conditions thereby inducing autophagy (more information in section 3.1.1.) (Zhao et al., 2013). Moreover, XBP1^{u} is able to protect endothelial cells from oxidative stress by physically interacting with HDAC3 and forming a complex with Akt1/mTOR. In this way, an upregulation of heme oxygenase, which is required for an anti-oxidative reaction, is achieved (Martin et al., 2014).

Remarkably, proteome-wide analyses on XBP1^{u} interactors did not reveal any of the above-mentioned interactors. It is possible that low XBP1^{u} expression levels or transient interactions account for the lack of identified protein interactions. Only few potential interactors were found that could have an influence on the ER stress response.

One of the potential interactors is thrombospondin 1 (THBS1). THBS1 has been proposed to have an influence on the ER stress response via both the PERK and ATF6 UPR branch (Cunha et al., 2016; Lynch et al., 2012). Another candidate is calponin 3 (CNN3), which is a regulatory protein binding to actin and calmodulin and involved in coordinating contractility of actin fibers (Ciuba et al., 2018).Actin stress fibers can be crosslinked via filamin A, which has been shown to interact with PERK resulting in stimulation of ER-plasma membrane contacts and maintenance of the actin cytoskeleton morphology (van Vliet et al., 2017). Another potential interactor of XBP1^{u} is the 26S proteasome regulatory subunit 11 (PSMD11) which regulates an increased proteasome activity in embryonic stem cells (Vilchez et al., 2012). The proteasome activity is tightly linked to ER stress since inhibition of the proteasomal function leads to increased ER stress levels (Lee et al., 2013).

It remains to be tested whether these proteins exert a regulatory role together with XBP1^{u} and whether XBP1^{u} acts on a post-transcriptional level. Under unstressed growth conditions, cell proliferation of RPE *XBP1*$^{-/-}$ cells was increased by expression of either *XBP1*^{u} or *XBP1*^{s}. However, it is unclear if both proteins resort to the same mechanism. In this case, the search for XBP1^{u}-specific interactors would be unrewarding and should be extended to proteins enriched in the presence of both XBP1^{u} and XBP1^{s}. On the other hand, it is still imaginable that there are two different strategies involved. XBP1^{u} could take over the ER stress regulation at low ER stress levels. As soon as ER stress can no longer be regulated by XBP1^{u} alone, IRE1α would be activated providing XBP1^{s}, which, in turn, would take over the regulatory function to restore ER homeostasis. In case of prolonged ER stress XBP1^{u} would induce degradation of XBP1^{s} leading the cells to cell death as suggested by Yoshida et al., 2006.

Due to the fact that the function of XBP1^{u} is only poorly understood, further research should be centered around a better understanding of the novel XBP1^{u}

role in the regulation of the ER stress response, which, due to the many parallels to Cib1^{u} in *U. maydis*, seems to be conserved in lower eukaryotes.

3.5. Linkage between the regulatory function of XBP1^{u} and its subcellular localization

XBP1^{u} is a highly unstable protein and this is probably the reason why information on its intracellular localization is scarce. In 2006, Yoshida and co-workers proposed a dual nuclear and cytoplasmic localization for XBP1^{u} in the cervical cancer cell line HeLa. While the very N-terminal part of the protein mediates nuclear localization, the C-terminal part of the protein is directed to the cytoplasm. The presence of an NLS and an NES provides a putative mechanistic basis for this dual localization of XBP1^{u}. Furthermore, they hypothesized that the XBP1^{u} localization is dynamic and that the protein shuttles between the cytoplasm and the nucleus. After prolonged ER stress, XBP1^{u} binds to XBP1^{s}, which is predominantly localized to the nucleus and forms a heterodimer resulting in nuclear export and degradation by the 26S proteasome (Yoshida et al., 2006). In another study in fibroblast-like cells derived from monkey kidney (COS-7), XBP1^{u} showed a localization to the ER and to the nucleus. Co-localization with Golgi and mitochondrial marker proteins could be excluded (Kanda et al., 2016). Nevertheless, Zhao and co-workers showed in lung cancer cells (H1299) via immunofluorescence that XBP1^{u} is mainly localized in the cytoplasm (Zhao et al., 2013). However, live cell imaging showing the dynamic interaction and the mobility of XBP1^{u} is still incomplete.

In the fluorescence microscopy analysis of the XBP1^{u} localization in RPE1 cells performed as part of this work, a nuclear and ER localization was observed. The nuclear localization of XBP1^{u} was reduced under ER stress conditions. Surprisingly, also XBP1^{s}, in contrast to the predominantly nuclear localization described in literature, showed a dual localization in the nucleus and the ER under conditions in which only little XBP1^{u} was produced. Moreover, FRAP analyses showed that XBP1^{u} and XBP1^{s} were similarly dynamic inside the nucleus. A similarly dynamic shuttling of XBP1^{s} or XBP1^{u} between the cytoplasm

and the nucleus was not observed.

All in all, these data imply that XBP1^{u} can be localized to the ER as well as the nucleus independent of ER stress levels. It would be interesting to see if a specific subcellular localization might be connected to the rescue of cell survival. By removing, for example, the NLS in XBP1^{u}, the protein would no longer be able to enter the nucleus. Assuming that only one of the two localizations is necessary to mediate cell proliferation, this would narrow down and simplify the search for the mode of action of XBP1^{u} to a large degree.

Surprisingly, Cib1^{u} did not localize to the ER but predominantly to the nucleus. In addition, it was observed that Cib1^{u} was not evenly distributed all over the nucleus but rather with a preference to certain areas. It cannot be excluded that XBP1^{u} binds to specific areas within the chromatin. Nonetheless, if the regulatory role of XBP1^{u} and Cib1^{u} was conserved on a mechanistic level, removal of the NLS would prevent XBP1^{u} from mediating cell survival. In contrast, removing the NES should not have a negative impact on cell proliferation.

3.6. Effect of XBP1^{u} on organelle morphology

ER stress not only affects the survival of cells but also their morphology. In rat fibroblasts, for example, heat-shock treatment induces flattening of the cells, an increase of actin-containing microfilaments and changes in the nuclear morphology (Welch and Suhan, 1985). However, in the analyses for this work, neither RPE1 WT nor RPE1 *XBP1*$^{-/-}$ cells exhibited changes in their actin network under unstressed conditions or TM-induced ER stress conditions. Certainly, this could be tied to the diverse ways in which cells were subjected to stress. Different sources of ER stress provoke different stress reactions. Similarly, these effects might be specific for certain cell lines as some cell lines may be more resistant to ER stress than others.

In some *XBP1*$^{-/-}$ cells, the nucleus seemed more fragmented than in WT. However, quantitative analyses showed that the fragmented appearance was equally likely to be found in WT cells independent of ER stress, which implies that these morphological changes are neither ER stress- nor XBP1-dependent. In the RPE1 *XBP1*$^{-/-}$ cells observed, the Golgi morphology was also altered

compared to WT cells. This observation is similar to previous reports where neuronal cells extendedly exposed to oxidative and pharmacological stress resulted in Golgi fragmentation (Machamer, 2015). In the absence of *XBP1*, the Golgi appeared larger and more fragmented, indicating that XBP1 might be involved in the maintenance of the Golgi morphology. Since the Golgi is part of the secretory apparatus and the organelle in which protein modification, sorting and packaging take place, it is reasonable that the deletion of *XBP1* also affects Golgi morphology.

Already in 1990, it was reported that in differentiating lymphocytes the size and shape of the ER change under ER stress conditions, such as a volume increase of more than threefold (Wiest et al., 1990). A potential involvement of XBP1^{u} was not investigated in any of the above-mentioned studies.

In this work it could be shown that both ER stress and the deletion of *XBP1* affect ER morphology. Already under unstressed conditions, the ER density in *XBP1* KO cells is reduced compared to RPE1 WT cells. ER stress induction leads to a more pronounced phenotype. In addition to the reduced density, the ER in *XBP1*$^{-/-}$ cells seems more fragmented compared to the ER in WT. Remarkably, under unstressed conditions, ER morphology could be restored by XBP1^{u} but not by XBP1^{s}. Under unstressed conditions, XBP1^{s} is normally not produced. Hence, the putative XBP1^{s} might have negatively affected the ER morphology under unstressed conditions. By contrast, under ER stress conditions, expression of both XBP1^{u} and XBP1^{s} restored ER morphology to a degree where no more differences to WT were discernible.

In conclusion, it could be shown that XBP1^{u} has a positive impact on the maintenance of the ER morphology, which, in turn, could be connected to increased cell survival. The underlying molecular mechanisms, however, are yet to be discovered. Hence, it would be important to investigate if the Cib1^{u} function is also conserved in this respect and sufficient to restore ER morphology.

3.7. XBP1^{u}: Mode of action

XBP1^{u} is a highly unstable protein whose regulatory role in the ER stress response was hardly covered in the past. The analyses for this work demonstrated that XBP1^{u} is able to rescue several cellular deficiencies caused by an *XBP1* deletion under unstressed and stressed conditions. XBP1^{u} was shown in this thesis to have an impact on cell proliferation, cell death, ER stress resistance and organelle morphology.

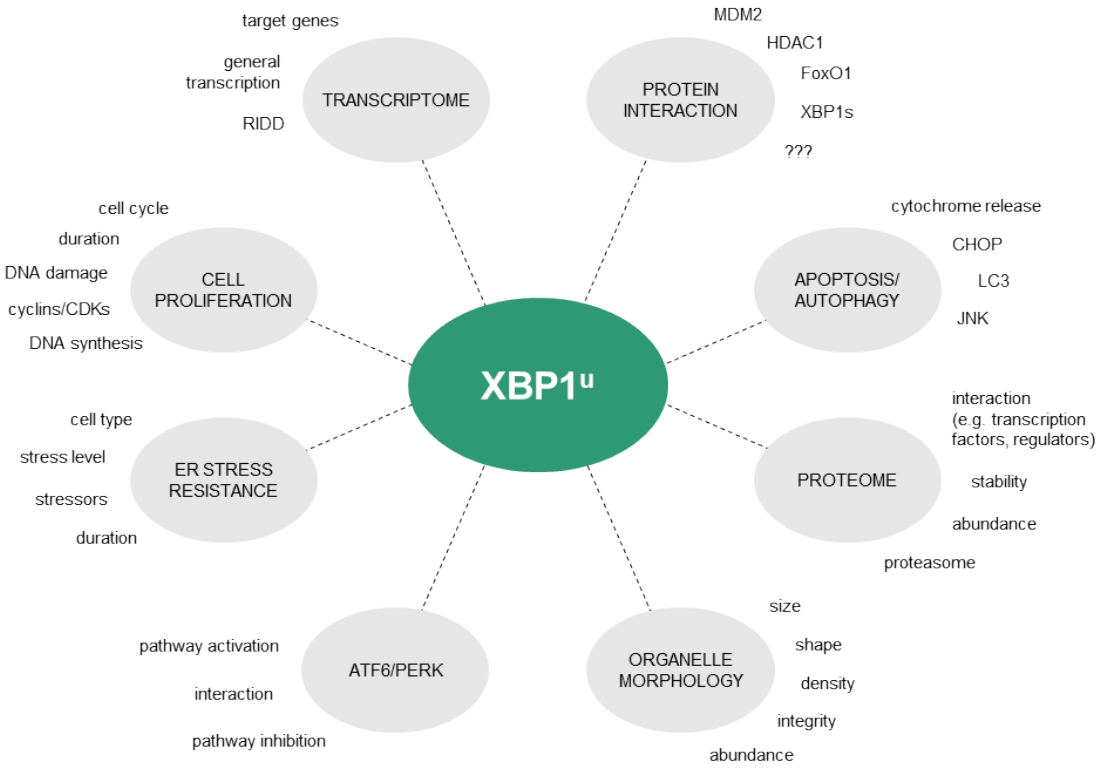

Figure 34: Overview on cellular processes affected by XBP1^{u}

XBP1^{u} most likely has an influence on cell proliferation, ER stress resistance as well as on apoptosis/autophagy. Duration of stress and type of the stressor selected play an important role. It remains to be clarified to which extent XBP1^{u} takes part in the regulation of the cell cycle on a molecular level as well as in the regulation of pathways that may lead to cell death. Moreover, XBP1^{u} could have an impact on the transcriptome/proteome. However, it remains to be investigated if certain targets or the transcript/protein stability are affected and how XBP1^{u} mechanistically affects the organelle morphology.

The molecular details and mechanism on how XBP1^{u} affects those processes will be a matter of future research. Interactions with other regulatory proteins, influence on the transcriptome, proteome, apoptosis and autophagy pathways as well as on the UPR branches PERK and ATF6 should be taken into consideration and further analyzed (Fig. 34).

4. Material and Methods

4.1. Material and source of supply

4.1.1. Chemicals

All chemicals used in this work were of p.a. quality, if not noted otherwise, and were obtained from BioRad, Carl Roth, Difco, Fluka, Invitrogen, Invivogen, New England Biolabs (NEB), Promega, Sigma-Aldrich, Macherey-Nagel, Merck, QIAGEN, Riedel-de-Haën and Thermo Fisher Scientific.

4.1.2. Enzymes

Restriction endonucleases were obtained from Thermo Fisher Scientific and NEB. As DNA polymerases either the Phusion DNA Polymerase (laboratory preparation and NEB) or the Q5 High-Fidelity DNA Polymerase were used. Gateway LR clonase enzyme mix as well as the Gibson assembly master mix were obtained from Thermo Fisher Scientific. For the generation of DNA probes, the Klenow polymerase (Thermo Fisher Scientific) was used. Ligation of DNA molecules was performed either with the T4 DNA Ligase (Thermo Fisher Scientific) or the Quick ligase (NEB). FastAP thermosensitive alkaline phosphatase (Thermo Fisher Scientific) was used for the dephosphorylation of DNA. For enzymatic digestion of RNA, RNase A (Serva and Invitrogen) was used. Lysing enzyme from *Trichoderma harzianum* was used for the digestion of fungal cell walls (Sigma-Aldrich).

4.1.3. **Antibodies**

Table 2: Used antibodies

Antibodies	Source of supply
α-HA	Sigma-Aldrich, H9658
α-HA Rhodamine-labeled	Boehringer
α-HA	Roche
α-GFP	Sigma-Aldrich, G1544
α-GFP	Roche, clones 7.1 and 13.1
α-XBP1^{s}	Biolegend, Poly6195
α-VapA	Sigma Prestige, HPA009174
α-GM130	BD Bioscience, 610822
α-phospho-Histone H3 (Ser10)	Merck, 06-570
α-Digoxigenin-AP	Roche, 11093274910
α-mouse IgG HRP conjugate	Promega, W402B
α-rabbit IgG HRP conjugate	Promega, W401B
α-Alexa568-donkey α-mouse IgG	Molecular Probes
α-Alexa488-goat α-rabbit IgG	Jackson

4.1.4. **Buffers and solutions**

Buffers and solutions needed for a specific method can be found below the description and were produced according to Ausubel et al., 1987; Sambrook et al., 1989, if not stated otherwise. All buffers and solutions were either autoclaved at 121°C for 20 min or sterilized by filtration (size of filter pores: 0.2 µm).

4.1.5. **Antibiotics/Fungicides**

Antibiotics/Fungicides were used as indicated in Table 3. Stocks were sterilized by filtration.

Table 3: Used antibiotics/fungicides

Antibiotic/Fungicide	Stock concentration	Final concentration
Ampicillin/Carbenicillin	100 mg/mL in H_2O	100 µg/mL
Blasticidin	10 mg/mL in HEPES	10 µg/mL
Carboxin	5 mg/mL in ethanol	2 µg/mL
G418	200 mg/mL in H_2O	400 µg/mL
Hygromycin	100 mg/mL in H_2O	200 µg/mL
Kanamycin	50 mg/mL in H_2O	30-50 µg/mL
Nourseothricin (clonNAT)	200 mg/mL in H_2O	75 µg/mL

4.1.6. **Kits**

All kits were used according to the manufacturer's protocol, if not stated otherwise.

Table 4: Used kits

Kits	Usage	Source of supply
QIAquick PCR Purification Kit	Purification of PCR products	QIAGEN
QIAquick Gel Extraction Kit	DNA extraction from agarose gels	QIAGEN
GeneJet Gel Extraction Kit	DNA extraction from agarose gels	Thermo Fisher Scientific
QIAprep Spin Miniprep Kit	Preparation and purification of plasmid DNA from *E. coli*	QIAGEN
DNA, RNA, and protein purification	Preparation and purification of plasmid DNA from *E. coli*	Macherey-Nagel
QIAGEN Plasmid Plus Midi Kit	Extraction and purification of plasmid DNA from *E. coli*	QIAGEN
Clone Jet PCR Cloning Kit	Subcloning of PCR fragments	Thermo Fisher Scientific
Phire Tissue Direct PCR Master Mix	PCR screen of *XBP1* KO clones	Thermo Fisher Scientific
Phusion Human Specimen Direct PCR	PCR screen of *XBP1* KO clones	Thermo Fisher Scientific
PureLink Genomic DNA Mini Kit	Extraction of genomic DNA from RPE1 cells	Invitrogen
SuperSignal West Dura Extended Duration Substrate	ECL substrate for HRP detection (Western Blot)	Thermo Fisher Scientific
Clarity Western ECL substrate	ECL substrate for HRP detection (Western Blot)	BioRad
Dual-Luciferase Reporter Assay System	Detection of firefly and renilla luciferase activity	Promega
RNeasy Mini Kit	Extraction of RNA	QIAGEN
RNeasy MinElute Cleanup Kit	RNA purification	QIAGEN
TurboDNase Kit	DNaseI digestion of purified RNA	Ambion
MesaGreen qPCR Master Mix	qRT-PCR	Eurogentech
cDNA synthesis Kit	Synthesis of cDNA	Thermo Fisher Scientific
iScript cDNA synthesis Kit	Synthesis of cDNA	BioRad
Amaxa Cell Line Nucleofector Kit L	Transfection of RPE1 cells	Lonza Bioscience
Trans-Blot Turbo RTA Midi/Mini PVDF Transfer Kit	Transfer of proteins (Western Blot with Trans-Blot Turbo Transfer System)	BioRad

4.1.7. **Miscellaneous**

Table 5: Miscellaneous

Product	Usage	Source of supply
Tunicamycin	Induction of ER stress	Sigma-Aldrich
Hoechst 33342	Staining of nuclei	Thermo Fisher Scientific
GFP-Trap	Immunoprecipitation of GFP-tagged proteins	ChromoTek
Alexa Fluor 647 Phalloidin	Staining of F-actin	Thermo Fisher Scientific
SYBR safe stain	DNA gel stain	Invitrogen
Ethidium bromide	DNA gel stain	Roth
Trizol	RNA preparation	Invitrogen
PhosSTOP	Inhibition of phosphatases	Sigma-Aldrich
cOmplete protease inhibitor cocktail	Inhibition of proteases	Roche
Fugene 6 Transfection reagent	Transfection of RPE1 cells	Promega
Lipofectamine 2000 Transfection reagent	Transfection of Lenti-X cells	Thermo Fisher Scientific
SYTOX Green	DNA stain for flow cytometry	Thermo Fisher Scientific
Pacific Blue Dye	Barcoding for flow cytometry	Thermo Fisher Scientific

4.2. Cultivation of microorganisms

4.2.1. **Cultivation of *Escherichia coli***

Liquid cultures of *E. coli* were cultivated in dYT- or LB-medium under aerobic conditions at 37°C with continuous shaking (Sambrook et al., 1989). For cultivation on solid medium either dYT- or LB-agar plates were used. 100 µg/mL ampicillin, 100 µg/mL carbenicillin or 30-50 µg/mL kanamycin were added to the medium when needed. *E. coli* cells used for Gateway cloning were incubated at 30°C. Optical density (OD) of liquid cultures was photometrically determined at 600 nm if not stated otherwise. For long-term storage at -80°C, a dense grown overnight culture was supplemented with 50 % (v/v) NSY-Glycerol-medium.

dYT-medium

16 g/L	Tryptone
10 g/L	Yeast extract
5 g/L	NaCl
1.5 % (w/v)	Agar for solid medium

Dissolve in $H_2O_{bid.}$ and autoclave at 121°C for 20 min.

LB-medium

10 g/L	Tryptone
5 g/L	Yeast extract
10 g/L	NaCL
1.5 % (w/v)	Agar for solid medium

Dissolve in $H_2O_{bid.}$ and autoclave at 121°C for 20 min.

NSY-Glycerol-medium

8 g/L	Nutrient Broth
1 g/L	Yeast extract
5 g/L	Saccharose
87 % (v/v)	Glycerol

Dissolve in $H_2O_{bid.}$ and autoclave at 121°C for 20 min.

4.2.2. **Cultivation of *Ustilago maydis***

U. maydis cells were cultivated in YEPS-L-medium, CM-medium or YNB-medium supplemented with 100 µg/mL ampicillin under aerobic conditions at 30°C with continuous shaking. For cultivation on solid medium, PD-agar plates supplemented, if required, with 2 µg/mL carboxin, 400 µg/mL G418 or 200 µg/mL hygromycin, were used. For long-term storage at -80°C, 50 % (v/v) NSY-Glycerol-medium was added to a dense overnight culture. Optical density (OD) of liquid cultures was photometrically determined at 600 nm if not stated otherwise. Logarithmic grown cells with an OD_{600} of 0.6-1.2 were used, unless stated differently. OD_{600} of 1.0 in *U. maydis* corresponds to 1-5 x 10^7 cells.

YEPS-L-medium (modified from Tsukuda et al., 1988)

10 g/L	Peptone
10 g/L	Yeast extract
10 g/L	Saccharose

Dissolve in $H_2O_{bid.}$ and autoclave at 121°C for 20 min.

CM-medium (Banuett and Herskowitz, 1989; Holliday, 1974)

1.5 g/L	Ammonium nitrate
2.5 g/L	Casamino acids
0.5 g/L	Herring sperm DNA
1.0 g/L	Yeast extract
1 % (v/v)	Vitamin solution
62.5 mL/L	Salt solution
1 mL/L	Trace element solution
2 % (w/v)	Bacto agar for solid medium
1 % (v/v)	50 % glucose (after autoclaving)

Dissolve in $H_2O_{bid.}$, adjust pH to 7.0 and autoclave at 121°C for 20 min.

Vitamin solution (Holliday, 1974)

100 mg/L	Thiamine
50 mg/L	Riboflavin
50 mg/L	Pyridoxine
200 mg/L	Calcium pantothenate
500 mg/L	p-Aminobenzoic acid
200 mg/L	Nicotinic acid
200 mg/L	Cholin chloride
1000 mg/L	Myo-Inositol

Dissolve in $H_2O_{bid.}$ and sterilize by filtration.

Salt solution (Holliday, 1974)

16 g/L	KH_2PO_4
4 g/L	Na_2SO_4
8 g/L	KCl
4 g/L	$MgSO_4 * 7\ H_2O$
1.32 g/L	$CaCl_2 * 2\ H_2O$
8 mL/L	Trace element solution

Dissolve in $H_2O_{bid.}$ and sterilize by filtration.

Trace element solution (Holliday, 1974)

60 mg/L	H_2BO_3
140 mg/L	$MnCl_2 * 4\ H_2O$
400 mg/L	$ZnCl_2$
40 mg/L	$NaMoO_4 * 2\ H_2O$
100 mg/L	$FeCl_3 * 6\ H_2O$
40 mg/L	$CuSO_4 * 5\ H_2O$

Dissolve in $H_2O_{bid.}$ and sterilize by filtration.

YNB-medium

1.7 g/L	YNB w/o aa, w/o $(NH_4)_2SO_4$
0.2 % (v/v)	20 % $(NH_4)_2SO_4$
1 % (v/v)	50 % Glucose
2 % (w/v)	Bacto agar for solid medium

Dissolve in $H_2O_{bid.}$, adjust pH to 5.8 and autoclave at 121°C for 20 min.

PD-agar plates

24 g/L	Potato dextrose broth
2 % (w/v)	Bacto agar

Dissolve in $H_2O_{bid.}$ and autoclave at 121°C for 20 min.

4.3. Cultivation of human cell lines

4.3.1. Cultivation of RPE1 cells

hTert-RPE1 cells (ATCC CRL-4000, human retinal pigmented epithelial cells immortalized with hTert) were cultivated according to ATCC guidelines in Dulbecco's modified Eagle's medium F12 (DMEM-F12, Sigma-Aldrich) supplemented with 10 % fetal bovine serum, 1 % penicillin/streptomycin (100 units/ mL penicillin, 100 µg/mL streptomycin) and maintained at 37 °C under 5 % CO_2. Cells were subcultured at 70-80 % of confluency. Therefore, cells were briefly rinsed in Trypsin/EDTA and afterwards incubated in 0.5-4 mL Trypsin/EDTA until all cells were fully detached and transferred to a new culture flask with full growth medium. For long-term storage, 80 % confluent cells were transferred to liquid nitrogen in complete growth medium supplemented with 10 % DMSO. Cells were regularly tested for mycoplasma contamination. Cell number was either determined with a Countess II FL automated cell counter (Thermo Fisher Scientific) or with a Coulter Counter (Beckman Coulter). RPE1 cells were transiently transfected with Fugene 6 using a ratio of 3:1 of reagent to DNA. 12 h after transfection, the cells were washed in order to remove the transfection reagent.

4.3.2. Cultivation of Lenti-X cells

Lenti-X cell line derived from the human embryonic kidney cell line Hek293 was used for lentiviral packaging and cultivated according to ATCC guidelines in Dulbecco's modified Eagle's medium (DMEM) high glucose (Sigma-Aldrich) supplemented with 10 % fetal bovine serum, 1 % penicillin/streptomycin (100 units/ mL penicillin, 100 µg/mL streptomycin) and maintained at 37 °C under 5 % CO_2. Cells were subcultured at 70-80 % of confluency.

4.4. Strains, cell lines, plasmids and oligonucleotides

4.4.1. *E. coli* strains

For all cloning procedures, the *E.coli* strain TOP10 (Invitrogen) with the following genotype was used:

F$^-$ *mcrA Δ(mrr-hsdRMS-mcrBC) Φ80lacZΔM15 ΔlacX74 recA1 araD139 Δ(ara-leu)7697 galU galK rpsL (Str^R) endA1 nupG*.

4.4.2. *U. maydis* strains

All *U. maydis* strains used and generated in this work are listed in Table 6 and Table 7, respectively. All generated strains were verified via Southern Blot and/or Western Blot if not stated otherwise.

Table 6: *U. maydis* strains used in this work

Strains	Genotype	Resistance	Reference
SG200	*a1::mfa2 bE1/bW2*	P	Kämper et al., 2006
SG200 Δ*cib1*	*a1::mfa2 bE1/bW2 Δcib1*	P, H	Heimel et al., 2010
SG200 Δ*cib1 cib1^{us}*	*a1::mfa2 bE1/bW2 Δcib1 ip^R[P$_{etef}$:cib1^{us}]ip^S*	P, H, C	Hampel, 2016
SG200 Δ*cib1 cib1*	*a1::mfa2 bE1/bW2 Δcib1 ip^R[P$_{etef}$:cib1]ip^S*	P, H, C	Hampel, 2016
FB1	*a1 b1*	–	Banuett and Herskowitz, 1989
FB1 Δ*cib1*	*a1 b1 Δcib1*	H	Heimel et al., 2010
SG200 Cib1-GFP	*a1::mfa2 bE1/bW2 P$_{etef}$:cib1-gfp*	H	Kai Heimel, pers. communication
SG200 eGFP	*a1::mfa2 bE1/bW2 ip^R[P$_{etef}$:egfp]ip^S*	P, C	Verena Siebert, pers. communication
SG200 Δ*cib1* Cib1^u-GFP	*a1::mfa2 bE1/bW2 Δcib1 ip^R[P$_{etef}$:cib1^{us}-gfp]ip^S*	P, H, C	Martin Hampel, pers. communication

Table 7: *U. maydis* strains generated in this work

Strains	Genotype	Resistance[1]	Integration frequency[2]
SG200 Δ*cib1 bZIP* cib1^{us}*	*a1::mfa2 bE1/bW2 Δcib1 ip^{R}[P$_{etef}$:bZIP* cib1^{us}]ip^{S}*	P, H, C	s and m
SG200 Δ*cib1 bZIP* cib1^{s}*	*a1::mfa2 bE1/bW2 Δcib1 ip^{R}[P$_{etef}$:bZIP* cib1^{s}]ip^{S}*	P, H, C	s
SG200 Δ*cib1 crg:cib1^{s}-3xHA*	*a1::mfa2 bE1/bW2 Δcib1 ip^{R}[P$_{crg}$:cib1^{s}-3xHA]ip^{S}*	P, H, C	m
SG200 3xHA-Cib1	*a1::mfa2 bE1/bW2 ip^{R}[P$_{etef}$:3xHA-cib1^{s}]ip^{S}*	P, C	s and m
FB1 Δ*cib1 crg:cib1^{us}-3xHA*	*a1 b1 Δcib1 ip^{R}[P$_{crg}$:cib1^{us}-3xHA]ip^{S}*	H, C	s and m
SG200 Cib1-GFP Cib1^{s}-3xHA	*a1::mfa2 bE1/bW2 P$_{etef}$:cib1-gfp ip^{R}[P$_{etef}$:cib1^{s}-3xHA]ip^{S}*	P, H, C	s and m
SG200 Cib1-GFP Cib1^{u}-3xHA	*a1::mfa2 bE1/bW2 P$_{etef}$:cib1-gfp ip^{R}[P$_{etef}$:cib1^{us}-3xHA]ip^{S}*	P, H, C	s and m
SG200 Cib1-GFP Cib1-N-term-3xHA	*a1::mfa2 bE1/bW2 P$_{etef}$:cib1-gfp ip^{R}[P$_{crg}$:cib1-N-term-3xHA]ip^{S}*	P, H, C	s and m
SG200 Cib1-GFP Cib1^{s}-C-term-3xHA	*a1::mfa2 bE1/bW2 P$_{etef}$:cib1-gfp ip^{R}[P$_{etef}$:cib1^{s}-C-term-3xHA]ip^{S}*	P, H, C	s and m
SG200 Cib1-GFP Cib1^{u}-C-term-3xHA	*a1::mfa2 bE1/bW2 P$_{etef}$:cib1-gfp ip^{R}[P$_{etef}$:cib1^{us}-C-term-3xHA]ip^{S}*	P, H, C	s and m
SG200 Δ*cib1* Cib1^{u}-GFP Cib1^{u}-3xHA	*a1::mfa2 bE1/bW2 Δcib1 ip^{R}[P$_{etef}$:cib1^{us}-gfp]ip^{S} ip^{R}[P$_{etef}$:cib1^{us}-3xHA]ip^{S}*	P, H, C, G	unknown
SG200 Δ*cib1* Cib1^{u}-GFP Cib1^{s}-3xHA	*a1::mfa2 bE1/bW2 Δcib1 ip^{R}[P$_{etef}$:cib1^{us}-gfp]ip^{S} ip^{R}[P$_{etef}$:cib1^{s}-3xHA]ip^{S}*	P, H, C, G	unknown
SG200 Δ*cib1* Cib1^{u}-GFP Cib1-N-term-3xHA	*a1::mfa2 bE1/bW2 Δcib1 ip^{R}[P$_{etef}$:cib1^{us}-gfp]ip^{S} ip^{R}[P$_{crg}$:cib1-N-term-3xHA]ip^{S}*	P, H, C, G	unknown
SG200 Δ*cib1* Cib1^{u}-GFP Cib1^{s}-C-term-3xHA	*a1::mfa2 bE1/bW2 Δcib1 ip^{R}[P$_{etef}$:cib1^{us}-gfp]ip^{S} ip^{R}[P$_{etef}$:cib1^{s}-C-term-3xHA]ip^{S}*	P, H, C, G	unknown
SG200 Δ*cib1* Cib1^{u}-GFP Cib1^{u}-C-term-3xHA	*a1::mfa2 bE1/bW2 Δcib1 ip^{R}[P$_{etef}$:cib1^{us}-gfp]ip^{S} ip^{R}[P$_{etef}$:cib1^{us}-C-term-3xHA]ip^{S}*	P, H, C, G	unknown
SG200 eGFP Cib1^{s}-3xHA	*a1::mfa2 bE1/bW2 ip^{R}[P$_{etef}$:egfp]ip^{S} ip^{R}[P$_{etef}$:cib1^{s}-3xHA]ip^{S}*	P, C, G	unknown
SG200 eGFP Cib1-N-term-3xHA	*a1::mfa2 bE1/bW2 ip^{R}[P$_{etef}$:egfp]ip^{S} ip^{R}[P$_{crg}$:cib1-N-term-3xHA]ip^{S}*	P, C, G	unknown
SG200 eGFP Cib1^{u}-C-term-3xHA	*a1::mfa2 bE1/bW2 ip^{R}[P$_{etef}$:egfp]ip^{S} ip^{R}[P$_{etef}$:cib1^{us}-C-term-3xHA]ip^{S}*	P, C, G	unknown
SG200 eGFP Cib1^{u}-3xHA	*a1::mfa2 bE1/bW2 ip^{R}[P$_{etef}$:egfp]ip^{S} ip^{R}[P$_{etef}$:cib1^{us}-3xHA]ip^{S}*	P, C, G	unknown
SG200 eGFP Cib1^{s}-C-term-3xHA	*a1::mfa2 bE1/bW2 ip^{R}[P$_{etef}$:egfp]ip^{S} ip^{R}[P$_{etef}$:cib1^{s}-C-term-3xHA]ip^{S}*	P, C, G	unknown

4.4.3. **Cell lines**

All cell lines used and generated in this work are listed in Table 8 and Table 9, respectively.

Table 8: Cell lines used in this work

Cell lines	Source of supply
hTert RPE1	ATCC CRL-4000
Lenti-X 293-T	Clontech

Table 9: Stable cell lines generated in this work

Cell lines	Description
RPE1 *XBP1*$^{-/-}$	KO_1 and KO_2 generated using CRISPR-Cas9
RPE1 *XBP1*$^{-/-}$ P_{PGK}*:XBP1*^{us}	Three independent XBP1^{u} rescue cell lines were generated using different viral titers (20 µL, 50 µL and 200 µL)
RPE1 *XBP1*$^{-/-}$ P_{PGK}*:XBP1*^{s}	Three independent XBP1^{s} rescue cell lines were generated using different viral titers (20 µL, 50 µL and 200 µL)
RPE1 *XBP1*$^{-/-}$ P_{PGK}*:bZIP* XBP1*^{us}	Two independent bZIP* XBP1^{u} cell lines were generated using different viral titers (25 µL and 50 µL)
RPE1 *XBP1*$^{-/-}$ P_{PGK}*:bZIP* XBP1*^{s}	Two independent bZIP* XBP1^{s} cell lines were generated using different viral titers (25 µL and 50 µL)
RPE1 *XBP1*$^{-/-}$ P_{PGK}*:eGFP*	Cell line was generated using a lentiviral system (virus titer 25 µL)
RPE1 *XBP1*$^{-/-}$ P_{PGK}*:GFP-XBP1*^{s}	Four independent GFP-XBP1^{s} cell lines were generated using different viral titers (20 µL, 50 µL, 250 and 300 µL).
RPE1 *XBP1*$^{-/-}$ P_{PGK}*:GFP-XBP1*^{us}	Four independent GFP-XBP1^{u} cell lines were generated using different viral titers (20 µL, 50 µL, 250 and 300 µL).
RPE1 *XBP1*$^{-/-}$ P_{PGK}*:cib1*^{s}*-1xHA*	Three independent Cib1^{s} cell lines were generated using different viral titers (20 µL, 50 µL and 200 µL).
RPE1 *XBP1*$^{-/-}$ P_{PGK}*:cib1*^{us}*-3xHA*	Three independent Cib1^{u} cell lines were generated using different viral titers (20 µL, 50 µL and 200 µL).

4.4.4. **Plasmids**

All plasmids used in this work are listed in Table 10. The correctness of the plasmids was validated by restriction digest and/or sequencing.

Table 10: Plasmids used in this work

Plasmids	Reference
pSpCas9(BB)-2A-GFP	pX458, Ran et al., 2013, Addgene #48138
pCDH-PGK-GW-IRES-BSD	Kay Oliver Schink, #577
pCDH-PGK-GW-IRES-Puro	Kia Wee Tan, #12
pENTR20 mEGFP-C1	Kay Oliver Schink, #754
pENTR20 mEGFP-N1	Kay Oliver Schink, #756
peGFP-T2A	Kay Oliver Schink, #172
pLenti-Tre3G-rtTA3-IRES-Puro	Kay Oliver Schink, #244
p5xATF6-GL3	Wang et al., 2000, Addgene #11976
pcDNA 3.1	Invitrogen
pRL-TK	Promega
pER-mCherry	Kay Oliver Schink, #382
pMDLg/pRRE	Dull et al., 1998, Addgene #12251
pRSV-Rev	Dull et al., 1998, Addgene #12253
pMD2.G	Addgene #12259
p123	Aichinger et al., 2003
pMF-1G	Baumann et al., 2012
pETEF-GFP-Ala6-MMXN-Cbx (1742)	Böhmer et al., 2008
pCRG-GFP-Ala6-MMXN-Cbx (1747)	Plasmid collection, group of Michael Bölker, Phillips-University Marburg
p123-*cib1*	Hampel, 2016
p123-*cib1*^{s}	Lara Schmitz, pers. communication
p123-*cib1*^{us}	Hampel, 2016
p123-*bZIP* cib1*^{us}	Kai Heimel, pers. communication
p123-*bZIP* cib1*^{s}	Oguz Bolgi, pers. communication
pDONR221-*XBP1*^{s}	Hampel, 2016
pDONR221-*XBP1*^{u}	Hampel, 2016

All generated plasmids in this work are listed below. Plasmids were verified by restriction digest and by sequencing. Oligonucleotides used for the generation of the corresponding plasmids are indicated in 5'-3' direction. Restriction sites are highlighted.

Plasmids used for the generation of RPE1 *XBP1* KO cell lines:

pX458-XBP1-gRNA1

The two single-stranded complementary oligonucleotides KS542 and KS543 were boiled for 5 min at 99°C in ligase buffer before slowly cooling down to 37°C. The formed duplex oligonucleotide was used for a ligation reaction with pX458 linearized with the restriction enzyme *Bbs*I. RPE1 cells were co-transfected with pX458-XBP1-gRNA1 and pX458-XBP1-gRNA3 in order to obtain *XBP1* KO cell lines lacking the entire *XBP1* ORF. The plasmid pX458 contains a Cas9-2A-GFP protein which enables selection of edited cells by fluorescence-activated cell sorting.

KS542: CACCGtgcgTAGTCTGGAGCTATGG
KS543: aaacCCATAGCTCCAGACTAcgcaC

pX458-XBP1-gRNA3

The two single-stranded complementary oligonucleotides KS546 and KS547 were boiled for 5 min at 99°C in ligase buffer before slowly cooling down to 37°C. The formed duplex oligonucleotide was used for a ligation reaction with pX458 linearized with the restriction enzyme *Bbs*I. RPE1 cells were co-transfected with pX458-XBP1-gRNA3 and pX458-XBP1-gRNA1 in order to obtain *XBP1* KO cell lines lacking the entire *XBP1* ORF. The plasmid pX458 contains a Cas9-2A-GFP protein which enables selection of edited cells by fluorescence-activated cell sorting.

KS546: CACCGAGATACCCAGCTCCGGAACG
KS547: aaacCGTTCCGGAGCTGGGTATCTC

pX458-XBP1-gRNA1-gRNA3

In order to increase the *XBP1* deletion efficiency in RPE1 cells, the expression of gRNA1 and gRNA3 was driven by the U6 promoter on the same plasmid. Therefore, *gRNA3* (with the U6 promoter) was amplified by PCR using the oligonucleotides KS642 and KS643. The pX458-XBP1-gRNA3 plasmid served as a template. The PCR product was digested with *Nhe*I + *Kpn*I and ligated with the *Xba*I-*Kpn*I linearized pX458-XBP1-gRNA1 plasmid. Alternatively, pX458-XBP1-gRNA1-gRNA3 was generated by Gibson assembly. For that, gRNA3 was amplified via PCR using the oligonucleotides KS640 and KS641. Selection of edited cells was accomplished by fluorescence-activated cell sorting.

KS640: cgccaattctgcagacaaatggcgctagcgagggcctatttcccatgattcc
KS641: cgggccatttaccgtaagttatgtaacgggtac
KS642: gatcatgctagcgagggcctatttcccatgattccttc
KS643: gtaacgggtacctctagagccatttgtctgc

Plasmids used for the generation of the rescue cell lines:

pENTR-XBP1^{u}

For the construction of this plasmid, *XBP1^{u}* was amplified via PCR from the plasmid pDONR221-*XBP1^{u}* using the oligonucleotides KS646 and KS647. The PCR product was digested with *BamH*I + *Not*I and ligated with the *BamH*I-*Not*I backbone of pENTR20 mNeonGreen-N1.

KS646: atatGGATCCatggtggtggtggcagccgcg
KS647: atatGCGGCCGCttagttcattaatggcttccagc

pENTR-XBP1^{s}

For the construction of this plasmid, *XBP1^{s}* was amplified via PCR from the plasmid pDONR221-*XBP1^{s}* using the oligonucleotides KS646 and KS648. The PCR product was digested with *BamH*I + *Not*I and ligated with the *BamH*I-*Not*I backbone of pENTR20 mNeonGreen-N1.

KS646: atatGGATCCatggtggtggtggcagccgcg
KS648: atatGCGGCCGCttagacactaatcagctgggg

pENTR-cib1^{s}-1xHA

For the construction of this plasmid, *cib1^{s}-1xHA* was amplified via PCR from the plasmid 1742-cib1^{s}-3xHA using the oligonucleotides KS649 and KS650. The PCR product was digested with *BamH*I + *Not*I and ligated with the *BamH*I-*Not*I backbone of pENTR20 mNeonGreen-N1.

KS649: atatGGATCCatgactagcaccaccacgtcaacg
KS650: atatGCGGCCGCctaatagtcgggcacgtcgtagg

pENTR-cib1^{us}-3xHA

For the construction of this plasmid, *cib1^{us}-3xHA* was amplified via PCR from the plasmid 1742-cib1^{us}-3xHA using the oligonucleotides KS649 and KS650. The PCR product was digested with *BamH*I + *Not*I and ligated with the *BamH*I-*Not*I backbone of pENTR20 mNeonGreen-N1.

KS649: atatGGATCCatgactagcaccaccacgtcaacg
KS650: atatGCGGCCGCctaatagtcgggcacgtcgtagg

pCDH-PGK-XBP1^{u}-IRES-BSD

For the construction of this plasmid, *XBP1^{u}* from pENTR-XBP1^{u} was inserted into the destination vector pCDH-PGK-GW-IRES-BSD through an LR reaction. The resulting plasmid was used for the generation of stable cell lines with a lentiviral system.

pCDH-PGK-XBP1^{s}-IRES-BSD

For the construction of this plasmid, *XBP1^{s}* from pENTR-XBP1^{s} was inserted into the destination vector pCDH-PGK-GW-IRES-BSD through an LR reaction. The resulting plasmid was used for the generation of stable cell lines with a lentiviral system.

pCDH-PGK-XBP1^{u}-IRES-Puro

For the construction of this plasmid, *XBP1^{u}* from pENTR-XBP1^{u} was inserted into the destination vector pCDH-PGK-GW-IRES-Puro through an LR reaction. The resulting plasmid was used for the generation of stable cell lines with a lentiviral system.

pCDH-PGK-XBP1^{s}-IRES-Puro

For the construction of this plasmid, *XBP1^{s}* from pENTR-XBP1^{s} was inserted into the destination vector pCDH-PGK-GW-IRES-Puro through an LR reaction. The resulting plasmid was used for the generation of stable cell lines with a lentiviral system.

pCDH-PGK-cib1^{s}-1xHA-IRES-BSD

For the construction of this plasmid, *cib1^{s}-1xHA* from pENTR-cib1^{s}-1xHA was inserted into the destination vector pCDH-PGK-GW-IRES-BSD through an LR reaction. The resulting plasmid was used for the generation of stable cell lines with a lentiviral system.

pCDH-PGK-cib1^{us}-3xHA-IRES-BSD

For the construction of this plasmid, *cib1^{us}-3xHA* from pENTR-cib1^{us}-3xHA was inserted into the destination vector pCDH-PGK-GW-IRES-BSD through an LR reaction. The resulting plasmid was used for the generation of stable cell lines with a lentiviral system.

Plasmids used for the generation of RPE1 cell lines expressing GFP-tagged XBP1$^{s/u}$:

pENTR-GFP-XBP1^{s}

The *GFP-XBP1^{s}* fragment was obtained by digesting the plasmid 1742-XBP1^{s} with *BamH*I + *Not*I and ligating the *BamH*I-*Not*I fragment with pENTR20 mEGFP-N1, which was digested the same way.

pENTR-GFP-XBP1^{u}

The *GFP-XBP1^{u}* fragment was obtained by digesting the plasmid 1742-XBP1^{u} with *BamH*I + *Not*I and ligating the *BamH*I-*Not*I fragment with pENTR20 mEGFP-N1, which was digested the same way.

pCDH-PGK-GFP-XBP1^{u}-IRES-BSD

For the construction of this plasmid, the GFP-XBP1^{u} from pENTR-GFP-XBP1^{u} was inserted into the destination vector pCDH-PGK-GW-IRES-BSD through an LR reaction. The resulting plasmid was used for the generation of stable cell lines with a lentiviral system.

pCDH-PGK-GFP-XBP1^{s}-IRES-BSD

For the construction of this plasmid, the GFP-XBP1^{s} from pENTR-GFP-XBP1^{s} was inserted into the destination vector pCDH-PGK-GW-IRES-BSD through an LR reaction. The resulting plasmid was used for the generation of stable cell lines with a lentiviral system.

pCDH-PGK-GFP-XBP1^{u}-IRES-Puro

For the construction of this plasmid, the GFP-XBP1^{u} from pENTR-GFP-XBP1^{u} was inserted into the destination vector pCDH-PGK-GW-IRES-Puro through an LR reaction. The resulting plasmid was used for the generation of stable cell lines with a lentiviral system.

pCDH-PGK-GFP-XBP1^{s}-IRES-Puro

For the construction of this plasmid, the GFP-XBP1^{s} from pENTR-GFP-XBP1^{s} was inserted into the destination vector pCDH-PGK-GW-IRES-Puro through an LR reaction. The resulting plasmid was used for the generation of stable cell lines with a lentiviral system.

Plasmids used for the generation of the bZIP* XBP1$^{s/u}$ cell lines:

pENTR-bZIP* XBP1^{s}

Three PCRs were performed for the construction of this plasmid. The first PCR amplified the 5' part of *XBP1* and at the same time inserted the mutation into the bZIP domain. pDONR221-*XBP1^{s}* served as a template and DM54 + DM56 served as oligonucleotides for the PCR. The second PCR amplified the 3' part of *XBP1* using pDONR221-*XBP1^{s}* as a template and DM55 + DM57 as oligonucleotides. The third PCR resulted in a fusion of the PCR fragments produced in the first two PCRs using the oligonucleotides DM54 and DM57.

DM54: TATAGGATCCATGGTGGTGGTGGCAGCCG
DM55: cctaagaagaagcgtaaggtcctggctcgaatgagtgagctggaa
DM56: caggaccttacgcttcttcttaggcagcgccttctcctcggg
DM57: atatgcggccgcttagacactaatcagctgg

pENTR-bZIP* XBP1^{u}

Three PCRs were performed for the construction of this plasmid. The first PCR amplified the 5' part of *XBP1* and at the same time inserted the mutation into the bZIP domain. pDONR221-*XBP1^{u}* served as a template and DM54 + DM56 served as oligonucleotides for the PCR. The second PCR amplified the 3' part of *XBP1* using pDONR221-*XBP1^{u}* as a template and DM55 + DM58 as oligonucleotides. The third PCR resulted in a fusion of the PCR fragments produced in the first two PCRs using the oligonucleotides DM54 and DM58.

DM54: TATAGGATCCATGGTGGTGGTGGCAGCCG
DM55: cctaagaagaagcgtaaggtcctggctcgaatgagtgagctggaa
DM56: caggaccttacgcttcttcttaggcagcgccttctcctcggg
DM58: atatgcggccgcttagttcattaatggcttccagc

pCDH-PGK-bZIP* XBP1^{u}-IRES-BSD

For the construction of this plasmid, the bZIP* XBP1^{u} from pENTR-bZIP* XBP1^{u} was inserted into the destination vector pCDH-PGK-GW-IRES-BSD through an LR reaction. The resulting plasmid was used for the generation of stable cell lines with a lentiviral system.

pCDH-PGK-bZIP* XBP1^{s}-IRES-BSD

For the construction of this plasmid, the bZIP* XBP1^{s} from pENTR-bZIP* XBP1^{s} was inserted into the destination vector pCDH-PGK-GW-IRES-BSD through an LR reaction. The resulting plasmid was used for the generation of stable cell lines with a lentiviral system.

Plasmid used for the generation of the control cell line for the LCMS analyses:

pCDH-PGK-eGFP-IRES-BSD

For the construction of this plasmid, the eGFP from pENTR20 mEGFP-N1 was inserted into the destination vector pCDH-PGK-GW-IRES-BSD through an LR reaction. The resulting plasmid was used for the generation of stable cell lines with a lentiviral system.

Plasmids used for the luciferase assays:

5xUPRE-FL-RL

pRL-TK was digested with *BamH*I + *Bgl*II and the fragment inserted into p5xATF6-GL3 linearized with *BamH*I. In this way, a plasmid containing five UPRE repeats, a firefly luciferase and a renilla luciferase was obtained.

pCDNA 3.1-XBP1^{u}-VP16

XBP1^{u} was amplified via PCR from pENTR20 XBP1^{u} using the oligonucleotides KS880 and KS881. *VP16* was amplified via PCR from pLenti-Tre3G-rtTA3-IRES-Puro using the oligonucleotides KS882 and KS883. Next the two PCR products were used as templates for an overlap-PCR using KS880 and KS883. The XBP1^{u}-VP16 fusion product was digested with *BamH*I + *Not*I and inserted into *BamH*I-*Not*I linearized pCDNA 3.1.

KS880: atatGGATCCatggtggtggtggcagcc
KS881: GTCAAAATCGTCAAGGGCGTCgttcattaatggcttccagcttgg
KS882: ccaagctggaagccattaatgaacGACGCCCTTGACGATTTTGAC
KS883: atatGCGGCCGCTTACCCGGGGAGCATGTCAAG

Plasmid used for XBP1$^{s/u}$ localization analyses:

pmCherry-XBP1^{s}-T2A-GFP-XBP1^{u}

This plasmid was generated in a three-step procedure. First of all, *GFP-XBP1^{u}* was amplified via PCR using the oligonucleotides KS980 and KS981. pENTR-GFP-XBP1^{u} served as a template. The PCR product was digested with *Asc*I + *Not*I and ligated with *Asc*I-*Not*I linearized peGFP-T2A. The resulting plasmid was linearized with *Kpn*I. Secondly, *mCherry* was amplified using pENTR20 mCherry-N1 as a template and the oligonucleotides KS982 and KS983. XBP1^{s} was amplified by PCR using pENTR-XBP1^{s} and the oligonucleotides KS984 and KS985. Thirdly, *mCherry* was fused to *XBP1^{s}* and inserted into the T2A-GFP-XBP1^{u} plasmid via Gibson assembly.

KS980: atatggcgcgccatggtgagcaagggcgagg
KS981: atatgcggccgcttagttcattaatggcttccagc
KS982: ctgcagtcgacggtaccgcgggcatggtgagcaagggcgaggagg
KS983: gcgcggctgccaccaccaccatcttgtacagctcgtccatgc
KS984: ggcggcatggacgagctgtacaagatggtggtggtggcagcc
KS985: gacttcctctgccctccccggtgacactaatcagctggggaaag

Plasmid used for the analysis of Cib1^{u}-Cib1^{s} ratio:

pETEF-3xHA-cib1

For the construction of this plasmid, the oligonucleotides 3xHA NcoI fwd and 3xHA NcoI rev were annealed and the resulting duplex ligated with the *Nco*I linearized plasmid p123-cib1.

3xHA NcoI fwd: CATGGCATACCCCTACGACGTGCCCGACTATGCCGGTGCCGCCTA
3xHA NcoI rev: CATGGCATAGTCGGGCACGTCGTAGGGGTAACCACCAGCCGAGTA

Plasmids used for CoIP analyses:

1742-cib1^{s}-3xHA

For the construction of this plasmid, the 3xHA tag including the *tnos* terminator was amplified from p123-3xHA (annealing of oligonucleotides as described for pETEF-3xHA-cib1 and insertion into p123 linearized with *Nco*I) via PCR using the oligonucleotides DM10 and DM12. Additionally, *cib1^{s}* was amplified from p123-cib1^{s} via PCR using the oligonucleotides cib1^{us}-SL fwd and DM24. Next, p123 was digested with *BamH*I and *EcoR*I in order to remove the GFP tag. Finally, the linearized p123 backbone, the 3xHA fragment and *cib1^{s}* fragment were fused using the seamless cloning technology.

DM10: ctgatatcatcgatgGCGGCCGCAATTCTCATGTTTGACAG
DM12: aaggtgcgtctgcccgccgccCGGGCCAACGCGGCCTACCCCT
DM24: AGCGACGATTGAGGCCATCAGACC
cib1^{us}-SL fwd: caacatcatccacggATGACTAGCACCACCACGTCAAC

1742-cib1^{us}-3xHA

For the construction of this plasmid, the 3xHA tag including the *tnos* terminator was amplified from p123-3xHA via PCR using the oligonucleotides DM10 and DM12. Additionally, *cib1^{us}* was amplified from p123-cib1^{us} via PCR using the oligonucleotides cib1^{us}-SL fwd and cib1^{us}-SL rev. Next, p123 was digested with *BamH*I and *EcoR*I in order to remove the GFP tag. Finally, the linearized p123 backbone, the 3xHA fragment and the *cib1^{us}* fragment were fused using the seamless cloning technology.

DM10: ctgatatcatcgatgGCGGCCGCAATTCTCATGTTTGACAG
DM12: aaggtgcgtctgcccgccgccCGGGCCAACGCGGCCTACCCCT
cib1^{us}-SL fwd: caacatcatccacggATGACTAGCACCACCACGTCAAC
cib1^{us}-SL rev: GGCTTGCGAGGTCACCT

1742-cib1^{s}-C-term-3xHA

For the construction of this plasmid, the 3xHA tag including the *tnos* terminator was amplified from p123-3xHA via PCR using the oligonucleotides DM10 and DM12. Additionally, the 3' part of *cib1^{s}* (aa273) was amplified from p123-cib1^{s} via PCR using the oligonucleotides DM22 and cib1^{us}-SL rev. Next, p123 was digested with *BamH*I and *EcoR*I in order to remove the GFP tag. Finally, the linearized p123 backbone, the 3xHA fragment and the *cib1^{s}* 3' fragment were fused using the seamless cloning technology

DM10: ctgatatcatcgatgGCGGCCGCAATTCTCATGTTTGACAG
DM12: aaggtgcgtctgcccgccgccCGGGCCAACGCGGCCTACCCCT
DM22: acagaCAACATCATCCACGGatgGATGCCCTCACACAGTTTGAG
cib1^{us}-SL rev: GGCTTGCGAGGTCACCT

1742-cib1^{us}-C-term-3xHA

For the construction of this plasmid, the 3xHA tag including the *tnos* terminator was amplified from p123-3xHA via PCR using the oligonucleotides DM10 and DM12. Additionally, the 3' part of *cib1^{us}* (aa273) was amplified from p123-cib1^{us} via PCR using the oligonucleotides DM6 and cib1^{us}-SL rev. Next, p123 was digested with *BamH*I and *EcoR*I in order to remove the GFP tag. Finally, the linearized p123 backbone, the 3xHA fragment and the *cib1^{us}* 3' fragment were fused using the seamless cloning technology

DM6: acagacaacatcatccacggATGGAGGCCACCTGCTCGGAC
DM10: ctgatatcatcgatgGCGGCCGCAATTCTCATGTTTGACAG
DM12: aaggtgcgtctgcccgccgccCGGGCCAACGCGGCCTACCCCT
cib1^{us}-SL rev: GGCTTGCGAGGTCACCT

pCRG-cib1-N-term-3xHA

The 5' part of *cib1* was amplified via PCR by using the oligonucleotides DM26 and DM27 and the template 1742-cib1^{s}-3xHA. The PCR product was digested with *BamH*I and *EcoR*I and ligated with the *BamH*I-*EcoR*I linearized plasmid 1747.

DM26: atatggatccatgactagcaccaccacg
DM27: atatgaattcctgatatcatcgatgcgc

Plasmids used for localization of XBP1$^{s/u}$ in *U. maydis*:

1742-XBP1^{u}

For the construction of this plasmid, *XBP1^{u}* was amplified from pDONR221-*XBP1^{u}* by PCR using the oligonucleotides DM39 and DM41. The PCR product was digested with *Msc*I + *Not*I and ligated into the *Msc*I-*Not*I linearized plasmid 1742.

DM39: ATATTGGCCATCatggtggtggtggcagcc
DM41: ATATGCGGCCGCttagttcattaatggcttccagc

1742-XBP1^{s}

For the construction of this plasmid, *XBP1^{s}* was amplified from pDONR221-*XBP1^{s}* by PCR using the oligonucleotides DM39 and DM40. The PCR product was digested with *Msc*I + *Not*I and ligated into the *Msc*I-*Not*I linearized plasmid 1742.

DM39: ATATTGGCCATCatggtggtggtggcagcc
DM40: ATATgcggccgcttagacactaatcagctgg

4.4.5. **Oligonucleotides**

Oligonucleotides used in this work are listed in Table 11. Sequence is displayed in 5'-3' direction. Oligonucleotides were synthesized from Eurofins Genomics and Biomers.net.

Table 11:Oligonucleotides used in this work

Primer	Identifier	Sequence (5'-3')	Usage
DM6	Cib^{us}-SL-274 fwd	acagacaacatcatccacggATGGAGGCCACC TGCTCGGAC	Generation of plasmids for CoIP
DM10	HA-nosT2-SL rev	ctgatatcatcgatgGCGGCCGCAATTCTCA TGTTTGACAG	Generation of plasmids for CoIP
DM12	HA-nosT-SL-NT3 fwd	aaggtgcgtctgcccgccgccCGGGCCAACGC GGCCTACCCCT	Generation of plasmids for CoIP
DM22	Cib1^{s}-CT273 fwd	acagaCAACATCATCCACGGatgGATGCC CTCACACAGTTTGAG	Generation of plasmids for CoIP
DM24	Cib1^{s}-SL rev	AGCGACGATTGAGGCCATCAGACC	Generation of plasmids for CoIP
DM26	cib1-NT crg BamHI	atatggatccatgactagcaccaccacg	Generation of the plasmid pCRG-cib1-N-term-3xHA
DM27	cib1-NT crg EcoRI	atatgaattcctgatatcatcgatgcgc	Generation of the plasmid pCRG-cib1-N-term-3xHA
DM39	GFP-XBP1 MscI fwd	ATATTGGCCATCatggtggtggtggcagcc	Generation of the plasmid 1742-XBP1$^{s/u}$
DM40	GFP-XBP1 lang NotI rev	ATATgcggccgcttagacactaatcagctgg	Generation of the plasmid 1742-XBP1^{s}
DM41	GFP-XBP1 kurz NotI rev	ATATGCGGCCGCttagttcattaatggcttccagc	Generation of the plasmid 1742-XBP1^{u}
DM54	XBP1 BamHI fwd	TATAGGATCCATGGTGGTGGTGGCAGC CG	Generation of pENTR-bZIP* XBP1$^{s/u}$
DM55	XBP1_mutbas fwd	cctaagaagaagcgtaaggtcctggctcgaatgagtga gctggaa	Generation of pENTR-bZIP* XBP1$^{s/u}$
DM56	XBP1_mutbas rev	caggaccttacgcttcttcttaggcagcgccttctcctcggg	Generation of pENTR-bZIP* XBP1$^{s/u}$
DM57	GFP-XBP1 lang NotI rev	atatgcggccgcttagacactaatcagctgg	Generation of pENTR-bZIP* XBP1^{s}
DM58	GFP-XBP1 kurz NotI rev	atatgcggccgcttagttcattaatggcttccagc	Generation of pENTR-bZIP* XBP1^{u}
DM98	RT_XBP1^{s} fwd	CTGCTGAGTCCGCAGCAG	qRT-PCR
DM99	FoxO1 fwd	CCCTACTTCAAGGATAAGGGTG	qRT-PCR
DM100	FoxO1 rev	CCTCTGGATTGAGCATCCACC	qRT-PCR
DM101	FoxO1 rev	CCAATGTATCTCCATCCATGAGG	qRT-PCR
DM102	FoxO1 fwd	CTCCGTGAGCAGCTGCAATG	qRT-PCR
DM103	ATF5 fwd	GGCAGGTGATGGCTTCTCTG	qRT-PCR
DM104	ATF5 rev	CCTTCTTGAGGAGGGAGGC	qRT-PCR
DM105	ATF5_2 fwd	GGGACCGCAAGCAAAAGAAGA	qRT-PCR
DM106	ATF5_2 rev	CCTTGACGTACTGGATCTCG	qRT-PCR
DM107	LC3b fwd	CGATACAAGGGTGAGAAGCAG	qRT-PCR
DM108	LC3b rev	CAGGAAGAAGGCCTGATTAGC	qRT-PCR
DM109	BECN1 fwd	CACGTTTTTGTCTTCCCTACAGG	qRT-PCR
DM110	BECN1 rev	GCTCCTCAGAGTTAAACTGGG	qRT-PCR

Primer	Identifier	Sequence (5'-3')	Usage
DM111	ATG5 fwd	GGAAGCAGAACCATACTATTTGC	qRT-PCR
DM112	ATG5 rev	GGTGTGCCTTCATATTCAAACC	qRT-PCR
DM113	ATG5_2 fwd	CGTCCTGTGGCTGCAGATG	qRT-PCR
DM114	ATG5_2 rev	CAGAGGTGTTTCCAACATTGGC	qRT-PCR
DM115	ATF6 fwd	CCCGTATTCTTCAGGGTGCTC	qRT-PCR
DM116	ATF6 rev	GCATAATACACTTGTAGCTCACTCC	qRT-PCR
DM117	ATF6_2 fwd	CTTTCTCCAGCCTCCTCAAG	qRT-PCR
DM118	ATF6_2 rev	GAGTTTTCACCATATAAGGAAAGGG	qRT-PCR
DM121	RT_XBP1^{s} intron fwd	GGAGTTAAGACAGCGCTTGGG	qRT-PCR
DM122	RT_XBP1^{s} intron rev	GGTGCACGTAGTCTGAGTGC	qRT-PCR
DM123	RT_XBP1^{s} intron outside fwd	ggatgccctggttgctgaag	qRT-PCR
DM124	RT_XBP1^{s} intron outside rev	caataccgccagaatccatgg	qRT-PCR
DM125	RT_Caspase 3 fwd	CGGTCTGGTACAGATGTCGA	qRT-PCR
DM126	RT_Caspase 3 rev	CATGGCTCAGAAGCACACAAAC	qRT-PCR
DM127	RT_TNFRSF10B fwd	cAAGACCCTTGTGCTCGTTG	qRT-PCR
DM128	RT_TNFRSF10B rev	GGTGGACACAATCCCTCTG	qRT-PCR
KS542	XBP1 gRNA1 fwd	CACCGtgcgTAGTCTGGAGCTATGG	Generation of *XBP1* KO cell lines
KS543	XBP1 gRNA1 rev	aaacCCATAGCTCCAGACTAcgcaC	Generation of *XBP1* KO cell lines
KS546	XBP1 gRNA3 fwd	CACCGAGATACCCAGCTCCGGAACG	Generation of *XBP1* KO cell lines
KS547	XBP1 gRNA3 rev	aaacCGTTCCGGAGCTGGGTATCTC	Generation of *XBP1* KO cell lines
KS548	XBP1 ver Exon1 fwd	CGCCGGACTCCATAGCCACG	Verification of KO lines
KS549	XBP1 ver Exon1 rev	AGCTCTGGTCATCTCTAACG	Verification of KO lines
KS550	XBP1 Exon1 int-ver rev	CGTGAGGCGCTGTCGCTTGC	Verification of KO lines
KS551	XBP1 ver fullORF rev	GGTTTACACCAAGCAGAGAGG	Verification of KO lines
KS552	XBP1 Exon5 int-ver fwd	TCTGAGACAGAGAGCCAAGC	Verification of KO lines
KS617	XBP1 Exon5 check fwd	gaacccagtacaaagtgttcc	Verification of KO lines
KS640	gRNA Multiplex Gibson fwd	cgccaattctgcagacaaatggcgctagcgagggcctatttcccatgattcc	Generation of *XBP1* KO cell lines

Primer	Identifier	Sequence (5'-3')	Usage
KS641	gRNA Multiplex Gibson rev	cgggccatttaccgtaagttatgtaacgggtac	Generation of *XBP1* KO cell lines
KS642	gRNA Multiplex fwd	gatcatgctagcgagggcctatttcccatgattccttc	Generation of *XBP1* KO cell lines
KS643	gRNA Multiplex rev	gtaacgggtacctctagagccatttgtctgc	Generation of *XBP1* KO cell lines
KS646	BamHI XBP1 fwd	atatGGATCCatggtggtggtggcagccgcg	Generation of XBP1 rescue cell lines
KS647	XBP1^{us} NotI rev	atatGCGGCCGCttagttcattaatggcttccagc	Generation of XBP1^{u} rescue cell lines
KS648	XBP1^{s} NotI rev	atatGCGGCCGCttagacactaatcagctgggg	Generation of XBP1^{s} rescue cell lines
KS649	BamHI cib1 fwd	atatGGATCCatgactagcaccaccacgtcaacg	Generation of *XBP1* KO cell lines expressing HA-tagged Cib1
KS650	Cib1$^{us/s}$ NotI rev	atatGCGGCCGCctaatagtcgggcacgtcgtagg	Generation of *XBP1* KO cell lines expressing HA-tagged Cib1
KS681	RT_atf4 fwd	GACAGCAGCCACTAGGTACC	qRT-PCR
KS682	RT_atf4 rev	GCCCTCTCTTTTAGAGCCTCG	qRT-PCR
KS683	RT_xbp1^{s} fwd	GGATGGATGCCCTGGTTGC	qRT-PCR
KS684	RT_xbp1^{s} rev	CCATGGGGAGATGTTCTGGAGG	qRT-PCR
KS685	RT_total xbp fwd	CCTTGACTATTACACTGCCTGG	qRT-PCR
KS686	RT_total xbp rev	GATGTCAAAAGACAATACCTGGG	qRT-PCR
KS687	RT_chop fwd	GAGGAAGACCAAGGGAGAACC	qRT-PCR
KS688	RT_chop rev	CATTCTCTTCAGCTAGCTGTGC	qRT-PCR
KS689	RT_gapdh fwd	GTGAAGCAGGCGTCGGAG	qRT-PCR
KS690	RT_gapdh rev	CGTTGAGGGCAATGCCAGC	qRT-PCR
KS691	RT_bip fwd	GATTCCAAGGAACACAGTGGTG	qRT-PCR
KS692	RT_bip rev	CCAGTCAGATCAAATGTACCCAG	qRT-PCR
KS693	RT_gadd34 fwd	GCAAAGGCGGCTCAAGCG	qRT-PCR
KS694	RT_gadd34 rev	CTGCCCAGACAGCCAGGAAAT	qRT-PCR
KS695	RT_p58 fwd	CCCATCCTATAATGCCTTTGTC	qRT-PCR
KS696	RT_p58 rev	CTATCCACGCCTTCATCAAGC	qRT-PCR
KS697	RT_Edem1 fwd	CCACTGAGACCAGAGTTAGTG	qRT-PCR
KS698	RT_Edem1 rev	CGTACCCACACTTGACTTTTGTG	qRT-PCR
KS699	RT_ramp4 fwd	CGTATGGCCAACGAGAAGC	qRT-PCR
KS700	RT_ramp4 rev	GAAGAGAGCCAATAACCAGGG	qRT-PCR

Primer	Identifier	Sequence (5'-3')	Usage
KS701	RT_erdj4 fwd	CCAAGAATTTTCTTTTGGAGGTGG	qRT-PCR
KS702	RT_erdj4 rev	CTGCAGTGCTTGCTAGATCC	qRT-PCR
KS880	XBP1^{u} BamHI fwd	atatGGATCCatggtggtggtggcagcc	Generation of the XBP1^{u}-VP16 plasmid
KS881	XBP1^{u} rev	GTCAAAATCGTCAAGGGCGTCgttcattaatggcttccagcttgg	Generation of the XBP1^{u}-VP16 plasmid
KS882	VP16 fwd	ccaagctggaagccattaatgaacGACGCCCTTGACGATTTTGAC	Generation of the XBP1^{u}-VP16 plasmid
KS883	VP16 rev	atatGCGGCCGCTTACCCGGGGAGCATGTCAAG	Generation of the XBP1^{u}-VP16 plasmid
KS884	LucNrev	CCTTATGCAGTTGCTCTCC	Sequencing of the XBP1^{u}-VP16 plasmid
KS980	Asc-GFP-XBP1^{u}	atatggcgcgcccatggtgagcaagggcgagg	Generation of pmCherry-XBP1^{s}-T2A-GFP-XBP1^{u}
KS981	GFP-XBP1^{u}-NotI	atatgcggccgcttagttcattaatggcttccagc	Generation of pmCherry-XBP1^{s}-T2A-GFP-XBP1^{u}
KS982	mCherry fwd	ctgcagtcgacggtaccgcgggcatggtgagcaagggcgaggagg	Generation of pmCherry-XBP1^{s}-T2A-GFP-XBP1^{u}
KS983	mCherry-XBP1 rev	gcgcggctgccaccaccaccatcttgtacagctcgtccatgc	Generation of pmCherry-XBP1^{s}-T2A-GFP-XBP1^{u}
KS984	XBP1 fwd	ggcggcatggacgagctgtacaagatggtggtggtggcagcc	Generation of pmCherry-XBP1^{s}-T2A-GFP-XBP1^{u}
KS985	XBP1 rev	gacttcctctgccctccccggtgacactaatcagctggggaaag	Generation of pmCherry-XBP1^{s}-T2A-GFP-XBP1^{u}
	3xHA_NcoI fwd	CATGGCATACCCCTACGACGTGCCCGACTATGCCGGTGCCGCCTACCCCTACGACGTGCCCGATTACTCGGCTGGTGGTTACCCCTACGACG TGCCCGACTATGC	Generation of pETEF-3xHA-cib1
	3xHA_NcoI rev	CATGGCATAGTCGGGCACGTCGTAGGGGTAACCACCAGCCGAGTAATCGGGCACGTCGTAGGGGTAGGCGGCACCGGCATAGTCGGGCACGTCGTAGGGGTATGC	Generation of pETEF-3xHA-cib1
	Cib1^{us}-SL fwd	caacatcatccacggATGACTAGCACCACCACGTCAAC	Generation of plasmids for CoIP
	Cib1^{us}-SL rev	GGCTTGCGAGGTCACCT	Generation of plasmids for CoIP
	cbx Sonde fwd	caggaaacagctatgaccatg	Generation of Cbx probe
	cbx Sonde rev	cgttgtaaaacgacggccagt	Generation of Cbx probe
	Hyg 5'out	cgacctctgttacccgattacc	sequencing
	pCDNA/pEGFP_Seq_f	GTCGTAACAACTCCGCCC	sequencing
	GFP 5'out Seq	accaggatgggcaccacc	sequencing
	pOTEF 3'out	CGCTTTCTTCTGCGTTGG	sequencing
	T7_term seq	gctagttattgctcagcgg	sequencing
	T7_promotor seq	TAATACGACTCACTATAGGG	sequencing
	cbx_5'out seq	gcacagatcaagaaggacatgg	sequencing

Primer	Identifier	Sequence (5'-3')	Usage
	mCherry5'out seq	gaactccttgatgatggcc	sequencing
	cib1all fwd	tatcgacctcgacgccaaac	qRT-PCR
	cib1all rev	tatctgtgggcgagggctat	qRT-PCR
	RT_Cib1 spliced	GCCTCCCTGCAGCGGATGC	qRT-PCR
	RT_cib1 rev	CATCGACGTTGTTTCCGGCCT	qRT-PCR
	RT_bip1 fwd	AGGCATGGCTCGACGAGAACA	qRT-PCR
	RT_bip1 rev	GGTAAATCTTGGCGGTGATGGG	qRT-PCR
	RT_eIF2b fwd	ATCCCGAACAGCCCAAAC	qRT-PCR
	RT_eIF2b rev	ATCGTCAACCGCAACCAC	qRT-PCR
	p58ipk_RT fwd	GTCCTCTCTGATCCAGAAATGAG	qRT-PCR
	p58ipk_RT rev	CCCTTGCCATGAGTTCCAGC	qRT-PCR

4.5. Microbiological and genetic methods

4.5.1. Generation of chemically competent *E. coli* cells

Chemically competent *E. coli* TOP10 cells were generated following the calcium-manganese-method modified after Hanahan et al., 1991. Therefore, cells were grown in SOB-medium without magnesium at 37°C with continuous shaking. The overnight culture was transferred to baffled shake flasks with SOB-medium lacking magnesium and incubated at 28°C until an OD_{550} of 0.3 which corresponds to 5 x 10^7 cells/mL, was reached. Afterwards, the cell culture was transferred to 50 mL tubes and incubated for 10 min on ice before being spun down at 3000 rpm for 15 min at 4°C. The cells were resuspended in 1/3 volume of ice-cold CCMB80-buffer and incubated for 20 min on ice. After centrifugation at 3000 rpm for 15 min at 4°C, the supernatant was discarded and the cells resuspended in CCMB80-buffer (1/12 of the original volume). The competent cells were either used immediately or aliquoted, flash frozen in liquid nitrogen and stored at -80°C.

SOB-medium w/o Mg

20 g/L	Tryptone
5 g/L	Yeast extract
0.58 g/L	NaCl
0.19 g/L	KCl

Dissolve in $H_2O_{bid.}$ and autoclave at 121°C for 20 min.

CCMB80-buffer

10 mM	KOAc (pH 7.0)
80 mM	$CaCl_2 * 2\ H_2O$
20 mM	$MnCl_2 * 4\ H_2O$
10 mM	$MgCl_2 * 6\ H_2O$
10 % (v/v)	Glycerol

Dissolve in $H_2O_{bid.}$, adjust pH to 6.4 and sterilize by filtration. Store at 4°C.

4.5.2. Transformation of chemically competent *E. coli* cells

For the transformation of chemically competent *E. coli* cells, 100 µL aliquots were thawed on ice. Thereafter, the cell suspension was mixed with the corresponding plasmid (1 µL for re-transformation and 10 µL of a ligation) and incubated for 20 min on ice following a 1 min heat-shock at 42°C. Afterwards, cells were kept on ice for 3 min. Then, 800 µL dYT/LB-medium was added to the cells and the mixture vigorously shaken for 35 min at 37°C (or 30°C for Gateway cloning) before being plated on selective dYT/LB-agar plates. Plates were incubated overnight at 37°C (30°C for Gateway cloning).

4.5.3. Generation of *U. maydis* protoplasts

U. maydis protoplast were prepared according to Schulz et al., 1990. Briefly, an *U. maydis* overnight culture was prepared in YEPS-L-medium. Next, OD of the cell suspension was adjusted to 0.25 and the cells incubated for 4 h or to an OD of 0.8-1.0 at 30°C with continuous shaking. After incubation, cells were collected by centrifugation (10 min, 2500 rpm, 4°C) and washed in 10 mL ice-cold SCS-buffer (10 min, 2500 rpm, 4°C). Next, the cells were resuspended in 2 mL SCS-lysing enzyme solution and incubated at RT until 70 % of the cells became protoplasts. Reaction was stopped with 10 mL ice-cold SCS-buffer and the cells collected by centrifugation (10 min, 2000 rpm, 4°C). Afterwards, the protoplasts were washed twice with ice-cold SCS-buffer (10 mL) and one time with ice-cold STC-buffer (5 mL, 10 min, 2000 rpm, 4°C). Finally, the protoplasts were resuspended in 500 µL ice-cold STC-buffer, aliquoted (70 µL per 1.5 mL reaction tube) and stored at -80°C.

SCS-buffer

20 mM	Sodium citrate buffer (pH 5.8)
1 M	Sorbitol

Dissolve in $H_2O_{bid.}$ and autoclave at 121°C for 20 min.

SCS-lysing enzyme solution

12.5 mg/mL	Lysing enzyme

Dissolve in SCS-buffer and sterilize by filtration.

STC-buffer

10 mM	Tris-HCl (pH 7.5)
100 mM	$CaCl_2$
1 M	Sorbitol

Dissolve in $H_2O_{bid.}$ and autoclave at 121°C for 20 min.

4.5.4. **Transformation of *U. maydis* protoplasts**

For transformation, the *U. maydis* protoplasts were thawed on ice and carefully mixed with 8-10 µL of the DNA to be introduced. After 10 min of incubation on ice, 500 µL STC/PEG was added. After another 15 min of incubation on ice, the mixture was plated on regeneration agar plates consisting of two layers. The bottom layer (10 mL) contained twice as much of the respective fungicide (carboxin: 4 µg/mL, hygromycin: 400 µg/mL, ClonNAT: 150 µg/mL, G418: 800 µg/mL) than usually used on selective PD-agar plates and the top layer (10 mL) was free of any fungicides. In this way, the usual concentration of the fungicide is established via diffusion over time. Hence, the transformed cells had enough time to regenerate and to establish the corresponding resistance. The plates were incubated for 4-6 days at 30°C.

STC-PEG

40 % (v/v)	PEG_{4000}

Dissolve in STC. and autoclave at 121°C for 20 min.

Regeneration agar

10 g/L	Yeast extract
10 g/L	Peptone
10 g/L	Sucrose
182.2 g/L	Sorbitol
1.3 % (w/v)	Bacto agar

Dissolve in $H_2O_{bid.}$ and autoclave at 121°C for 20 min.

4.5.5. **Growth and stress assay in *U. maydis***

Cell growth and stress resistance of *U. maydis* was tested on YNB-agar plates supplemented with 1 %glucose and 0.2 % ammonium sulfate and different concentrations of tunicamycin (TM). Therefore, cells were grown overnight in YEPS-L-medium. Next, cells were adjusted to an OD of 0.25 in YEPS-L-medium. After 4 h of incubation at 30°C under continuous shaking, cells were washed in YNB-medium and collected at 2500 rpm for 5 min at RT. OD was adjusted to 1.0 in YNB-medium and 10-fold serial dilutions were prepared (10^0-10^{-5}). 3.5 µL of each dilution was spotted on the corresponding YNB-agar plates. Plates were incubated for 2-4 days at 30°C.

4.5.6. ***Zea mays* infection assay with *U. maydis***

Pathogenic development of *U. maydis* strains was tested by infection of 8 days old maize plants (Early Golden Bantam). For infection assays the solopathogenic SG200 WT and its derivatives were used. The strains were grown overnight at 30°C in YEPS-L-medium. The OD of the overnight culture was adjusted to 0.25 and incubated for another 4 h or until an OD of 0.8-1.0 was reached. Afterwards, the cells were washed in H_2O (2500 rpm, 5 min, RT) and adjusted to an OD of 1.0. 500 µL of each fungal cell suspension was injected approximately 1 cm above the soil into the inner leaf whorl of the maize plant. Inoculated maize plants were incubated in a plant chamber (GroBanks CLF Plant Climatics) with the following settings: 14 h daylight and 28°C and 10 h night at 22°C. Scoring of plant symptoms took place 8 days post inoculation following the symptom classification described in Kämper et al., 2006 (Tab. 12).

Table 12: Classification of maize plant disease symptoms

Plant symptoms	Description
Chlorosis	Yellowish coloration on infected leaves
Anthocyan	Brownish-purple colorations on infected leaves
Small tumors	Tumor size <2 mm
Large tumors	Tumor size >2 mm
Stem bending	Plant stems are completely surrounded by tumors
Dead	Infection resulted in plant death

4.5.7. **Integration of vectors into the *sdh*-locus of *U. maydis***

The *U. maydis sdh*-locus, also called *ip*-locus, codes for the succinate dehydrogenase. A substitution of the amino acid histidine to leucine at position 257 leads to resistance against the fungicide carboxin (Broomfield and Hargreaves, 1992; Keon et al., 1991). Carboxin (Cbx) usually inhibits the iron-sulfur subunit of the succinate dehydrogenase. This mutation can be used for the targeted integration into the *sdh*-locus by homologous recombination. For that, *U. maydis* protoplast transformation was performed with a plasmid containing the mutated version of *sdh* in the presence of Cbx, resulting in strains containing the desired construct flanked by the mutated version of *sdh* (ip^r) and the native version of *sdh* (ip^s). Not only single but also multiple integration events can be observed. The integration frequency can be determined via Southern blot analysis.

4.6. Cell culture methods

4.6.1. **Deletion of *XBP1* via CRISPR/Cas9**

hTert-RPE1 cells containing an *XBP1* deletion were generated using CRISPR/Cas9. The Benchling software (www.benchling.com) was used for the design of the guide RNAs (gRNAs). gRNA1 recognizes a region directly upstream of the *XBP1* start codon, whereas gRNA3 is complementary to a region within exon 5. 70-80 % confluent RPE1 cells were transfected with pX458-derived plasmids containing both Cas9-2A-GFP and the gRNAs using Fugene 6 or the Nucleofection technology. pX458 (pSpCas9(BB)-2A-GFP) was a gift from Feng Zhang (Addgene plasmid #48138). 48 h post-transfection, GFP-positive cells were sorted with a Sony SH800 cell sorter into 96-well plates containing conditioned DMEM-F12-medium. After sorting, every well contained a single GFP-positive cell. Cells were incubated for several days until colonies were formed. Afterwards, gDNA was extracted and analyzed for an *XBP1* deletion via PCR. The following combinations of oligonucleotides were used: KS548+KS550,

KS550+KS551, KS549+KS551, KS548+KS551. Clones lacking *XBP1* were further analyzed by Western blot using an XBP1^{s}-specific antibody.

4.6.2. **Generation of stable cell lines via a lentiviral system**

All generated stable cell lines were lentivirus-generated pools based on RPE1 *XBP1*$^{-/-}$. The cell lines were generated using a third-generation-lentivirus system. The genes to be stably introduced into the genome were subcloned into Gateway ENTRY plasmids using either conventional restriction-enzyme based cloning or Gibson assembly cloning. Based on these vectors, lentiviral transfer vectors were created through Gateway LR recombination into lentiviral destination vectors derived from pCDH-PGK-MCS-IRES-PURO (System Biosciences). VSV-G pseudotyped lentiviral particles were packaged using the system described in Dull et al., 1998. The required plasmids pRSV-Rev (Rev), pMDLg/pRRE (Gag/Pol) and pMD2.G (VSV-G) were gifts from Didier Trono (Addgene plasmids #12251, #12253, #12259).

Briefly, Lenti-X cells were transfected with the plasmid containing the construct to be introduced, Gag/Pol, Rev and VSV-G using Lipofectamine 2000. Three days post-transfection lentiviral particles were harvested from the Lenti-X cell supernatant. RPE1 *XBP1*$^{-/-}$ cells were transduced with three different virus titers. Antibiotic selection which resulted in cell populations with stable expression was started two days after transduction and lasted at least for 8 days.

Production of lentiviral particles

15 µg	Construct to be introduced
15 µg	Gag/Pol
6 µg	Rev
3 µg	VSV-G
50 µL	Lipofectamine 2000
1000 µL	Optimem

Mix and incubate for 15 min at RT
before cell transfection.

4.6.3. **Clonogenic assay**

70-80 %confluent RPE1 cells and its derivatives were seeded in 6 cm dishes (100-250 cells per dish). Cells were either incubated overnight or until they were

attached before TM treatment. TM (0.5-0.6 µg/mL) was added to the cells for 4.5 h. Afterwards, the cells were washed twice in DMEM-F12-medium without TM before further incubation (8-10 days). After the corresponding incubation time, the medium was removed and the attached cells washed with PBS. Next, the cells were fixed with 2 mL 70 % ethanol for 15 min at RT. The ethanol was removed and the dishes rinsed in H_2O before being put upside down on paper towels for drying. After at least 60 min of drying, the colonies were stained with 0.01 % crystal violet (in H_2O) and washed again with H_2O. For the evaluation, only colonies containing more than 50 cells and only assays in which the number of colonies in KO was at least 35 % reduced compared to WT, were considered.

4.6.4. **Dual luciferase reporter assay**

RPE1 cells (70-80 % confluency) were seeded into 6-well plates (1.5 x 10^5 cells per dish). Cells were transfected using Fugene 6 with 1 µg plasmid containing the UPRE-luciferase reporter. This plasmid (p5 x ATF6-GL3, Addgene plasmid #11976) was a gift from Ron Prywes. 24 h post-transfection, the cells were washed twice with PBS and passively lysed with 500 µL PLB buffer for 15 min on a rocking platform at RT. 20 µL of the cell lysates was transferred to a 96-well plate. All following steps were performed according to the manufacturer's protocol (Dual-Luciferase Reporter Assay System for the products E1910 and E1960). The firefly and renilla luciferase activity was measured on a BioTek Gen5 wellplate reader. The activity of the renilla luciferase was used for normalization purposes.

4.6.5. **Flow cytometry**

For flow cytometry analyses, 70-80 % confluent RPE1 cells were seeded into 10 cm dishes (10^6 cells per dish). If needed, cells were treated with TM for 4.5 h before fixation. 24 h after seeding, cells were trypsinized and collected in 15 mL falcons (5 min, 1000 rpm). Cells were washed with PBS and fixed with 70 % ethanol (ice-cold). The ethanol was added drop-wise while vortexing to prevent formation of cell clumps. Cells were afterwards stored at -20°C for at least 30 min. For staining, the cells were collected into 1.5 mL tubes (5 min, 1000 rpm) and washed in PBS. Afterwards, the cell pellet was resuspended in 50 µL flow

detergent buffer for blocking of non-specific binding. The cells were incubated for 5 min in the detergent buffer before adding 50 µL of α-H_3P antibody diluted in flow detergent buffer (final concentration 1:500) to the cells. The cells were incubated for 1 h with the antibody at RT. Then, the cells were washed with PBS and incubated for 30 min at RT with flow detergent buffer containing the secondary Alexa488-goat α-rabbit IgG antibody (1:500). After the incubation, the cells were washed again with PBS and resuspended in 500 µL PBS containing Hoechst 33342 (1.5 µL in 1 mL PBS) and filtered into a flow test tube through a cell strainer snap cap. Finally, the stained cells were incubated in darkness overnight at 4°C before running the flow cytometry analyses. Measurements were performed in collaboration with Viola Nähse (Oslo University Hospital, Institute for Cancer Research). Sample preparation for cell cycle analyses in *U. maydis* was performed according to Boye et al., 2016. Measurements were performed in collaboration with Beata Grallert (Oslo University Hospital, Institute for Cancer Research).

Analyses were performed either on a BD LSR II UV laser flow cytometer equipped with UV, 405, 488 and 633 nm line lasers or on a BD LSR II Yellow laser flow cytometer equipped with 406, 488, 561 and 640 nm line lasers. Data was analyzed using the BD FACSDiva software.

Flow cytometry analyses were supported by the Flow Cytometry Core Facility (FCCF) of the Oslo University Hospital.

Flow detergent buffer

50 µL	Igepal
50 µL	0.5 M EDTA (pH 8.0)
4 % (w/v)	Milk powder

Dissolve in 50 mL PBS.

4.7. Molecular biological methods

4.7.1. Isolation of plasmid DNA from *E. coli*

For analytic purposes, plasmid DNA was isolated from dense grown *E. coli* cultures by destroyer lysis preparation. Cell pellets were resuspended in 50 µL destroyer buffer and incubated for 5 min at RT. Afterwards, the samples were

incubated for 1 min at 98°C before being cooled down on ice and spun down for 8 min at 13000 rpm at RT. 5 µL of the supernatant was used for restriction digest. Plasmid isolation for sequencing, transformations and PCRs was performed using either the QIAprep Spin Miniprep Kit (Qiagen) or the DNA, RNA, and protein purification Kit (Macherey-Nagel) according to the manufacturer's protocol.

Destroyer lysis buffer

10 mM	Tris-HCl (pH 8.0)
1 mM	EDTA (pH 8.0)
50 % (w/v)	Sucrose
2 mg/mL	Lysozym
100 µg/mL	BSA
200 µg/mL	RNase A

Dissolve in $H_2O_{bid.}$ and store at -20°C.

4.7.2. **Isolation of genomic DNA from *U. maydis***

For the isolation of genomic DNA from *U. maydis*, cells were grown in dense overnight cultures in YEPS-L-medium (30°C under continuous shaking). Cells were collected in 2 mL tubes containing 300 mg glass beads (150-200 µm diameter) and resuspended in 500 µL lysis buffer (1:2 with TE buffer). After 15 min incubation on the Vibrax shaker at 1800 rpm, the samples were incubated another 15 min at 65°C and 5 min on ice. 100 µL of 8 M potassium acetate were added to the samples and inverted 10 times before centrifugation (15 min, 13300 rpm, RT). 500 µL of the supernatant was transferred into a 1.5 mL tube containing 300 µL isopropanol. After mixing the samples and centrifugation at 13000 rpm for 15 min at RT, the supernatant was discarded, the DNA pellet washed with 750 µL 70 % ethanol, dried and dissolved in 50 µL TE/RNase buffer. DNA was stored at -20°C.

Lysis buffer

50 mM	Tris-HCl (pH 7.5)
50 mM	Na_2-EDTA (pH 8.0)
1 % (w/v)	SDS

Dissolve in $H_2O_{bid.}$ and store at RT.

TE-buffer

10 mM	Tris-HCl (pH 8.0)
1 mM	Na_2-EDTA (pH 8.0)

Dissolve in. $H_2O_{bid.}$ and autoclave at 121°C for 20 min.

TE/RNase buffer

20 mg/mL RNaseA

Dissolve in TE-buffer and store at RT.

4.7.3. **Isolation of genomic DNA from RPE1 cells**

Genomic DNA (gDNA) from RPE1 cells was isolated and purified using the PureLink Genomic DNA Mini Kit (Invitrogen). At least 2 x 10^5 cells were collected and washed twice with 1xPBS (250 g, 5 min, RT). Lysates were prepared according to the manufacturer's 'Mammalian Cells Lysate' protocol. 1 µL of the corresponding gDNA was used for subsequent PCR analysis. gDNA was stored at -20°C.

10xPBS buffer

25.6 g/L Na_2HPO_4 x 7 H_2O
80 g/L NaCl
2 g/L KCl
2 g/L KH_2PO_4

Dissolve in $H_2O_{bid.}$, adjust to pH 7.4 and autoclave at 121°C for 20 min.

4.7.4. **RNA preparation from *U. maydis***

For the preparation of RNA from *U. maydis*, cells were grown overnight in CM-medium containing 1 % (v/v) glucose at 30°C and continuous shaking. OD of the overnight culture was adjusted to 0.25 and incubated for another 4 h or until an OD of 0.8-1.0 was reached. ER stress was induced, when needed, during this 4 h incubation step with TM. Next, cells from 15 mL cell suspension was collected by centrifugation (3500 rpm, 5 min, RT). The pellets were flash-frozen in liquid nitrogen and stored at -80°C (long-term storage possible at this step). Directly before preparing the RNA, the tubes containing the frozen pellets were transferred to -20°C. Cells were resuspended in 1 mL Trizol and transferred to 2 mL tubes containing 300 mg glass beads (150-200 µm diameter, washed in HCl). Cells were broken open on a Vibrax-VXR shaker for 8 min at 2000 rpm. Afterwards, the samples were incubated for 5 min at RT and 200 µL chloroform

added. The samples were mixed and incubated for another 2-3 min at RT. Samples were spun down for 10 min at 13000 rpm. The upper aqueous phase was carefully transferred to a 1.5 mL tube and the RNA precipitated by the addition of 500 µL isopropanol (10 min, RT). RNA pellets were collected by centrifugation (15 min, 13000 rpm) and washed with 1 mL 70 % ethanol (5 min, 13000 rpm). Finally, the RNA pellets were dissolved in 30 µL RNase-free H_2O (10 min, 55°C, 300 rpm) and the RNA quality tested on an agarose gel. Successful RNA preparation results in two distinct bands. Smear on the gel is an indication of poor quality.

Before cDNA synthesis, the isolated RNA was treated with Turbo-DNaseI (Ambion) according to the manufacturer's recommendation. Afterwards the RNA was reverse transcribed into cDNA using the Revert Aid First Strand cDNA Synthesis Kit (Thermo Fisher Scientific). cDNA was stored at -80°C. Exclusively nuclease-free tubes, tips and H_2O were used.

4.7.5. **RNA preparation for RNAseq analysis and data analysis**

RNA was isolated as described in 2.7.4. Samples were additionally purified with the QIAGEN RNeasy MinElute Cleanup Kit according to the manufacturer's protocol and the RNA quality examined with the Agilent 2100 Bioanalyzer. All following steps in sample preparation and sequencing were performed by the Göttingen Genomics Laboratory (G2L). Briefly, mRNA was enriched using the NEB Next Poly(A) mRNA Magnetic Isolation Module following the manufacturer's protocol. For the construction of strand-specific cDNA libraries NEB Next Ultra directional RNA library preparation kit for Illumina was used. Quality and size of the cDNA libraries were assessed using the Agilent High Sensitivity DNA Kit on an Agilent Bioanalyzer 2100. Library concentration was determined using the Qubit® dsDNA HS Assay Kit according to the manufacturer's protocol. A minimum of 15 Million raw reads were generated per sample.

Alignment of raw RNAseq reads to the *U. maydis* genome, calculation of read counts and RPM values as well as the assessment of differential expression with DESeq2 were performed by Florian Finkernagel (IMT Marburg).

Markus Esswein (University Duisburg-Essen) wrote the R script (see Appendix A) for the preparation and analysis of the RPKM values. Briefly, the script loads

RPKM values, subsets by relevant columns, filters for two-fold change, visualizes the results and saves the output.

4.7.6. RNA preparation from RPE1 cells

RNA was automatically isolated from RPE1 cells using the QIAcube and the RNeasy Mini Kit according to the manufacturer's protocol. In total, 10^6 cells were seeded in 10 cm dishes and incubated overnight. Cells were afterwards washed with ice-cold PBS and lysed on ice in 350 µL lysis buffer. RNA concentration and purity were determined by a NanoDrop Spectrophotometer and stored at -80°C. cDNA was synthesized using the iScript cDNA synthesis Kit (BioRad) following the manufacturer's protocol. cDNA was stored at -80°C.

4.7.7. Cleavage of DNA by restriction enzymes

In order to cut DNA at a defined position, restriction enzymes were used. Enzyme concentration, buffer concentration, duration of incubation and temperature followed the manufacturer's information. Also in case of a restriction digest with several enzymes the recommendation of the manufacturer was complied.

4.7.8. Dephosphorylation of DNA

To minimize re-ligation of linearized vectors, FastAP thermosensitive alkaline phosphatase (Thermo Fisher Scientific) was added to the restriction digest and inactivated for 5 min at 75°C.

4.7.9. Ligation of DNA fragments

For covalent linkage of DNA fragments, the fragments to be ligated were mixed in a tube (in an appropriate ratio, e.g. 1/10 backbone and 9/10 DNA fragment to be inserted). Either the T4-DNA ligase or the Quick ligase were used according to the manufacturer's protocol. 5-10 µL of the ligation was utilized for *E. coli* transformations.

4.7.10. **Determination of nucleic acid concentration**

Nucleic acid concentrations were determined by photometric measurements using a NanoDrop ND-1000 spectrophotometer (Thermo Fisher Scientific). The 260 nm and 280 nm ratio was used to ascertain the purity of nucleic acids.

4.7.11. **Separation of DNA fragments via agarose gel electrophoresis**

DNA fragments were separated via agarose gel electrophoresis (Sharp et al., 1973). Therefore, an 0.8-1.3 % agarose gel was prepared in either 0.5 x TBE or 1 x TAE buffer. To visualize the DNA, either ethidium bromide (final concentration of 0.5 µg/mL) or SYBR safe (1:10000 diluted), were used. DNA fragments were separated at 90-150 volts. As a size standard the Generuler DNA LadderMix (Thermo Fisher Scientific) was used. For documentation, DNA bands were made visible by UV light exposure at 304 nm.

4.7.12. **DNA amplification by polymerase chain reaction (PCR)**

The PCR is used for the amplification of specific double-stranded DNA fragments. For the amplification a thermo-stable polymerase, specific primers and dNTPs are required. Different polymerases were used in this work. For the amplification of DNA fragments required for subsequent cloning, either the Phusion DNA-Polymerase (laboratory preparation and NEB) or the Q5 High-Fidelity DNA Polymerase (NEB) were used. Both polymerases possess a 5'-3' polymerase activity with 3'-5' exonuclease activity and generate blunt-end products. The PCR consists of 4 characteristic steps: Double-stranded DNA is denatured at 98°C in order to generate single-stranded DNA. The oligonucleotides anneal to the single-stranded DNA at 52-72°C and mark the initiation site for the polymerase. The polymerase synthesizes the complementary DNA strand. By subsequent denaturation the PCR cycle re-starts.

Phusion PCR mixture

100 ng	DNA template
1.5 µL	5’ primer (15 pmol)
1.5 µL	3’ primer (15 pmol)
1 µL	dNTPs (10 mM each)
10 µL	5 x PCR buffer (GC)
1.5 µL	DMSO
0.5 µL	Phusion
ad 50 µL	H_2O

Q5 PCR mixture

100 ng	DNA template
1.5 µL	5’ primer (15 pmol)
1.5 µL	3’ primer (15 pmol)
1 µL	dNTPs (10 mM each)
10 µL	5 x Q5 buffer
1.5 µL	DMSO
0.5 µL	Q5 polymerase
ad 50 µL	H_2O

PCR program

98°C	∞ (preheating)	
98°C	30 sec (initial denaturation)	
98°C	10 sec (denaturation)	x 35
52-72°C	15 sec (primer annealing)	
72°C	30 sec/1 kb (elongation)	
72°C	5 min (fill-up reaction)	
12°C	∞	

For the verification of the RPE1 KO cells, the ‘Phire Tissue Direct PCR Master Mix’ and ‘Phusion Human Specimen Direct PCR Kit’ were used according to the manufacturer’s protocol.

4.7.13. **Gateway cloning and Gibson assembly**

Gateway cloning and Gibson assembly were performed using the Gateway LR clonase enzyme mix as well as the Gibson assembly master mix (Thermo Fisher Scientific), respectively, according to the manufacturer’s protocol.

4.7.14. **DNA sequencing**

All plasmids used were verified by restriction digest and afterwards sequenced. Sequencing was performed at GATC or Microsynth Seqlab. Sample preparation followed the sample requirements of the respective company.

4.7.15. **Quantitative real-time PCR (qRT-PCR)**

For the determination of relative transcript levels, a mixture of 1 µL cDNA, 5 µL 2 x SYBR Green qPCR MasterMix, 2 µL primer mix (1:50 dilution of 5’ and 3’ primer) and 2 µL H_2O was prepared. qRT-PCR was performed in a CFX Connect

Real Time System (BioRad). Data analysis was performed using the BioRad CFX Manager Software (v3.1). Melting curves were used to analyze the specificity of the amplification. *eIF2b* (*U. maydis*), *GAPDH* and *β-Actin* (RPE1) were used as reference genes.

4.7.16. **Transfer and detection of DNA (Southern Blot)**

DNA fragments cleaved by restriction endonucleases were transferred to a nylon membrane through capillary action (Southern, 1975). 15 µL of gDNA was digested overnight with the respective enzymes and loaded afterwards on a 0.8 % TBE-agarose gel. DNA fragments were separated for 2.5 h at 90 volts. Afterwards, the agarose gel was incubated in 0.25 M HCl for 20 min, rinsed in H_2O, incubated in DENAT solution for 20 min, washed in H_20 and incubated for another 20 min in RENAT solution. The DNA fragments were transferred to a positively charged nylon membrane (Roti-Nylon Plus, Carl Roth) by capillary action with the aid of 20 x SSC transfer solution.

DNA probes were generated according to the DIG-High Prime protocol (Roche). Briefly, Digoxigenin-11-dUTP (DIG) was incorporated into the DNA-probe fragments. In total 1.5 µg DNA was denatured for 10 min at 99°C. After cooling down on ice, 1 µL 10 x Random Primer Mix, 1 µL 10 x BSA, 1 µL 10 x DIG dNTP-Mix (1 mM dATP, 1 mM dCTP, 1 mM dGTP, 0.65 mM dTTP and 0.35 mM DIG-dUTP) and 0.4 µL Klenow polymerase were added. The mixture was incubated overnight at 37°C and the reaction stopped by incubation at 65°C for 10 min. The DNA probe was diluted in 15 mL southern hybridization buffer and stored at -20°C.

After successful blotting, the nylon membrane was dried at RT and transferred into a hybridization tube. The membrane was incubated two times in southern hybridization buffer at 65°C in a hybridization oven (Biometra). The denatured DNA probe (99°C, 10 min) was added to the membrane and incubated overnight at 65°C. Next, the probe was removed from the membrane and stored for re-use at -20°C. Before detecting the DNA fragments, the nylon membrane was washed for 15 min with 2 x SSPE + 0.1 % SDS buffer at 65°C, for 15 min with 1 x SSPE + 0.1 % SDS buffer at 65°C and for 15 min with 0.5 x SSPE + 0.1 % SDS buffer at 65°C. All following washing/incubation steps were performed at 25°C. First of

all, the membrane was washed in DIG wash buffer for 5 min and incubated for 30 min in DIG2 (blocking reaction). Afterwards, 10 mL anti-DIG antibody solution was added to the membrane and incubated for 30 min. After incubation, the membrane was washed two times in DIG wash buffer for 15 min and one time in DIG3 buffer for 5 min. After that, the membrane was incubated for 5 min with CDP-Star solution and the DNA fragments visualized using the Fusion XT Chemiluminescence/Fluorescence detection system (Peqlab).

Southern hybridization buffer

0.5 M	Na-phosphate buffer (pH 7.0)
7 % (w/v)	SDS

Dissolve in $H_2O_{bid.}$ and store at 65°C.

1 M Na-phosphate buffer

1 M	Na_2HPO_4 x 2 H_20 (solution 1)
1 M	NaH_2PO_4 x 2 H_20 (solution 2)

Add solution 2 to solution 1 until pH of 7.0 is reached.

20 x SSC buffer

3 mM	NaCl
0.3 mM	Na-citrate x 2 H_2O

Dissolve in $H_2O_{bid.}$ and adjust to pH 7.0 with HCl.

DENAT solution

1.5 M	NaCl
0.4 M	NaOH

Dissolve in. $H_2O_{bid.}$ and store at RT.

RENAT solution

1.5 M	NaCl
282 mM	Tris-HCl
218 mM	Tris-Base

Dissolve in $H_2O_{bid.}$ and store at RT.

DIG wash buffer

0.3 % (v/v)	Tween-20

Dissolve in 1 L $H_2O_{bid.}$ and store at RT.

DIG1 buffer

0.1 M	Maleic acid
0.15 M	NaCl

Dissolve in $H_2O_{bid.}$ and adjust pH to 7.5 with NaOH.

DIG2 buffer

5 % (v/v)	Milk powder

Dissolve in 50 mL DIG1 buffer. (freshly prepare before usage).

DIG3 buffer

0.1 M	NaCl
0.5 M	$MgCl_2$ x 6 H_2O

Dissolve in $H_2O_{bid.}$ and adjust pH to 9.5 with HCl.

20 x SSPE buffer

3 mM	NaCl
227 mM	Na_2HPO_4 x H_2O
20 mM	Na_2-EDTA

Dissolve in $H_2O_{bid.}$ and adjust pH to 7.5 with NaOH.

CDP-Star solution

20 µL	CDP-Star solution

Mix with 10 mL DIG3 buffer and store at -20°C.

anti-DIG antibody solution

6 mL	DIG2 buffer
4 mL	DIG1 buffer
1 µL	anti-DIG antibody

Freshly prepare before usage.

4.8. Biochemical methods

4.8.1. Protein extraction from *U. maydis*

For the extraction of proteins, *U. maydis* cells from a 50 mL cell suspension were collected via centrifugation (3500 rpm, 5 min, 4°C) and washed in ice-cold TBS buffer (3500 rpm, 5 min, 4°C). Next, the cells were resuspended in 150 µL lysis buffer and transferred into a 2 mL tube containing 300 mg glass beads. The samples were flash frozen in liquid nitrogen and thawed for 30 min at 4°C on a Vibrax shaker at 2000 rpm. The samples were spun down for 10 min at 13000 rpm and the clear supernatant containing the protein lysate was transferred into a fresh tube. For storage, the proteins were flash frozen and stored at -80°C.

TBS buffer

150 mM	NaCl
50 mM	Tris-HCl (pH 7.5)

Dissolve in $H_2O_{bid.}$ and adjust pH to 7.5. Store at RT.

Lysis buffer

0.1 % (v/v)	TritonX-100
2 x	Protease inhibitor cocktail

Freshly prepare in TBS buffer.

Preparation of proteins from larger culture volumes was performed according to the protocol described in section 4.8.7.

4.8.2. **Protein extraction from RPE1 cells**

For the preparation of proteins from RPE1 cells, 1.5 x 10^5 cells were seeded in 6-well plates and incubated overnight. After incubation, the cells were washed two times with ice-cold PBS buffer and lysed in 50 µL Laemmli lysis buffer on ice using a cell scraper (BioRad). The lysates were transferred into 1.5 mL tubes and boiled for 7 min at 99°C. After 3 min centrifugation at 13000 rpm (RT), the samples were stored at -20°C.
Proteins for subsequent LCMS analysis were prepared as described in section 4.8.6.

4.8.3. **Determination of protein concentration**

For the determination of the protein concentration, protein lysates were diluted in an appropriate amount of H_2O and the concentration measured using a NanoDrop ND-1000 spectrophotometer (Thermo Fisher Scientific).

4.8.4. **Protein separation via SDS-polyacrylamide gel electrophoresis**

The separation of proteins was achieved by discontinuous SDS-polyacrylamide gel electrophoresis (SDS-PAGE) (Laemmli, 1970). Proteins for the mammalian part of this work were separated on 4-20 % Mini-PROTEAN TGX Precast Gradient Gels using the premixed Tris/Gylcine/SDS (TGS) electrophoresis buffer (BioRad). As size standard the Precision Plus Protein Dual Color Standard (BioRad) was used.
Proteins for the fungal part of this work were separated on SDS-gels prepared with the Mini PROTEAN II equipment (BioRad) according to the manufacturer's protocol. Proteins were mixed with Roti Load-1 sample buffer (Carl Roth) and boiled for 5 min at 95°C. As a size standard, the PageRuler Prestained Protein Ladder (Thermo Fisher Scientific) was used. Protein separation took place at 100 V for 2 h in running buffer on ice.

10 % Separation gel (for 2 gels)

2.8 mL	H_20
3.75 mL	1 M Tris-HCl (pH 8.8)
100 µL	10 % SDS
3.3 mL	30 Acrylamide
12 µL	TEMED
52 µL	10 % Ammonium persulfate (APS)

4 % Stacking gel (for 2 gels)

3.67 mL	H_20
625 µL	1 M Tris-HCl (pH 6.8)
50 µL	10 % SDS
650 µL	30 Acrylamide
7 µL	TEMED
27 µL	10 % Ammonium persulfate (APS)

Running buffer (10 x)

30 g/L	NaCl
188 g/L	Tris-HCl (pH 7.5)
10 g/L	SDS

Dissolve in $H_2O_{bid.}$ and autoclave for 20 min at 121°C.

4.8.5. **Protein transfer and detection (Western Blot)**

For the transfer of proteins on a PVDF membrane (Amersham Hybond P 0,45 GE Healthcare), a semi-dry electro-blot system (Peqlab) was used. The membrane was activated for 1 min in either methanol or ethanol and briefly rinsed in transfer buffer. The blot was assembled as follows:
bottom-3 x Whatman paper-PVDF membrane-SDS gel-3 x Whatman paper-**top**
The protein transfer was performed at 75 mA/gel for 2 h at RT. Next, the membrane was rinsed in TBS-T buffer and incubated for 35 min in 5 % milk-TBS-T. The membrane was incubated with the primary antibody diluted in 5 % milk-TBS-T either overnight at 4°C or for 2 h at RT. After incubation with the primary antibody, the membrane was washed 3 times in TBS-T buffer for 5 min before being incubated with the corresponding secondary antibody diluted in 5 % milk-TBS-T. Incubation with the secondary antibody took at least 2 h at RT. After that, the membrane was again washed three times in TBS-T buffer and one time in TBS buffer for 5 min before detection of the proteins. For the detection, the membrane was incubated with 1 mL ECL solution (Luminata Crescendo Western HRP Substrate, Merck) and the blot developed using the Fusion XT Chemiluminescence/Fluorescence detection system. As a loading control Ponceau S staining was used. Stripping of the membrane was performed via incubation in Ponceau S for 1 h at RT.

Transfer buffer (10 x)

1.92 M	Glycine
0.25 M	Tris-HCl

Dissolve in $H_2O_{bid.}$ and store at RT. Before usage, add 20 % methanol to the 1 x transfer buffer.

Ponceau S

0.1 % (w/v)	Ponceau S
5 % (v/v)	Acetic acid

Prepare in H_2O_{bid} and store at RT. Solution can be reused.

TBS-T

0.1 % (v/v)	Tween-20

Mix in TBS buffer and store at RT.

Milk-TBS-T

5 % (w/v)	Milk powder

Dissolve in TBS-T buffer. Storage at 4°C possible up to several days.

Alternatively, the Trans-Blot Turbo Blotting System (BioRad) was used according to the manufacturer's description. Membranes and transfer buffer included in the Trans-Blot Turbo Transfer Kit (BioRad) were used. Membrane stripping was performed using the Restore Western Blot Stripping buffer (Thermo Fisher Scientific) following the manufacturer's advice.

4.8.6. **GFP-Trap and LCMS analysis**

For the interactor analysis of $XBP1^s$/$XBP1^u$, GFP-traps were performed using GFP-Trap beads (ChromoTek). All following steps were performed at 4°C. RPE1 cells were lysed in L1 lysis buffer using a cell scraper (1 mL per 15 cm dish). Before collection and transfer of the cells into 1.5 mL, the scraped plates were incubated for 5 min on ice. Cell lysates were homogenized by ten times passing through a 27G syringe. After another 20 min of incubation on ice, centrifugation of the samples was performed at 14000 rpm for 20 min. The supernatant containing the cleared lysates was stored at -80°C after the addition of 8 % glycerol and snap-freezing in liquid nitrogen.

For the immunoprecipitation (IP) the GFP-Trap beads were washed three times in L1 lysis buffer. Protein lysates were thawed on ice and were added to the GFP-Trap beads and incubated for 3 h under continuous rotation. After that, the GFP-Trap beads were washed five times in L1 lysis buffer and three times in L1 lysis buffer without any detergents and protease/phosphatase inhibitors. Beads were transferred into a fresh 1.5 mL tube and washed another three times in PBS

buffer. All following steps in sample preparation and the subsequent LCMS analysis were performed by the Proteomics Core Facility (PCF) of the Oslo University Hospital. Markus Esswein (University Duisburg-Essen) wrote the R script (see Appendix A) for the preparation and analysis of the raw data. Briefly, the script loads raw data from both experiments, joins by protein IDs (full outer join), subsets by relevant columns, filters for twofold change, visualizes the results and saves the output.

L1 lysis buffer

50 mM	Tris-HCl (pH 7.5)
150 mM	NaCl
0.2 % (v/v)	TritonX-100
1 mM	EDTA
1 mM	DTT
1 x	Protease inhibitor cocktail
1 x	PhosSTOP
5 mM	NaPPi
100 mM	NaF
1 mM	Na_3VO_4
5 % (v/v)	Glycerol

Dissolve in H_2O_{bid} (final volume 50 mL).
Store buffer at RT. Add the inhibitors and DTT right before usage.

4.8.7. **Co-immunoprecipitation**

For co-immunoprecipitation (CoIP) analysis, the corresponding *U. maydis* cells were grown overnight in CM-medium supplemented with 1 % glucose/arabinose. The cultures were adjusted to OD 0.3 in at least 300 mL culture volume and incubated for another 4 h at 30°C under continuous shaking. Afterwards, cells were collected via centrifugation at 3500 rpm for 5 min at 4°C. The supernatant was discarded, the cells washed in ice-cold B300 buffer containing 2 x protease inhibitor cocktail and transferred into 2.0 mL tubes. After another round of centrifugation, the supernatant was discarded and the cell pellet snap-frozen in liquid nitrogen. The cells were broken open using two times a Retsch MM200 mill at 30 Hz for 1.45 min. Next, the cell ‘powder’ was carefully resuspended in B300 buffer. After centrifugation at 22000 rpm for 30 min at 4°C, the supernatant containing the cleared protein lysates was added to 30 µL in B300 buffer washed

GFP-Trap beads and incubated for 3 h at 4°C under continuous rotation. Before adding the GFP-Trap beads, 20 µL of the lysates were mixed with Roti Load-1 sample buffer, boiled for 5 min at 95°C and stored at -20°C. These samples served as input controls to test the expression of the proteins for which interaction should be analyzed. After 3 h of incubation, the GFP-Trap beads were washed four times with B300 buffer at 4°C. Finally, the beads were resuspended in 50 µL Roti Load-1 sample buffer and boiled for 5 min at 95°C. The supernatant contained the IP fraction and was stored at -20°C. Input and IP fractions were loaded on SDS acrylamide gels following the protocol described in section 4.8.4. and 4.8.5.

B300 buffer

300 mM	NaCl
100 mM	Tris-HCl (pH 7.5)
10 % (v/v)	Glycerol
0.1 % (v/v)	NP-40
1 mM	EDTA
2 x	Protease inhibitor cocktail

Dissolve in H_2O_{bid} and store buffer at 4°C.
Add the protease inhibitor cocktail right before usage.

4.8.8. **Cycloheximide chase analysis**

Protein stability was determined performing a cycloheximide (CHX) chase analysis. Therefore, logarithmically grown *U. maydis* cells were treated with 100 µg/mL CHX for 15 min, 30 min, 60 min and 90 min at 30°C under continuous shaking. Afterwards, the cells were collected via centrifugation (3500 rpm, 5 min, RT), washed in TBS buffer and the proteins extracted according to the procedure described in section 4.8.1.

4.9. Microscopy

4.9.1. Live cell imaging *U. maydis*

For live cell imaging, *U. maydis* cells were grown overnight in YEPS-L-medium at 28°C under continuous shaking. OD of the culture was adjusted to 0.25 in YNB-medium supplemented with 1 % glucose and 0.2 %ammonium sulfate and incubated for another 4 h at 28°C. After incubation, the cells were collected via centrifugation at 2500 rpm for 5 min at RT and washed in YNB-medium. Afterwards, the cells were resuspended in 100 µL YNB-medium. 20 µL of the cell suspension was transferred onto MatTek 35 mm glass-bottom dishes and covered with a 2 % agarose plug in order to prevent the cells to dry out. Imaging was performed on a Deltavision OMX V4 microscope (GE Healthcare) equipped with three water-cooled PCO.edge sCMOS cameras, a solid-state light source and a laser-based autofocus. Deconvolution was performed using softWoRx software and image processing using Fiji (Schindelin et al., 2012).

4.9.2. Live cell imaging RPE1 cells

For live cell imaging, RPE1 cells were grown in MatTek 35 mm glass-bottom dishes in DMEM-F12-medium. Cells were washed and imaged in Live Cell Imaging buffer (Invitrogen) containing 20 mM glucose. A heated stage and an objective heater (20-20 Technologies) enabled stable environmental imaging conditions. Imaging and image analysis were performed as described in section 4.9.1.

For FRAP analyses, RPE1 cells were grown in MatTek 35 mm glass-bottom dishes in DMEM-F12-medium and transfected with the mCherry-XBP1^{s}-T2A-GFP-XBP1^{u} plasmid. 24 h post-transfection, cells were imaged in Live Cell Imaging buffer (Invitrogen) supplemented with 20 mM glucose. FRAP experiments were performed using an OMX V4 system equipped with a solid state light source and 405, 488, 568, 647 nm laser lines. Images were acquired every second. After 1-3 timepoints, selected regions were bleached using 488 nm light and recovery was measured for at least 26 timepoints. Images were analyzed using Fiji (Schindelin et al., 2012). Mean intensities in defined ROIs were measured in every frame and plotted versus time. FRAP analyses were

performed in collaboration with Kay Oliver Schink (Oslo University Hospital, Institute for Cancer Research).

4.9.3. **Confocal microscopy**

For confocal microscopy, RPE1 cells were grown on coverslips in DMEM-F12-medium, washed in PBS and fixed in 3 % paraformaldehyde (PFA) for 15 min on ice. After fixation, cells were washed three times in PBS and incubated with NH_4Cl for 10 min at RT (quenching). After quenching, cells were washed again one time in PBS and one time in PBS/0.05 % Saponin. The primary antibodies (α-VapA, α-GM130, α-GFP) were diluted in PBS/0.05 % Saponin and carefully applied on the coverslips and incubated for 1 h at RT in darkness. Coverslips were washed three times in PBS/0.05 % Saponin and incubated in darkness for 45 min with the corresponding secondary antibodies as well as Alexa Fluor 647 Phalloidin diluted in PBS/0.05 % Saponin. Next, the coverslips were washed three times in PBS/0.05 % Saponin and three times in PBS. After that, the coverslips were briefly dipped in H_2O_{bid} and mounted on Mowiol containing 2 µg/mL Hoechst 33342. The cells were examined using a Zeiss LSM 780 (Carl Zeiss MicroImaging GmbH) equipped with an Ar-Laser Multiline (458/488/514 nm), a DPSS-561 10 (561 nm), a Laser diode 405-30 CW (405 nm) and a HeNe-laser (633 nm). A Zeiss plan-Apochromat x 63/1.4 Oil DIC III objective was used. Image processing was performed using Fiji (Schindelin et al., 2012). Confocal microscopy was supported by the core facility for Advanced Light Microscopy at the Oslo University Hospital.

Quantification of the nuclear localization was automatically performed using a Python script (see Appendix A). This script was written by Kay Oliver Schink (Oslo University Hospital, Institute for Cancer Research) and contains segmentation of nuclei and intensity measurements within this region of interest. Z-projections were used for qualitative and quantitative analyses.

PBS/0.05 % Saponin buffer	**NH_4Cl buffer**
0.05 % (v/v) 10 % Saponin	50 mM NH_4Cl
Add to PBS buffer and mix properly. Freshly prepare before immunostaining.	Dissolve in PBS and store at RT.

4.9.4. **Electron microscopy**

For electron microscopy analysis, *U. maydis* cells were grown overnight in YEPS-L-medium. Afterwards, the OD was adjusted to 0.25 and the cells incubated under continuous shaking for another 4 h at 28°C. After incubation, the cells were washed twice in YNB-medium supplemented with 1 % glucose and 0.2 % ammonium sulfate and collected via centrifugation (2500 rpm, 5 min, RT). All following steps were performed by Andreas Brech and Maja Radulovic (Oslo University Hospital, Institute for Cancer Research). Further information can be requested from Andreas Brech.

4.10. Statistical analysis

Statistical analyses were performed using Graphpad Prism 7. The tests used as a measure for statistical significance are provided in figure captions and in the corresponding results section. The sample size and the significance levels are reported in the figure legends.

4.11. Icon library used for creation of figures

Icons for biological compartments and receptors, e.g. in Figure 1, were taken from the ‘library of science and medical illustrations’ (http://www.somersault1824.com/resources/).

References

Acosta-Alvear D, Zhou Y, Blais A, Tsikitis M, Lents NH, Arias C, Lennon CJ, Kluger Y, Dynlacht BD. 2007. XBP1 Controls Diverse Cell Type- and Condition-Specific Transcriptional Regulatory Networks. *Mol Cell* **27**:53–66. doi:10.1016/j.molcel.2007.06.011

Adachi Y, Yamamoto K, Okada T, Yoshida H, Harada A, Mori K. 2008. ATF6 is a transcription factor specializing in the regulation of quality control proteins in the endoplasmic reticulum. *Cell Struct Funct* **33**:75–89. doi:doi.org/10.1247/csf.07044

Aichinger C, Hansson K, Eichhorn H, Lessing F, Mannhaupt G, Mewes W, Kahmann R. 2003. Identification of plant-regulated genes in Ustilago maydis by enhancer-trapping mutagenesis. *Mol Genet Genomics* **270**:303–314. doi:10.1007/s00438-003-0926-z

Alberts B, Johnson A, Lewis J, Raff M, Roberts K, Walter P. 2002. The Endoplasmic Reticulum.

Aragón T, van Anken E, Pincus D, Serafimova IM, Korennykh A V., Rubio CA, Walter P. 2009. Messenger RNA targeting to endoplasmic reticulum stress signalling sites. *Nature* **457**:736–740. doi:10.1038/nature07641

Arendt D. 2008. The evolution of cell types in animals: emerging principles from molecular studies. *Nat Rev Genet* **9**:868–882. doi:10.1038/nrg2416

Ausubel F, Kingston R, Moore D, Seidman J, Smith J, Struhl K. 1987. Current Protocols in Molecular Biology. *Wiley Interscience, New York*.

Banuett F, Herskowitz I. 1996. Discrete developmental stages during teliospore formation in the corn smut fungus, Ustilago maydis. *Development* **122**:2965–2976.

Banuett F, Herskowitz I. 1989. Different a alleles of Ustilago maydis are necessary for maintenance of filamentous growth but not for meiosis. *Proc Natl Acad Sci U S A* **86**:5878–5882.

Bauer DE, Canver MC, Orkin SH. 2015. Generation of genomic deletions in mammalian cell lines via CRISPR/Cas9. *J Vis Exp* **95**. doi:10.3791/52118

Baumann S, Pohlmann T, Jungbluth M, Brachmann A, Feldbrugge M. 2012. Kinesin-3 and dynein mediate microtubule-dependent co-transport of mRNPs and endosomes. *J Cell Sci* **125**:2740–2752. doi:10.1242/jcs.101212

Bertolotti A, Wang X, Novoa I, Jungreis R, Schlessinger K, Cho JH, West AB, Ron D. 2001. Increased sensitivity to dextran sodium sulfate colitis in IRE1β-deficient mice. *J Clin Invest* **107**:585–593. doi:10.1172/JCI11476

Bertolotti A, Zhang Y, Hendershot LM, Harding HP, Ron D. 2000. Dynamic interaction of BiP and ER stress transducers in the unfolded-protein response. *Nat Cell Biol* **2**:326–332. doi:10.1038/35014014

Böhmer C, Böhmer M, Bölker M, Sandrock B. 2008. Cdc42 and the Ste20-like kinase Don3 act independently in triggering cytokinesis in Ustilago maydis. *J Cell Sci* **121**:143–148. doi:10.1242/jcs.014449

Bölker M, Basse CW, Schirawski J. 2008. Ustilago maydis secondary metabolism-from genomics to biochemistry. *Fungal Genet Biol* **45**:88–93. doi:10.1016/j.fgb.2008.05.007

Bölker M, Böhnert HU, Braun KH, Görl J, Kahmann R. 1995. Tagging pathogenicity genes in Ustilago maydis by restriction enzyme-mediated integration (REMI). *Mol Gen Genet* **248**:547–552.

Bölker M, Urban M, Kahmann R. 1992. The a mating type locus of U. maydis specifies cell signaling components. *Cell* **68**:441–450.

Boye E, Anda S, Rothe C, Stokke T, Grallert B. 2016. Analyzing Schizosaccharomyces pombe DNA Content by Flow Cytometry. *Cold Spring Harb Protoc* **6**. doi:10.1101/pdb.prot091280

Brachmann A, König J, Julius C, Feldbrügge M. 2004. A reverse genetic approach for generating gene replacement mutants in Ustilago maydis. *Mol Genet Genomics* **272**:216–226. doi:10.1007/s00438-004-1047-z

Brachmann A, Weinzierl G, Kämper J, Kahmann R. 2001. Identification of genes in the bW/bE regulatory cascade in Ustilago maydis. *Mol Microbiol* **42**:1047-1063. doi:10.1046/j.1365-2958.2001.02699.x|

Brewer JW, Hendershot LM, Sherr CJ, Diehl JA. 1999. Mammalian unfolded protein response inhibits cyclin D1 translation and cell-cycle progression. *Proc Natl Acad Sci U S A* **96**:8505–8510. doi:10.1073/pnas.96.15.8505

Broomfield PLE, Hargreaves JA. 1992. A single amino-acid change in the iron-sulphur protein subunit of succinate dehydrogenase confers resistance to carboxin in Ustilago maydis. *Curr Genet* **22**:117–121.doi:10.1007/BF00351470

Cabrera E, Hernández-Pérez S, Koundrioukoff S, Debatisse M, Kim D, Smolka MB, Freire R, Gillespie DA. 2017. PERK inhibits DNA replication during the Unfolded Protein Response via Claspin and Chk1. *Oncogene* **36**:678–686. doi:10.1038/onc.2016.239

Calfon M, Zeng H, Urano F, Till JH, Hubbard SR, Harding HP, Clark SG, Ron D. 2002. Erratum: IRE1 couples endoplasmic reticulum load to secretory capacity by processing the XBP-1 mRNA. *Nature* **415**:92–96. doi:10.1038/415092a

Carrara M, Prischi F, Nowak PR, Kopp MC, Ali MM. 2015. Noncanonical binding of BiP ATPase domain to Ire1 and Perk is dissociated by unfolded protein CH1 to initiate ER stress signaling. *Elife* **4**. doi:10.7554/eLife.03522

Castillo K, Rojas-Rivera D, Lisbona F, Caballero B, Nassif M, Court FA, Schuck S, Ibar C, Walter P, Sierralta J, Glavic A, Hetz C. 2011. BAX inhibitor-1 regulates autophagy by controlling the IRE1α branch of the unfolded protein response. *EMBO J* **30**:4465–78. doi:10.1038/emboj.2011.318

Chapman RE, Walter P. 1997. Translational attenuation mediated by an mRNA intron. *Curr Biol* **7**:850–9.

Chen C, Malchus NS, Hehn B, Stelzer W, Avci D, Langosch D, Lemberg MK. 2014. Signal peptide peptidase functions in ERAD to cleave the unfolded protein response regulator XBP1u. *EMBO J* **33**:2492–506. doi:10.15252/embj.201488208

Chen X, Iliopoulos D, Zhang Q, Tang Q, Greenblatt MB, Hatziapostolou M, Lim E, Tam WL, Ni M, Chen Y, Mai J, Shen H, Hu DZ, Adoro S, Hu B, Song M, Tan C, Landis MD, Ferrari M, Shin SJ, Brown M, Chang JC, Liu XS, Glimcher LH. 2014. XBP1 promotes triple-negative breast cancer by controlling the HIF1α pathway. *Nature* **508**:103–107. doi:10.1038/nature13119

Chen X, Shen J, Prywes R. 2002. The Luminal Domain of ATF6 Senses Endoplasmic Reticulum (ER) Stress and Causes Translocation of ATF6 from the ER to the Golgi. *J Biol Chem* **277**:13045–13052. doi:10.1074/jbc.M110636200

Cheon SA, Jung K-W, Bahn Y-S, Kang HA. 2014. The unfolded protein response (UPR) pathway in Cryptococcus. *Virulence* **5**:341–350. doi:10.4161/viru.26774

Cheon SA, Jung K-W, Chen Y-L, Heitman J, Bahn Y-S, Kang HA. 2011. Unique Evolution of the UPR Pathway with a Novel bZIP Transcription Factor, Hxl1, for Controlling Pathogenicity of Cryptococcus neoformans. *PLoS Pathog* **7**. doi:10.1371/journal.ppat.1002177

Ciuba K, Hawkes W, Tojkander S, Kogan K, Engel U, Iskratsch T, Lappalainen P. 2018. Calponin-3 is critical for coordinated contractility of actin stress fibers. *Sci Rep* **8**. doi:10.1038/s41598-018-35948-6

Cohen N, Breker M, Bakunts A, Pesek K, Chas A, Argemí J, Orsi A, Gal L, Chuartzman S, Wigelman Y, Jonas F, Walter P, Ernst R, Aragón T, van Anken E, Schuldiner M. 2017. Iron affects Ire1 clustering propensity and the amplitude of endoplasmic reticulum stress signaling. *J Cell Sci* **130**:3222–3233. doi:10.1242/jcs.201715

Cox JS, Shamu CE, Walter P. 1993. Transcriptional induction of genes encoding endoplasmic reticulum resident proteins requires a transmembrane protein kinase. *Cell* **73**:1197–1206. doi:10.1016/0092-8674(93)90648-A

Cox JS, Walter P. 1996. A novel mechanism for regulating activity of a transcription factor that controls the unfolded protein response. *Cell* **87**:391–404. doi:10.1016/S0092-8674(00)81360-4

Cribb AE, Peyrou M, Muruganandan S, Schneider L. 2005. The Endoplasmic Reticulum in Xenobiotic Toxicity. *Drug Metab Rev* **37**:405–442. doi:10.1080/03602530500205135

Cullinan SB, Zhang D, Hannink M, Arvisais E, Kaufman RJ, Diehl JA. 2003. Nrf2 is a direct PERK substrate and effector of PERK-dependent cell survival. *Mol Cell Biol* **23**:7198–7209. doi:10.1128/MCB.23.20.7198-7209.2003

Cunha DA, Cito M, Carlsson P-O, Vanderwinden J-M, Molkentin JD, Bugliani M, Marchetti P, Eizirik DL, Cnop M. 2016. Thrombospondin 1 protects pancreatic β-cells from lipotoxicity via the PERK-NRF2 pathway. *Cell Death Differ* **23**:1995–2006. doi:10.1038/cdd.2016.89

Di Santo R, Aboulhouda S, Weinberg DE. 2016. The fail-safe mechanism of post-transcriptional silencing of unspliced HAC1 mRNA. *Elife* **5**. doi:10.7554/eLife.20069

Diehn M, Eisen MB, Botstein D, Brown PO. 2000. Large-scale identification of secreted and membrane-associated gene products using DNA microarrays. *Nat Genet* **25**:58–62. doi:10.1038/75603

Doebley J. 1992. Mapping the genes that made maize. *Trends Genet* **8**:302–307. doi:10.1016/0168-9525(92)90261-2

Dull T, Zufferey R, Kelly M, Mandel RJ, Nguyen M, Trono D, Naldini L. 1998. A third-generation lentivirus vector with a conditional packaging system. *J Virol* **72**:8463–8471.

Eichhorn H, Lessing F, Winterberg B, Schirawski J, Kämper J, Müller P, Kahmann R. 2006. A ferroxidation/permeation iron uptake system is required for virulence in Ustilago maydis. *Plant Cell* **18**:3332–3345. doi:10.1105/tpc.106.043588

Fordyce PM, Pincus D, Kimmig P, Nelson CS, El-Samad H, Walter P, DeRisi JL. 2012. Basic leucine zipper transcription factor Hac1 binds DNA in two distinct modes as revealed by microfluidic analyses. *Proc Natl Acad Sci* **109**:3084–3093. doi:10.1073/pnas.1212457109

Friedlander R, Jarosch E, Urban J, Volkwein C, Sommer T. 2000. A regulatory link between ER-associated protein degradation and the unfolded protein response. *Nat Cell Biol* **2**:379–384. doi:10.1038/35017001

Gambella M, Rocci A, Passera R, Gay F, Omede P, Crippa C, Corradini P, Romano A, Rossi D, Ladetto M, Boccadoro M, Palumbo A. 2014. High XBP1 expression is a marker of better outcome in multiple myeloma patients treated with bortezomib. *Haematologica* **99**:14–16. doi:10.3324/haematol.2013.090142

Gardner BM, Walter P. 2011. Unfolded Proteins Are Ire1-Activating Ligands That Directly Induce the Unfolded Protein Response. *Science* **333**:1891–1894. doi:10.1126/science.1209126

Gething M-J. 1999. Role and regulation of the ER chaperone BiP. *Semin Cell Dev Biol* **10**:465–472. doi:10.1006/scdb.1999.0318

Gillissen B, Bergemann J, Sandmann C, Schroeer B, Bölker M, Kahmann R. 1992. A two-component regulatory system for self/non-self recognition in Ustilago maydis. *Cell* **68**:647–657.

Glazier VE, Kaur JN, Brown NT, Rivera AA, Panepinto JC. 2015. Puf4 regulates both splicing and decay of HXL1 mRNA encoding the unfolded protein response transcription factor in Cryptococcus neoformans. *Eukaryot Cell* **14**:385–395. doi:10.1128/EC.00273-14

Gonzalez TN, Sidrauski C, Dörfler S, Walter P. 1999. Mechanism of non-spliceosomal mRNA splicing in the unfolded protein response pathway. *EMBO J* **18**:3119–3132. doi:10.1093/emboj/18.11.3119

Guo J, Polymenis M. 2006. Dcr2 targets Ire1 and downregulates the unfolded protein response in Saccharomyces cerevisiae. *EMBO Rep* **7**:1124–1127. doi:10.1038/sj.embor.7400813

Gupta S, Deepti A, Deegan S, Lisbona F, Hetz C, Samali A. 2010. HSP72 Protects Cells from ER Stress-induced Apoptosis via Enhancement of IRE1α-XBP1 Signaling through a Physical Interaction. *PLoS Biol* **8**:e1000410. doi:10.1371/journal.pbio.1000410

Halliwell B. 2003. Oxidative stress in cell culture: an under-appreciated problem? *FEBS Lett* **540**:3–6. doi:10.1016/S0014-5793(03)00235-7

Hampel M. 2016. Analyse der UPR vermittelten Stressantwort und ihrer Funktion während der biotrophen Entwicklung von Ustilago maydis.

Hampel M, Jakobi M, Schmitz L, Meyer U, Finkernagel F, Doehlemann G, Heimel K. 2016. Unfolded Protein Response (UPR) Regulator Cib1 Controls Expression of Genes Encoding Secreted Virulence Factors in Ustilago maydis. *PLoS One* **11**. doi:10.1371/journal.pone.0153861

Hanahan D, Jessee J, Bloom FR. 1991. [4] Plasmid transformation of Escherichia coli and other bacteria. *Methods Enzymol* **204**:63–114. doi:10.1016/0076-6879(91)04006-A

Harding HP, Novoa I, Zhang Y, Zeng H, Wek R, Schapira M, Ron D. 2000. Regulated translation initiation controls stress-induced gene expression in mammalian cells. *Mol Cell* **6**:1099–1108. doi:10.1016/S1097-2765(00)00108-8

Harding HP, Zhang Y, Scheuner D, Chen J-J, Kaufman RJ, Ron D. 2009. Ppp1r15 gene knockout reveals an essential role for translation initiation factor 2 alpha (eIF2α) dephosphorylation in mammalian development. *Proc Natl Acad Sci* **106**:1832–1837. doi:10.1073/pnas.0809632106

Harding HP, Zhang Y, Zeng H, Novoa I, Lu PD, Calfon M, Sadri N, Yun C, Popko B, Paules R, Stojdl DF, Bell JC, Hettmann T, Leiden JM, Ron D. 2003. An integrated stress response regulates amino acid metabolism and resistance to oxidative stress. *Mol Cell* **11**:619–633. doi:10.1016/S1097-2765(03)00105-9

Hawksworth DL. 2001. The magnitude of fungal diversity: the 1.5 million species estimate revisited. *Mycol Res* **105**:1422–1432. doi:10.1017/S0953756201004725

Haze K, Yoshida H, Yanagi H, Yura T, Mori K. 1999. Mammalian Transcription Factor ATF6 Is Synthesized as a Transmembrane Protein and Activated by Proteolysis in Response to Endoplasmic Reticulum Stress. *Mol Biol Cell* **10**:3787–3799. doi:10.1091/mbc.10.11.3787

Hegde RS, Lingappa VR. 1999. Regulation of protein biogenesis at the endoplasmic reticulum membrane. *Trends Cell Biol* **9**:132–137. doi:10.1016/S0962-8924(99)01504-4

Heimel K. 2015. Unfolded protein response in filamentous fungi-implications in biotechnology. *Appl Microbiol Biotechnol* **99**:121–132. doi:10.1007/s00253-014-6192-7

Heimel K, Freitag J, Hampel M, Ast J, Bölker M, Kamper J. 2013. Crosstalk between the Unfolded Protein Response and Pathways That Regulate Pathogenic Development in Ustilago maydis. *Plant Cell* **25**:4262–4277. doi:10.1105/tpc.113.115899

Heimel K, Scherer M, Schuler D, Kämper J. 2010. The Ustilago maydis Clp1 protein orchestrates pheromone and b-dependent signaling pathways to coordinate the cell cycle and pathogenic development. *Plant Cell* **22**:2908–2922. doi:10.1105/tpc.110.076265

Hermann BG, Patel M. 2007. Today's and tomorrow's bio-based bulk chemicals from white biotechnology: a techno-economic analysis. *Appl Biochem Biotechnol* **136**:361–388. doi:10.1007/s12010-007-9031-9

Herzog B, Popova B, Jakobshagen A, Shahpasandzadeh H, Braus GH. 2013. Mutual cross talk between the regulators Hac1 of the unfolded protein response and Gcn4 of the general amino acid control of Saccharomyces cerevisiae. *Eukaryot Cell* **12**:1142–1154. doi:10.1128/EC.00123-13

Hetz C. 2012. The unfolded protein response: controlling cell fate decisions under ER stress and beyond. *Nat Rev Mol Cell Biol* **13**:89–102. doi:10.1038/nrm3270

Hetz C, Papa FR. 2018. The Unfolded Protein Response and Cell Fate Control. *Mol Cell* **69**:169–181. doi:10.1016/j.molcel.2017.06.017

Hinnebusch AG. 1997. Translational regulation of yeast GCN4. A window on factors that control initiator-tRNA binding to the ribosome. *J Biol Chem* **272**:21661–21664. doi:10.1074/jbc.272.35.21661

Holliday R. 1974. Ustilago maydisBacteria, Bacteriophages, and Fungi. Boston, MA: Springer US. pp. 575–595. doi:10.1007/978-1-4899-1710-2-31

Hollien J. 2013. Evolution of the unfolded protein response. *Biochim Biophys Acta - Mol Cell Res* **1833**:2458–2463. doi:10.1016/j.bbamcr.2013.01.016

Hollien J, Weissman JS. 2006. Decay of Endoplasmic Reticulum-Localized mRNAs During the Unfolded Protein Response. *Science* **313**:104–107. doi:10.1126/science.1129631

Huang C, Wu S, Ji H, Yan X, Xie Y, Murai S, Zhao H, Miyagishi M, Kasim V. 2017. Identification of XBP1-u as a novel regulator of the MDM2/p53 axis using an shRNA library. *Sci Adv* **3**. doi:10.1126/sciadv.1701383

Hurtley SM, Bole DG, Hoover-Litty H, Helenius A, Copeland CS. 1989. Interactions of misfolded influenza virus hemagglutinin with binding protein (BiP). *J Cell Biol* **108**:2117–2126. doi:10.1083/jcb.108.6.2117

Janssens S, Pulendran B, Lambrecht BN. 2014. Emerging functions of the unfolded protein response in immunity. *Nat Immunol* **15**:910–919. doi:10.1038/ni.2991

Joubert A, Simoneau P, Campion C, Bataillé-Simoneau N, Iacomi-Vasilescu B, Poupard P, François JM, Georgeault S, Sellier E, Guillemette T. 2011. Impact of the unfolded protein response on the pathogenicity of the necrotrophic fungus Alternaria brassicicola. *Mol Microbiol* **79**:1305–1324. doi:10.1111/j.1365-2958.2010.07522.x

Jung K-W, So Y-S, Bahn Y-S. 2016. Unique roles of the unfolded protein response pathway in fungal development and differentiation. *Sci Rep* **6**. doi:10.1038/srep33413

Kämper J, Kahmann R, Bölker M, Ma L-J, Brefort T, Saville BJ, Banuett F, Kronstad JW, Gold SE, Müller O, Perlin MH, Wösten HAB, de Vries R, Ruiz-Herrera J, Reynaga-Peña CG, Snetselaar K, McCann M, Pérez-Martín J, Feldbrügge M, Basse CW, Steinberg G, Ibeas JI, Holloman W, Guzman P, Farman M, Stajich JE, Sentandreu R, González-Prieto JM, Kennell JC, Molina L, Schirawski J, Mendoza-Mendoza A, Greilinger D, Münch K, Rössel N, Scherer M, Vranes M, Ladendorf O, Vincon V, Fuchs U, Sandrock B, Meng S, Ho ECH, Cahill MJ, Boyce KJ, Klose J, Klosterman SJ, Deelstra HJ, Ortiz-Castellanos L, Li W, Sanchez-Alonso P, Schreier PH, Häuser-Hahn I, Vaupel M, Koopmann E, Friedrich G, Voss H, Schlüter T, Margolis J, Platt D, Swimmer C, Gnirke A, Chen F, Vysotskaia V, Mannhaupt G, Güldener U, Münsterkötter M, Haase D, Oesterheld M, Mewes H-W, Mauceli EW, DeCaprio D, Wade CM, Butler J, Young S, Jaffe DB, Calvo S, Nusbaum C, Galagan J, Birren BW. 2006. Insights from the genome of the biotrophic fungal plant pathogen Ustilago maydis. *Nature* **444**:97–101. doi:10.1038/nature05248

Kämper J, Reichmann M, Romeis T, Bölker M, Kahmann R. 1995. Multiallelic recognition: nonself-dependent dimerization of the bE and bW homeodomain proteins in Ustilago maydis. *Cell* **81**:73–83. doi:10.1016/0092-8674(95)90372-0

Kanda S, Yanagitani K, Yokota Y, Esaki Y, Kohno K. 2016. Autonomous translational pausing is required for XBP1u mRNA recruitment to the ER via the SRP pathway. *Proc Natl Acad Sci U S A* **113**:5886–5895. doi:10.1073/pnas.1604435113

Karagöz GE, Acosta-Alvear D, Walter P. 2019. The Unfolded Protein Response: Detecting and Responding to Fluctuations in the Protein-Folding Capacity of the Endoplasmic Reticulum. *Cold Spring Harb Perspect Biol*. doi:10.1101/cshperspect.a033886

Kaufman RJ. 2002. Orchestrating the unfolded protein response in health and disease. *J Clin Invest* **110**:1389–1398. doi:10.1172/JCI0216886

Kaufman RJ. 1999. Stress signaling from the lumen of the endoplasmic reticulum: coordination of gene transcriptional and translational controls. *Genes Dev* **13**:1211–1233.

Kawahara T, Yanagi H, Yura T, Mori K. 1997. Endoplasmic reticulum stress-induced mRNA splicing permits synthesis of transcription factor Hac1p/Ern4p that activates the unfolded protein response. *Mol Biol Cell* **8**:1845–1862.

Keon JPR, White GA, Hargreaves JA. 1991. Isolation, characterization and sequence of a gene conferring resistance to the systemic fungicide carboxin from the maize smut pathogen, Ustilago maydis. *Curr Genet* **19**:475–481. doi:10.1007/BF00312739

Kimmig P, Diaz M, Zheng J, Williams CC, Lang A, Aragón T, Li H, Walter P. 2012. The unfolded protein response in fission yeast modulates stability of select mRNAs to maintain protein homeostasis. *Elife* **1**. doi:10.7554/eLife.00048

Kohno K, Normington K, Sambrook J, Gething MJ, Mori K. 1993. The promoter region of the yeast KAR2 (BiP) gene contains a regulatory domain that responds to the presence of unfolded proteins in the endoplasmic reticulum. *Mol Cell Biol* **13**:877–890. doi:10.1128/MCB.13.2.877

Kozutsumi Y, Segal M, Normington K, Gething M-J, Sambrook J. 1988. The presence of malfolded proteins in the endoplasmic reticulum signals the induction of glucose-regulated proteins. *Nature* **332**:462–464. doi:10.1038/332462a0

Laemmli UK. 1970. Cleavage of Structural Proteins during the Assembly of the Head of Bacteriophage T4. *Nature* **227**:680–685. doi:10.1038/227680a0

Lane DJR, Mills TM, Shafie NH, Merlot AM, Saleh Moussa R, Kalinowski DS, Kovacevic Z, Richardson DR. 2014. Expanding horizons in iron chelation and the treatment of cancer: Role of iron in the regulation of ER stress and the epithelial–mesenchymal transition. *Biochim Biophys Acta - Rev Cancer* **1845**:166–181. doi:10.1016/j.bbcan.2014.01.005

Lanver D, Müller AN, Happel P, Schweizer G, Haas FB, Franitza M, Pellegrin C, Reissmann S, Altmüller J, Rensing SA, Kahmann R. 2018. The Biotrophic Development of Ustilago maydis Studied by RNA-Seq Analysis. *Plant Cell* **30**:300–323. doi:10.1105/tpc.17.00764

Lee A-H, Chu GC, Iwakoshi NN, Glimcher LH. 2005. XBP-1 is required for biogenesis of cellular secretory machinery of exocrine glands. *EMBO J* **24**:4368–4380. doi:10.1038/sj.emboj.7600903

Lee A-H, Iwakoshi NN, Glimcher LH. 2003. XBP-1 Regulates a Subset of Endoplasmic Reticulum Resident Chaperone Genes in the Unfolded Protein Response. *Mol Cell Biol* **23**:7448–7459. doi:10.1128/MCB.23.21.7448-7459.2003

Lee A-H, Scapa EF, Cohen DE, Glimcher LH. 2008. Regulation of hepatic lipogenesis by the transcription factor XBP1. *Science* **320**:1492–1496. doi:10.1126/science.1158042

Lee AS. 2001. The glucose-regulated proteins: stress induction and clinical applications. *Trends Biochem Sci* **26**:504–510. doi:10.1016/S0968-0004(01)01908-9

Lee CS, Ho D V, Chan JY. 2013. Nuclear factor-erythroid 2-related factor 1 regulates expression of proteasome genes in hepatocytes and protects against endoplasmic reticulum stress and steatosis in mice. *FEBS J* **280**:3609–3620. doi:10.1111/febs.12350

Lee JW, Kim HU, Choi S, Yi J, Lee SY. 2011. Microbial production of building block chemicals and polymers. *Curr Opin Biotechnol* **22**:758–767. doi:10.1016/j.copbio.2011.02.011

Liu CY, Wong HN, Schauerte JA, Kaufman RJ. 2002. The Protein Kinase/Endoribonuclease IRE1α That Signals the Unfolded Protein Response Has a Luminal N-terminal Ligand-independent Dimerization Domain. *J Biol Chem* **277**:18346–18356. doi:10.1074/jbc.M112454200

Liu J-X, Srivastava R, Che P, Howell SH. 2007. Salt stress responses in Arabidopsis utilize a signal transduction pathway related to endoplasmic reticulum stress signaling. *Plant J* **51**:897–909. doi:10.1111/j.1365-313X.2007.03195.x

Liu Y, Adachi M, Zhao S, Hareyama M, Koong AC, Luo D, Rando TA, Imai K, Shinomura Y. 2009. Preventing oxidative stress: a new role for XBP1. *Cell Death Differ* **16**:847–857. doi:10.1038/cdd.2009.14

Lo Presti L, Lanver D, Schweizer G, Tanaka S, Liang L, Tollot M, Zuccaro A, Reissmann S, Kahmann R. 2015. Fungal Effectors and Plant Susceptibility. *Annu Rev Plant Biol* **66**:513–545. doi:10.1146/annurev-arplant-043014-114623

Lo Presti L, López Díaz C, Turrà D, Di Pietro A, Hampel M, Heimel K, Kahmann R. 2016. A conserved co-chaperone is required for virulence in fungal plant pathogens. *New Phytol* **209**:1135–1148. doi:10.1111/nph.13703

Lodish H, Berk A, Zipursky SL, Matsudaira P, Baltimore D, Darnell J. 2000. Cell-Type Specification in Animals.

Lynch JM, Maillet M, Vanhoutte D, Schloemer A, Sargent MA, Blair NS, Lynch KA, Okada T, Aronow BJ, Osinska H, Prywes R, Lorenz JN, Mori K, Lawler J, Robbins J, Molkentin JD. 2012. A Thrombospondin-Dependent Pathway for a Protective ER Stress Response. *Cell* **149**:1257–1268. doi:10.1016/J.CELL.2012.03.050

Ma Y, Brewer JW, Diehl JA, Hendershot LM. 2002. Two distinct stress signaling pathways converge upon the CHOP promoter during the mammalian unfolded protein response. *J Mol Biol* **318**:1351–1365. doi:10.1016/S0022-2836(02)00234-6

Ma Y, Hendershot LM. 2004. The role of the unfolded protein response in tumour development: friend or foe? *Nat Rev Cancer* **4**:966–977. doi:10.1038/nrc1505

Ma Y, Hendershot LM. 2002. The mammalian endoplasmic reticulum as a sensor for cellular stress. *Cell Stress Chaperones* **7**:222–229.

Machamer CE. 2015. The Golgi complex in stress and death. *Front Neurosci* **9**. doi:10.3389/fnins.2015.00421

Marciniak SJ, Ron D. 2006. Endoplasmic Reticulum Stress Signaling in Disease. *Physiol Rev* **86**:1133–1149. doi:10.1152/physrev.00015.2006

Marciniak SJ, Yun CY, Oyadomari S, Novoa I, Zhang Y, Jungreis R, Nagata K, Harding HP, Ron D. 2004. CHOP induces death by promoting protein synthesis and oxidation in the stressed endoplasmic reticulum. *Genes Dev* **18**:3066–3077. doi:10.1101/gad.1250704

Margariti A, Li H, Chen T, Martin D, Vizcay-Barrena G, Alam S, Karamariti E, Xiao Q, Zampetaki A, Zhang Z, Wang W, Jiang Z, Gao C, Ma B, Chen Y-G, Cockerill G, Hu Y, Xu Q, Zeng L. 2013. *XBP1* mRNA Splicing Triggers an Autophagic Response in Endothelial Cells through *BECLIN-1* Transcriptional Activation. *J Biol Chem* **288**:859–872. doi:10.1074/jbc.M112.412783

Martin D, Li Y, Yang J, Wang G, Margariti A, Jiang Z, Yu H, Zampetaki A, Hu Y, Xu Q, Zeng L. 2014. Unspliced X-box-binding protein 1 (XBP1) protects endothelial cells from oxidative stress through interaction with histone deacetylase 3. *J Biol Chem* **289**:30625–30634. doi:10.1074/jbc.M114.571984

Masaki T, Yoshida M, Noguchi S. 1999. Targeted Disruption of CRE-Binding Factor TREB5 Gene Leads to Cellular Necrosis in Cardiac Myocytes at the Embryonic Stage. *Biochem Biophys Res Commun* **261**:350–356. doi:10.1006/BBRC.1999.0972

Maurel M, Chevet E, Tavernier J, Gerlo S. 2014. Getting RIDD of RNA: IRE1 in cell fate regulation. *Trends Biochem Sci* **39**:245–254. doi:10.1016/j.tibs.2014.02.008

Moore K, Hollien J. 2015. Ire1-mediated decay in mammalian cells relies on mRNA sequence, structure, and translational status. *Mol Biol Cell* **26**:2873–2884. doi:10.1091/mbc.E15-02-0074

Mori K, Kawahara T, Yoshida H, Yanagi H, Yura T. 1996. Signalling from endoplasmic reticulum to nucleus: transcription factor with a basic-leucine zipper motif is required for the unfolded protein response pathway. *Genes Cells* **1**:803–817. doi:10.1046/j.1365-2443.1996.d01-274.x|

Mori K, Ma W, Gething MJ, Sambrook J. 1993. A transmembrane protein with a cdc2+/CDC28-related kinase activity is required for signaling from the ER to the nucleus. *Cell* **74**:743–756. doi:10.1016/0092-8674(93)90521-Q

Mori K, Ogawa N, Kawahara T, Yanagi H, Yura T. 1998. Palindrome with spacer of one nucleotide is characteristic of the cis-acting unfolded protein response element in Saccharomyces cerevisiae. *J Biol Chem* **273**:9912–9920. doi:10.1074/jbc.273.16.9912

Mori K, Sant A, Kohno K, Normington K, Gething MJ, Sambrook JF. 1992. A 22 bp cis-acting element is necessary and sufficient for the induction of the yeast KAR2 (BiP) gene by unfolded proteins. *EMBO J* **11**:2583–2593.

Murray JI, Whitfield ML, Trinklein ND, Myers RM, Brown PO, Botstein D. 2004. Diverse and specific gene expression responses to stresses in cultured human cells. *Mol Biol Cell* **15**:2361–2374. doi:10.1091/mbc.e03-11-0799

Nagashima Y, Mishiba K-I, Suzuki E, Shimada Y, Iwata Y, Koizumi N. 2011. Arabidopsis IRE1 catalyses unconventional splicing of bZIP60 mRNA to produce the active transcription factor. *Sci Rep* **1**. doi:10.1038/srep00029

Navon A, Gatushkin A, Zelcbuch L, Shteingart S, Farago M, Hadar R, Tirosh B. 2010. Direct proteasome binding and subsequent degradation of unspliced XBP-1 prevent its intracellular aggregation. *FEBS Lett* **584**:67–73. doi:10.1016/j.febslet.2009.11.069

Newman JRS, Keating AE. 2003. Comprehensive Identification of Human bZIP Interactions with Coiled-Coil Arrays. *Science* **300**:2097–2101. doi:10.1126/science.1084648

Nikawa J-I, Yamashita S. 1992. IRE1 encodes a putative protein kinase containing a membrane-spanning domain and is required for inositol phototrophy in Saccharomyces cerevisiae. *Mol Microbiol* **6**:1441–1446. doi:10.1111/j.1365-2958.1992.tb00864.x

Okabe M, Lies D, Kanamasa S, Park EY. 2009. Biotechnological production of itaconic acid and its biosynthesis in Aspergillus terreus. *Appl Microbiol Biotechnol* **84**:597–606. doi:10.1007/s00253-009-2132-3

Olivares S, Henkel AS. 2015. Hepatic *Xbp1* Gene Deletion Promotes Endoplasmic Reticulum Stress-induced Liver Injury and Apoptosis. *J Biol Chem* **290**:30142–30151. doi:10.1074/jbc.M115.676239

Oliveira SJ, de Sousa M, Pinto JP. 2011. ER Stress and Iron Homeostasis: A New Frontier for the UPR. *Biochem Res Int* **2011**. doi:10.1155/2011/896474

Oslowski CM, Urano F. 2011. Measuring ER Stress and the Unfolded Protein Response Using Mammalian Tissue Culture System. *Methods Enzymol* **490**:71–92. doi:10.1016/B978-0-12-385114-7.00004-0

Patil CK, Li H, Walter P. 2004. Gcn4p and Novel Upstream Activating Sequences Regulate Targets of the Unfolded Protein Response. *PLoS Biol* **2**. doi:10.1371/journal.pbio.0020246

Pérez-Martín J, Castillo-Lluva S, Sgarlata C, Flor-Parra I, Mielnichuk N, Torreblanca J, Carbó N. 2006. Pathocycles: Ustilago maydis as a model to study the relationships between cell cycle and virulence in pathogenic fungi. *Mol Genet Genomics* **276**:211–229. doi:10.1007/s00438-006-0152-6

Peschek J, Acosta-Alvear D, Mendez AS, Walter P. 2015. A conformational RNA zipper promotes intron ejection during non-conventional XBP1 mRNA splicing. *EMBO Rep* **16**:1688–1698. doi:10.15252/embr.201540955

Pozarowski P, Darzynkiewicz Z. 2004. Analysis of Cell Cycle by Flow CytometryCheckpoint Controls and Cancer. New Jersey: Humana Press. pp. 301–312. doi:10.1385/1-59259-811-0:301

Puscheck EE, Awonuga AO, Yang Y, Jiang Z, Rappolee DA. 2015. Molecular Biology of the Stress Response in the Early Embryo and its Stem Cells. *Adv Exp Med Biol* 77–128. doi:10.1007/978-1-4939-2480-6_4

Raines DJ, Sanderson TJ, Wilde EJ, Duhme-Klair A-K. 2015. SiderophoresReference Module in Chemistry, Molecular Sciences and Chemical Engineering. Elsevier. doi:10.1016/B978-0-12-409547-2.11040-6

Rambhatla L, Chiu C-P, Glickman RD, Rowe-Rendleman C. 2002. In vitro differentiation capacity of telomerase immortalized human RPE cells. *Invest Ophthalmol Vis Sci* **43**:1622–1630.

Ran FA, Hsu PD, Wright J, Agarwala V, Scott DA, Zhang F. 2013. Genome engineering using the CRISPR-Cas9 system. *Nat Protoc* **8**:2281–2308. doi:10.1038/nprot.2013.143

Reimold AM, Etkin A, Clauss I, Perkins A, Friend DS, Zhang J, Horton HF, Scott A, Orkin SH, Byrne MC, Grusby MJ, Glimcher LH. 2000. An essential role in liver development for transcription factor XBP-1. *Genes Dev* **14**:152–157. doi:10.1101/GAD.14.2.152

Reimold AM, Iwakoshi NN, Manis J, Vallabhajosyula P, Szomolanyi-Tsuda E, Gravallese EM, Friend D, Grusby MJ, Alt F, Glimcher LH. 2001. Plasma cell differentiation requires the transcription factor XBP-1. *Nature* **412**:300–307. doi:10.1038/35085509

Ribeiro CMP, Lubamba BA. 2017. Role of IRE1α/XBP-1 in Cystic Fibrosis Airway Inflammation. *Int J Mol Sci* **18**. doi:10.3390/ijms18010118

Riccardi C, Nicoletti I. 2006. Analysis of apoptosis by propidium iodide staining and flow cytometry. *Nat Protoc* **1**:1458–1461. doi:10.1038/nprot.2006.238

Richie DL, Hartl L, Aimanianda V, Winters MS, Fuller KK, Miley MD, White S, McCarthy JW, Latgé J-P, Feldmesser M, Rhodes JC, Askew DS. 2009. A Role for the Unfolded Protein Response (UPR) in Virulence and Antifungal Susceptibility in Aspergillus fumigatus. *PLoS Pathog* **5**. doi:10.1371/journal.ppat.1000258

Romero-Ramirez L, Cao H, Nelson D, Hammond E, Lee A-H, Yoshida H, Mori K, Glimcher LH, Denko NC, Giaccia AJ, Le Q-T, Koong AC. 2004. XBP1 Is Essential for Survival under Hypoxic Conditions and Is Required for Tumor Growth. *Cancer Res* **64**:5943–5947. doi:10.1158/0008-5472.CAN-04-1606

Ron D, Walter P. 2007. Signal integration in the endoplasmic reticulum unfolded protein response. *Nat Rev Mol Cell Biol* **8**:519–529. doi:10.1038/nrm2199

Roy B, Lee AS. 1999. The mammalian endoplasmic reticulum stress response element consists of an evolutionarily conserved tripartite structure and interacts with a novel stress-inducible complex. *Nucleic Acids Res* **27**:1437–1443. doi:10.1093/nar/27.6.1437

Ruegsegger U, Leber JH, Walter P. 2001. Block of HAC1 mRNA translation by long-range base pairing is released by cytoplasmic splicing upon induction of the unfolded protein response. *Cell* **107**:103–114. doi:10.1016/S0092-8674(01)00505-0

Rutkowski DT, Arnold SM, Miller CN, Wu J, Li J, Gunnison KM, Mori K, Sadighi Akha AA, Raden D, Kaufman RJ. 2006. Adaptation to ER stress is mediated by differential stabilities of pro-survival and pro-apoptotic mRNAs and proteins. *PLoS Biol* **4**. doi:10.1371/journal.pbio.0040374

Rutkowski DT, Kaufman RJ. 2007. That which does not kill me makes me stronger: adapting to chronic ER stress. *Trends Biochem Sci* **32**:469–476. doi:10.1016/j.tibs.2007.09.003

Sahni S, Bae D-H, Lane DJR, Kovacevic Z, Kalinowski DS, Jansson PJ, Richardson DR. 2014. The Metastasis Suppressor, N-myc Downstream-regulated Gene 1 (NDRG1), Inhibits Stress-induced Autophagy in Cancer Cells. *J Biol Chem* **289**:9692–9709. doi:10.1074/jbc.M113.529511

Saloheimo M, Valkonen M, Penttilä M. 2003. Activation mechanisms of the HACI-mediated unfolded protein response in filamentous fungi. *Mol Microbiol* **47**:1149–1161. doi:10.1046/j.1365-2958.2003.03363.x

Sambrook J, Fritsch EF, Maniatis T. 1989. Molecular Cloning: A Laboratory Manual. Cold Spring Harbor laboratory press, New York.

Scheuner D, Song B, McEwen E, Liu C, Laybutt R, Gillespie P, Saunders T, Bonner-Weir S, Kaufman RJ. 2001. Translational control is required for the unfolded protein response and in vivo glucose homeostasis. *Mol Cell* **7**:1165–1176. doi:10.1016/S1097-2765(01)00265-9

Schindelin J, Arganda-Carreras I, Frise E, Kaynig V, Longair M, Pietzsch T, Preibisch S, Rueden C, Saalfeld S, Schmid B, Tinevez J-Y, White DJ, Hartenstein V, Eliceiri K, Tomancak P, Cardona A. 2012. Fiji: an open-source platform for biological-image analysis. *Nat Methods* **9**:676–682. doi:10.1038/nmeth.2019

Schirawski J, Böhnert HU, Steinberg G, Snetselaar K, Adamikowa L, Kahmann R. 2005. Endoplasmic Reticulum Glucosidase II Is Required for Pathogenicity of Ustilago maydis. *Plant Cell* **17**:3532–3543. doi:10.1105/TPC.105.036285

Schröder M. 2008. Endoplasmic reticulum stress responses. *Cell Mol Life Sci* **65**:862–894. doi:10.1007/s00018-007-7383-5

Schröder M, Kaufman RJ. 2005. ER stress and the unfolded protein response. *Mutat Res Mol Mech Mutagen* **569**:29–63. doi:10.1016/j.mrfmmm.2004.06.056

Schuck S, Prinz WA, Thorn KS, Voss C, Walter P. 2009. Membrane expansion alleviates endoplasmic reticulum stress independently of the unfolded protein response. *J Cell Biol* **187**:525–536. doi:10.1083/jcb.200907074

Schulz B, Banuett F, Dahl M, Schlesinger R, Schäfer W, Martin T, Herskowitz I, Kahmann R. 1990. The b alleles of U. maydis, whose combinations program pathogenic development, code for polypeptides containing a homeodomain-related motif. *Cell* **60**:295–306.

Schuster M, Schweizer G, Kahmann R. 2018. Comparative analyses of secreted proteins in plant pathogenic smut fungi and related basidiomycetes. *Fungal Genet Biol* **112**:21–30. doi:10.1016/J.FGB.2016.12.003

Selye H. 1975. Implications of stress concept. *N Y State J Med* **75**:2139–2145.

Shamu CE, Walter P. 1996. Oligomerization and phosphorylation of the Ire1p kinase during intracellular signaling from the endoplasmic reticulum to the nucleus. *EMBO J* **15**:3028–3039.

Sharp PA, Sugden B, Sambrook J. 1973. Detection of two restriction endonuclease activities in Haemophilus parainfluenzae using analytical agarose--ethidium bromide electrophoresis. *Biochemistry* **12**:3055–3063. doi:10.1021/bi00740a018

Shen J, Chen X, Hendershot L, Prywes R. 2002. ER stress regulation of ATF6 localization by dissociation of BiP/GRP78 binding and unmasking of Golgi localization signals. *Dev Cell* **3**:99–111. doi:10.1016/S1534-5807(02)00203-4

Shen X, Ellis RE, Lee K, Liu CY, Yang K, Solomon A, Yoshida H, Morimoto R, Kurnit DM, Mori K, Kaufman RJ. 2001. Complementary signaling pathways regulate the unfolded protein response and are required for C. elegans development. *Cell* **107**:893–903. doi:10.1016/S0092-8674(01)00612-2

Sherr CJ, DePinho RA. 2000. Cellular Senescence. *Cell* **102**:407–410. doi:10.1016/S0092-8674(00)00046-5

Shore GC, Papa FR, Oakes SA. 2011. Signaling cell death from the endoplasmic reticulum stress response. *Curr Opin Cell Biol* **23**:143–149. doi:10.1016/j.ceb.2010.11.003

Shoulders MD, Ryno LM, Genereux JC, Moresco JJ, Tu PG, Wu C, Yates JR, Su AI, Kelly JW, Wiseman RL, Wiseman RL. 2013. Stress-independent activation of XBP1s and/or ATF6 reveals three functionally diverse ER proteostasis environments. *Cell Rep* **3**:1279–1292. doi:10.1016/j.celrep.2013.03.024

Sidrauski C, Cox JS, Walter P. 1996. tRNA ligase is required for regulated mRNA splicing in the unfolded protein response. *Cell* **87**:405–413. doi:10.1016/S0092-8674(00)81361-6

Smith MH, Ploegh HL, Weissman JS. 2011. Road to Ruin: Targeting Proteins for Degradation in the Endoplasmic Reticulum. *Science* **334**:1086–1090. doi:10.1126/science.1209235

Snetselaar KM. 1993. Microscopic Observation of Ustilago maydis Mating Interactions. *Exp Mycol* **17**:345–355. doi:10.1006/emyc.1993.1033

Snetselaar KM, Mims CW. 1992. Sporidial fusion and infection of maize seedlings by the smut fungus Ustilago maydis. *Mycol Soc Am* **84**:193–203. doi:10.2307/3760250

Southern EM. 1975. Detection of specific sequences among DNA fragments separated by gel electrophoresis. *J Mol Biol* **98**:503–517. doi:10.1016/S0022-2836(75)80083-0

Sriburi R, Jackowski S, Mori K, Brewer JW. 2004. XBP1. *J Cell Biol* **167**:35–41. doi:10.1083/JCB.200406136

Steinberg G, Perez-Martin J. 2008. Ustilago maydis, a new fungal model system for cell biology. *Trends Cell Biol* **18**:61–67. doi:10.1016/j.tcb.2007.11.008

Szymczak AL, Vignali DA. 2005. Development of 2A peptide-based strategies in the design of multicistronic vectors. *Expert Opin Biol Ther* **5**:627–638. doi:10.1517/14712598.5.5.627

Tam AB, Koong AC, Niwa M. 2014. Ire1 has distinct catalytic mechanisms for XBP1/HAC1 splicing and RIDD. *Cell Rep* **9**:850–858. doi:10.1016/j.celrep.2014.09.016

Tavernier SJ, Osorio F, Vandersarren L, Vetters J, Vanlangenakker N, Van Isterdael G, Vergote K, De Rycke R, Parthoens E, van de Laar L, Iwawaki T, Del Valle JR, Hu C-CA, Lambrecht BN, Janssens S. 2017. Regulated IRE1-dependent mRNA decay sets the threshold for dendritic cell survival. *Nat Cell Biol* **19**:698–710. doi:10.1038/ncb3518

Thuerauf DJ, Marcinko M, Belmont PJ, Glembotski CC. 2007. Effects of the Isoform-specific Characteristics of ATF6α and ATF6β on Endoplasmic Reticulum Stress Response Gene Expression and Cell Viability. *J Biol Chem* **282**:22865–22878. doi:10.1074/jbc.M701213200

Tirasophon W, Welihinda AA, Kaufman RJ. 1998. A stress response pathway from the endoplasmic reticulum to the nucleus requires a novel bifunctional protein kinase/endoribonuclease (Ire1p) in mammalian cells. *Genes Dev* **12**:1812–1824.

Todd DJ, Lee A-H, Glimcher LH. 2008. The endoplasmic reticulum stress response in immunity and autoimmunity. *Nat Rev Immunol* **8**:663–674. doi:10.1038/nri2359

Travers KJ, Patil CK, Wodicka L, Lockhart DJ, Weissman JS, Walter P. 2000. Functional and genomic analyses reveal an essential coordination between the unfolded protein response and ER-associated degradation. *Cell* **101**:249–258. doi:10.1016/S0092-8674(00)80835-1

Treiman M. 2002. Regulation of the endoplasmic reticulum calcium storage during the unfolded protein response--significance in tissue ischemia? *Trends Cardiovasc Med* **12**:57–62. doi:10.1016/S1050-1738(01)00147-5

Tsaytler P, Harding HP, Ron D, Bertolotti A. 2011. Selective Inhibition of a Regulatory Subunit of Protein Phosphatase 1 Restores Proteostasis. *Science* **332**:91–94. doi:10.1126/science.1201396

Tsukuda T, Carleton S, Fotheringham S, Holloman WK. 1988. Isolation and characterization of an autonomously replicating sequence from Ustilago maydis. *Mol Cell Biol* **8**:3703–3709. doi:10.1128/MCB.8.9.3703

van Huizen R, Martindale JL, Gorospe M, Holbrook NJ. 2003. P58 IPK , a Novel Endoplasmic Reticulum Stress-inducible Protein and Potential Negative Regulator of eIF2α Signaling. *J Biol Chem* **278**:15558–15564. doi:10.1074/jbc.M212074200

van Vliet AR, Giordano F, Gerlo S, Segura I, Van Eygen S, Molenberghs G, Rocha S, Houcine A, Derua R, Verfaillie T, Vangindertael J, De Keersmaecker H, Waelkens E, Tavernier J, Hofkens J, Annaert W, Carmeliet P, Samali A, Mizuno H, Agostinis P. 2017. The ER Stress Sensor PERK Coordinates ER-Plasma Membrane Contact Site Formation through Interaction with Filamin-A and F-Actin Remodeling. *Mol Cell* **65**:885–899. doi:10.1016/j.molcel.2017.01.020

Vecchi C, Montosi G, Zhang K, Lamberti I, Duncan SA, Kaufman RJ, Pietrangelo A. 2009. ER stress controls iron metabolism through induction of hepcidin. *Science* **325**:877–880. doi:10.1126/science.1176639

Venugopal R, Jaiswal AK. 1998. Nrf2 and Nrf1 in association with Jun proteins regulate antioxidant response element-mediated expression and coordinated induction of genes encoding detoxifying enzymes. *Oncogene* **17**:3145–3156. doi:10.1038/sj.onc.1202237

Vilchez D, Boyer L, Morantte I, Lutz M, Merkwirth C, Joyce D, Spencer B, Page L, Masliah E, Berggren WT, Gage FH, Dillin A. 2012. Increased proteasome activity in human embryonic stem cells is regulated by PSMD11. *Nature* **489**:304–308. doi:10.1038/nature11468

Vincenz L, Jäger R, O'Dwyer M, Samali A. 2013. Endoplasmic Reticulum Stress and the Unfolded Protein Response: Targeting the Achilles Heel of Multiple Myeloma. *Mol Cancer Ther* **12**:831–843. doi:10.1158/1535-7163.MCT-12-0782

Wahl R, Zahiri A, Kämper J. 2010. The Ustilago maydis b mating type locus controls hyphal proliferation and expression of secreted virulence factors in planta. *Mol Microbiol* **75**:208–220. doi:10.1111/j.1365-2958.2009.06984.x

Walter F, Schmid J, Düssmann H, Concannon CG, Prehn JHM. 2015. Imaging of single cell responses to ER stress indicates that the relative dynamics of IRE1/XBP1 and PERK/ATF4 signalling rather than a switch between signalling branches determine cell survival. *Cell Death Differ* **22**:1502–1516. doi:10.1038/cdd.2014.241

Walter P, Ron D. 2011. The unfolded protein response: From stress pathway to homeostatic regulation. *Science* **334**:1081–1087. doi:10.1126/science.1209038

Wang M, Kaufman RJ. 2014. The impact of the endoplasmic reticulum protein-folding environment on cancer development. *Nat Rev Cancer* **14**:581–597. doi:10.1038/nrc3800

Wang P, Li J, Sha B. 2016. The ER stress sensor PERK luminal domain functions as a molecular chaperone to interact with misfolded proteins. *Acta Crystallogr Sect D, Struct Biol* **72**:1290–1297. doi:10.1107/S2059798316018064

Wang P, Li J, Tao J, Sha B. 2018. The luminal domain of the ER stress sensor protein PERK binds misfolded proteins and thereby triggers PERK oligomerization. *J Biol Chem* **293**:4110–4121. doi:10.1074/jbc.RA117.001294

Wang S, Kaufman RJ. 2012. The impact of the unfolded protein response on human disease. *J Cell Biol* **197**:857–867. doi:10.1083/jcb.201110131

Wang X-Z, Harding HP, Zhang Y, Jolicoeur E, Kuroda M, Ron D. 1998. Cloning of mammalian Ire1 reveals diversity in the ER stress responses. *EMBO J* **17**:5708–5717. doi:10.1093/emboj/17.19.5708

Wang Y, Shen J, Arenzana N, Tirasophon W, Kaufman RJ, Prywes R. 2000. Activation of ATF6 and an ATF6 DNA Binding Site by the Endoplasmic Reticulum Stress Response. *JBC* **275**:27013–27020. doi:10.1074/jbc.M003322200

Welch W, Suhan J. 1985. Morphological study of the mammalian stress response: characterization of changes in cytoplasmic organelles, cytoskeleton, and nucleoli, and appearance of. *JcbRupressOrg* **101**:1198–1211. doi:10.1083/JCB.101.4.1198

Welihinda AA, Kaufman RJ. 1996. The unfolded protein response pathway in Saccharomyces cerevisiae. Oligomerization and trans-phosphorylation of Ire1p (Ern1p) are required for kinase activation. *J Biol Chem* **271**:18181–18187. doi:10.1074/jbc.271.30.18181

Wiest DL, Burkhardt JK, Hester S, Hortsch M, Meyer DI, Argon Y. 1990. Membrane biogenesis during B cell differentiation: most endoplasmic reticulum proteins are expressed coordinately. *J Cell Biol* **110**:1501–1511. doi:10.1083/JCB.110.5.1501

Xu J. 2005. Preparation, Culture, and Immortalization of Mouse Embryonic FibroblastsCurrent Protocols in Molecular Biology. Hoboken, NJ, USA: John Wiley & Sons, Inc. pp. 2811–2818. doi:10.1002/0471142727.mb2801s70

Xu T, Yang L, Yan C, Wang X, Huang P, Zhao F, Zhao L, Zhang M, Jia W, Wang X, Liu Y. 2014. The IRE1α-XBP1 pathway regulates metabolic stress-induced compensatory proliferation of pancreatic β-cells. *Cell Res* **24**:1137–40. doi:10.1038/cr.2014.55

Yamamoto K, Sato T, Matsui T, Sato M, Okada T, Yoshida H, Harada A, Mori K. 2007. Transcriptional Induction of Mammalian ER Quality Control Proteins Is Mediated by Single or Combined Action of ATF6α and XBP1. *Dev Cell* **13**:365–376. doi:10.1016/j.devcel.2007.07.018

Yamamoto K, Yoshida H, Kokame K, Kaufman RJ, Mori K. 2004. Differential Contributions of ATF6 and XBP1 to the Activation of Endoplasmic Reticulum Stress-Responsive cis-Acting Elements ERSE, UPRE and ERSE-II. *J Biochem* **136**:343–350. doi:10.1093/jb/mvh122

Yanagitani K, Imagawa Y, Iwawaki T, Hosoda A, Saito M, Kimata Y, Kohno K. 2009. Cotranslational targeting of XBP1 protein to the membrane promotes cytoplasmic splicing of its own mRNA. *Mol Cell* **34**:191–200. doi:10.1016/j.molcel.2009.02.033

Yanagitani K, Kimata Y, Kadokura H, Kohno K. 2011. Translational pausing ensures membrane targeting and cytoplasmic splicing of XBP1u mRNA. *Science* **331**:586–589. doi:10.1126/science.1197142

Yang J, Cheng D, Zhou S, Zhu B, Hu T, Yang Q, Yang J, Cheng D, Zhou S, Zhu B, Hu T, Yang Q. 2015. Overexpression of X-Box Binding Protein 1 (XBP1) Correlates to Poor Prognosis and Up-Regulation of PI3K/mTOR in Human Osteosarcoma. *Int J Mol Sci* **16**:28635–28646. doi:10.3390/ijms161226123

Ye J, Rawson RB, Komuro R, Chen X, Davé UP, Prywes R, Brown MS, Goldstein JL. 2000. ER Stress Induces Cleavage of Membrane-Bound ATF6 by the Same Proteases that Process SREBPs. *Mol Cell* **6**:1355–1364. doi:10.1016/S1097-2765(00)00133-7

Yoshida H, Haze K, Yanagi H, Yura T, Mori K. 1998. Identification of the cis-acting endoplasmic reticulum stress response element responsible for transcriptional induction of mammalian glucose-regulated proteins. Involvement of basic leucine zipper transcription factors. *J Biol Chem* **273**:33741–33749. doi:10.1074/jbc.273.50.33741

Yoshida H, Matsui T, Yamamoto A, Okada T, Mori K. 2001. XBP1 mRNA is induced by ATF6 and spliced by IRE1 in response to ER stress to produce a highly active transcription factor. *Cell* **107**:881–891. doi:10.1016/S0092-8674(01)00611-0

Yoshida H, Okada T, Haze K, Yanagi H, Yura T, Negishi M, Mori K. 2000. ATF6 activated by proteolysis binds in the presence of NF-Y (CBF) directly to the cis-acting element responsible for the mammalian unfolded protein response. *Mol Cell Biol* **20**:6755–6767. doi:10.1128/MCB.20.18.6755-6767.2000

Yoshida H, Oku M, Suzuki M, Mori K. 2006. pXBP1(U) encoded in XBP1 pre-mRNA negatively regulates unfolded protein response activator pXBP1(S) in mammalian ER stress response. *J Cell Biol* **172**:565–575. doi:10.1083/jcb.200508145

Yoshida H, Uemura A, Mori K. 2009. pXBP1(U), a negative regulator of the unfolded protein response activator pXBP1(S), targets ATF6 but not ATF4 in proteasome-mediated degradation. *Cell Struct Funct* **34**:1–10. doi:10.1247/csf.06028

Zeng L, Xiao Q, Chen M, Margariti A, Martin D, Ivetic A, Xu H, Mason J, Wang W, Cockerill G, Mori K, Li JY, Chien S, Hu Y, Xu Q. 2013. Vascular Endothelial Cell Growth–Activated XBP1 Splicing in Endothelial Cells Is Crucial for Angiogenesis. *Circulation* **127**:1712–1722. doi:10.1161/CIRCULATIONAHA.112.001337

Zeng L, Zampetaki A, Margariti A, Pepe AE, Alam S, Martin D, Xiao Q, Wang W, Jin Z-G, Cockerill G, Mori K, Li Y -s. J, Hu Y, Chien S, Xu Q. 2009. Sustained activation of XBP1 splicing leads to endothelial apoptosis and atherosclerosis development in response to disturbed flow. *Proc Natl Acad Sci* **106**:8326–8331. doi:10.1073/pnas.0903197106

Zhang L, Zhang C, Wang A. 2016. Divergence and Conservation of the Major UPR Branch IRE1-bZIP Signaling Pathway across Eukaryotes. *Sci Rep* **6**. doi:10.1038/srep27362

Zhao Y, Li X, Cai M-Y, Ma K, Yang J, Zhou J, Fu W, Wei F-Z, Wang L, Xie D, Zhu W-G. 2013. XBP-1u suppresses autophagy by promoting the degradation of FoxO1 in cancer cells. *Cell Res* **23**:491–507. doi:10.1038/cr.2013.2

Zhou Y, Lee J, Reno CM, Sun C, Park SW, Chung J, Lee J, Fisher SJ, White MF, Biddinger SB, Ozcan U. 2011. Regulation of glucose homeostasis through a XBP-1–FoxO1 interaction. *Nat Med* **17**:356–365. doi:10.1038/nm.2293